

Open Research Online

The Open University's repository of research publications and other research outputs

Preclinical Models to study the Biology and Therapy of Ovarian Cancer

Thesis

How to cite:

Bizzaro, Francesca (2019). Preclinical Models to study the Biology and Therapy of Ovarian Cancer. PhD thesis The Open University.

For guidance on citations see [FAQs](#).

© 2018 The Author



<https://creativecommons.org/licenses/by-nc-nd/4.0/>

Version: Version of Record

Link(s) to article on publisher's website:

<http://dx.doi.org/doi:10.21954/ou.ro.0000e718>

Copyright and Moral Rights for the articles on this site are retained by the individual authors and/or other copyright owners. For more information on Open Research Online's data [policy](#) on reuse of materials please consult the policies page.

oro.open.ac.uk

Thesis submitted by

Francesca Bizzaro

Istituto di Ricerche Farmacologiche Mario Negri IRCCS

Milan, Italy

**PRECLINICAL MODELS TO STUDY THE
BIOLOGY AND THERAPY
OF OVARIAN CANCER**

for the degree of

Doctor of Philosophy

Discipline of Life and Biomolecular Sciences

The Open University, UK

September 2018

ABSTRACT

Ovarian cancer (OC) is one of the most common gynaecological malignancies and a cause of mortality among western women. Standard-of-care treatment consists of platinum/taxane-based chemotherapy, but 5-years survival rate remains low.

Germline and somatic mutations in *BRCA* are present in half of the high grade serous (HGS) ovarian cancer. Olaparib, a PARP inhibitor affecting DNA damage repair pathway, has been approved in the treatment of germline-*BRCA*-mutated patients. The combination with cediranib, an angiogenesis inhibitor, has shown promising results, increasing progression-free survival in women with recurrent HGS ovarian cancer.

In this thesis, patient-derived ovarian cancer xenografts (OC-PDX) were used to study olaparib therapy and mechanisms underlying the observed benefit of the combination.

Next Generation Sequencing and gene expression analysis were performed on OC-PDX to identify mutations/aberrations in *BRCA1/2* and other genes connected to the DNA repair pathway. A cohort (n=13) of OC-PDX was selected and classified as BRCAness and Not BRCAness, accordingly to their proficiency or deficiency in DNA damage repair.

Olaparib and cediranib were administered in short-term (4 weeks) or maintenance (until progression) regimens.

Olaparib showed activity in BRCAness OC-PDX; the effect was improved by cediranib, inducing durable responses even after treatment suspension. Of note, the combination was also beneficial in Not BRCAness OC-PDX, promoting stable disease and regression.

The effect of the combination on changes in tumor-associated vasculature and hypoxia (likely due to cediranib) and DNA damage repair (due to olaparib), together with preliminary data on gene expression and mutational status, suggested a potential “cumulative” effect of the combination after 4 weeks of treatment. Studies are ongoing, to understand the molecular determinants that accompany the response of OC-PDX to the combination.

The results obtained compel us to believe that the combination of olaparib with cediranib is advantageous both in DNA repair proficient and, most importantly, in deficient patients, and has to be administered until tumor progression.

Preface

The work described herein was performed at the Istituto di Ricerche Farmacologiche Mario Negri IRCCS, Milan, Italy, from October 2014 to October 2018.

The PhD research project was performed under the supervision and direction of Dr. Raffaella Giavazzi (director of the studies) and Prof. Suzanne Eccles (external supervisor).

Declaration

This PhD research project has not been submitted in whole or in part for a degree or diploma or other qualification to any other university.

The experimental work described herein was performed by myself, Francesca Bizzaro, and includes work carried out in collaboration with:

- Dr. Lucia Minoli and Prof. Eugenio Scanziani, pathologists of the Department of Veterinary Medicine of the University of Milan and Mouse and Animal Pathology Lab (MAPLab) of the Fondazione Filarete, Milan, performed immunohistochemical analyses on hypoxia and tumor-associated vasculature.

- Dr. Daniele Tolomeo and Dr. Edoardo Micotti, magnetic resonance imaging (MRI) experts from the Laboratory of Biology of Neurodegenerative Disorders, Istituto di Ricerche Farmacologiche Mario Negri IRCCS, Milan, Italy.

- Dr. Paola Ostano and Dr. Giovanna Chiorino, from the Cancer Genomics Laboratory, Fondazione Edo and Elvo Tempia Valenta, Biella, Italy, performed genome-wide gene expression analyses and elaborated data from genome-wide gene expression and fluidigm experiments.

- Dr. Simon Barry from AstraZeneca, Oncology, IMED Biotech Unit at the CRUK Institute of Cambridge, hosted me during my period as a visiting scientist and outstandingly and fruitfully collaborated with us during the entire project.

- Dr. Molly Taylor from AstraZeneca, Bioscience, Oncology, IMED Biotech Unit at the CRUK Institute of Cambridge, taught and performed with me fluidigm experiments.

- Dr. Vidalba Rocher Ros and her team from AstraZeneca, Oncology, IMED Translational Science, Molecular Pathology Group at the Cambridge Science Park performed the immunohistochemical analyses on HR DNA repair markers.

- Dr. Zhounghwu Lai and Dr. Steven Criscione from AstraZeneca, Bioscience, Oncology Translational Sciences, IMED Biotech Unit, Waltam, MA, US, supervised and analyzed data from next generation sequencing (NGS) experiments on DNA and RNA.
- Novogene: Genome Sequencing Company (Chula Vista, California), which performed whole transcriptome shotgun sequencing (RNA sequencing).

Acknowledgment

Firstly, I would like to thank my supervisor Dr. Raffaella Giavazzi, for her guidance and support throughout all the years that I spent at the Istituto di Ricerche Farmacologiche Mario Negri IRCCS.

I would like to thank Prof. Sue Eccles, my external supervisor. Your precious guidance and advice, your kindness and continuous encouragement have helped me during these “not always easy” years of PhD.

A special thanks to my third party monitor Mabi. Thank you for have constantly challenged and helped me to figure out which was the best way to face every difficulty that popped up during the journey.

A big big big thanks to the entire Laboratory of Biology and Treatment of Metastasis, former and present members, both in Milano and Bergamo.

Each of you, in different ways and moments, have taught me something that helped me to grow as a researcher and mostly as a person.

I will always bring with me our shared achievements and our defeats, our genuine laughs and our equally genuine fights.

Thanks for have made me feel part of a “little family”...and, in this regard, a special hug goes to Vivi!

Thanks to the entire Department of Oncology, former and present members. In particular Sarah, Bene, Miky, Eu, Nico, Frizz e Roby. Moreover, I would like to express my sincere gratitude to Paolo Ubezio and Francesca Falcetta.

Thanks to Molly and Simon, for literally gave me a home in Cambridge. It was a fundamental life-experience for my personal growth. All of you made me feel happy even in that “cold-grey-rainy-WONDERFUL” city!

A huge thanks to Chiara, Pietro, Laura and Silvia. You were my lifeline during all these years. None of this would have been possible without your never-ending support and help! I would have probably left after the probationary period if it wasn't for you!

My most important thanks go to Mum and Dad, for have always believed and supported me, even when I was making the “not-so-right” choice. Your love has been, is and always will be my strength.

Finally, no words could ever explain how much I love you, Alessio. Thanks for your special encouragement, patience and understanding in every single moment of all these years. It was not always easy, but you have always been by my side. It is finally time to start OUR life together!

List of Abbreviation

Δ Ct	Delta Ct
μ l	Microliters
μ m	Micrometres
μ g	Micrograms
AGD	Absolute Growth Delay
ATM	Ataxia-telangiectasia mutated gene serine/threonine kinase
ATRX	Alpha-Thalassemia X-Linked ATP-dependent helicase
BER	Base Excision Repair
BEV	Bevacizumab
bp	Base pair
BRAF	v-raf murine sarcoma viral oncogene homolog B
BRCA 1	Breast Cancer Type 1 Susceptibility Protein
BRCA 2	Breast Cancer Type 2 Susceptibility Protein
BSA	Bovine Serum Albumin
c DNA	Complementary Deoxyribonucleic acid
C57BL/6	C57 black 6 mice
CA9	Carbonic anhydrase 9
CCC	Clear Cell Carcinoma
CD31/PECAM 1	Platelet endothelial cell adhesion molecule-1,cluster of differentiation 31
CED	Cediranib
c-KIT	KIT proto-oncogene receptor tyrosine kinase
Ct	Threshold cycle
CTNNB1	Catenin beta 1
DDP	Cisplatin
DDR	DNA Damage Repair
DMEM	Dulbecco's Modified Eagle Medium

DMSO	Dimethylsulphoxide
DNA	Deoxyribonucleic Acid
DSBs	Double Strand Breaks
DTregrowth	Doubling Time at regrowth
EA	Epithelial Area
EDTA	Ethylene-Diamine-Tetraacetic Acid
EGFR	Epidermal Growth Factor Receptor
EMA	European Medicines Agency
FANCA	Fanconi anaemia, complementation group A
FANCB	Fanconi anaemia, complementation group B
FBS	Fetal Bovine Serum
FDA	Food and Drug Administration
FFPE	Formalin Fixed-Paraffin Embedded
FIGO	Federation of Gynecologist and Obstetricians
FLT1 (VEGFR-1)	fms related tyrosine kinase 1, VEGF receptor 1
FLT4 (VEGFR-3)	fms related tyrosine kinase 4, VEGF receptor 3
GEM	Genetically Engineered Mouse models
γ H2AX	Phosphorylated H2A histone family, member X
H&E	Hematoxylin and Eosin
HBSS	Hank's Balanced Salt Solution
HGE	High Grade Endometrioid carcinoma
HGS	High Grade Serous carcinoma
HR	Homologous Recombination
i.o	Intraovarian
i.p	Intraperitoneal
i.v	Intravenous
IHC	Immuno-Histo-Chemistry
ILS	Increment of Lifespan
KDR (VEGFR-2)	Kinase insert Domain Receptor, VEGF receptor 2

kg	Kilograms
KRAS	Kirsten rat sarcoma viral oncogene homolog
LGE	Low Grade Endometrioid carcinoma
LGS	Low Grade Serous carcinoma
mg	Milligrams
ml	Millilitres
mRNA	Messenger RNA
MMR	Mismatch Repair
MNHOC	Mario Negri Human Ovarian Carcinoma
MOSEC	Mouse Ovarian Surface Epithelial Cells
MRI	Magnetic Resonance Imaging
MST	Median Survival Time
MUC	Mucinous carcinoma
MVD	Micro Vessel Density
NCr-nu/nu	Athymic Nude Mice
NER	Nucleotide Excision Repair
ng	Nanograms
nm	Nanometres
NGS	Next Generation Sequencing
NHEJ	Non Homologous End Joining
NHR	Non Homologous Recombination
NSG	NOD Scid Gamma Mice
OC-PDX	Ovarian Cancer-Patient Derived Xenografts
OCT	Optimal Cutting Temperature Compound
OLA	Olaparib
p.o	Per os
PALB2	Partner And Localizer of BRCA2
PARP	Poly (ADP-ribose) Polymerase
PARP4	Poly(ADP-ribose) Polymerase family member 4

PCR	Polymerase Chain Reaction
PDGFR-alpha/-beta	Platelet Derived Growth Factor Receptor-alpha/-beta
PIK3CA	Phosphatidyl-Inositol-4,5-bisphosphate 3-Kinase Catalytic subunit Alpha
Pimo	Pimonidazole
PPP2R1A	Protein Phosphatase 2 Scaffold Subunit Alpha
PTEN	Phosphatase And Tensin Homolog
RNA	Ribonucleic Acid
rpm	Revolution per minutes
s.c	Subcutaneous
SCID	Severe Combined Immunodeficiency Mice
SD	Standard Deviation
SSBs	Single Strand Breaks
TP53	Tumor Protein 53
Tween-80	Polysorbate 80
TWnadir	Tumor Weight at Nadir
VEGFA	Vascular Endothelial Growth Factor A
VEGFR	Vascular Endothelial Growth Factor Receptor
VH	Vehicle

Table of Contents

ABSTRACT	ii
Preface	v
Declaration	vi
Acknowledgment	viii
List of Abbreviation	ix
Table of Contents	xiii
Table of Figures	xix
CHAPTER 1	2
Introduction	2
1.1 EPITHELIAL OVARIAN CANCER	3
1.1.1 Epidemiology and risk factors	3
1.1.2 Pathology	5
1.1.3 Dualistic model	7
1.1.4 Classification	7
<i>1.1.4.1 Type I</i>	7
<i>1.1.4.2 Type II</i>	9
1.2 TREATMENT OF OVARIAN CANCER	12
1.2.1 Cytoreductive surgery	12
1.2.2 Chemotherapy	13
<i>Platinum-derivatives</i>	13
<i>Taxane-derivatives</i>	13
<i>Other cytotoxic agents</i>	14
1.2.3 Targeted therapies	15
1.3 ANGIOGENESIS AND TUMOR ANGIOGENESIS	15
1.3.1 Inhibitors of angiogenesis as cancer therapy	19
1.3.2 Cediranib	25
1.4 DNA REPAIR TARGETED THERAPY	29
1.4.1 Poly(ADP-ribose) polymerase (PARP) inhibitors as cancer therapy	31
1.4.2 BRCA1 and BRCA2 mutations	35
1.4.3 Olaparib	40
1.5 PARP INHIBITORS IN COMBINATION WITH ANGIOGENESIS INHIBITORS	43
1.6 ANIMAL MODELS FOR OVARIAN CANCER	44
1.6.1 Patient-derived ovarian cancer xenografts (OC-PDX)	45

CHAPTER 1.....	49
Aim of the study.....	49
CHAPTER 2.....	53
Materials and Methods.....	53
2.1 PATIENT-DERIVED OVARIAN CANCER XENOGRAFTS (OC-PDX).....	54
2.1.1 Models.....	54
2.1.2 Animals.....	55
2.1.2.1 <i>Anaesthesia and euthanasia in mice</i>	55
2.1.3 Ectopic tumor models.....	56
2.1.4 Orthotopic tumor models.....	57
2.1.4.1 <i>Intraperitoneal models</i>	57
2.1.4.2 <i>Intraovarian model ID8</i>	57
2.1.4.3 <i>Necropsy examination</i>	59
2.1.5 The biobank of OC-PDX.....	60
2.1.5.1 <i>Patients' tumor collection</i>	60
2.1.5.2 <i>Subcutaneous tumor specimen collection</i>	60
2.1.5.3 <i>Ascites collection</i>	60
2.1.5.4 <i>Sample storage</i>	60
2.1.5.5 <i>Blood sample collection and storage</i>	61
2.2 MOLECULAR ANALYSIS.....	61
2.2.1 Nucleic Acid Extraction.....	61
2.2.2 Next Generation Sequencing.....	65
2.2.3 Sanger validation.....	66
2.2.4 RealTime PCR.....	70
2.2.5 Fluidigm.....	72
2.2.6 RNA sequencing.....	77
2.3 <i>IN VIVO</i> PRECLINICAL STUDIES.....	77
2.3.1 Animals for preclinical studies.....	77
2.3.2 Drug preparation and administration.....	78
2.3.2.1 <i>Schedule of treatments</i>	78
2.3.3 Evaluation of treatment.....	79
2.3.3.1 <i>Ectopic tumor models</i>	79
2.3.3.2 <i>Intraperitoneal tumor models</i>	80
2.3.3.3 <i>Intraovarian model ID8</i>	80
2.4 <i>EX VIVO</i> ANALYSIS.....	82

2.4.1 Histological and immunohistochemical analysis on hypoxia and tumor-associated vasculature.....	82
2.4.2 Histological and immunohistochemical analysis of HR DNA repair markers.....	83
2.5 STATISTICAL ANALYSES.....	84
CHAPTER 3.....	86
Results.....	86
CHARACTERIZATION OF <i>IN VIVO</i> PATIENT-DERIVED OVARIAN CANCER XENOGRAFTS.....	86
(OC-PDX).....	86
3.1 THE PLATFORM OF OC-PDX.....	87
3.1.1 Characteristics of original patients’ tumors.....	91
3.1.2 OC-PDX recapitulate the morphology and histopathology of ovarian cancer.....	93
3.1.3 OC-PDX biological behaviour.....	95
3.1.4 NGS to study the mutational landscape of OC-PDX.....	95
3.1.5 Gene expression profile analysis to characterize OC-PDX.....	101
3.2 THE COHORT OF OC-PDX SELECTED TO PERFORM PRECLINICAL DRUG TESTING.....	109
3.3 SUMMARY OF RESULTS AND DISCUSSION.....	111
CHAPTER 4.....	116
Results.....	116
PRECLINICAL THERAPY TESTING.....	116
4.1 CORRELATION BETWEEN THE BRCA ^{NESS} STATUS AND RESPONSE TO OLAPARIB MONOTHERAPY.....	117
4.2 THE IMPORTANCE OF THE COMBINATION OF OLAPARIB AND CEDIRANIB.....	120
Summary of results.....	123
4.3 THE COMBINATION OF OLAPARIB AND CEDIRANIB IN ECTOPIC MODELS OF OVARIAN CANCER.....	123
4.3.1 Case-report: MNHOC 18, Not BRCA ^{ness}	123
4.3.2 Case-report: MNHOC 182, Not BRCA ^{ness}	126
4.3.3 Case-report: MNHOC 508, BRCA ^{ness}	128
4.3.4 Cases-report: MNHOC 511 and MNHOC 513, BRCA ^{ness}	131
4.3.5 Case-report: MNHOC 154, BRCA ^{ness}	134
Summary of results.....	136
4.4 THE COMBINATION OF OLAPARIB AND CEDIRANIB IN ORTHOTOPIC MODELS OF OVARIAN CANCER.....	138
4.4.1 Case-report: MNHOC 8, BRCA ^{ness}	138

<i>The combination administered in a short-term regimen (4 weeks)</i>	138
<i>The combination administered in a maintenance regimen</i>	139
<i>The importance of drug sequence in the combination</i>	141
Summary of results.....	144
4.5 THE COMBINATION OF OLAPARIB WITH OTHER ANGIOGENESIS INHIBITORS	145
4.5.1 Case-report: MNHOC 18, Not BRCAness.....	145
4.5.2 Case-report: MNHOC 8, BRCAness.....	147
Summary of results.....	149
4.6 THE ADVANTAGE OF THE COMBINATION IN OLAPARIB RESISTANT BRCA NESS MODELS	149
4.6.1 Case-report: MNHOC 22, BRCAness.....	149
Summary of results.....	152
4.7 MODELS NOT RESPONSIVE TO THE COMBINATION TO STUDY NEW TREATMENT MODALITIES	152
4.7.1 Case-report: MNHOC 94/2-C, Not BRCAness.....	152
4.7.2 Case-report: MNHOC 506, Not BRCAness.....	155
Summary of results.....	157
4.8 A SYNGENEIC MODEL OF OVARIAN CANCER IN IMMUNOCOMPETENT MICE	157
Summary of results.....	162
4.9 MOLECULAR CHARACTERIZATION AFTER TREATMENT	162
4.10 DISCUSSION	166
CHAPTER 5	174
Results.....	174
BIOMARKERS OF RESPONSE (IMMUNOHISTOCHEMICAL ANALYSES)	174
5.1 EFFECTS OF THE COMBINATION ON THE TUMOR MICROENVIRONMENT AND HR DNA REPAIR MARKERS	175
5.1.1 Subcutaneous tumor models.....	177
5.1.1.1 MNHOC 18, Not BRCAness.....	177
5.1.1.2 MNHOC 182, Not BRCAness.....	180
5.1.1.3 MNHOC 508, BRCAness.....	183
5.1.2 Intraperitoneal models.....	186
5.1.2.1 MNHOC 8, BRCAness.....	186
5.2 SUMMARY OF RESULTS AND DISCUSSION	190
CHAPTER 6	195
Results.....	195

PRELIMINARY APPROACHES TO DETERMINE MECHANISMS UNDERLYING THE BENEFIT OF COMBINATION THERAPY..... 195

6.1 GENE EXPRESSION ANALYSIS AFTER TREATMENT: FLUIDIGM DATA... 196

6.2 CEDIRANIB TARGET BASELINE LEVELS OF EXPRESSION..... 205

6.3 SUMMARY OF RESULTS AND DISCUSSION..... 211

CHAPTER 7..... 216

Conclusions and Future Perspective..... 216

BIBLIOGRAPHY..... 228

APPENDICES..... 244

A.1 Work by the candidate preceding the work described in this thesis..... 244

A.2 Work by the candidate emanating from the work described in this thesis..... 245

A.3 Work by the candidate not pertaining to the work described in this thesis..... 246

A.4 Abstract from paper as a first name author..... 249

Table of Figures

Figure 1.1 The major histologic subtypes of epithelial ovarian cancer.....	11
Figure 1.2 New blood-vessel formation.....	16
Figure 1.3 Angiogenic balance and angiogenic switch.....	18
Figure 1.4 VEGF signaling inhibitors and their targets.....	20
Figure 1.5 Structure of cediranib.....	25
Figure 1.6 DNA damage repair pathways.....	30
Figure 1.7 Mechanism of action of PARP inhibitors.....	34
Figure 1.8 Structure and Binding Partners of BRCA1.....	36
Figure 1.9 Structure and Binding Partners of BRCA2.....	36
Figure 1.10 Structure of olaparib.....	40
Figure 2.1 Predisposed cartridge of Maxwell ® 16 Tissue DNA purification kit.....	63
Figure 2.2 Diagram of a Fluidigm 96.96 primed chip (IFC) layout.....	75
Figure 3.1 The application of the platform of OC-PDX.....	90
Figure 3.2 Representative histological section of subcutaneous OC-PDX and corresponding patient tumor.....	94
Figure 3.3 Gene expression analysis of OC-PDX from RT-PCR: BRCA1 level of expression.....	102
Figure 3.4 Gene expression analysis of OC-PDX from genome-wide gene expression.	104
Figure 3.5 Gene expression analysis of OC-PDX at baseline from Fluidigm.....	106
Figure 3.6 Gene expression analysis of OC-PDX from RNAseq.....	108
Figure 3.7 The cohort of OC-PDX selected for drug testing.....	110
Figure 4.1 Correlation between BRCAness status and response to olaparib monotherapy in a short-term versus maintenance regimen.....	119
Figure 4.2 The combination of olaparib and cediranib in a short-term and in maintenance (until tumor progression) regimen.....	122
Figure 4.3 The combination in maintenance regimen: the case of MNHOC 18, Not BRCAness.....	125
Figure 4.4 The combination in maintenance regimen: the case of MNHOC 182, Not BRCAness.....	127
Figure 4.5 The combination in maintenance regimen: the case of MNHOC 508, BRCAness.....	130
Figure 4.6 The combination in maintenance regimen: the cases of MNHOC 511 and MNHOC 513, BRCAness.....	133
Figure 4.7 The combination in maintenance regimen: the case of MNHOC 154, BRCAness.....	135
Figure 4.8 The combination in the orthotopic model MNHOC 8, BRCAness.....	140

Figure 4.9 The importance of drug sequence in the combination olaparib plus cediranib..... 143

Figure 4.10 Olaparib in combination with different angiogenesis inhibitors: the case of the ectopic MNHOC 18, Not BRCAness..... 146

Figure 4.11 Olaparib in combination with a different angiogenesis inhibitor, bevacizumab: the case of the orthotopic MNHOC 8, BRCAness..... 148

Figure 4.12 The advantage of the combination in olaparib-resistant BRCAness model: the case of the orthotopic MNHOC 22, BRCAness.....151

Figure 4.13 The resistance to the combination: the case of the subcutaneous MNHOC 94/2-C, Not BRCAness..... 154

Figure 4.14 The resistance to the combination: the case of the orthotopic MNHOC 506, Not BRCAness..... 156

Figure 4.15 The combination in a syngeneic orthotopic model: the intraovarian ID8. 159

Figure 4.16 The combination in a syngeneic orthotopic model: the intraovarian ID8. 161

Figure 4.17 OC-PDX classification after treatment..... 165

Figure 5.1 Tumor hypoxia: CA-9 vs Pimonidazole representative staining on MNHOC 513.....176

Figure 5.2 Analysis on subcutaneous MNHOC 18..... 179

Figure 5.3 Analysis on subcutaneous MNHOC 182..... 182

Figure 5.4 Analysis on subcutaneous MNHOC 508..... 185

Figure 5.5 Analysis on intraperitoneal MNHOC 8..... 187

Figure 5.6 Analysis on intraperitoneal MNHOC 8..... 189

Figure 6.1 OC-PDX models selected to perform gene expression data analysis..... 198

Figure 6.2 Gene expression analysis after 4-week treatment with the combination. 200

Figure 6.3 Heatmap of relative gene expression ($-\Delta\Delta C_t$ values) induced by 4-week treatment..... 202

Figure 6.4 Heatmap of relative gene expression ($-\Delta\Delta C_t$ values) induced by 4-week treatment..... 204

Figure 6.5 Cediranib-target expression level of OC-PDX..... 206

Figure 6.6 Cediranib-target expression level in 13 OC-PDX from RT-PCR.....208

Figure 6.7 Cediranib-target level in MNHOC 18, MNHOC 124 and MNHOC 182.. 210

Table 1.1 Panel of 31 genes associated with homologous recombination.....39

Table 2.1 Genes and primer pairs used in Sanger validation..... 69

Table 2.2 Panel of genes for Fluidigm prepared in a 96-well plate assay..... 76

Table 3.1 The platform of OC-PDX: histopathology and route of engraftment.....88

**Table 3.2 Patients’ tumors characteristics of the 26 OC-PDX used in this PhD thesis.
..... 92**

**Table 3.3 Mutational spectrum of most commonly mutated genes in ovarian cancer,
verified by Sanger sequencing.....97**

**Table 3.4 Mutational spectrum of different HR genes, verified by Sanger sequencing.
..... 99**

CHAPTER 1.

Introduction

1.1 EPITHELIAL OVARIAN CANCER

1.1.1 Epidemiology and risk factors

Ovarian cancer is the seventh most common gynaecological malignancy and one of the most significant causes of mortality among women, with an estimated incidence of 239.000 cases per year worldwide and accounting for 152.000 deaths per year (Banerjee et al., 2010; Banerjee and Kaye, 2013).

The high mortality is due to difficulties in diagnosing early stage disease; indeed the majority of cases (75%-80%) continue to be diagnosed at advanced stage (Banerjee and Kaye, 2013).

Cytoreductive surgery plays a key role in the initial treatment of ovarian cancer patients, to remove the tumor mass in order to achieve either a complete ablation or to leave residual tumors <1 cm (optimal cytoreductive surgery) (Saitou et al., 2015).

After debulking, the majority of patients are referred to standard of care therapy with platinum/taxane-based first line chemotherapy, resulting in an 80% response rate. However, the 5-year survival rate remains at 31%, with the majority of the patients relapsing and becoming resistant to first line treatment (Jemal et al., 2009; Korkmaz et al., 2016). Stage at diagnosis deeply influences the progression-free survival (PFS) and overall survival (OS) of the patients. To date, an effective screening tool for ovarian cancer has not been identified, mainly because symptoms preceding the diagnosis are neither specific nor sensitive. Indeed, pelvic and abdominal pain, increasing girth or bloating of the abdomen, difficulty with eating are all symptoms that could be confused with gastrointestinal diseases. Moreover, in many cases symptoms may not even be present until the tumor has reached an advanced stage (Cragun, 2011; Karst and Drapkin, 2010).

An important issue to be addressed for ovarian cancer are risk factors. The most important is a strong family history of ovarian or breast cancer, although an identifiable genetic predisposition, such as Breast Cancer Type 1 and 2 Susceptibility Proteins (*BRCA1* and

BRCA2) tumor suppressor gene mutations, is present only in 10-15% of patients (Bast et al., 2009). Early menarche, late menopause, nulliparity and increasing age are also connected with increased risk, whereas oral contraceptive usage, pregnancy, breastfeeding and tubal ligation are associated with reduced risk (Edmondson and Monaghan, 2001). Incessant ovulation could explain these epidemiological data; the repetitive wounding of the ovarian surface epithelium and cell proliferation in postovulatory repair could result in a stepwise accumulation of genomic alterations. The accumulation of ovarian epithelial inclusion cysts might increase the risk of carcinogenesis by entrapping cells in a hormone- and growth factor-rich environment (Fathalla, 1971). Gonadotropin could also be involved in the development of ovarian cancer; its high concentration during ovulation and its persistence after menopause stimulate the epithelial cells of the ovary, inducing genomic instability and increasing carcinogenesis risk (Cramer et al., 1983).

Inflammation and changes in the redox potential could also play a role in the setting of ovulation and surface-epithelium repair, accounting for the increased risk of epithelial ovarian cancer associated with talc or asbestos exposure, endometriosis, pelvic inflammatory disease and mumps (Cramer et al., 1983).

In this scenario, an effective screening test might help to decrease mortality from ovarian cancer.

CA-125 is a glycoprotein produced by the uterus, cervix and Fallopian tubes and released in serum in case of tissue damage and inflammation. In general, levels of CA-125 higher than 35 U/ml are considered elevated, even though not unequivocally correlated with cancer.

Indeed, elevated levels of CA-125 are present also in physiological conditions such as pregnancy, menstrual cycle, hepatic disease and endometriosis.

Transvaginal ultrasonography has been evaluated as an early screening method, but resulted not to be a completely reliable screening test (Partridge et al., 2009). Women

carrying mutations in *BRCA1* and *BRCA2* genes are recommended to undergo periodical measurements of levels of CA-125 in association with ultrasonography. Moreover, a salpingo-oophorectomy is advised after 40 years or after pregnancy in these women (Bast et al., 2009).

1.1.2 Pathology

The term “ovarian cancer” refers not to a single disease, but to a heterogeneous subset of malignancies involving the ovary, with different morphology and biological behaviour.

Generally, ovarian cancer may arise from one of three cell types: epithelial cells, sex cord-stromal cells (i.e. granulosa, theca and hilus cells), or germ cells (i.e. oocytes).

Although approximately 40% of all ovarian tumors are non-epithelial in origin, such lesions may progress to malignancies, accounting for 10% of ovarian cancer (Chen et al., 2003). Approximately 90% of ovarian cancers are carcinomas (malignant epithelial tumors) and considered as a heterogeneous group of neoplastic diseases, exhibiting a wide range of tumor morphologies, clinical manifestations and genetic alterations (Prat and FIGO Committee on Gynecologic Oncology, 2015).

According to the International Federation of Gynecology and Obstetrics (FIGO) criteria, epithelial ovarian tumors can be classified upon the grade of invasion and diffusion at diagnosis in four stages, from I to IV (Prat and FIGO Committee on Gynecologic Oncology, 2015), as reported in the following table.

Stage I: confinement to the ovary.	
IA	Tumor limited to one ovary with an intact capsule or to Fallopian tubes.
IB	Tumor limited to both the ovaries with intact capsules or to both the Fallopian tubes.
IC	Tumor limited to one or both the ovaries or Fallopian tubes, but with capsule rupture or the presence of malignant cells on the epithelial surface. Malignant cells are also present in the ascites or peritoneal washings.
Stage II: involvement one or both the ovaries or Fallopian tubes, with pelvic extension or primary peritoneal cancer.	
IIA	Tumor is extended and/or implanted on the uterus and/or Fallopian tubes and/or ovaries.
IIB	Tumor has extended to other pelvic intraperitoneal tissues.
Stage III: involvement of one or both ovaries or Fallopian tubes, or primary peritoneal cancer with spreading to the peritoneum outside the pelvis, and/or metastasis to the retroperitoneal lymph nodes.	
IIIA	Cytologically or histologically proven positive retroperitoneal lymph nodes only or microscopic extrapelvic peritoneal involvement.
IIIB	Macroscopic peritoneal metastasis beyond the pelvis up to 2 cm diameter with or without metastasis to retroperitoneal lymph nodes.
IIIC	Macroscopic peritoneal metastasis beyond the pelvis more than 2 cm diameter with or without metastasis to retroperitoneal lymph nodes.
Stage IV indicates tumors with distant metastasis, with malignant cells present in the pleural effusion and involving abdominal organs with parenchymal and extra-abdominal metastasis.	

Five main subtypes of epithelial ovarian cancer can be recognized based on their histopathology: high grade serous (HGS, 70%) and low grade serous (LGS, <5%)

carcinomas, high grade endometrioid carcinomas (HGE, 10%), clear cell carcinomas (CCC, 10%), mucinous carcinomas (MUC, 3%) (Figure 1.1) (Prat, 2012; Robert J. Kurman et al., 2014). They differ completely in epidemiologic and genetic risk factors, precursor lesions, patterns of spread and molecular events during cancer development, other than response to first line chemotherapy and prognosis (Gilks and Prat, 2009).

1.1.3 Dualistic model

Over the last several years a so-called “dualistic model” has been proposed to explain the pathogenesis of epithelial ovarian cancer, based on origin, morphological and molecular features (Bowtell, 2010; Kurman and Shih, 2010; Wu et al., 2013).

Serous carcinomas arise from the Fallopian tube epithelium, while endometriosis is considered the precursor of endometrioid and clear cell tumors (Kurman and Shih, 2010). Moreover, low grade serous carcinomas differ from high grade serous on both the morphological and molecular aspects. Even though they both seem to arise from Fallopian tubes, the former develops from papillary hyperplasia that invades the ovary forming benign cysts that evolve later to neoplasia, which are not related to *BRCA* abnormalities. The latter arises from the tube and invades the ovary by direct contact. The finding of high grade serous tubal intraepithelial carcinoma (STIC) in patients with *BRCA* mutations drives the idea that STIC cannot be considered a real *in situ* carcinoma, but rather metastasizing tubal-origin cells, sharing typical tube Mullerian markers with high grade serous carcinomas, rather than ovarian epithelial markers (Piek et al., 2001). Accordingly to these findings, epithelial ovarian tumors can be divided into Type I and Type II.

1.1.4 Classification

1.1.4.1 Type I

The type I group includes low grade serous, clear cell and mucinous carcinomas, which develop in a stepwise fashion from well-established precursor lesions, such as borderline tumors and endometriosis. These types of tumor are generally indolent and confined to the

ovary (stage I), genetically stable and displaying a variety of somatic sequence mutations but very rarely tumor protein p53 (*TP53*) (Jones et al., 2010; Shih and Kurman, 2004).

Low grade serous (LGS) carcinomas

LGS are uncommon (less than 5% of all cases of ovarian carcinoma), originate from papillary hyperplasia of the Fallopian tube, that subsequently colonizes the ovary forming benign cysts. They are generally associated with a good prognosis. LGS lack chromosomal instability and the most frequent mutations are on Kirsten rat sarcoma viral oncogene homolog (*KRAS*) and v-raf murine sarcoma viral oncogene homolog B (*BRAF*) genes.

Low grade endometrioid (LGE) carcinomas

LGE account for approximately 10% of ovarian carcinomas and resemble tumors encountered frequently in the endometrium. They are diagnosed at early stage and for this reason prognosis is generally favourable. The most frequent mutation occurs in the Catenin (cadherin-associated protein) beta 1 (*CTNNB1*) gene (50% of the cases) and to a lesser extent phosphatase and tensin homolog (*PTEN*) is mutated (20% of the cases) or lost (40%).

Clear cell carcinomas (CCC)

CCC account for approximately 10% of ovarian carcinomas and patients are generally diagnosed at early stages of disease. These types of tumors are frequently related to endometriosis and have a good prognosis (Komiyama et al., 1999). From the histological point of view, a papillary architecture defines this group of tumors. CCC lack *BRCA* abnormalities and chromosomal instability (Press et al., 2008), but inactivating mutations on the AT rich interactive domain 1A (SWI-like) (*ARID1A*) gene and activating mutations of phosphatidylinositol-4,5-bisphosphate 3-kinase, catalytic subunit alpha (*PIK3CA*) gene are present in ~ 50% of cases.

Mucinous carcinomas (MUC)

MUC account for 3% of ovarian carcinomas. They are generally associated with a good prognosis because they are usually confined to the ovary, without the involvement of the ovarian surface. Tumor cells of MUC resemble those of the endocervix, gastric pylorus and intestine. *KRAS* mutations are the most common alterations in this type of tumor.

1.1.4.2 Type II

Type II includes high grade serous and high grade endometrioid carcinomas, malignant mixed mesodermal tumors (carcinosarcomas), and undifferentiated carcinomas, which present at an advanced stage (stages II-IV) in more than 75% of cases. These types of tumors are generally aggressive and rapidly evolving, highly chromosomally unstable, presenting mutations in *TP53* (more than 95% of the cases) and rarely displaying mutations found in the type I tumors (Kurman and Shih, 2011). *BRCA* inactivation, either by mutation or loss of expression, and its downstream genes via promoter methylation, occurs in up to 40% to 50% of high grade serous carcinoma.

High grade serous (HGS) carcinomas

HGS is the most common type of ovarian carcinoma, arising from the Fallopian tube and reaching the ovary by direct contact (Piek et al., 2003). This type accounts for approximately 70% of all cases of ovarian carcinomas and they are usually related to a poor prognosis, mainly due to their rapid growth and aggressiveness. Primary cytoreductive surgery is the initial approach in most patients; thereafter tumors are generally sensitive to platinum/taxane-based first line chemotherapy, but the majority of the patients eventually experience chemotherapy resistant recurrence.

Up to 50% of HGS show abnormalities in *BRCA1* and *BRCA2* genes (such as germline and somatic mutation, deletion, promoter methylation and therefore low expression) and more than 95% in *TP53* (mutation or deletion) (Esteller et al., 2000; Kindelberger et al., 2007; Leitao et al., 2004; Medeiros et al., 2006; Singer et al., 2005). Moreover, HGS are characterized by homologous recombination dysfunction and widespread copy number

changes. All these changes result in a loss of ability to repair DNA double strand breaks and in an increase in chromosomal instability, that increases intratumoral heterogeneity.

Recently has been reported that germline mutations in *BRCA1* and *BRCA2* are mutually exclusive with aberrations in cyclin E1 (CCNE1), one of the few recognized molecular therapeutic target in HGS.

High CCNE1 expression occurs up to 50% of HGS cases, but only half the cases are linked to 19q12 locus amplification accordingly to the Cancer Genome Atlas (Cancer Genome Atlas Research Network, 2011).

The CCNE1-high/amplified subset of tumors has intact *BRCA1/2*, unfavorable outcome, since they are poorly responsive to platinum therapy and have limited responsiveness to PARP inhibitors.

High grade endometrioid (HGE) carcinomas

HGE can barely be distinguished from HGS. Unlike LGE, *CTNNB1* and *PIK3CA/PTEN* pathways are not defective, but mutations in *TP53* are frequently present (Wu et al., 2007).

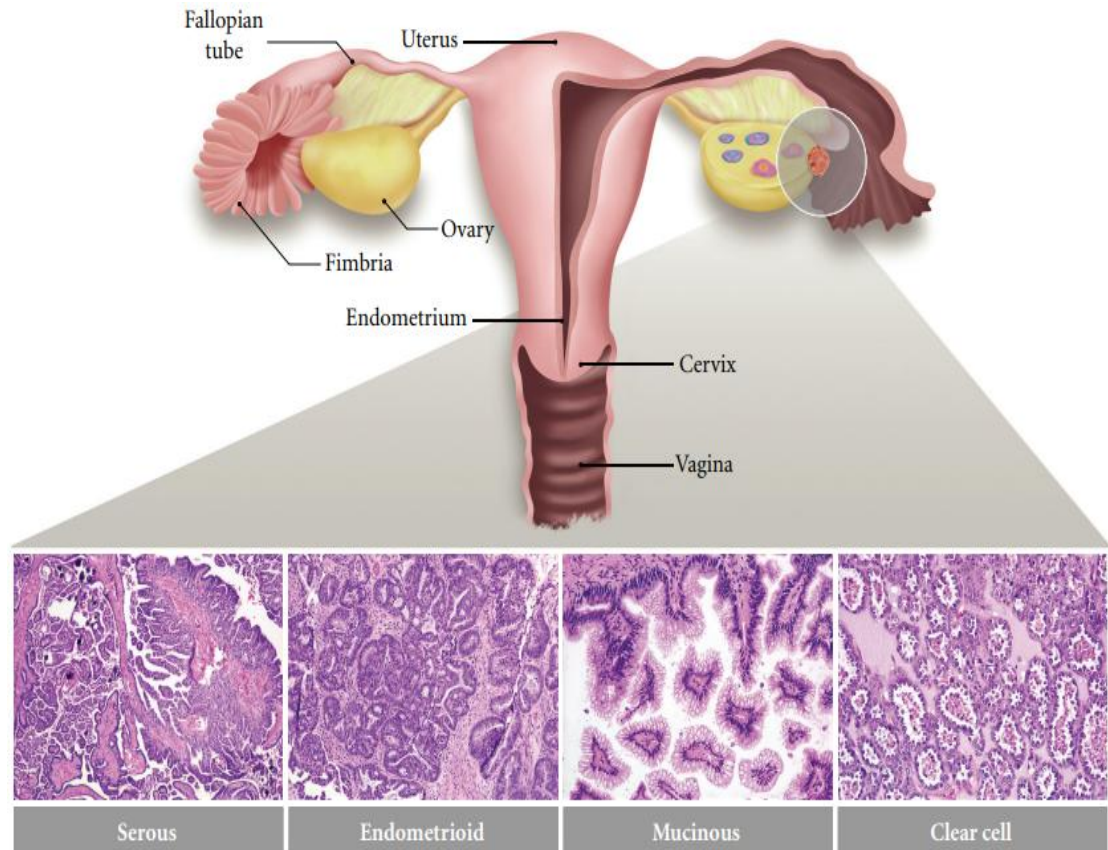


Figure 1.1 The major histologic subtypes of epithelial ovarian cancer.

Serosus carcinomas mirror fallopian tube epithelium, endometrioid carcinomas resemble endometrial glands, and mucinous carcinomas look like endocervical epithelium.

Picture shows representative tumor section stained with haematoxylin and eosin. The shaded circle represents the general anatomical location from which ovarian carcinomas are thought to arise.

Modified from Karst A.M. and Drapkin R, Ovarian Cancer Pathogenesis: A Model in Evolution, Journal of Oncology, 2010.

1.2 TREATMENT OF OVARIAN CANCER

1.2.1 Cytoreductive surgery

Peritoneal washing and/or paracentesis, hysterectomy, bilateral salpingo-oophorectomy, pelvic and para-aortic lymph node sampling, diaphragmatic biopsies, omentectomy, biopsy of suspicious lesions and random biopsies through the peritoneum are used to collect material for histological analysis to formulate a diagnosis and decide the optimum post-operative treatment (Ozols, 2003).

Since the majority of ovarian cancers are diagnosed at advanced stage and grade of disease, chemotherapy alone rarely results in a complete cure. For this reason, optimising surgery continues to be essential for patients.

Complete surgical debulking is the standard of care for early stage ovarian cancer, whereas primary cytoreductive surgery followed by platinum/taxane-based chemotherapy is to date the current management for advanced ovarian cancer. Optimal cytoreduction is one of the most significant predictors of survival: indeed residual disease < 1 cm is considered optimal debulking and prognosis correlates with the extent of residual disease (Griffiths, 1975).

Moreover, the timing of cytoreduction is becoming a critical point; cytoreduction at the time of diagnosis is a standard practice, although only 50% of patients can be effectively reduced at the initial laparotomy.

Patients in whom the initial cytoreduction is not successful are committed to three cycles of chemotherapy, and if responsive, undergo another attempt at cytoreduction (interval cytoreduction) followed by additional chemotherapy (Martinek and Kehoe, 2010). Interval debulking has generally a significant effect both on time to progression and median survival for patients (6 months).

Ovarian cancer is frequently considered a chronic disease, and while cure remains the ultimate goal of therapy, prolongation of survival, together with palliation of symptoms, is a clinically meaningful accomplishment.

1.2.2 Chemotherapy

The 2010 consensus meeting defined standard of care treatment in ovarian cancer. The recommended treatment paradigm for advanced disease has been debulking surgery followed by platinum-based chemotherapy, initially cisplatin-based and more recently with carboplatin/paclitaxel (Stuart et al., 2011).

Platinum-derivatives

Platinum-derivatives were introduced as chemotherapeutic agents in the 1960s. Cisplatin was the first platinum-based drug developed, before oxaliplatin and then carboplatin, a drug with fewer and less severe side effects introduced in the 1980s and to date the drug of choice for the treatment of ovarian cancer.

Cisplatin is a cytotoxic drug, classified as an alkylating agent, whose mechanism of action is the formation of platinum complexes interacting with DNA. The formation of DNA adducts, primarily intra-strand crosslink adducts, activates several signal transduction pathways and culminates in the activation of apoptosis.

Several randomized studies have demonstrated the efficacy of platinum-based therapy in ovarian cancer, particularly when given in combination. Gynaecologic Oncology Group Trial No.47 (Omura et al., 1986) has compared the efficacy of doxorubicin-cyclophosphamide (AC) with doxorubicin-cyclophosphamide-cisplatin (PAC); the progression-free survival and median survival time were significantly increased in the PAC group.

Taxane-derivatives

Paclitaxel was isolated in 1967 from the bark of the Pacific yew tree, *Taxus brevifolia*. Together with docetaxel, it comprised the category of taxanes. Paclitaxel is a mitotic

inhibitor that stabilizes microtubules (tubulin dimers) and as a result, interferes with the normal breakdown of microtubules during cell division because chromosomes are thus unable to achieve a metaphase spindle configuration. This blocks progression of mitosis and prolonged activation of the mitotic checkpoint triggers apoptosis or reversion to the G-phase of the cell cycle without cell division.

The consensus meeting in 2010 acknowledged that acceptable variations to the recommended therapies existed, but their use must be supported by at least one trial demonstrating superiority or non-inferiority. Initially, improvements to standard platinum/taxane chemotherapy were seen through the addition of a third chemotherapeutic agent with demonstrable activity in the relapsed setting. First line trials investigated the addition of drugs, including pegylated liposomal doxorubicin (PLD), topotecan and gemcitabine (Bolis et al., 2010; Bookman et al., 2009; du Bois et al., 2010; Hoskins et al., 2010), but unfortunately demonstrated only increased toxicity without survival benefits.

Other cytotoxic agents

After first line treatment with platinum/taxane-based chemotherapy, patients are monitored periodically to evaluate the response; tumors are defined as platinum resistant if the relapse occurs within 6 months from the last dose of treatment. In this case, a second line chemotherapy is proposed.

Pegylated liposomal doxorubicin is a newly available formulation of doxorubicin, an anthracycline antibiotic intercalating DNA that is encapsulated in a pegylated liposome. The size of the liposomes prevents them from entering tissues with tight capillary junctions, such as the heart and gastrointestinal tract, and in contrast to other nanoparticles, the pegylation allows these molecules to be protected from destruction by the reticuloendothelial system (Green and Rose, 2006).

Topotecan is a derivative of camptothecin that inhibits topoisomerase I, thus blocking cell cycle S-phase (Armstrong, 2004).

Gemcitabine is a nucleoside analogue of deoxycytidine that replaces cytidine during DNA replication, thus blocking DNA synthesis and inducing apoptosis (Poveda, 2005).

Recently, trabectedin demonstrated efficacy as a second-line treatment in platinum-sensitive ovarian cancer. The mechanism of action is binding of the DNA minor groove and interference with cell division, gene transcription mechanisms and DNA repair (Colombo, 2011).

A more successful strategy seems likely to be the addition of targeted therapies to chemotherapy.

1.2.3 Targeted therapies

During recent years the search for new cancer therapies has been addressed to the development of specifically targeted drugs that block cancer growth and dissemination by interfering with multiple molecular targets, such as growth factor receptors, signal transduction pathways, cell cycle regulators, and angiogenic mechanisms specifically expressed by tumor cells or the tumor environment. For this reason, these therapies are theoretically very effective against cancer cells and less harmful to normal cells.

Two of the major molecular targeted agents applied to ovarian cancer are inhibitors of angiogenesis (chapter 1.3.1 Inhibitors of angiogenesis as cancer therapy) and inhibitors of the poly(ADP-ribose) polymerases (chapter 1.4.1 Poly(ADP-ribose)polymerase (PARP) inhibitors as cancer therapy) (Grunewald and Ledermann, 2017; Lim and Ledger, 2016).

1.3 ANGIOGENESIS AND TUMOR ANGIOGENESIS

The term angiogenesis refers to all those processes that lead to blood vessel formation and sprouting, starting from the existing vasculature. In physiological conditions, angiogenesis plays a key role in embryonal development, formation of the uterus lining prior to menstruation and of the placenta after fertilization, pregnancy, normal tissue growth and wound healing (Figure 1.2) (Carmeliet and Jain, 2000).

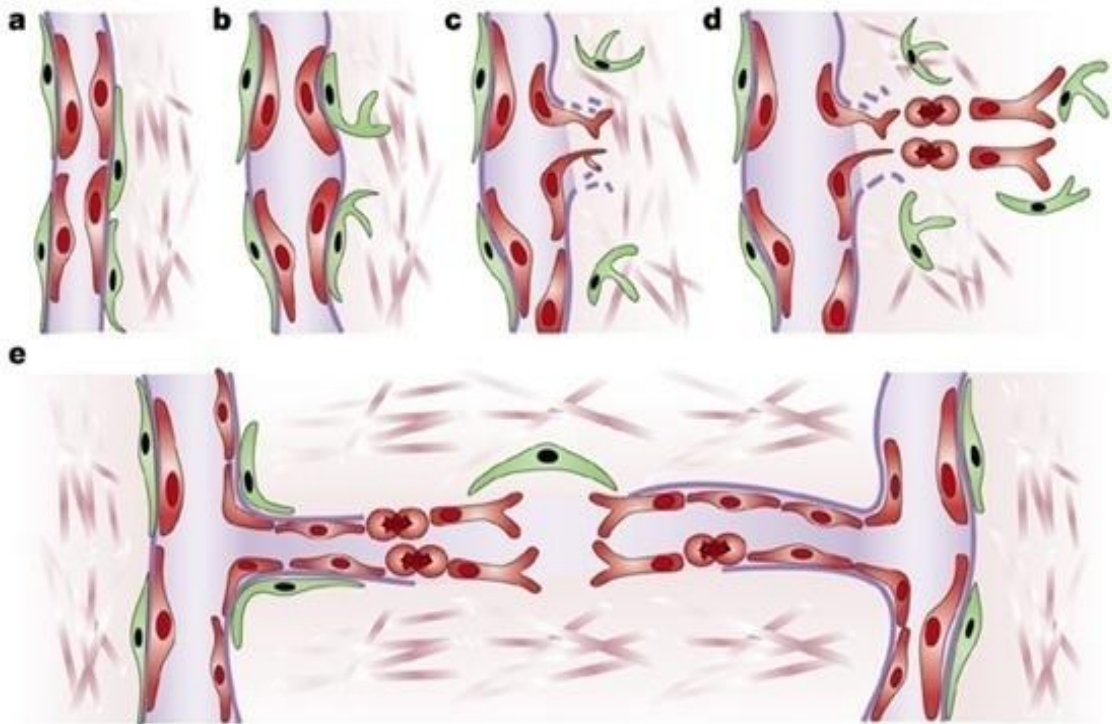


Figure 1.2 New blood-vessel formation.

Angiogenic signals lead to the preferential differentiation of certain endothelial cells into so-called “tip cells”, which start to migrate and exist at the leading front of the growing vessels.

Number of factors including VEGF receptor (VEGFR)-3 (for lymphatic-endothelial cells), VEGFR-1 and -2 (for blood endothelial cells), PDGF-B and the Notch ligand delta-like ligand (Dll)-4 have been shown to contribute to the endothelial tip cell phenotype.

a) Vessel in normal physiological conditions.

b) Detachment of pericytes and dilatation of blood vessels before the basement membrane and extracellular matrix are degraded.

c) Migration of endothelial cells, following angiogenic stimuli.

d) Proliferation of endothelial cells.

e) Adhesion of endothelial cells to each other, consequently creation of a lumen and formation of a basement membrane, surrounded by pericytes.

Modified from Bergers and Benjamin, Tumorigenesis and angiogenic switch, Nature Review, 2003.

Nevertheless, angiogenesis is fundamental in many pathological conditions such as chronic inflammation and cancer (Folkman, 1971). Angiogenesis is a critical component for the growth and metastasis of cancer (Ellis and Hicklin, 2008) and it is one of the hallmarks of cancers that have been extensively studied (Hanahan and Weinberg, 2011). Accordingly to Folkman et al (Hanahan and Folkman, 1996), endothelial cells switch from a resting state to a rapid growth phase, induced by factors released by the tumor. The switch depends on the increased production of positive regulators of angiogenesis such as vascular endothelial growth factor (VEGF), fibroblast growth factor (FGF), placental growth factor (PlGF), transforming growth factor beta (TGF-beta), angiopoietins (Angs), interleukin-8 (IL-8) and others (Bergers and Hanahan, 2008) induced by tumor cells, or released from the microenvironment upon tumor stimulation. In parallel, the switch involves downregulation of negative regulators of angiogenesis, such as endostatin, angiostatin and thrombospondin (Hanahan and Folkman, 1996; Ribatti, 2009). During pathological angiogenesis the tight balance and control of factors which regulated the process are lost and tumor vessels fail to remain quiescent (Figure 1.3) (Bergers and Benjamin, 2003).

In this scenario, tumor blood vessels display abnormalities both at the structural and functional level. Typical tumor vessels are leaky, tortuous and sinusoidal, poorly covered in pericytes and smooth muscle cells, leading to a poor functionality and perfusion (Hosaka et al., 2013; Nagy et al., 2012; Xue et al., 2011) and facilitating invasion and metastatic dissemination of tumor cells (Kassis et al., 2007). Moreover tumor vessel density is highly heterogeneous within the tumor, resulting in chaotic blood flow, hypoxia, hyperpermeability that may also influence the delivery and effectiveness of anticancer therapy (Figure 1.3) (Dowlati et al., 2008; Ghosh et al., 2008; Giavazzi et al., 2003; Yu et al., 2002) and thus may influence the patients' outcome (Hollingsworth et al., 1995).

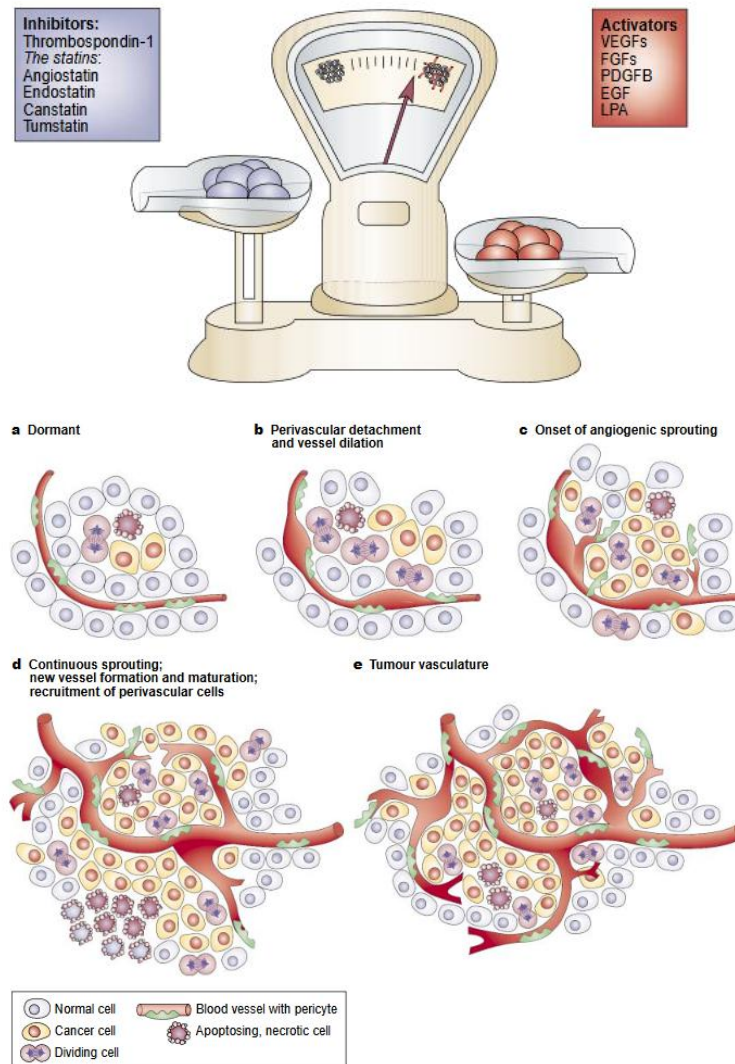


Figure 1.3 Angiogenic balance and angiogenic switch.

Physiologically, angiogenesis is a process tightly regulated by a multitude of pro- and anti-angiogenic factors. However, this delicate equilibrium is lost in tumor tissues and pro-angiogenic factors prevail over angiogenesis inhibitors, thus promoting the angiogenic switch.

a) “Dormant” tumor nodule.

b) Starting of the “switch”: perivascular detachment and vessels dilatation. Angiogenic switch occurs to ensure exponential tumor growth.

c) and d) Onset of the sprouting of the new tumor vessels, that continuously grow and mature, recruiting perivascular cells.

e) Permanent tumor vessels formation to feed hypoxic and necrotic areas of the tumor.

Modified from Bergers and Benjamin, Tumorigenesis and angiogenic switch, Nature Review, 2003.

1.3.1 Inhibitors of angiogenesis as cancer therapy

An effective antiangiogenic strategy is to block the VEGF / VEGFR (vascular endothelial growth factor receptor) pathway (Leung et al., 1989). VEGFA, known also as vascular permeability factor, was first described in the malignant ascites of human ovarian cancer (Dvorak et al., 1995) and it is mainly induced by hypoxia (Forsythe et al., 1996). To date, VEGFA is the most studied non-oncogene-specific target that can be blocked directly with humanized monoclonal antibodies such as bevacizumab. The VEGF receptor family, that includes VEGFR1, VEGFR2 and VEGFR3, is the target of numerous kinase inhibitors, such as sunitinib, sorafenib, pazopanib and cediranib (Figure 1.4).

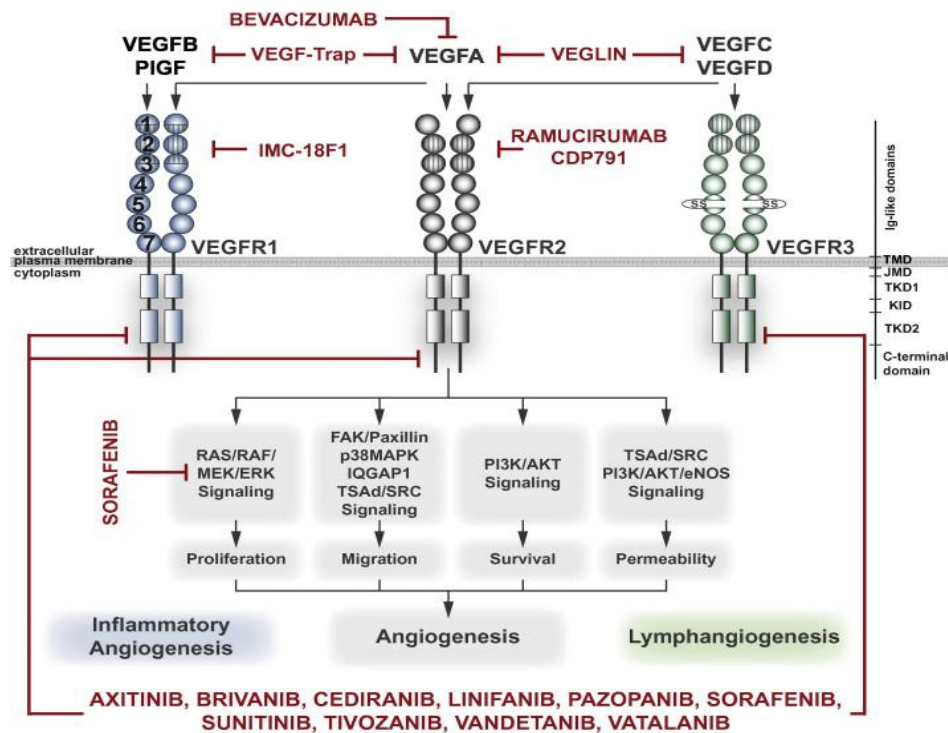


Figure 1.4 VEGF signaling inhibitors and their targets.

The VEGF family of ligands (VEGFA, PlGF, VEGFB, VEGFC, and VEGFD) bind to their receptors (VEGFR1; blue, VEGFR2; grey, VEGFR3; green).

VEGF antagonists display their activity:

- interfering with binding of VEGF ligands on the extracellular domain (e.g. Bevacizumab, VEGF-Trap, Veglin, IMC-18F1, Ramucirumab/CDP791);
- competing for ATP-binding to the intracellular kinase domain (e.g. axitinib, brivanib, cediranib, linifanib, pazopanib, sorafenib, sunitinib, tivozanib, vandetanib, vatalanib).

Modified from Tugues et al, Vascular endothelial growth factors and receptors: Anti-angiogenic therapy in the treatment of cancer, Molecular Aspects of Medicine, 2011.

Bevacizumab (Avastin ®) is a humanized antibody that targets directly VEGF and blocks its binding with VEGFR (Kim et al., 1992). The antitumor activity of bevacizumab has been demonstrated in preclinical studies (Gerber and Ferrara, 2005; Hu et al., 2002; Mabuchi et al., 2008) and in several clinical trials (Burger et al., 2007; Chura et al., 2007; Nimeiri et al., 2008; O'Malley et al., 2011) on ovarian cancer. Recently, two randomized controlled clinical trials have been carried out with bevacizumab added to first line chemotherapy (GOG-0218 and ICON7) (Burger et al., 2011; Perren et al., 2011) and results led to the approval of bevacizumab in combination with platinum/taxane-based frontline therapy by EMEA (European Medicines Evaluation Agency).

The AURELIA and OCEANS trials have evaluated the activity of bevacizumab combined with chemotherapy also in platinum-resistant (Pujade-Lauraine et al., 2014) and platinum-sensitive (Aghajanian et al., 2012) recurrent ovarian cancer.

Interestingly the AURELIA trial suggested a positive trend in overall survival in patients treated with bevacizumab combined with dose-dense weekly paclitaxel. Although this regimen of paclitaxel is considered a reasonable option to enhance antitumor activity and prolong survival (Katsumata et al., 2009; Pignata et al., 2014) and paclitaxel displays potent antiangiogenic properties (Miller et al., 2001), the relevance of doses and schedules of paclitaxel in a combination with bevacizumab was not completely clear. Recently, the GOG-0262 clinical trial reported that in combination with bevacizumab (and carboplatin), 3-weekly or weekly paclitaxel (PTX) regimens were equally effective (reported as PFS), with the former giving fewer adverse events (Chan et al., 2016). This study also indicated similar PFS with weekly paclitaxel without bevacizumab (14.2 months) and with weekly or every-3-weeks PTX with bevacizumab (respectively 14.9 and 14.7 months), thus questioning the advantage of adding bevacizumab to the treatment regimens. A further issue in these trials is that, although the delay in tumor progression (PFS) was a major

achievement for women with ovarian cancer receiving bevacizumab-containing chemotherapy, this usually led to a scanty OS increase (Burger et al., 2011; Perren et al., 2011).

The escape of the tumor from antiangiogenic treatments is well documented in preclinical studies, including in our models of patient-derived ovarian cancer (OC-PDX) treated with bevacizumab, which under certain circumstances increased survival but also increased tumor dissemination (Decio et al., 2015; Oliva et al., 2012; Mitamura et al., 2016).

A number of other antiangiogenic agents have been tested in clinical trials in ovarian cancer (as reported in the table below, **Angiogenesis inhibitors tested in ovarian cancer clinical trials**).

Nintedanib, an oral tyrosine kinase inhibitor (TKI) targeting VEGF receptor 1-3, FGFR 1-3 and PDGFR α and β , has been studied as a first line therapy in chemotherapy-naïve patients in combination with carboplatin and paclitaxel in the randomised, double-blind, placebo-controlled phase 3 trial AGO-OVAR 12. A statistically significant improvement in PFS was noted although the actual magnitude of benefit in median PFS was modest (du Bois et al., 2016).

Pazopanib, a multi-targeted receptor tyrosine kinase inhibitor (VEGFR 1-3, PDGFR α and β and c-kit) has also been studied in the first line setting in ovarian cancer. In a randomized, double-blind, placebo-controlled, phase III trial of maintenance pazopanib (for up to 24 months) following no evidence of progression after surgery and platinum-taxane chemotherapy, progression-free survival was significantly improved (12.3 vs 17.9 months; HR 0.766 p=0.021) (du Bois et al., 2014).

Trebananib, a peptide fusion protein (or peptibody), displays its activity by preventing the binding of angiopoietin-1 (Ang1) and angiopoietin-2 (Ang2) to their receptor Tie2. Trebananib has shown antiangiogenic activity on preclinical models of ovarian cancer (Coxon et al., 2010) and as a single-agent in relapsed epithelial ovarian cancer in phase I

trial (Herbst et al., 2009), prolonging progression-free survival in phase II study (Karlan et al., 2012). Results of a phase III trial investigated the addition of trebananib to paclitaxel, showing an increase in progression-free survival (7·2 months vs 5·4 months), associated with higher incidence of oedema (Monk et al., 2016).

Angiogenesis inhibitors tested in ovarian cancer clinical trials.

Drug	Clinical trial	Eligibility	Arms	Clinical outcome	
Bevacizumab	GOG218	1 st line	PTX+carbo± beva concurrent/ maintenance	PFS (months) -PTX+carbo 11.0 -PTX+carbo+beva concurrent 12.3 -PTX+carbo+beva maintenance 15.3	OS (months) -PTX+carbo 40.6 -PTX+carbo+beva concurrent 38.7 -PTX+carbo+beva maintenance 43.8
	ICON7	1 st line	PTX+carbo± beva concurrent+ maintenance	PFS (months) -PTX+carbo 17.5 -PTX+carbo+beva 19.9	OS (months) -PTX+carbo 58.6 -PTX+carbo+beva 58.0
	OCEANS	Platinum-sensitive, recurrent	Gemcitabine+ carbo±beva concurrent+ maintenance (until disease progression)	PFS (months) -Gemcitabine+ carbo 8.4 -Gemcitabine+ carbo+beva 12.4	OS (months) -Gemcitabine+ carbo 32.9 -Gemcitabine+ carbo+beva 33.6
	AURELIA	Platinum-resistant, recurrent	PTX weekly or topotecan w. or PLD w.±beva concurrent+ maintenance (until disease progression)	PFS (months) -PTX weekly or topotecan w. or PLD w. 3.4 -PTX weekly or topotecan w. or PLD w.+beva 6.7	OS (months) -PTX weekly or topotecan w. or PLD w. 13.3 -PTX weekly or topotecan w. or PLD w.+beva 16.6
	GOG213	Platinum-sensitive, recurrent	PTX+carbo± beva	PFS (months) -PTX+carbo 10.4 -PTX+carbo+beva 13.8	OS (months) -PTX+carbo 37.3 -PTX+carbo+beva 42.4
Nintedanib	AGO-OVAR12	1 st line /Advanced stage	PTX+carbo± nintedanib	PFS (months) -PTX+carbo 16.6 -PTX+carbo+ nintedanib 17.2	OS (months) -PTX+carbo 62.8 -PTX+carbo+ nintedanib 62.0
Pazopanib	AGO-OVAR16	Advanced stage with no evidence of progression	Surgery and PTX+carbo → pazopanib	PFS (months) -PTX+carbo 12.3 -PTX+carbo → pazopanib 17.9	OS (months) -PTX+carbo 64.0 -PTX+carbo → pazopanib 59.1
Trebananib	TRINOVA-1	Recurrent	Weekly PTX± trebananib	PFS (months) -PTX 5.4 -PTX+trebananib 7.2	OS (months) -PTX 18.3 -PTX+trebananib 19.3
Cediranib	ICON6	Platinum-sensitive, recurrent	PTX+DDP or DDP+gemcitabine or carbo±CED concurrent/maintenance	PFS (months) -Chemo 8.7 -Chemo+CED concurrent 9.9 -Chemo+CED maintenance 11.0	OS (months) -Chemo 19.9 -Chemo+CED concurrent 26.6 -Chemo+CED maintenance 27.3
PTX: paclitaxel; DDP: cisplatin; carbo: carboplatin; CED: cediranib; PLD: pegylated liposomal doxorubicin					

In this scenario, cediranib, a VEGFR tyrosine kinase inhibitor, has a response rate similar to bevacizumab given as single-agent (Hirte et al., 2015; Matulonis et al., 2009).

1.3.2 Cediranib

Cediranib (AZD2171) is a potent, oral, small molecule tyrosine kinase inhibitor that blocks the three VEGF receptors (VEGFR1, VEGFR2, VEGFR3), and targets also c-KIT and PDGFR-alpha and PDGFR-beta (Figure 1.5) (Wedge et al., 2005; Smith et al., 2007; Heckman et al., 2008; Brave et al., 2011).

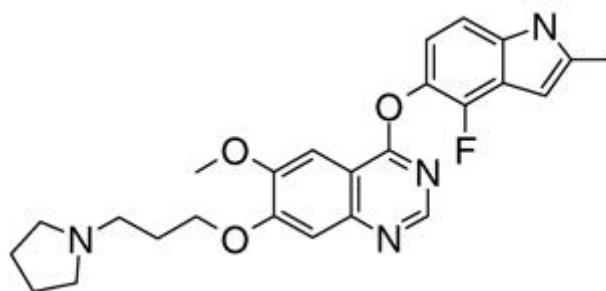


Figure 1.5 Structure of cediranib.

[(4-fluoro-2-methyl-1H-indol-5-yl)oxy]-6-methoxy-7-(3-pyrrolidin-1-yl)propoxy) quinazoline maleate (AZD2171).

Modified from Brave et al, Assessing the Activity of Cediranib, a VEGFR-2/3 Tyrosine Kinase Inhibitor, against VEGFR-1 and Members of the Structurally Related PDGFR Family, Molecular Cancer Therapeutics, 2011.

Cediranib competes for the ATP-binding site within the receptor kinase domain in particular of VEGFR2, that predominantly transduce the angiogenic and permeability activity of VEGFA, but also of VEGFR1 and VEGFR3 (Heckman et al., 2008), preventing the ATP catalysis and propagation of receptor signaling. Consequently, a reduced activation of downstream signaling molecules ERK1/2, Akt, and CREB is observed.

The unique structural features adjacent to the ATP-binding site allows the achievement of selectivity. However, cediranib has additional activity against PDGFR-alpha, PDGFR-beta and c-Kit. Indeed, these receptors have some structural homologies with the VEGFR family members, having a kinase-insert sequence in the intracellular domain.

The simultaneous inhibition of multiple kinases may provide additional therapeutic opportunities, but also impact adversely on tolerability or in combination usage with concurrent cytotoxic drugs.

Additionally, cellular functions associated with VEGFR activation, including proliferation, survival, and migration, are all compromised by cediranib. Interestingly, cellular migration seems to be particularly sensitive to cediranib treatment. Low concentrations of the compound inhibit blood endothelial cell migration, but only slight inhibition of ligand-induced receptor phosphorylation at the same concentration was observed. Furthermore, cediranib compromises the growth of tumor-associated blood vessels and also induces regression and inhibition of VEGFR3 mediated lymphangiogenesis. The growth of human non-small cell lung adenocarcinomas in cediranib treated animals is impaired (Heckman et al., 2008). Cediranib inhibits human umbilical vein endothelial cell (HUVEC) proliferation and diminishes microvessel density, causing reversible epiphyseal zone hypertrophy in rodent models (Wedge et al., 2005) and was described effective in reducing lymphatic metastasis, independent of the effect on blood vessels (Padera et al., 2008), but also blocking VEGFC-induced VEGFR3 activity and lymphangiogenesis in lung cancer

(Heckman et al., 2008). Also, cediranib is active in a wide variety of human tumor xenografts (Decio et al., 2015; Lobo et al., 2015; Melsens et al., 2017). It has demonstrated single-agent activity in preclinical models of ovarian cancer and activity in combination with other small molecule inhibitors or chemotherapy, inhibiting tumor progression and dissemination to metastatic organs even in OC-PDX poorly responsive to platinum (Decio et al., 2015).

In the randomized, double-blind NCIC clinical trial BR24 in advanced non-small-cell lung cancer (NSCLC), the addition of cediranib to carboplatin/paclitaxel resulted in improved response and increased PFS (Goss et al., 2010).

In the double-blind, randomized phase III study (HORIZON III) in advanced metastatic colorectal cancer, cediranib activity, in terms of PFS and OS, was comparable to that of bevacizumab when added to mFOLFOX6. However, the predefined boundary for PFS non-inferiority was not met (Schmoll et al., 2012).

Cediranib monotherapy was studied in a phase II study in patients with recurrent glioblastoma. Encouraging proportions of radiographic response and an increase in the 6-month PFS was observed after cediranib treatments (Batchelor et al., 2013).

Cediranib monotherapy demonstrated significant evidence of antitumor activity in a randomised phase II study in patients with advanced renal cell carcinoma (Mulders et al., 2012).

In a prospective trial of systemic therapy for metastatic alveolar soft tissue sarcoma, it was observed that cediranib had substantial single-agent activity, producing an objective response rate (ORR) of 35% and a disease control rate of 84% at 24 weeks (Kummar et al., 2013).

In an open-label, phase I study of cediranib in patients with acute myeloid leukemia, cediranib showed preliminary evidence of activity as a monotherapy (Fiedler et al., 2010).

In particular, in ovarian cancer cediranib has demonstrated activity as monotherapy in two phase II single-agent studies with either platinum-resistant or -sensitive recurrent disease; all the patients that had benefitted from the administration of cediranib were high grade serous cases with a maximum of one previous line of treatment for relapsed disease (Matulonis et al., 2009).

Following these phase II trials, studies with cediranib given in combination with chemotherapy and other targeted therapies were carried out.

A pivotal phase III trial of cediranib in combination with platinum-based chemotherapy with or without cediranib maintenance demonstrated improved PFS in patients treated with cediranib compared with placebo and the outcome measure of safety demonstrated that is feasible to add cediranib to carboplatin/cisplatin (DDP) and paclitaxel chemotherapy without major unexpected toxicities (Raja et al., 2011).

ICON6, a multi-stage phase III, randomized, placebo-controlled Gynaecological Cancer InterGroup (GCIG) trial, evaluated the activity of cediranib in combination with chemotherapy in patients with relapsed-sensitive ovarian, Fallopian tube or primary peritoneal cancer. Treatment arms were chemotherapy plus placebo then placebo in maintenance (arm A), chemotherapy plus cediranib once a day then placebo in maintenance (arm B), chemotherapy plus cediranib once a day then cediranib in maintenance (arm C). PFS was the primary end-point. Median PFS was 11.0 months in arm C and 8.7 months in arm A. The majority (90%) of patients in arm B had disease progression, and median progression-free survival was 9.9 months. ICON 6 was prematurely interrupted, due to toxic effects, particularly diarrhoea, fatigue and hypertension, but PFS was greater in the chemotherapy plus cediranib in maintenance group than chemotherapy plus cediranib followed by placebo (Ledermann et al., 2016).

The promising activity in terms of PFS in ICON6 prompted the investigation of cediranib in combination with other therapies (such as PARP inhibitors) for ovarian cancer.

1.4 DNA REPAIR TARGETED THERAPY

DNA repair pathways are intrinsic cell mechanisms that evolved to allow the tolerance and repair of DNA damage associated with normal cell functions and with the extrinsic injuries such as environmental radiation, reactive oxygen species and chemical agents.

Genome instability caused by the great variety of DNA damaging agents would be an overwhelming problem for cells and organisms if it were not for DNA repair systems (Friedberg et al., 2006; Glazer et al., 2013; Sancar et al., 2004; Wood et al., 2001).

The human genome encodes information to protect its own integrity. DNA repair enzymes have the role to continuously monitor the chromosome to correct damaged nucleotides with five main mechanisms of action (Figure 1.6).

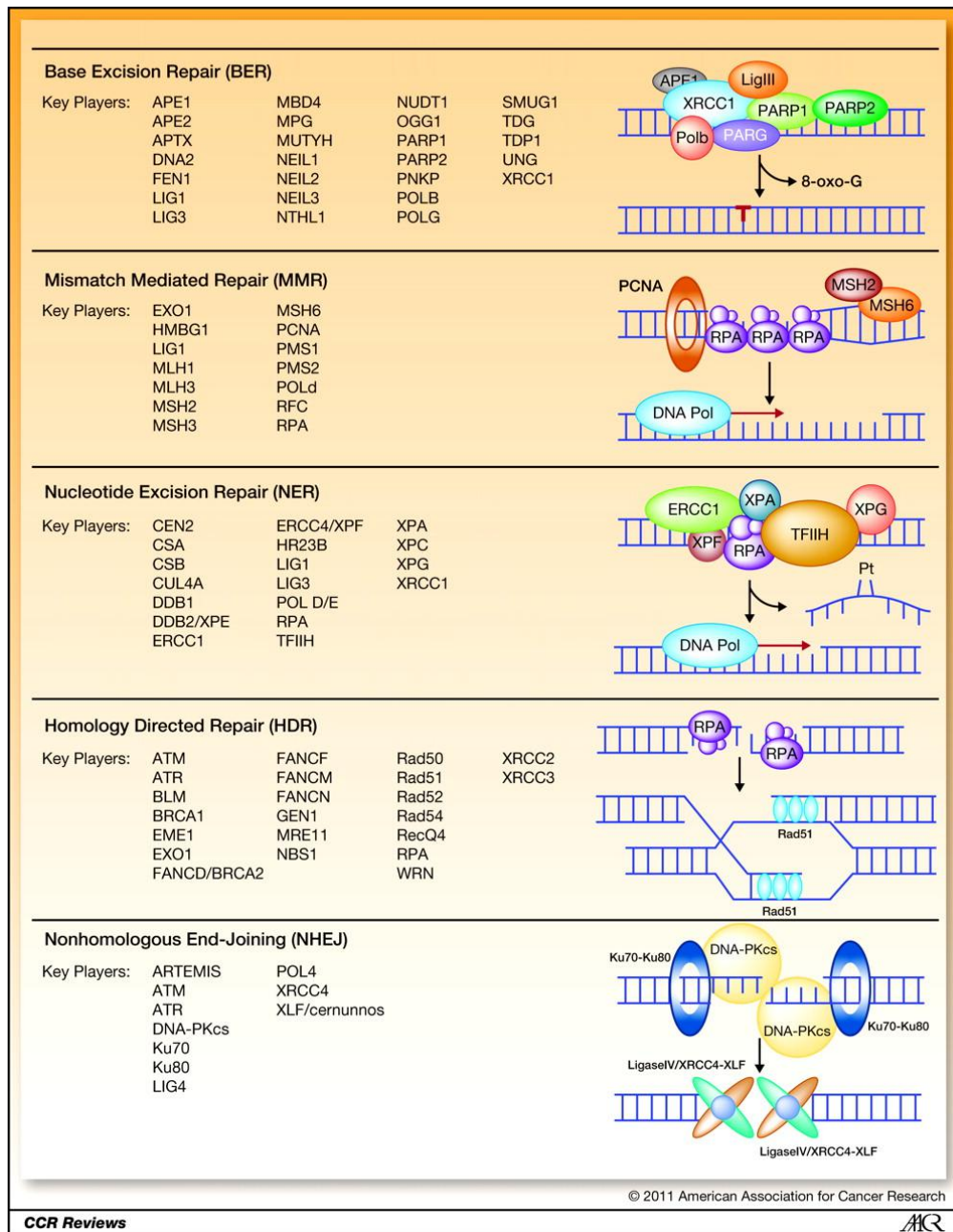


Figure 1.6 DNA damage repair pathways.

The five DNA damage response pathways are presented with key proteins involved and the critical repair steps within each of the pathways are pictured.

Modified from Jalal et al, DNA Repair: From Genome Maintenance to Biomarker and Therapeutic Target, Clin Cancer Res, 2011.

Two major forms of injury can occur on DNA: single strand breaks (SSBs) that involve only one DNA filament, and double strand breaks (DSBs) that involve the double helix.

Direct reversal repair (DDR) directly restores the native nucleotide residues by removing the non-native chemical modification. Functions for excision repair are base-excision repair (BER), nucleotide excision repair (NER) and mismatch repair (MMR); the BER system excises single damaged bases and replaces them, NER mainly removes bulky adducts and MMR corrects occasional errors of DNA replication as well as abnormalities formed during recombination.

Homologous (HR) and non-homologous (NHR) recombination pathways, such as non-homologous end-joining (NHEJ), correct DSBs. The former repairs DNA double strand breaks using the homologous DNA strand as a template to resynthesize a new filament and for this is considered a high fidelity repair pathway; the latter ligates the ends resulting from DNA double strand breaks with an error-prone mechanism of repair.

Interest in targeting DNA repair proteins has increased over the last few decades, in particular because their impact in platinum resistance is well documented in several types of cancer, including ovarian (Nguewa et al., 2006).

1.4.1 Poly(ADP-ribose) polymerase (PARP) inhibitors as cancer therapy

PARP inhibitors are the latest class of agents to gain approval in ovarian cancer (George et al., 2017).

PARP1 and 2 are enzymes that sense the DNA damage and signal transducers that operate by synthesizing negatively charged poly(ADP-ribose) (PAR) chains, via PARylation, on target proteins as a form of posttranslational modification (Sato and Lindahl, 1992).

PARP1 works by binding DNA single strand breaks and other DNA lesions. The recognition of the damage induces allosteric changes in the structure of PARP1, activating its catalytic function (Figure 1.7). This leads to the PARylation and recruitment of DNA

repair effectors (such as *BRCA1/2*, substrates of PARP) and also to the remodelling of the chromatin around the site of damage. To shut down the process, PARP1 autoPARylates itself and it is released from the repaired DNA (Dawicki-McKenna et al., 2015; De Vos et al., 2012; Krishnakumar and Kraus, 2010; Satoh and Lindahl, 1992).

The rationale to use PARP inhibitors is that tumor cells can be made more sensitive to conventional treatments that damage DNA, such as chemotherapy or radiotherapy. It was recently shown that PARP inhibition, as well as blocking the PARylation process, also induces a “trap” of PARP on the site of DNA damage. This effect induces the block of the replication forks; in conditions of effective DNA repair systems, such as HR (chapter 1.4 DNA repair target therapy), the activity of the forks is restored and the tumor cell survives. Conversely, the concept of synthetic lethality is related to the blockade of PARP activity in the presence of defects in mechanisms of DNA repair. Mutations in DNA repair effector genes (such as *BRCA1/2*) and consequent production of a non-functional protein, added to PARP1 blockade, induce a non-resolution of the DNA damage, driving genomic instability, mediated by an error-prone mechanism of repair, such as NHEJ, that eventually leads to death (Ashworth et al., 2011; Terada et al., 1979).

For these reasons, drug discovery efforts led to the development of a plethora of PARP inhibitors that show different effects in terms of cytotoxicity and ability to “trap” PARP on DNA.

To date there are five principal PARP inhibitors that have been developed and are used clinically: veliparib (Abbvie), rucaparib (Pfizer/Clovis), olaparib (KuDOS/AstraZeneca) and niraparib (Merck/Tesaro) and the second generation, more potent PARPi, talazoparib (Lead/Biomarin/Medivation/Pfizer) (Shen et al., 2013). Talazoparib is approximately 100 times more potent than niraparib in term of capacity to “trap” PARP on DNA, and niraparib itself is more potent than olaparib and rucaparib; it has been demonstrated that the PARP inhibitor with least “trap” ability is veliparib (Murai et al., 2014).

Preclinical testing of PARP inhibitors demonstrated anti-tumor activity both alone and in combination with DNA damaging chemotherapy.

Farmer and colleagues (Farmer et al., 2005) showed *in vitro* and *in vivo* activity of PARP inhibitor on *BRCA1* and *2* deficient embryonic stem cells (ES). Similarly, De Soto (De Soto et al., 2006) reported *in vivo* demonstration of PARP-1 in *BRCA1* deficient mammary tumors, mouse and human breast cells, thus indicating that the inhibition of PARP could improve the outcome for patients with defects in DNA repair effector genes.

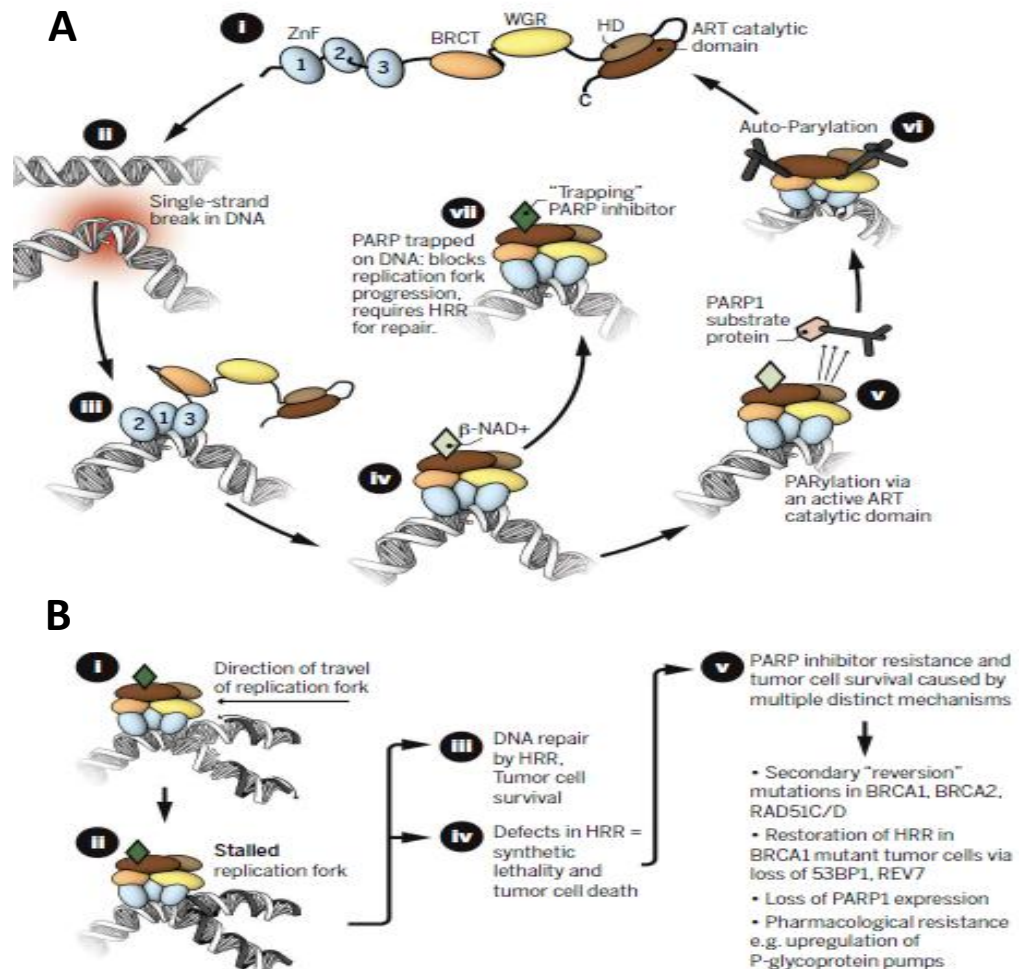


Figure 1.7 Mechanism of action of PARP inhibitors.

A. PARP1 catalytic cycle.

i) Non-DNA bound state. PARP1 includes three zinc-finger related domains (ZnF1,2,3), BRCA1 C-terminus domain (BRCT), tryptophan-,glycine-, arginine-rich domain (WGR) and the catalytic domain composed by an helical domain (HD) and an ADP-ribosyltransferase (ART) domain. HD acts as an autoinhibitory domain preventing the bound to DNA. ii) DNA single strand breaks (SSBs) make the DNA double helix turn. iii) SSBs are recognized by ZnF1,2,3. iv) HD domain changes conformation and losses the autoinhibitory activity. v) ART domain drives the PARylation by mediating the recruitment of DNA repair effectors that are PARP1 substrates. vi) PARP1 autoPARylation causes the restoration of a catalytically inactive state. vii) PARPi, that binds catalytic domains of PARP1, prevents the release of PARP1 from DNA, by “trapping” it at the site of damage.

B. PARP inhibitors mechanism of action.

i) When PARP1 is trapped on DNA, it causes the impairment of the progression of replication forks. ii) Stalled replication forks normally induce DNA damage response. iii) Homologous recombination (HRR), that involves BRCA1/2, allows the forks to restart and damage is resolved. iv) Defective HRR induces the cell to switch on error prone DNA damage repair systems, which cause large-scale genomic rearrangements, which can lead to cell death and synthetic lethality. v) Resistance to PARP inhibitor can occur also in case of HRR deficiency.

Modified from Lord and Ashworth, PARP inhibitors: Synthetic lethality in the clinic, Science, 2017

1.4.2 *BRCA1* and *BRCA2* mutations

Breast cancer susceptibility genes (*BRCA*) 1 and 2 were discovered in the early 90's (Hall et al., 1990; Wooster et al., 1995). *BRCA1* spans approximately 100 kb on the genomic DNA and consists of 5592 base pairs in 22 exons, that encodes an 1863 amino acid protein (Figure 1.8) (Miki et al., 1994). *BRCA2* is a large gene of 10524 nucleotides, including 27 exons and encoding for a protein of 3418 amino acids (Figure 1.9) (Tavtigian et al., 1996).

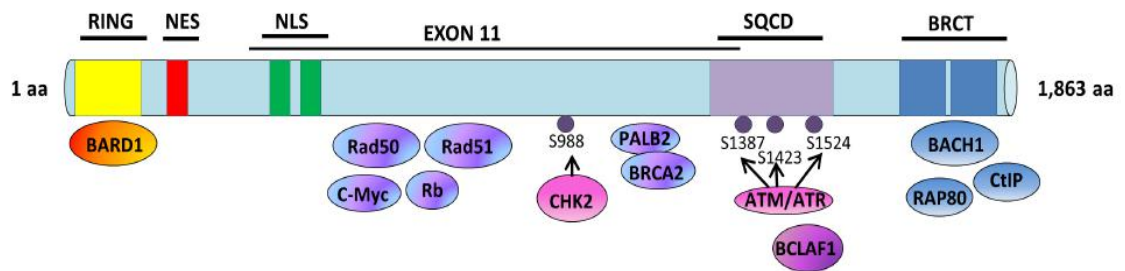


Figure 1.8 Structure and Binding Partners of BRCA1.

BRCA1 encodes for 24 exons, translating into an 1863 amino acid protein. Main functional domains are:

- RING finger domain, located at the N-terminus. It mediates the binding with BARD1, that it is necessary for BRCA1 stability. This domain has also a E3 ligase activity.
- BRCT domains, located at the C-terminus. These two domains are responsible for the binding with phosphorylated protein to signal the DNA damage response pathway.
- Region between the exon 11 and 13. This region plays a key role in binding Rad50, Rad51, PALB2 and BRCA2. Moreover it contains two nuclear localization signals (NLS) and a SQ cluster domain (SQCD) that mediates the binding with ATM and ATR.

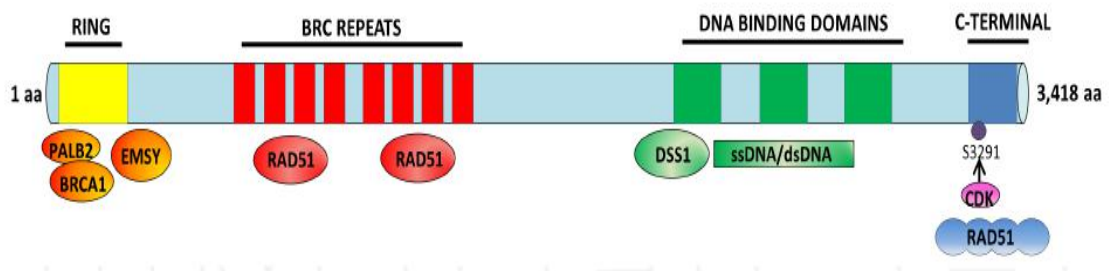


Figure 1.9 Structure and Binding Partners of BRCA2.

BRCA2 coding sequence translates for a 3418 amino acid protein. Main functional domains are:

- RING finger domain, located at the N-terminus. It mediates the binding with PALB2, BRCA1 and EMSY.
- C-terminus domain. It mediates the binding with multimeric Rad51.
- BRC repeats domains. These eight domains mediate the binding with 6-8 monomeric molecules of Rad51.
- DNA binding domains. These three domains are able to associate with single strand DNA and double strand DNA.

Modified from Orr and Savage, The BRCA1 and BRCA2 Breast and Ovarian Cancer Susceptibility Genes — Implications for DNA Damage Response, DNA Repair and Cancer Therapy, Advances in DNA repair, Chapter 7, 2015. 9

These two genes are considered tumor-suppressors because germline mutations are associated with tumor development and predisposition to familial forms of breast, ovarian and (as more recently discovered) pancreatic cancer (Antoniou et al., 2003; O'Donovan and Livingston, 2010).

Moreover, the loss of the wild type allele (loss of heterozygosis) is frequently observed in sporadic breast and ovarian tumors. This is likely due to the fact that both the *BRCA1* and *BRCA2* genes adhere to the Knudson “two-hit” hypothesis in which both alleles of a tumor suppressor gene must be mutated for the pathogenic phenotype to become apparent. Hence one inherited a copy of mutant *BRCA1/2* is the “first hit” and the “second hit” comes from acquiring a somatic mutation (Knudson, 1971).

BRCA1 and *BRCA2* play a key role in maintaining genomic integrity, being involved in the regulation of DNA repair pathways. Specifically, *BRCA1* is a multi-functional protein involved in transcriptional regulation, ubiquitination, oestrogen metabolism, chromatin remodelling and mRNA splicing (Turner et al., 2004). The main function of *BRCA2* identified to date is to promote the NHEJ recombination pathway.

BRCA1 and *BRCA2* are highly mutated in HGS, with a rate of germline mutation of approximately 8-18% (Pal et al., 2005; Risch et al., 2001). Nevertheless, it is important to note that germline mutations are reported also in other types of ovarian cancer, including endometrioid, clear cell and mucinous, with lower mutation rates (5-15%) (Pennington et al., 2014; Soegaard et al., 2008; Zhang et al., 2011).

HGS tumors display a loss of the second copy of *BRCA1/2*, thus having a homozygous deficiency in the HR repair pathway. Germline *BRCA*-mutated ovarian cancers demonstrate a specific clinical behaviour, such as earlier stage diagnosis, improved patient survival, high response to platinum and high sensitivity to PARP inhibitors (Alsop et al., 2012; Banerjee et al., 2010; Fong et al., 2010; Tan et al., 2013). Even somatic mutations play a fundamental role; accordingly to The Cancer Genome Atlas Research Network

(Cancer Genome Atlas Research Network, 2011), an additional 3% of HGS show somatic mutations on *BRCA1/2* genes. Pennington (Pennington et al., 2014) described a 9% somatic mutation rate in one or more genes belonging to the HR pathway, including *BRCA1* and *BRCA2*.

To date, the clinical relevance of harbouring germline mutations is widely established, but the same could not be claimed for somatic abnormalities. Hennessy (Hennessy et al., 2010) demonstrated that PFS was longer in patients with somatic mutations in *BRCA1/2* compared with wild type, but no improvement was seen in OS. No significant differences in OS were highlighted in somatic mutation carriers compared with wild type cases after platinum (Pennington et al., 2014). Prospective studies such as ARIEL-3 are planning to clarify the relevance of somatic mutations in *BRCA1/2* as biomarkers for therapy.

Also, the deficiency in HR could be driven by epigenetic alterations that lead to *BRCA1* and *BRCA2* silencing. *BRCA1* promoter hypermethylation (an epigenetic modification that leads to loss of expression of the protein) was seen in ovarian cancer patients (Baldwin et al., 2000). Moreover, promoter hypermethylation has been reported to be associated with loss of heterozygosity (Ledermann et al., 2012).

In this scenario, *BRCA1* and *BRCA2* are not the only players. Recently it is becoming evident that a proportion of sporadic ovarian cancers share pathological features of *BRCA* mutation-association cases, without *BRCA* germline or somatic mutations. The concept of “BRCAness” includes situations where defects in the HR pathway are present but associated with genes other than *BRCA1* and 2 (Turner et al., 2004). This aspect is becoming increasingly relevant especially relating to the activity of PARP inhibitors in ovarian cancer (Konstantinopoulos et al., 2010). Indeed, in this project it was decided to focus on germinal and somatic mutations in *BRCA1* and 2 to select OC-PDX for *in vivo* trials, but also to take into consideration the mutational status of a panel of HR related genes (Table 1.1) (Coleman et al., 2017; McNeish et al., 2015).

BRCA	Other HR repair pathway genes	
<i>BRCA1</i>	<i>ATM</i>	<i>FANCI</i>
<i>BRCA2</i>	<i>ATR</i>	<i>FANCL</i>
	<i>ATRX</i>	<i>FANCM</i>
	<i>BARD1</i>	<i>MRE11A</i>
	<i>BLM</i>	<i>NBN</i>
	<i>BRIP1</i>	<i>PALB2</i>
	<i>CHEK1</i>	<i>RAD50</i>
	<i>CHEK2</i>	<i>RAD51</i>
	<i>FANCA</i>	<i>RAD51B</i>
	<i>FANCB</i>	<i>RAD51C</i>
	<i>FANCC</i>	<i>RAD51D</i>
	<i>FANCD</i>	<i>RAD52</i>
	<i>FANCE</i>	<i>RAD54L</i>
	<i>FANCF</i>	<i>RPA</i>
	<i>FANCG</i>	

Table 1.1 Panel of 31 genes associated with homologous recombination.

Modified from Coleman RL et al, Rucaparib maintenance treatment for recurrent ovarian carcinoma after response to platinum therapy (ARIEL3): a randomised, double-blind, placebo-controlled, phase 3 trial, Lancet, 2017.

1.4.3 Olaparib

Olaparib (AZD2281) is a potent oral inhibitor of poly(adenosine diphosphate [ADP]-ribose) polymerase that induces synthetic lethality in *BRCA1/2*-deficient tumors and generally in HR deficient tumors (Figure 1.10) (Evers et al., 2008; Rottenberg et al., 2008).

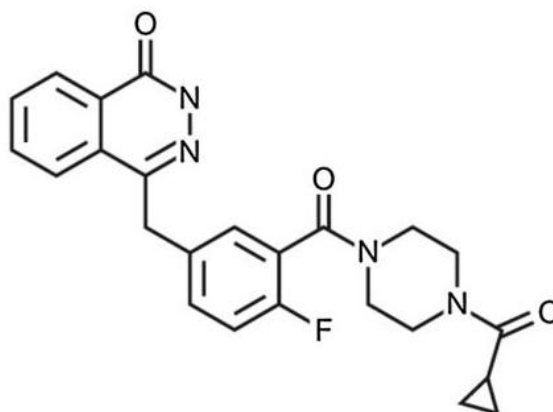


Figure 1.10 Structure of olaparib.

4-[[3-[4-(cyclopropanecarbonyl)piperazine-1-carbonyl]-4-fluorophenyl]methyl]-2H-phthalazin-1-one (Lynparza TM, AZD2281, KU-0059436).

Modified from O'Connor et al, The PARP Inhibitor AZD2461 Provides Insights into the Role of PARP3 Inhibition for Both Synthetic Lethality and Tolerability with Chemotherapy in Preclinical Models, Cancer Research, 2016.

Olaparib has EMA (European Medicine Agency) approval as maintenance of second or later therapy for patients with platinum-sensitive relapsed *BRCA* mutated (germline and somatic) HGS, who had a complete or partial response to platinum-based chemotherapy. Moreover, FDA (Food and Drug Administration) approved it as a treatment for patients with germline *BRCA* mutated ovarian cancer who have received three or more lines of chemotherapy.

Olaparib inhibits DNA repair of SSBs, through a catalytic inhibition of the PARP enzyme, both blocking DNA PARylation and trapping PARP in DNA complexes, leading to termination of replication forks (Lord and Ashworth, 2017). Eventually, in the case of repair pathway deficiency, SSBs evolve to DSBs, leading to an accumulation of DNA damage and tumor cell death.

A comprehensive characterization of 41 ovarian cell lines, sequenced in *BRCA1/2* genes, mRNA expression of *BRCA1/2* and gene methylation status, allowed testing of olaparib *in vitro*. In this study deleterious mutations, heterozygous mutations and promoter methylation were correlated to a higher sensitivity to the PARP inhibitor, following long-term exposure (Stordal et al., 2013).

Indraccolo (Indraccolo et al., 2006) derived two ovarian cancer cell lines from patients previously treated with chemotherapy, both showing loss of the *BRCA1* wild type allele, accompanied by gain of one or more copies of the mutant allele, thus providing a useful tool to test the activity of PARP inhibitors.

The efficacy of olaparib was tested *in vivo* in several studies. Kortman (Kortmann et al., 2011) investigated the synthetic lethality efficacy in *BRCA2* germline mutated xenograft models, developed directly from ovarian cancer tissue, either alone or in combination with carboplatin. Results indicated that olaparib greatly delayed tumor growth only in the *BRCA2* mutated xenografts and not in the wild type counterpart, significantly decreasing proliferation, increasing apoptosis (cleaved caspase 3 and Ki67 stains), and reducing

PARP1 activity.

Topp (Topp et al., 2014) generated a biobank of patient-derived xenografts, including two mutated in *BRCA1*, two mutated in *BRCA2* and one *BRCA1* promoter methylated, demonstrating the correlation between an impaired DNA repair pathway and platinum activity.

Fong (Fong et al., 2009) carried out the first phase I trial of olaparib in 60 patients including 22 *BRCA* mutated; the primary end-point was to establish the maximum tolerated dose as 400 mg twice daily. An additional study on 50 patients with *BRCA* mutated tumors showed that there was a significant association between the clinical benefit rate and progression-free survival across the platinum-sensitive, -resistant and -refractory group; moreover, an association between platinum sensitivity and extended response to olaparib was highlighted (Fong et al., 2010).

A Phase II trial in patients with recurrent *BRCA* mutated ovarian cancer, comparing 400 mg olaparib twice a day versus 100 mg twice a day, showed that the higher dose gave a better clinical outcome (Audeh et al., 2010). In the phase II trial Study 42 by Kaufman (Kaufman et al., 2015) olaparib was given as a monotherapy in patients with different types of cancer, including ovarian, breast, pancreatic and prostate; the response to olaparib was observed across the different types of tumors, associated with germline mutations in *BRCA1/2*. These results led to the FDA licencing of olaparib.

Interesting data on olaparib monotherapy as a maintenance regimen in patients with platinum-sensitive relapsed HGS were assessed in a pivotal phase II randomized placebo-controlled study (Study 19), in which patients were not selected accordingly to their *BRCA* status (Ledermann et al., 2012); PFS was significantly longer in the olaparib treated group. PFS benefit was significant in patients with *BRCA* wild type tumors, suggesting for the first time the advantage of the administration of the drug also in this group of patients. Following these results, EMA approved olaparib for maintenance treatment of patients

with platinum-sensitive relapsed *BRCA* mutated HGS who have received three or more lines of chemotherapy.

A variety of phase III trials of olaparib in ovarian cancer are currently in progress, such as SOLO-1 and SOLO-2, that are evaluating the maintenance of olaparib in patients with *BRCA*-mutated cancer who have responded to first line or second or later line platinum-based chemotherapy (Kathleen N. Moore et al., 2014; Pujade-Lauraine et al., 2017). PAOLA-1 is evaluating the efficacy of olaparib in patients who have received platinum/taxane-based chemotherapy plus bevacizumab (Ray-Coquard et al., 2016).

1.5 PARP INHIBITORS IN COMBINATION WITH ANGIOGENESIS INHIBITORS

Interest in the combination of PARP inhibitors and antiangiogenic strategy is growing. Enhanced PARP inhibition has been shown under hypoxic conditions and to reduce VEGF-induced angiogenesis (Pyriochou et al., 2008).

In this scenario, it has been postulated that the dual use of PARP inhibitors and antiangiogenic agents may have a synergistic effect (Bindra et al., 2005; Tentori et al., 2007).

A preclinical study led by Lim (Lim et al., 2014) reported that the inhibition of VEGFR3 in ovarian cancer cells is associated with decreased levels of *BRCA1* and *BRCA2*, inducing a downregulation of the expression levels of the two genes. In this way cells are restored to chemosensitivity, suggesting that the downregulation of *BRCA* genes can be obtained by inhibiting angiogenesis. Thus, it may be a pharmacologically relevant strategy also for *BRCA* wild type patients.

Preclinical antiangiogenic interaction of olaparib and cediranib led to the clinical investigation of the activity of the combination. A phase I study, aiming to explore tolerability and safety in patients with ovarian, Fallopian tube, primary peritoneal and

breast cancers, has been conducted (Liu et al., 2013). In this study, patients were allocated to receive olaparib plus cediranib in 28-day cycles until disease progression, toxicity or withdrawal. Activity was observed both in platinum-sensitive and -resistant patients, both *BRCA* mutated and wild type.

A following phase II trial evaluated PFS. Patients were randomized to receive olaparib as a single-agent or in combination with cediranib. PFS was higher in the latter group (17.7 vs 9 months), and there was also a slight increase in OS at 24 months (81% versus 65%). Subsequently, *ad hoc* analysis revealed that not only patients with *BRCA* mutations gained an advantage from the combination, but the magnitude of improvement was greater in *BRCA* wild type/unknown patients, encouraging the administration of the two agents together also in this population (Liu et al., 2014). Taking together, these results suggest that the combination of olaparib and cediranib has encouraging activity, regardless of *BRCA* mutational status, both in platinum-sensitive and -resistant ovarian cancers, thus providing a new therapeutic option, especially for *BRCA* wild type patients.

1.6 ANIMAL MODELS FOR OVARIAN CANCER

The scarcity of *in vivo* preclinical models that closely reproduce the complexity and heterogeneity of ovarian cancer has limited - and still limits - the development of new and effective therapeutic strategies.

In this scenario, clinically-derived cell lines play a critical role, being reproducible and easy to use, especially if the focus is on specific mechanisms. However, their resemblance to the original tumor is very limited, thus affecting their therapeutic predictive value (Domcke et al., 2013).

In vivo animal models more accurately recapitulate the biological and molecular characteristics of primary tumors, thus being a more valuable preclinical platform. The development of peritoneal metastasis and ascites, the interaction between tumor and

microenvironment are crucial to accurately recapitulate the progression of human disease (Ricci et al., 2014, 2013; Masazza et al., 1991; Massazza et al., 1989; Lengyel et al., 2014). In recent years, two types of mouse models have expanded the understanding of the disease, the investigation of tumorigenic mechanisms and the testing of novel therapeutic strategies.

Genetically engineered mouse (GEM) models are generated by introducing transgenes or gene mutations into the mouse genetic background, mirroring natural disease initiation, progression and physiological states.

Two main examples are the tetracycline-inducible system and the Cre/loxP recombinase system, which ensure gene induction/inactivation in a tissue-specific manner at temporally regulated points (Gama Sosa et al., 2010; Jaisser, 2000). A major limitation of GEM models is that they cannot entirely mirror a patient's disease from the molecular aspect, because they are generally engineered only with one or a limited number of putative key alterations/mutations, in genetically homogeneous animals. However, the genetic background in patients is more heterogeneous and their lifetime exposure to additional environmental influences renders the clinical situation infinitely more complex. On the other hand, GEM have a functional immune system that can be exploited to focus on the role of the microenvironment and especially the innate and adaptive immune systems in relation to drug response (Chen et al., 2014; Smith et al., 2014).

1.6.1 Patient-derived ovarian cancer xenografts (OC-PDX)

Xenograft models are typically generated by establishing tumor cell lines *in vitro* and then injecting them into immunocompromised mice, such as thymus-deficient nude, severe combined immunodeficient (SCID) and NOD/SCID//IL2R γ null (NSG) strains. However, the use of an established cell line can result in a population that is not truly representative of the original tumor, producing responses that are different from those seen in patients (Ricci et al., 2013).

In light of this, patient-derived xenograft models are generated by injecting tumors from patients directly into immunodeficient mice. These models benefit from their limited diversity from the patient's tumor, retaining the natural heterogeneity, allowing for further evolution during progression and following drug treatment (Ricci et al., 2014; Sausville and Burger, 2006; Siolas and Hannon, 2013; Tentler et al., 2012).

Ovarian cancer patient-derived xenografts (OC-PDX) retain the biological behaviour, histological and molecular profiles of the original patients, even if it is crucial to use the OC-PDX within a few *in vivo* passages in mice, in order to avoid changes in the phenotypes or acquisition of new mutations.

OC-PDX are a useful tool to test new therapeutic strategies and efficacy can be determined by mimicking the response of the patients (Weroha et al., 2014). A strong correlation between patient and OC-PDX responsiveness to therapy has been demonstrated in ovarian cancer, thus endorsing the reliability of the model to lead translational preclinical and co-clinical trials (Ricci et al., 2014; Masazza et al., 1991; Massazza et al., 1989; Fiebig et al., 1984). Unfortunately, the biggest issue with OC-PDX is the lack of a mouse immune system that makes it impossible to study the effect of the immune system to boost the therapy. It has been widely demonstrated that the immune system plays a critical role in cancer initiation and expansion (Colvin, 2014; Hansen et al., 2016; McLean and Mehta, 2017; Pogge von Strandmann et al., 2017).

PDX could nevertheless accomplish this goal thanks to the recent development of "humanized xenograft" models, which are created by co-engrafting patient's tumor fragments with hematopoietic stem cells or human peripheral blood mononuclear cells (Siolas and Hannon, 2013), ideally derived from the same patient to avoid allogenic and graft-versus-host phenomena (Shultz et al., 2012).

In the Department of Oncology, where this PhD research has been carried out, a platform of transplantable patient-derived ovarian tumor xenografts (OC-PDX) has been established

and some models have been used to perform all of the studies described in this thesis. Our bio-bank of OC-PDX has been shown to comprise all the main subtypes of ovarian carcinoma and retain the features of patients' original tumors, on the histopathological, molecular and biological behaviour points of view (Ricci et al., 2014).

To summarize, OC-PDX models are a preferred tool for drug discovery and translation, despite some limitations. These models resemble patients' biological, histological and molecular features and enable the identification of predictive biomarkers and novel therapeutic strategies. Moreover, the possibility to repeat experiments and include treatment groups not feasible in the clinic, make this a unique and powerful tool.

CHAPTER 1.

Aim of the study

Epithelial ovarian cancer is still a leading cause of cancer deaths due to difficulties in diagnosis and lack of effective therapies.

Thus, there is an ongoing need to identify selective pathways and investigate targets for therapy.

Preclinical models that more closely recapitulate the heterogeneity of ovarian tumor are useful for more efficient drug development. To accelerate the process of data integration and translation between preclinical and clinical efforts, a preclinical trial should be conducted in OC-PDX established directly from patients, and where possible in parallel to the clinical trial.

Models of OC-PDX, which are molecularly and biologically representative of patient tumors, have been recently shown to be a valuable tool in predicting clinical outcome. The advantage is that freshly xeno-transplanted human tumor, without *in vitro* manipulation, maintains the biological and molecular features of the original tumor (Ricci et al., 2014).

To address this goal, in this study specimens from patients were transplanted immediately after surgical resection into immune-incompetent mice, such as SCID and NSG strains. OC-PDX were established subcutaneously (s.c. ectopic models) or orthotopically into the peritoneal cavity (i.p. intraperitoneal models or i.o. intraovarian model ID8).

Because they can be propagated perpetually, these models are an important source of tumor material for biological and pharmacological studies, overcoming the limitation often encountered with small biopsies. Patients' original tumors and corresponding OC-PDX were analyzed for histopathologic phenotype and for molecular genetic alterations, *via* the Next Generation Sequencing technique complemented by traditional Sanger Sequencing.

The molecular characterization is a useful tool to select appropriated OC-PDX for testing new therapeutic agents, such as poly(ADP-ribose)polymerase inhibitors (e.g. olaparib), in combination with angiogenesis inhibitors (e.g. cediranib).

Indeed, germinal and somatic defects in the DNA repair pathways have been proved to be a promising target of PARP inhibitors, but several preclinical and clinical trials demonstrated that the combination with angiogenesis inhibitors could be a compelling strategy for those patients with functional DNA repair pathways, even though no clear mechanisms of action have so far been determined.

Altogether, the aims of this project were to:

- Enlarge the collection of OC-PDX already established in the Department of Oncology, where this PhD research has been carried out (Ricci et al., 2014). Additional patients' tumor samples have been received during this PhD research program and established *in vivo*.
- Profile the expanded platform of OC-PDX and corresponding patient tumor, when available, at a histopathological and molecular level, exploiting new techniques, such as Next Generation Sequencing, RNA Sequencing and Fluidigm for gene expression.
- Take advantage of this improved and properly analyzed biobank to provide insights into better treatment modalities for ovarian cancer. In particular, based on histopathological and molecular features, a smaller cohort of *ad hoc* OC-PDX has been selected to perform preclinical studies aimed at elucidating the responsiveness to PARP inhibitor olaparib and to the combination with the angiogenesis inhibitor cediranib, and explore possible mechanisms of action underlying it.

CHAPTER 2.

Materials and Methods

2.1 PATIENT-DERIVED OVARIAN CANCER XENOGRAFTS (OC-PDX)

2.1.1 Models

Clinical specimens (primary ovarian tumors, metastases, ascitic fluid) were obtained from patients undergoing surgery for ovarian tumor by laparotomy or paracentesis at the San Gerardo Hospital in Monza (Italy) and IEO Hospital (European Institute of Oncology) in Milan (Italy). Tumor specimens were engrafted into immunodeficient mice within 24h, as described below, or stored as frozen stocks (Masazza et al., 1991; Massazza et al., 1989; Ricci et al., 2014). The study protocol for tissue collection and clinical information was approved by the institutional review board and patients provided written informed consent authorizing the collection and use of the tissue for study purposes.

Detailed clinical and follow-up data were obtained from medical records at predefined intervals: post-surgery, after primary chemotherapy, at six-month intervals up to five years and annually thereafter. Patients underwent primary surgery of the ovary and disseminated disease for diagnosis, staging and debulking. Surgical staging was based on the FIGO (Fédération Internationale des Gynaecologistes et Obstetristes) classification. Optimal debulking was defined as less than 1 cm (diameter) residual disease, and sub-optimal debulking as more than 1 cm. Patients were followed up with a physical examination, including the pelvic examination and serum CA-125 assay. When there were abnormal findings a CT scan was done, and relapse was defined according to RECIST criteria (Response Evaluation Criteria In Solid Tumors) (Therasse et al., 2000) as tumor re-growth after a standard course of platinum-based primary chemotherapy.

A complete clinical response (cCR) was defined as resolution of all clinical and radiographic evidence of disease, and normal CA-125 after completion of first line chemotherapy, which was considered the last treatment. Persistent disease was defined as the lack of complete response to first-line chemotherapy. For patients who achieved a cCR, progression-free survival (PFS) was defined as the interval between the end of first-line

chemotherapy and first confirmed sign of disease recurrence. Overall survival (OS) was defined as the interval between the date of diagnosis and the date of death from any cause.

2.1.2 Animals

For all the studies reported, six- to eight-week-old athymic female NCr-nu/nu and SCID mice were obtained from Envigo Laboratories (Udine, Italy). NOD scid gamma (NSG) mice were bred in-house at the Mario Negri Institute. Mice were maintained under specific pathogen-free conditions, housed in isolated vented cages (IVC), and handled using aseptic procedures. For the syngeneic intraovarian model ID8, seven-week-old pathogen-free C57BL/6 were obtained from Envigo Laboratories (Udine, Italy). Procedures involving animals and their care were conducted in accordance with institutional guidelines that comply with national (Legislative Decree 26, March, 2014) and international laws and policies (EEC Council Directive 2010/63, August, 2013), in line with guidelines for the welfare and use of animals in cancer research (Workman et al., 2010). Animal studies were approved by the Mario Negri Institute Animal Care and Use Committee and Italian Ministerial decree no. 84-2013. Additionally, intensive *in vivo* training is required by Istituto di Ricerche Farmacologiche Mario Negri IRCCS guidelines to ensure respect of and compliance with the laws. The training program consists of lectures (12 hours), concerning animal welfare, and hands-on practical sessions (30 days) under the supervision of an expert.

2.1.2.1 Anaesthesia and euthanasia in mice

In order to transplant tumor fragments subcutaneously, animals were placed individually in a transparent acrylic chamber and anaesthetized using an automatic delivery system that provides a mixture of 3-4% isoflurane (Florane, Abbot Laboratories) in 1% oxygen. Anaesthetic depth was assessed by testing the pedal withdrawal reflex. At the end of each study, mice were euthanized by cervical dislocation. This technique used in physical euthanasia of small animals consists in applying pressure to the neck to dislocate the spinal

column from the skull or brain. Euthanasia was performed either at predetermined days (end of short-term treatment, 4 weeks), when subcutaneous tumors reached a volume of 1500 mm³ (maximum 10% of animal body weight) or when animals showed sign of discomfort (survival). Subcutaneous tumor samples and representative organs of the peritoneal cavity were then collected.

2.1.3 Ectopic tumor models

Patient-derived solid specimens from tumor masses (ovary and omentum) were dissected free of necrotic tissue. Working under sterile conditions, tumor fragments (2-4mm³) were transferred to a petri dish of 100mm, filled with medium RPMI 1640 (BioWest) supplemented with 50% fetal bovine serum (FBS) (Microgem), then transferred to a second petri dish containing RPMI 1640 supplemented with 20% FBS. Subsequently, fragments were rinsed in HBSS (BioWest) and prepared for transplantation (Masazza et al., 1991; Ricci et al., 2014). The subcutaneous transplant was performed in the right flank of mice under anaesthesia. Briefly, the skin was disinfected with Betadine and a 1-2 cm lateral skin incision performed to access the subcutis, where tumor fragments were placed using a sterile trocar. The incision was then closed with metal wound clips. For these ectopic models, tumor growth s.c. was measured with a Vernier caliper, and tumor weight (mg=mm³) was calculated as [length (mm) x width² (mm²)]/2. Measurements were acquired with software “*Study Director*” version 2.5 (Studylog System, Inc.)

To store and enlarge the biobank of OC-PDX, s.c tumors from 3-5 mice were collected, minced (2-4 mm³) and pooled together to avoid selection of subpopulations and to maintain heterogeneity. Fragments were then frozen in a solution containing 50% Cryoprotective Medium (Lonza) with 15% DMSO and 50% FBS and then stored in liquid nitrogen for future experiments, or transplanted serially in mice for further studies (i.e therapy).

2.1.4 Orthotopic tumor models

2.1.4.1 Intraperitoneal models

Patient-derived ovarian cancer cells from were obtained from patients' ascites.

Working under sterile condition, ascites fluids were centrifuged at 8000 g for 10 minutes at 4°C. Pellets of cells were resuspended in HBSS (BioWest) and again centrifuged. Then viable cells were counted by trypan blue exclusion with the aid of a Bürker chamber and resuspended in HBSS at the concentration of 5×10^7 cells/ml.

A suspension of 0.2 ml (10×10^6 cells) was injected intraperitoneally in the lower right quadrant of the mouse abdomen using a syringe with a 21 gauge needle. Animals were checked at least twice a week for tumor formation (abdominal distension) in the peritoneal cavity and killed when they presented signs of discomfort (survival), ascites was harvested and the volume recorded.

To store and enlarge the biobank of OC-PDX, ascites from 3-5 mice were collected, pooled and frozen in a solution containing 50% Cryoprotective Medium (Lonza) with 15% DMSO and 50% FBS and then stored in liquid nitrogen or transplanted serially in mice for further studies (i.e. therapy).

2.1.4.2 Intraovarian model ID8

Cell culture conditions

The murine ID8 cell line was obtained from MOSEC (mouse ovarian surface epithelial cells), isolated from the ovaries of virgin wild type mice and cultured repeatedly before transplantation into syngeneic recipient mice of seven weeks age (Greenaway et al., 2008).

Cells were resurrected from the cell bank by rapidly thawing the vial (to 37° in a water bath) and the viable cells counted by Trypan blue exclusion dye (Fluka Analytical) with the aid of a Burker chamber and transferred to a fresh tube. About 10 ml of fresh medium containing 10% of heat-inactivated FBS (Microgem) was added. After centrifugation, cells were transferred to a T25 tissue culture flask in 5 ml fresh culture medium containing

Dulbecco's Modified Eagle Medium (DMEM), 10% v/v FBS and 1% v/v L-glutamine. Cells were maintained in 5% CO₂ in air incubator and were passaged routinely twice a week to maintain logarithmic growth. Cell culture procedures were carried out aseptically in class II laminar flow cabinet and the cells were tested for Mycoplasma contamination, with qPCR, upon thawing. Cell lines were not maintained in culture for long periods in order to avoid changes in their growth and biological behaviour.

Four or five days before each study, cell cultures were split (1:10 to 1:20) and plated in 75 cm² flasks ensuring that they did not develop beyond semi-confluence. The culture medium was changed 24h before harvesting cells for injection into mice.

On the day of the injection, the medium was removed and the monolayer washed once with phosphate-buffered saline (PBS). PBS was then removed and the monolayer was overlaid with Trypsin–EDTA solution (0.05% w/v trypsin and 0.02% w/v EDTA in Ca²⁺/Mg²⁺-free PBS, Bio-West) and then poured off. After few minutes, the flask was tapped until the cells lifted away from the surface. Approximately 10 mL of complete medium containing FBS (to neutralize the trypsin) were added, and the suspension pipetted up and down in order to obtain a single-cell suspension. Cells were then transferred into a 50 mL polypropylene conical tube, pelleted by centrifugation (8000 g for 10 min), washed twice again with Ca²⁺/Mg²⁺-free Hank's balanced salt solution (HBSS) and pelleted each time.

Cells were counted using Trypan blue exclusion dye with the aid of a Bürker chamber and resuspended in HBSS at the concentration of 2×10^8 /ml.

Orthotopic intrabursa transplant

Cell suspensions were obtained from cell lines as described above.

Pathogen-free C57BL/6 mice were anaesthetized with isoflurane and placed on the surgery table warmed to 37°C. Animals were shaved on one side to allow rapid and clean surgery. Work was conducted in aseptic/sterile conditions. Briefly, the skin was disinfected with Betadine and a 1-2 cm lateral midline skin incision was performed to access the left ovary

and exteriorize the ovary and the oviduct. 1×10^6 ID8 cells were injected in 5-10 μ L HBSS under the bursa of the ovary of the mice, using a Hamilton syringe with a 26-gauge needle. The ovary was replaced in the peritoneal cavity, the incision closed with surgical thread and the skin with metal wound clips, then disinfected with Betadine (Decio and Giavazzi, 2016). Tumor formation was followed by magnetic resonance imaging (MRI), in collaboration with the experts of the Laboratory of Biology of Neurodegenerative Disorders of the Istituto di Ricerche Farmacologiche Mario Negri IRCCS (see Section 2.3.3.3).

2.1.4.3 Necropsy examination

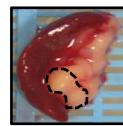
Both for intraperitoneal and intraovarian tumor models, the peritoneal cavity was macroscopically examined to ascertain the presence of tumor at necropsy (sacrifice and/or prefixed end-points). Macroscopical analysis of the organs of the peritoneal cavity (liver, diaphragm, omentum, pancreas, uterus/ovary, nodes) and lungs was performed by at least two independent scientists and tumor dissemination was rated using an arbitrary score, as reported:



0 = not infiltrated



1 = small masses



2 = evident masses



3 = completely
invaded



4 = extremely
invaded

Tumor burden was then calculated by summing the scores for each animal. The images of the liver, diaphragm, omentum, pancreas, uterus/ovary, lungs and lymph nodes were acquired with a macro-digital imaging system (MacroPATH; Milestone S.r.l.).

2.1.5 The biobank of OC-PDX

2.1.5.1 Patients' tumor collection

Patients' original tumors were snap frozen then stored at -80°C and formalin fixed for further analysis. When possible, patients' tumors were frozen in a solution containing 50% Cryoprotective Medium (Lonza) with 15% DMSO and 50% FBS and then stored in liquid nitrogen as primary stocks.

2.1.5.2 Subcutaneous tumor specimen collection

Subcutaneous tumors were collected when they reached a volume of 1500 mm^3 . Mice were sacrificed as previously described. A skin incision was then performed to access the tumor mass, which was collected using sterile scissors and forceps.

2.1.5.3 Ascites collection

Ascitic fluid and subsequent peritoneal washings (3 mL 0.9% NaCl) were harvested using a 5 mL syringe, collected separately in 15 mL tubes, and centrifuged at 8000 g for 10 minutes at 4°C . The volume of original ascites and pellet (representative of tumor burden) were recorded for each animal.

2.1.5.4 Sample storage

After collection, s.c. and abdominal tumor masses were minced, placed into tubes and immediately frozen in dry ice. Pellets and supernatants of ascites were separately collected and snap frozen in dry ice. Samples were stored at -80°C until analysis. For histopathological and immunohistochemical analysis, part of the subcutaneous tumor mass and organs cavity (liver, diaphragm, omentum, pancreas, lungs and uterus/ovary) were frozen in Optimal Cutting Compound (OCT) or fixed in 10% phosphate-buffered formalin (Bio Optica) for 24h prior to embedding in paraffin. Prolonged contact with formalin causes excessive crosslink formation and increasing loss of antigenicity. If samples could not be processed to paraffin blocks after 24h in formalin, they were transferred to 70%

ethanol for holding until the samples could be put on the processor. Samples were then washed twice with 100% ethanol (absolute ethanol) and embedded in paraffin with the aid of a microwave rapid tissue processor (Histos5, Milestone S.r.l.).

2.1.5.5 Blood sample collection and storage

Blood samples were collected from the retro-ocular plexus of anaesthetized mice. At the end of the collection, mice were immediately sacrificed by cervical dislocation.

Plasma was collected using 10% EDTA disodium salt (1:50 final volume) and then centrifuged at 12000 g for 10 minutes at 4°C. Blood serum was collected without any anticoagulant, warmed at 37°C for 30 minutes and then centrifuged at 12000 g for 10 minutes at 4°C. The supernatant was collected and stored at -80°C.

2.2 MOLECULAR ANALYSIS

2.2.1 Nucleic Acid Extraction

RNA isolation

Frozen fragments of patients' original tumors, ascites pellet and subcutaneous tumor tissues were placed into 2 mL microcentrifuge tubes containing one stainless steel bead (5 mm mean diameter) and 1 mL QIAzol Lysis Reagent (Qiagen). QIAzol Lysis Reagent is a monophasic solution of phenol and guanidine thiocyanate, which in addition to lysing action prevents the activity of RNases. Tubes were then placed in the TissueLyser LT Adapter (Qiagen) and the instrument was switched on at 20-30 Hz until no tissue debris was visible (about 2 minutes). Tubes containing the homogenates were placed on the bench top at room temperature (25°C) for 5 minutes. The homogenates were then transferred to new 2 mL microcentrifuge tubes and 200 µL chloroform were rapidly added. Tubes were shaken vigorously for 15 seconds and left on the bench top for about 2 minutes to favour the extraction of RNA. Tubes were then centrifuged at 12000 g for 15 minutes at 4°C to separate the phases: an upper colourless aqueous phase containing RNA; a white

interphase (DNA); and a lower organic phase containing protein. The aqueous phase was transferred into 2 mL collection tubes.

RNA purification was performed using the RNeasy[®] mini Kit along with the QIAcube[®] robotic workstation (Qiagen). According to the RNeasy[®] mini Kit protocol, 350 μ L of ethanol 70% were added to the aqueous phase, creating conditions that promote selective binding of RNA to the column. The samples were then applied to the RNeasy[®] mini spin columns and centrifuged for 15 seconds at 8000 g. After centrifugation, contaminants were washed away using RPE and RTW buffers and samples were again centrifuged. Finally, the total RNA was eluted in 30 μ L RNase-free water. At the end of the method, collection tubes containing the purified RNA were securely capped and stored at -80°C until analysed.

DNA isolation

Genomic DNA from frozen fragments of patients' original tumors, ascites pellets and subcutaneous tumor tissues were extracted using Maxwell[®] 16 Tissue DNA purification kit, to be used with the Maxwell[®] 16 Instrument for automated purification of genomic DNA.

Frozen samples of approximately 30 mg were placed in the #1 well of the pre-dispensed cartridge (Figure 2.1) after have removed the seal. In each cartridge, a plunger was placed in the #7 well. Cartridges containing samples and plungers were transferred onto the Maxwell[®] 16 Instrument platform. In parallel, one blue elution tube for each cartridge was placed into the elution tube slots at the front of the platform, with 300 μ L of elution buffer in each blue tube.

At the end of the automated run, genomic DNA of each sample was eluted in the elution buffer and collected. DNA samples were stored at -20°C until analysed.

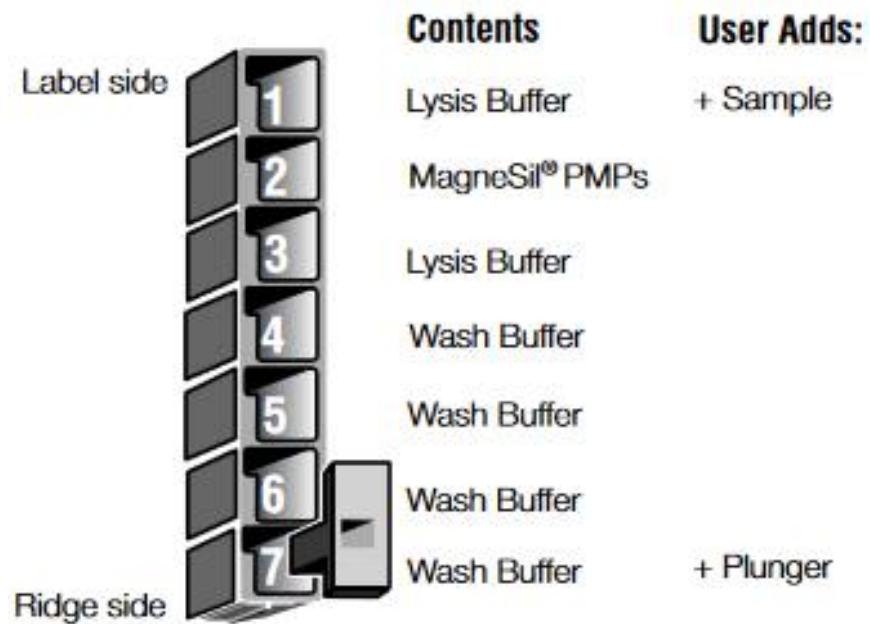


Figure 2.1 Predispensed cartridge of Maxwell ® 16 Tissue DNA purification kit.

30 mg of tumor tissue were placed in Lysis Buffer in #1 well on the label side of the cartridge, plunger in Wash Buffer in #7 well on the ridge side. #2 well from #6 well contained different reagent buffers to perform the automated run of extraction.

Analysis of DNA and RNA concentration and purity by Nanodrop® Spectrophotometer

Concentration and purity of nucleic acid samples were determined by spectrophotometric analysis (Nanodrop® Spectrophotometer). Before starting the software module, both the top and the bottom sensors of the Nanodrop® Spectrophotometer were cleaned with a tissue moistened with ddH₂O to remove any dried samples that might be present. Then 1 µL of RNase-free water was pipetted onto the bottom sensor to calibrate the instrument. The sensors were then wiped and 1 µL of purified DNA or RNA solution was loaded. The absorbance of DNA and RNA samples was measured at 260 nm, 280 nm, and 230 nm. The nucleic acid concentration was calculated using the Beer-Lambert law, which relates the amount of light absorbed to the concentration of the absorbing molecule.

The 260/280 and 260/230 ratios were calculated to determine the purity of nucleic acids. 260/280 = nucleic acid and proteins/proteins only. 260/230 = nucleic acid and contaminants/contaminants only. The optimum value for both 260/280 and 260/230 is between 1,7 and 2,1.

Analysis of RNA integrity by Agilent Bioanalyzer®

The Agilent 6000 Nano Assay was used to check for RNA integrity (Agilent Bioanalyzer®). This assay is similar to gel electrophoresis in concept, but it is more efficient and only requires a very small amount of sample (25-500 ng). 1 µL of each total RNA sample was loaded into each of the 12 sample wells in the RNA Nano Chip by Agilent Technologies. The chip contains an interconnected set of microchannels in which nucleic acid fragments are sieved by size as they are driven through it by an electrical current. Results are either shown as an electropherogram image or as bands on a gel. To determine RNA integrity, Agilent Technologies introduced the RNA Integrity Number (RIN). Generally, RIN numbers greater than 6 are considered acceptable for further RealTime PCR analyses.

2.2.2 Next Generation Sequencing

Next Generation Sequencing was conducted on a panel of 26 OC-PDX, in collaboration with AstraZeneca, Bioscience, Oncology Translational Sciences, IMED Biotech Unit, Waltham, MA, US.

Library construction and next generation sequencing (NGS)

Two hundred nanograms of purified genomic DNA were used for NGS library construction. Libraries were generated using the Kapa Biosystems HyperPrep kit following the manufacturer's protocol. All libraries were visualized on the Agilent TapeStation and the concentration was determined using the Kapa Biosystems NGS Library Quantification qPCR kit.

Exome sequencing and variant calling

Whole genome libraries were pooled together and used for the exome hybridization capture using xGen®Exome Research Panel v1.0 (Integrated DNA Technologies). Libraries were sequenced on the Illumina HiSeq 4000 platform (2 x 150) using TruSeq SBS (sequencing by synthesis) reagents (Illumina). The NGS data were aligned and analysed within the BCBio framework (<https://bcbio-nextgen.readthedocs.org/en/latest/>) using an AstraZeneca-developed variant calling algorithm (<https://github.com/AstraZeneca-NGS/VarDict>) (Lai et al., 2016).

For this PhD thesis the focus was on those aberrations and mutations in a set of genes previously described as being mutated in ovarian cancer (e.g. *TP53*, *KRAS*, *BRAF*, *PIK3CA*, *CTNNB1*, *PTEN*) and genes belonging to the HR DNA repair pathway (e.g. *BRCA1/2* and others from Coleman RL et al, Lancet 2017 and reported in Table 1.1 Introduction). For these genes, Sanger sequencing was performed to validate mutations.

2.2.3 Sanger validation

To validate the results from the Next Generation Sequencing analysis, *ad hoc* Sanger sequencing was performed for each mutation of interest, both on patients' original tumors and samples derived from OC-PDX.

PCR reaction

For each tumor model found to be mutated, 50 ng of DNA, extracted and quality checked as reported in Section 2.2.1, was amplified by GoTaq® PCR Core System (Promega), accordingly to manufacturers' instruction.

PCR reaction mix components	Single reaction (µL)
5X Colourless GoTaq® Flexi Buffer	10
10 uM specific forward primer	2
10 uM specific reverse primer	2
PCR Nucleotide Mix, 10 mM each	1
25 mM MgCl ₂	5
GoTaq® Hot Start Polymerase (5u/ul)	1
H ₂ O	9

Ad hoc specific primer pairs tagged with M13F and M13R were chosen using PRIMER-3 software (<https://primer3plus.com/>).

The primer specificity for human DNA and not murine DNA was verified using NCBI BLAST: Basic Local Alignment Search Tool (<https://blast.ncbi.nlm.nih.gov/Blast.cgi>) and optimal cycling conditions were verified by detecting single-band amplicons of the PCR products with a 1.5% agarose gel. PCR amplification of genomic DNA was done in a thermocycler (2720 Thermal Cycler, Applied Biosystem) following the conditions reported below.

Thermal Conditions for BRCA1 and BRCA2 primers	Initial denaturation	PCR 35 cycles			Final extension
		Denaturation	Annealing	Extension	
Temperature (°C)	94	94	53	72	72
Time	2 min	15 sec	30 sec	45 sec	5 min

Thermal Conditions for CTNNB1 exon 3	Initial denaturation	PCR 35 cycles			Final extension
		Denaturation	Annealing	Extension	
Temperature (°C)	94	94	55	72	72
Time	2 min	15 sec	30 sec	45 sec	5 min

Thermal Condition for PIK3CA exon 10	Initial denaturation	PCR 35 cycles			Final extension
		Denaturation	Annealing	Extension	
Temperature (°C)	94	94	57	72	72
Time	2 min	15 sec	30 sec	45 sec	5 min

Thermal Condition for PPP2R1A exons 5-6	Initial denaturation	PCR 3 cycles			PCR 3 cycles			PCR 3 cycles			PCR 35 cycles			Final extension
Temperature (°C)	94	94	64	70	94	61	70	94	58	70	94	57	70	70
Time	2 min	15 sec	30 sec	30 sec	15 sec	30 sec	30 sec	15 sec	30 sec	30 sec	15 sec	30 sec	30 sec	5 min

Thermal Condition for all the other primers	Initial denaturation	PCR 35 cycles			Final extension
		Denaturation	Annealing	Extension	
Temperature (°C)	94	94	60	72	72
Time	2 min	15 sec	30 sec	45 sec	5 min

PCR product purification

Amplified DNA was purified with Illustra™ GFX PCR DNA and Gel Band Purification kit (GE Healthcare) following the manufacturer's instructions. Briefly, 500 µl of capture buffer were added to each sample and transferred to a GFX column, centrifuged at 13000 g for 30 seconds. The flow-through was discarded. Then 500 µl of wash buffer were added to each column, centrifuged at 13000 g for 30 seconds, the flow-through discarded and each column placed into a new 1.5 ml collection tube. Elution buffer (20 µl) was added to each column directly to the top of the glass fibre matrix. Columns were finally centrifuged at 13000 g for 1 minute to recover purified DNA.

DNA was then quantified with a Nanodrop® Spectrophotometer (see Section 2.2.1) and prepared to be sequenced.

Sequencing of amplified DNA

The sequencing of PCR products was performed as a service by Microsynth SeqLab (Switzerland). DNA was prepared at 6 ng/µl, in a volume of 12 µl, to obtain a total amount of 72 ng.

Primer solution (3 µl of 10 µM primer) was added to the DNA template, keeping separate the tube with DNA and forward primer and the tube with DNA and reverse primer.

Sequencing results consisted of an electropherogram for each reaction. Electropherograms were then analysed and mutations confirmed using Sequencer 5.1 software and FinchTV software.

All the genes and primer pairs sequenced are reported in Table 2.1.

GENE	MUTATION	PROTEIN	FORWARD PRIMER	REVERSE PRIMER
TP53	c.3384eIT	p.F113fs	GTAAAACGACGGCCAGTGAAGCTCCAGAAATGCCAG	CAGGAAACAGCTATGACCCGACAGGAAAGCCAAAGGGTGA
TP53	c.470T>A	p.V157D	GTAAAACGACGGCCAGTGTTCCTTATCTGTCACTTGTGC	CAGGAAACAGCTATGACCCGACCTGACAAACCCCTTTA
TP53	c.514G>T	p.V172F	GTAAAACGACGGCCAGTGAAGCTCCCAAGATGCCAG	CAGGAAACAGCTATGACCCGACAGGAAAGCCAAAGGGTGA
TP53	c.524G>A	p.R175H	GTAAAACGACGGCCAGTGTTCCTTATCTGTCACTTGTGC	CAGGAAACAGCTATGACCCGACCTGACAAACCCCTTTA
TP53	c.523C>G	p.R175G	GTAAAACGACGGCCAGTGAAGCTCCCAAGATGCCAG	CAGGAAACAGCTATGACCCGACAGGAAAGCCAAAGGGTGA
TP53	c.527G>T	p.C176F	GTAAAACGACGGCCAGTGTTCCTTATCTGTCACTTGTGC	CAGGAAACAGCTATGACCCGACCTGACAAACCCCTTTA
TP53	c.641A>G	p.H214R	GTAAAACGACGGCCAGTGAAGCTCCCAAGATGCCAG	CAGGAAACAGCTATGACCCGACAGGAAAGCCAAAGGGTGA
TP53	c.993+1G>A splice site		GTAAAACGACGGCCAGTCAAGGGTGGTGGGAGTGA	CAGGAAACAGCTATGACCCGCCCAATTCAGGTTAAAACA
TP53	c.844C>T	p.R282W	GTAAAACGACGGCCAGTCAAGGGTGGTGGGAGTGA	CAGGAAACAGCTATGACCCGCCCAATTCAGGTTAAAACA
TP53	c.782+1G>A splice site		GTAAAACGACGGCCAGTGTTCCTTGTCCACAGGTTCTCC	CAGGAAACAGCTATGACCCGGTCAAGGCAAGCAGAGG
KRAS	c.35G>A	p.G12D	GTAAAACGACGGCCAGTCTTAAGCGTCCGATGGAGGAG	CAGGAAACAGCTATGACCCAGATGGTCTCCACCAAGTAA
PIK3CA	exon 10		GTAAAACGACGGCCAGTGAAGATGTAATTTGCTTTTCTGT	CAGGAAACAGCTATGACCCACATGCTGAGATCAGCCAAA
PIK3CA	exon 21		GTAAAACGACGGCCAGTGTTCCTTGTACGAAAAGCCTCT	CAGGAAACAGCTATGACCCATGCTGTGTTATGGATTGTGC
BRAF	exon 11		GTAAAACGACGGCCAGTGAAGGGGATCTTCTCTGTATCC	CAGGAAACAGCTATGACCCGAAAACCTTTTGGAGGATCCTGA
BRAF	exon 15		GTAAAACGACGGCCAGTAAACACATTTCAAAGCCCCAAA	CAGGAAACAGCTATGACCCCTGATTTTGTGAAATACTGGGAAT
CTNNB1	exon 3		GTAAAACGACGGCCAGTAAAGTAAACATTTCCAATCTACTAATGC	CAGGAAACAGCTATGACCCCTCAAAAATGCTTCTGACTTTCA
PPP2R1A	exon 5		GTAAAACGACGGCCAGTACTTCCGGAAACCTGTGGTCT	CAGGAAACAGCTATGACCCAGGAAAGCAAAACTCACT
PPP2R1A	exon 6		GTAAAACGACGGCCAGTGTTCCTGCCCATGAAAGAGA	CAGGAAACAGCTATGACCTTATTTGCTCAACGCCCAAT
BRC1	c.168C>T	p.Q363*	GTAAAACGACGGCCAGTGAAGCCCTTCACTCTGAGGAT	CAGGAAACAGCTATGACCCGCTGCTTATAGGTTCAAGCTTCC
BRC1	c.181T>G	p.C61G	GTAAAACGACGGCCAGTGGCATGCTGAAACTTCTCAACCA	CAGGAAACAGCTATGACCTTCTTCTGCTGCTGCTTCTCC
BRC1	c.190T>C	p.C64R	GTAAAACGACGGCCAGTGGCATGCTGAAACTTCTCAACCA	CAGGAAACAGCTATGACCTTCTTCTGCTGCTGCTTCTCC
BRC1	c.1088delA	p.N363fs	GTAAAACGACGGCCAGTCCGACTCCACGACAGAAA	CAGGAAACAGCTATGACCCAGCTCCCAATCATGTGAGTCA
BRC2	c.3199A>G	p.T1067A	GTAAAACGACGGCCAGTGGAAATCAAGTCTCTGAAACATAACA	CAGGAAACAGCTATGACCCAGTAGAAAGTTCGTGTAATTTCTGGCT
BRC2	c.5722_5723delCT	p.L1908fs	GTAAAACGACGGCCAGTGGCCACCTGGCAATTTAGGATAG	CAGGAAACAGCTATGACCTGACACTGACTGACTTATGAAAGCTTCCC
BRC2	c.6212G>C	p.S2071T	GTAAAACGACGGCCAGTACGAAATTCAGACCAAGCTCA	CAGGAAACAGCTATGACCTGTTGAAATTCAGAGAGATATGGAGA
BRC2	c.7177dupA	p.M2399fs	GTAAAACGACGGCCAGTAAATTTTACCGCACTGGTCA	CAGGAAACAGCTATGACCACTTTGGTGTGGCTGTGT
ATM	c.6067G>A	p.G2023R	GTAAAACGACGGCCAGTACATAACATTAGAGTTGGGAGTTACA	CAGGAAACAGCTATGACCCGATGATTCCTGCTGCTGGGGGT
ATM	c.6167C>T	p.P2056L	GTAAAACGACGGCCAGTGTGTGGGAGGGAAGATG	CAGGAAACAGCTATGACCTTGCATCCCTCTCTGCTCAGG
ATM	c.6660C>G	p.L2223M	GTAAAACGACGGCCAGTGTCTGTGTCACTACAAAAGTTCCT	CAGGAAACAGCTATGACCCAGGAAAGTCAAGAGTAAAGTACA
ATRX	c.2595C>G	p.H865Q	GTAAAACGACGGCCAGTACGACAAACCCAGTCTGAGTC	CAGGAAACAGCTATGACCTGTTTTTGTGATGCTGCTCT
ATRX	c.2093delA	p.K698fs	GTAAAACGACGGCCAGTGTGGACTGTGGACAGGAAACA	CAGGAAACAGCTATGACCTGTGACTGACTCTCTGCTCAACC
EGFR	c.2884C>T	p.R962C	GTAAAACGACGGCCAGTACTAGCTGGCCAAAGACAGAA	CAGGAAACAGCTATGACCTGAGGGCTTGCCTTAATGGG
EGFR	c.3282T>A	p.Y110N	GTAAAACGACGGCCAGTGGTTCAGAAACCCAGGGATCC	CAGGAAACAGCTATGACCCAGGCTAAATTTGGTGGCTGC
FANCA	c.2134G>A	p.E12K	GTAAAACGACGGCCAGTACTTTCAGCGGAGGGCGGA	CAGGAAACAGCTATGACCCCAAAACAGACTGTGGCAGC
FANCA	c.33G>C	p.S11S	GTAAAACGACGGCCAGTGGCCGACCAATAGGAAAGG	CAGGAAACAGCTATGACCCGGGGAAGGGATCGGGGA
FANCB	c.1004G>A	p.G35E	GTAAAACGACGGCCAGTGTGACACTACATGAAACAAAGGACT	CAGGAAACAGCTATGACCCAGGTCAAAAGCTTTTGGAGACT
PALB2	c.850A>C	p.T284P	GTAAAACGACGGCCAGTATTCACCAACTGCCCAACC	CAGGAAACAGCTATGACCCGCTCTAAATTAGAACTTTGGGGC
PTEN	c.388C>T	p.R130*	GTAAAACGACGGCCAGTGTGTTATCTTTTACCACAGTTGAC	CAGGAAACAGCTATGACCTCCAGGAAAGGAAACA

Table 2.1 Genes and primer pairs used in Sanger validation.

Most frequently mutated genes in ovarian carcinoma and belonging to the homologous recombination deficiency (HRD) pathway were analysed.

2.2.4 RealTime PCR

FLT1 gene (VEGFR1), *KDR* gene (VEGFR2), *FLT4* gene (VEGFR3), *KIT* gene (c-Kit protooncogene Receptor Tyrosine Kinase) and *PDGFRA* gene (PDGFR-Alpha) transcripts were analysed by real-time reverse transcription-PCR (RT-PCR) using *TaqMan® Gene Expression Assay* (Applied Biosystems, Monza, Italy).

Briefly, total RNA was extracted from tumor cells and tumor masses snap frozen in liquid nitrogen with Trizol® protocol (Invitrogen, Life-Technologies, Monza, Italy) as described in Section 2.2.1 then purified and reverse-transcribed with High Capacity cDNA Reverse Transcription Kit (Applied Biosystems™) to cDNA, according to manufacturer's instructions.

RT reaction

2 × RT master mix was prepared following the instruction provided by the High Capacity cDNA Reverse Transcription Kit (Applied Biosystems™), which is intended for the quantitative conversion of up to 2 µg of total RNA to single-stranded cDNA for each single reaction.

Component	Volume/Reaction (µL)
10 × RT Buffer	2.0
25 × dNTP Mix	0.8
10 × RT Random Primers	2.0
Multiscribe™ Reverse Transcriptase	1.0
Nuclease-free H ₂ O	4.2
Total per Reaction	10.0

All required reagents were collected into a microcentrifuge tube and gently mixed. 10 µL of 2 × RT master mix were pipetted into each well of a 96-well reaction plate kept in a tabletop cooler box. 500 ng – 1 µg of total RNA were pipetted into the 96-well reaction plate containing the 2 × RT master mix and enough nuclease-free water was added to reach the final volume of 20 µL. The plate was then sealed, briefly centrifuged to spin

down the contents and to eliminate any air bubbles, and finally load onto the thermal cycler.

Thermal cycler conditions were programmed as described below.

	Step 1	Step 2	Step 3
Temperature (°C)	25	37	85
Time	10 min	120 min	5 min

At the end of the procedure, the plate was stored at -20°C until used for PCR analysis. RT reactions were diluted 1:20 in ddH₂O before qPCR reactions.

qPCR reaction

The expression of human receptors VEGFR1, VEGFR2, VEGFR3, c-Kit and PDGFRA was determined using qPCR and human ACTB (beta-actin) was chosen as a housekeeping gene.

Experiments were run in triplicate.

For the amplification and quantification of a chosen target, the TaqMan[®] probes labelled with FAM[™] reporter dye on the 5' end and the quencher dye on the 3' end were purchased from Applied Biosystems[™] along with the primers and the Universal PCR Master Mix. The qPCR reaction mix was prepared following the instructions provided by the TaqMan[®] Gene Expression Assay protocol, as reported below.

PCR reaction mix components	Single reaction (µL)
2 × TaqMan [®] Universal PCR Master mix*	5
20 × primers	0.5
RNase-free water	0.5
Total per Reaction	6

* TaqMan[®] Universal PCR Master mix contains AmpliTaq Gold[®] Polymerase, Uracil-DNA Glycosylate, dNTPs with dUTP, ROX[™] dye (passive internal standard), and optimized buffer components.

The qPCR was run in a 384-well plate at a final volume of 10 μL in each well. To aid in loading the plate, a robotic liquid handling system (epMotion[®] 5075 TMX) was used. epMotion[®] 5075 transferred 6 μL of mix and 4 μL of diluted cDNA sample in each well of 384-well plate to reach the predetermined final volume of 10 μL .

The default thermal cycling protocol was used for all target and reference genes.

	Step 1	PCR 40 cycles	
Temperature ($^{\circ}\text{C}$)	95	95	60
Time	10 min	15 sec	1 min

Amplification reactions were performed with the 7900HT Fast RealTime PCR System (Applied Biosystems[™]). Quantitative PCR data were subsequently analysed using the Sequence Detection System (SDS) version 2.3 (Applied Biosystems[™]).

VEGFR1, VEGFR2, VEGFR3, c-Kit and PDGFRA mRNA were normalized to beta-actin housekeeping gene: $\Delta\text{Ct} = \text{Ct}_{\text{target}} - \text{Ct}_{\text{housekeeping}}$ (Schmittgen and Livak, 2008), mean \pm SD of three replicates from one experiment representative of three.

2.2.5 Fluidigm

The Fluidigm platform allowed the analysis of expression levels of a broader panel of genes of interest, using chip supports. Experiments were run in biological triplicates and technical duplicates.

All the procedures were conducted in collaboration with AstraZeneca, Bioscience, Oncology, IMED Biotech Unit at the CRUK Institute of Cambridge.

PreAmp pool and assay plate preparation

The panel of chosen genes was prepared in two 96-well plates assay (Table 2.2 and 2.3).

TaqMan[®] Gene expression assays were supplied at 20x. The pooled assays were diluted in 1x TE buffer so that each assay was run at a final concentration of 0.2x.

To prepare the PreAmp pool, 1 μ l of each TaqMan[®] probe was added to a 1.5 ml tube and made up to a volume of 100 μ l with TE buffer. 7.5 μ l of each assay mix was dispensed into a 96 well plate following the assay scheme plate reported above.

cDNA preamplification

For each sample, cDNA was obtained as described in Section 2.2.4 and pre-amplified. Briefly, 200 μ l of PreAmp TaqMan[®] Master Mix was added to 100 μ l PreAmp pool+TE and then dispensed into a 96 well plate. cDNA was added to each well, following the designed sample plate layout. The plate containing cDNA was run on a thermal cycler as previously reported.

	Step 1	Step 2 14 cycles		Step 3
Temperature (°C)	95	95	60	4
Time	10 min	15sec	4 min	hold

Successively primed chip (IFC) was loaded.

Briefly, the control line fluid was injected into the two control line fluid reservoirs on the IFC (see Figure 2.2). Then the chip was loaded into the instrument and the prime script run for 10 minutes. At this point, the chip was ready to be loaded with samples and assays as described in Figure 2.2.

Finally, the IFC was run on BioMark system as reported below.

Step	Thermal Mix			UNG	Hot Start	PCR 40 cycles	
Temperature (°C)	50	70	25	50	95	95	60
Time	2 min	30 min	10 min	2 min	10 min	15 sec	1 min

Data analysis

For Fluidigm, data analysis was performed in collaboration with Dr. Paola Ostano and Dr. Giovanna Chiorino of the Cancer Genomics Laboratory, Fondazione Edo and Elvo Tempia Valenta, Biella, Italy.

For each biological replicate, the technical replicate Ct mean was calculated. Then the mean was normalized to housekeeping genes (IPO8 and HPRT1 for human; Hprt1 and Ipo8 for mouse) and $\Delta Ct = Ct_{\text{target}} - Ct_{\text{housekeeping}}$ assessed.

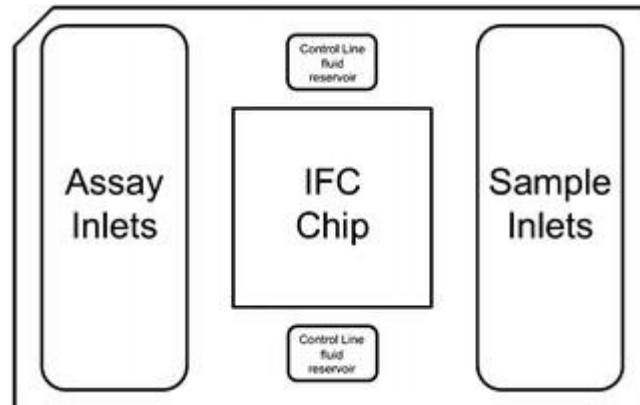


Figure 2.2 Diagram of a Fluidigm 96.96 primed chip (IFC) layout.

Control line fluid was injected into each of the control line fluid reservoirs and primed using the IFC Controller (Control line fluid is pressurized causing it to enter the chip allowing control of various valves). Ninety-six assays and 96 samples were then loaded into their respective inlets. Assays and samples were then forced into the IFC chip using the IFC controller.

Assay Plate 1												
	1	2	3	4	5	6	7	8	9	10	11	12
A	18S	BRCA2	CDH2	CXCL11	DMC1	GADD45A	HNF4A	IL6	MDC1	NFE2L2	H18S	RAD51D
B	ABL1	CA9	CHEK1	CXCL12	ELANE	GAPDH	HPRT1	IL6R	ME1	PDK1	PRKDC	RAD52
C	ANGPT2	CCL11	CPT1A	CXCL14	ENO2	HSP90B2P	HUS1	IL8	MLH1	PDK4	PSAT1	TP53
D	ARG1	CCL17	CPT1B	CXCL2	EPAS1	H2AFX	IDH2	IPO8	MMP7	PFKFB3	RAD21	RAD54L
E	ATF4	CCL2	CSF1	PARP1	ESR1	HGF	IL10	ITGAM	MMP9	PFKFB4	RAD50	S100A4
F	ATM	CCL22	CX3CL1	CXCL5	FEN1	HIF1A	IL12A	KEAP1	MRE11A	PGF	RAD51	SCD
G	BLM	CCL5	CXCL1	CXCL9	FGF1	HK2	IL1B	LIG1	NBN	PHGDH	RAD51B	SLC16A3
H	BRCA1	CDH1	CXCL10	PLAUR	FLT4	HMGCS1	IL23A	LIG4	NCF1	PIGF	RAD51C	SLC1A4

Assay Plate 2												
	1	2	3	4	5	6	7	8	9	10	11	12
A	SLC25A10	TP53BP1	Angpt2	Cpt1a	Cxcr1	Esr1	Hnf4a	Il6ra	Mmp9	Pgf	Slc25a10	Tnf
B	SOD1	TXNIP	Arg1	Cpt1b	Cxcr4	Fgf1	Hprt	Cxcr2	Ncf1	Phgdh	Sod1	Txnip
C	SOD2	VEGFA	Atf4	Csf1	Ackr3	Gadd45a	Idh2	Ipo8	Nfe2l2	Pigf	Sod2	Vegfa
D	SOD3	XRCC2	Car9	Csf1r	Dll4	Gapdh	Il10	Itgam	Nrp1	m18S	Sod3	SERPINE1
E	SREBF1	XRCC3	Cd17	Cxcl1	Elane	Hgf	Il12a	Kdr	Pdk1	Psat1	Srebf1	Serpine1
F	TFRC	XRCC4	Cd2	Cxcl10	Eng	Hif1a	Il1b	Keap1	Pdk4	Scd1	Tek	IGFBP3
G	TGFB1	XRCC5	Cd22	Cxcl14	Eno2	Hk2	Il23a	Me1	Pfkfb3	Slc16a3	Tfrc	Igf1r
H	TNF	XRCC6	Cd5	Cxcl2	Epas1	Hmgcs1	Il6	Mmp7	Pfkfb4	Slc1a4	Tgfb1	Plaur

Table 2.2 Panel of genes for Fluidigm prepared in a 96-well plate assay.

Capital case letters: human genes; lower case letters: murine genes; red letters: housekeeping genes.

2.2.6 RNA sequencing

In collaboration with Novogene: Genome Sequencing Company (Chula Vista, California), whole transcriptome shotgun sequencing was performed. Briefly, RNA sequencing uses next generation sequencing techniques to reveal the presence and quantity of RNA in a biological sample at a given moment. In this way, the continuous modifications of the cellular transcriptome can be analysed, by looking at alternative gene spliced transcripts, post-transcriptional modifications, gene fusions, mutations and changes in gene expression over time in different groups of treatments. With this technique, it is possible also to examine different populations of RNA (total and small RNA).

To perform this analysis, RNA samples, extracted and quality checked as reported in Section 2.2.1, were prepared at 50 ng in 50 µl and sent to Novogene for a 150 base pair-paired end sequencing with 50 million reads per sample.

RNAseq data analysis was performed in collaboration with AstraZeneca, Bioscience, Oncology Translational Sciences, IMED Biotech Unit, Waltam, MA, US.

2.3 *IN VIVO* PRECLINICAL STUDIES

2.3.1 Animals for preclinical studies

For preclinical testing, six- to eight-week-old female NCr-nu/nu mice or seven-week-old pathogen-free C57BL/6 for the syngenic intraovarian model ID8 were obtained from Envigo Laboratories. Mice were maintained under specific-pathogen-free conditions, housed in isolated vented cages, and handled using aseptic procedures. Procedures involving animals and their care were conducted in conformity with institutional guidelines that comply with national (Legislative Degree 26, March, 2014) and international (EEC Council Directive 2010/63, August, 2013) laws and policies, in line with guidelines for the welfare and use of animals in cancer research (Workman et al., 2010). Animal studies were approved by the Mario Negri Institute Animal Care and Use Committee and Italian

Ministerial decree no. 84-2013.

2.3.2 Drug preparation and administration

Cisplatin (cis-diamminedichloroplatinum, DDP, Sigma-Aldrich, Milan, Italy) was dissolved in 0.9% NaCl and administered intravenously (i.v) at the dose of 4 mg/kg, in a volume of 10 ml/kg. DDP was administered every week for 3 cycles. DDP was used as a reference drug.

Olaparib (OLA, AZD2281, AstraZeneca, Alderley Park, Macclesfield, UK) was dissolved in 10%v/v DMSO in 10%w/v Kleptose (HP- β -CD) in purified deionized water and administered by oral gavage (p.o) daily at the dose of 100 mg/kg, in a volume of 20 ml/kg.

Cediranib (CED, AZD2171, AstraZeneca, Alderley Park, Macclesfield, UK) was suspended 0.5%w/v HPMC (hydroxyl propyl methyl cellulose) 0.1% Tween80 (Sigma-Aldrich, Milan, Italy) in deionised water, vortexed and stirred overnight prior to dosing. Cediranib was administered by oral gavage (p.o) daily at the dose of 3 mg/kg, in a volume of 10 ml/kg.

For a particular set of experiments (see Section 4.5, Chapter 4, Results), bevacizumab (Roche) and B20 4.1 (Genentech, provided by AstraZeneca) were tested along with the PARP inhibitor olaparib. Bevacizumab is an antibody that recognized selectively human VEGF, and B20 recognizes both human and mouse VEGF exhibiting with equal affinity (EC₅₀ 0.17 nmol/L for h-VEGF and EC₅₀ 0.17 nmol/L for m-VEGF) (Liang et al., 2006). Bevacizumab (BEV) was diluted in saline and administered at the dose of 5 mg/kg, i.v, once a week for 4 cycles; B20 was diluted in saline and administered at the dose of 5 mg/kg, i.v, twice and once a week for short-term treatment of 4 cycles.

2.3.2.1 Schedule of treatments

Olaparib and cediranib, alone or in combination, were administered every day for 5 days on and 2 days off (Q1x5), for four cycles (4 weeks, short-term treatment regimen) or until

tumor progression (maintenance regimen). In models that were very responsive (regression of tumor volume > -30%), treatments were stopped and tumor growth monitored.

2.3.3 Evaluation of treatment

2.3.3.1 Ectopic tumor models

For ectopic models (3-7 mice per group), tumor measurements were taken twice a week during and after treatments. Tumor growth s.c. was measured with a Vernier caliper, and tumor weight ($\text{mg}=\text{mm}^3$) was calculated as $[\text{length (mm)} \times \text{width}^2 (\text{mm}^2)]/2$.

Subcutaneous tumor-bearing mice were randomized at a calculated tumor volume of 280-330 mm^3 (300 mm^3 average) and assigned to treatment groups. Animals were euthanized when primary tumor volume reached approximately 1500 mm^3 and never beyond it exceeded 15% of animal body weight. Tumor-free mice at approximately 200 days post therapy were considered cured.

Treatment efficacy was expressed as best tumor growth inhibition: $\%T/C = (\text{median weight of treated tumors}/\text{median weight of control tumors}) \times 100$, and evaluated also from the tumor weight curve of individual mice using three independent parameters: the tumor weight at nadir (TW_{nadir}), the absolute growth delay (AGD) and the doubling time of tumor regrowth (DT_{regrowth}). TW_{nadir} is the smallest tumor volume measured after treatment. Where no regression was seen, TW_{nadir} was set as the weight at the start of treatment. AGD was calculated as the difference (in days) between the time to reach a target size of 1500 mm^3 in treated tumors and the average time to reach the same size in the control group. DT_{regrowth} was calculated from the exponential fit of the last part of the growth curve when there was a frank and persisting increase in tumor size.

Treatment efficacy was also expressed as % tumor variation after 4 weeks (day 28) and 12 weeks (day 100) of treatment: $\% \text{tumor variation} = [(\text{tumor volume day 28 or 100} - \text{tumor volume day 0}) / \text{tumor volume day 0}] \times 100$, considering day 0 as the day in which each mouse was randomized to treatment. Disease was considered progressive: tumor variation

> 20%; stable : -30% < tumor variation > 20%; regressive : tumor variation > -30% (Fournier et al., 2014).

2.3.3.2 Intraperitoneal tumor models

For intraperitoneal models, mice (8-11 mice per group) were monitored and checked twice a week for tumor formation (abdominal distension) in the peritoneal cavity. Mice were randomized to treatment at an advanced stage of disease (i.e. 25% of expected median survival time, MST) unless otherwise stated. For ethical reasons, survival was defined as the day of appearance of signs of distress, at which time mice were euthanized (Garofalo et al., 2003; Oliva et al., 2012; Ricci et al., 2014). At necropsy, the peritoneal cavity was macroscopically examined to ascertain the presence of tumor. Survival time was recorded and increment of lifespan was calculated: %ILS = [(median survival day of treated group – median survival day of control group) / median survival day of control group] x 100. Results were plotted as the percentage of survival against days after tumor transplant. Complete response, confirmed macroscopically at necropsy, was the absence of tumor in animals still alive 200 days after transplant.

2.3.3.3 Intraovarian model ID8

For the intraovarian tumor model ID8, mice (5-10 per group) were randomized at an advanced stage of disease (i.e. 25% of MST from previous experiments). In parallel two randomly selected mice were scanned by MRI and sacrificed to ascertain the presence of the tumor.

After 4 weeks of treatment, mice were scanned by MRI, and from that point on tumor burden and progression were monitored every two-four weeks until the median survival time was reached for each group. The appearance of signs of distress was considered as survival and mice were immediately sacrificed; a complete necropsy was performed, primary tumor in the ovary weighed and organs of the peritoneal cavity macroscopically scored (see Section 2.1.4.3). Survival time was recorded and increment of lifespan was

calculated: %ILS = [(median survival day of treated group – median survival day of control group) / median survival day of control group] x 100. Results were plotted as the percentage survival against days after tumor transplant.

Magnetic Resonance Imaging

Tumor formation was followed by MRI, in collaboration with the experts of the Laboratory of Biology of Neurodegenerative Disorders of the Istituto di Ricerche Farmacologiche Mario Negri IRCCS, Milan, Italy.

Briefly, animals were imaged under general gas anaesthesia (1.4% isoflurane in O₂). Respiratory rate and temperature were continuously monitored. Experiments were performed on a 7T Bruker Biospin 70/30 Avance III system, equipped with a 12 cm diameter gradient coil (400 mT/m maximum amplitude). A transmit cylindrical radiofrequency (rf) coil (7.2 cm inner diameter) and a receive surface rf (2×2cm) coil array positioned over the animal body were used.

In order to identify the tumor location, an initial axial image was first obtained using a rapid acquisition with relaxation enhancement (RARE) sequence (TR/TE=2000/36ms, RARE factor 8, Number of average 2, Field of View 30x30mm, Matrix 256x256, Slice thickness 1mm, Number of slices 16). The anatomical image was then acquired using a coronal RARE sequence triggered on respiration (TR/TE=4000/36ms, RARE factor 8, Number of average 2, Field of View 30x20mm, Matrix 256x176) with a different slice thickness from 0.8 to 1.1 mm depending on the extension of the tumor. Tumor volumes were manually calculated by an expert tracer using ITK-SNAP software (Yushkevich et al., 2006).

2.4 *EX VIVO* ANALYSIS

2.4.1 Histological and immunohistochemical analysis on hypoxia and tumor-associated vasculature

Histological and immunohistochemical analyses were performed in collaboration with an expert pathologist of the Department of Veterinary Medicine of the University of Milan and Mouse and Animal Pathology Lab (MAPLab) of the Fondazione Filarete, Milan.

Analyses were performed on subcutaneous tumors (s.c. models) and tumor masses at the ovaries (i.p. models) collected at the end of short-term treatment (4 weeks, 5 days on and 2 days off), 6 hours after the last received dose of drugs.

Antibodies used are listed in the table below.

Marker	Application	Clone	Supplier	Code	Clonality	Dilution
CD31	Detection of tumor vessel	SZ31	Dianova	DIA310	Rat monoclonal	1:100
Pimonidazole	Detection of hypoxia	-	Hypoxyprobe	PAb-2627AP	Rabbit polyclonal	1:700
CA9	Detection of hypoxia	-	LS biosciences	LS-B273	Rabbit polyclonal	1:2000

Pimonidazole and CA-9 were used to assess levels of hypoxia in the vehicle at random (VH at random, when available), VH, OLA, CED and COMBO treatment group (n=2-3/per group).

When possible, pimonidazole was administered 60 mg/kg, i.v, 30 minutes before the sacrifice of the mice. Tumors and organs were fixed in 10% neutral buffered formalin and paraffin embedded for histopathological analyses. 4 µm serial sections from each sample were routinely stained with Hematoxylin and Eosin for morphology and by immunohistochemistry for features shown above.

For immunohistochemistry, deparaffinization, rehydration and antigen retrieval were performed in a single step method: sections were immersed for 40' at 94°C in a pH 9 buffer solution (Dewax and HIER Buffer H, Thermo Scientific). Endogenous peroxidase

activity was blocked by incubating sections in 3% H₂O₂ for 15 min. To reduce nonspecific background staining, slides were rinsed and treated, for 30 min, with 10% normal serum from the species in which the secondary antibody was produced (rabbit serum for anti-CD31 and goat serum for anti-pimonidazole and anti-CA9) and then incubated for 1 hour at room temperature with the primary antibody.

An appropriate biotinylated secondary antibody (Vector Laboratories) was then added for 30 min and sections were labelled by the avidin-biotin-peroxidase (ABC) procedure with a commercial immunoperoxidase kit (Vectastain Standard Elite, Vector Laboratories). The immunoreaction was revealed with 3,3'-diaminobenzidine substrate (DAB, Vector Laboratories) for 5 minutes and sections were counterstained with Mayer's hematoxylin.

Digital Image Analysis.

The tumor-associated vasculature was evaluated by computing the number of CD31-positive vessels (Microvessel Density, MVD) and by measuring the CD31-immunopositive areas (Endothelial Area, EA, not considering vascular lumen) in 3 200x microscopic fields, randomly selected throughout the neoplastic tissue, using ImageJ software (Schneider et al., 2012). Tumor hypoxia was calculated by measuring the extension of pimonidazole- or CA9- intensely stained area in 2 50x microscopic fields, with Orbit.bio software (<http://www.orbit.bio>).

2.4.2 Histological and immunohistochemical analysis of HR DNA repair markers

Histological and immunohistochemical (IHC) analyses on γ H2AX were performed in collaboration with AstraZeneca, Oncology iMed Translational Science, Molecular Pathology Group at the Cambridge Science Park.

Briefly, subcutaneous tumors were collected at the end of short-term treatment (4 weeks, 5 days on and 2 days off), 6 hours after the last received dose of drugs. Tumors were fixed in 10% neutral buffered formalin and paraffin embedded for histopathological analyses. 4 μ m serial sections from each sample were routinely stained with Hematoxylin and Eosin for

morphology and by immunohistochemistry for features shown above. Subsequently, sections were deparaffinized in xylene and rehydrated using graded ethanol and analyses were performed with γ H2AX, using a Ventana BenchMark XT immunostainer.

Digital Image Analysis.

Foci of γ H2AX (% γ H2AX+ foci with a different pattern of expression) were evaluated 3 200x fields, randomly chosen across neoplastic tissue in VH, OLA, CED and COMBO group (n=2-3/per group). Whole slide scans were analysed with Aperio ImageScope Software.

2.5 STATISTICAL ANALYSES

Statistical analyses were done using Prism Software (Prism 7; GraphPad Software, La Jolla, CA). Differences in Kaplan Meier survival curves were analysed by the Log-Rank test. Differences in microvessel density (MVD), endothelial area (EA), foci of γ H2AX, gene expression and $-\Delta$ Ct values after treatment were analysed by the Kruskal Wallis test followed by Dunn's multiple comparison post-test.

CHAPTER 3.

Results

CHARACTERIZATION OF *IN VIVO* PATIENT- DERIVED OVARIAN CANCER XENOGRAPHS (OC-PDX)

3.1 THE PLATFORM OF OC-PDX

Part of the data presented in this section is reported in the manuscript entitled “Patient-Derived Ovarian Tumor Xenografts Recapitulate Human Clinicopathology and Genetic Alterations”, by Ricci/Bizzaro et al, Cancer Res, 2014; DOI: 10.1158/0008-5472.CAN-14-0274.

In the Department of Oncology, where this PhD research has been carried out, a platform of transplantable patient-derived ovarian cancer xenografts (OC-PDX) has been established over the last years. We have previously demonstrated that our bio-bank of OC-PDX comprise all the main subtypes of human ovarian carcinomas and retain the features of patients’ original tumors, in terms of biological behaviour, histopathological and molecular profiling. Moreover, the availability of orthotopic intraperitoneally growing OC-PDX, able to disseminate in the organs of the peritoneal cavity of mice, is a powerful tool to resemble the typical pattern of dissemination seen in patients, with the formation of ascites and carcinomatosis (Ricci et al., 2014).

One of the tasks of this PhD project was to establish new OC-PDX directly from patients’ fresh tumor tissue, thus enlarging the existing platform.

To date, the platform of OC-PDX available in the Department of Oncology of the Mario Negri Institute includes 43 models, 34 previously described (Ricci et al., 2014) and 9 newly established, which I directly contributed to characterize during my PhD research project.

Our collaboration with the San Gerardo Hospital in Monza (Italy) and IEO Hospital (European Institute of Oncology) in Milan (Italy) is ongoing.

The 43 OC-PDX have been established and grow in immunodeficient mice, with different routes of injection, as reported in Table 3.1.

ID	OC-PDX Histotype	Specimen source	Route of injection and growth
MNHOC 8	HGS	A	I.P
MNHOC Y8	HGS	A	I.P
MNHOC 10	HGS	A	I.P
MNHOC 22	HGS	A	I.P
MNHOC 76	HGS	A	I.P
MNHOC 84	HGS	A	S.C/I.P
MNHOC 106	HGS	Om	S.C
MNHOC 107	HGS	Om	S.C
MNHOC 111/2	HGS	A	I.P
MNHOC 125	HGS	Ov	S.C
MNHOC 143	HGS	Ov	S.C
MNHOC 148	HGS	Ov	S.C
MNHOC 149	HGS	Ov	S.C
MNHOC 229	HGS	Ov	S.C
MNHOC 239	HGS	Om	S.C
MNHOC 241	HGS	Ov	S.C
MNHOC 244	HGS	Ov	S.C
MNHOC 500	HGS	Ov	S.C
MNHOC 506	HGS	A	I.P
MNHOC 508	HGS	Om	S.C
MNHOC 511	HGS	Om	S.C
MNHOC 513	HGS	Om	S.C
MNHOC 124	HGS/HGE	Ov	S.C
MNHOC 212	HGS/HGE	Ov	S.C
MNHOC 18	HGE	Ov	I.P
MNHOC 78	HGE	A	S.C/I.P
MNHOC 154	HGE	Om	S.C
MNHOC 218	HGE	Ov	S.C
MNHOC 230	HGE	Om	S.C
MNHOC 503	HGE	Ov	S.C
MNHOC 79	HGE/CCC	A	I.P
MNHOC 109	LGE	Om	S.C
MNHOC 232	LGS/LGE	Ov	S.C
MNHOC 94/2-C	CCC	A	S.C
MNHOC 119	CCC	Ov	I.P
MNHOC 142	CCC	A	I.P
MNHOC 164	MUC	Om	S.C
MNHOC 182	MUC	Ov	S.C
MNHOC 135	MMT	Ov	S.C
MNHOC 195	MMT	Ov	S.C
MNHOC 88	UNDIFF.	Om	S.C
MNHOC 213	UNDIFF.	Ov	S.C
MNHOC 9	UNDIFF.	A	S.C

Table 3.1 The platform of OC-PDX: histopathology and route of engraftment.

Abbreviations: HGS, high grade serous; HGE, high grade endometrioid; LGE, low grade endometrioid; CCC, clear cell carcinomas; MUC, mucinous; MMT, mixed Mullerian tumor; UNDIFF., undifferentiated. S.C: subcutaneously growing OC-PDX.

I.P: intraperitoneally growing OC-PDX. Squared in red are the 26 OC-PDX selected to perform molecular and pharmacological studies reported in this PhD research project.

[§] OC-PDX reported in "Patient-Derived Ovarian Tumor Xenografts Recapitulate Human Clinicopathology and Genetic Alterations", by Ricci/Bizzaro et al, *Cancer Res*, 2014.

Routinely, patients' solid tumors from ovary and omentum, primary or relapsed, were transplanted subcutaneously (s.c) in the flanks of mice, as reported in Materials and Methods, Section 2.1.3.

Patients' primary or relapsed ascites were injected directly into the peritoneal cavity (i.p) of mice, as reported in Materials and Methods, Section 2.1.4.

Our pathologist, taking into account the available data of the corresponding patients, confirmed the histotype of the 43 OC-PDX.

Half of the models (53%) were high grade serous, followed by 13% of high grade endometrioid, 5% of high grade serous/endometrioid, 2% of high grade endometrioid/clear cell, 2% of low grade endometrioid, 2% low grade serous/endometrioid, 6% of clear cell carcinomas, 5% of mucinous, 5% of mixed Mullerian tumor and 6% of undifferentiated ovarian carcinoma, mimicking the clinical pattern and frequency of human ovarian carcinomas (Table 3.1).

The established platform of OC-PDX is an instructive framework that can be used to perform characterization studies on generic molecular, morphological and biological aspects and also to selected representative OC-PDX for drug testing (Figure 3.1).

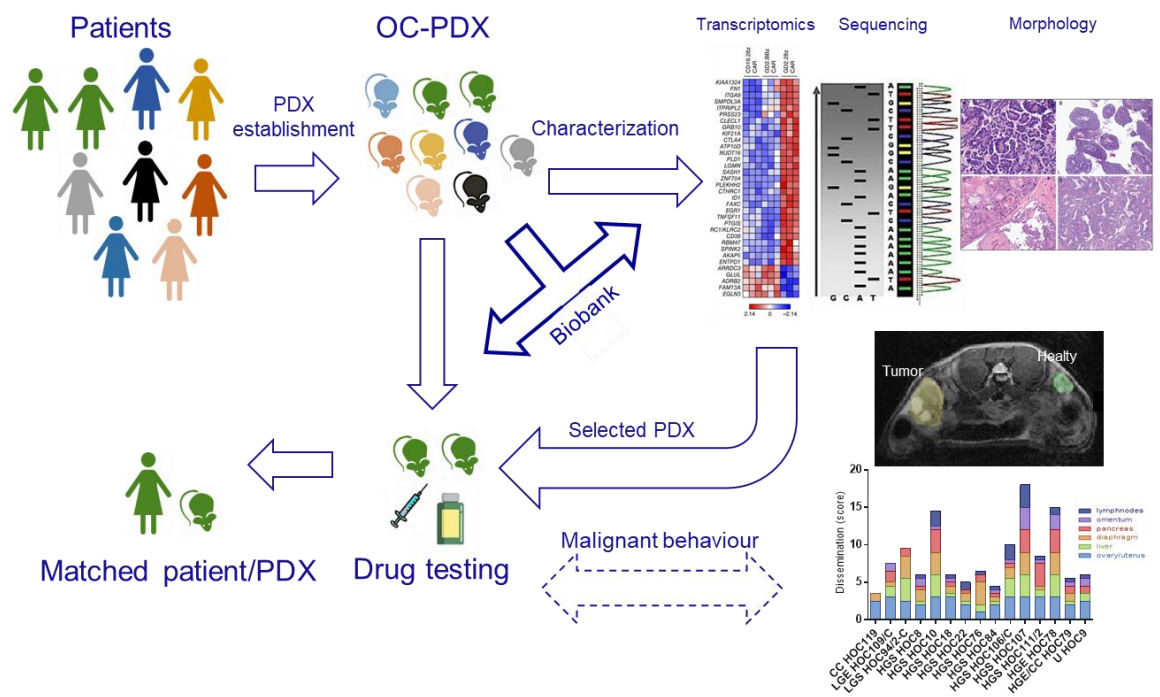


Figure 3.1 The application of the platform of OC-PDX.

After patient surgery, tumor fragments or ascites were transplanted in immunocompromised mice, without previous *in vitro* passage, obtaining different OC-PDX models. After the *in vivo* establishment, OC-PDX were expanded and cryopreserved at different passages. In parallel, tumor samples were collected and stored (formalin-fixed paraffin-embedded and snap-frozen) to constitute the bio-bank for further studies. Pharmacological studies were performed on OC-PDX to test several compounds and combination.

To perform all the studies reported in this PhD research project, we decided to focus our attention on 26 OC-PDX (Table 3.1), based on their biological behaviour and histological features and analysed them with whole genome libraries sequenced on the Illumina HiSeq 4000 platform. The Next Generation Sequencing (NGS) data were aligned and analysed within the BCBio framework (Lai et al., 2016) as reported in Materials and Methods, Chapter 2.2.2. The ultimate goal was to select a smaller cohort of OC-PDX for drug testing with the PARP inhibitor olaparib in combination with the angiogenesis inhibitor cediranib (see Chapter 4, Results).

3.1.1 Characteristics of original patients' tumors

Diagnosis (histotype, grade and stage), sample source and origin, patients' treatments and follow up of the 26 OC-PDX used in this PhD research project are reported in Table 3.2.

The origin and source of patients' specimens included 3 primary ascites, 8 primary ovary, 3 primary tumors located in the omentum, 8 ascites and 4 omental metastasis collected at relapse.

Patients experienced different treatments before primary surgery, peritoneal washing or omentectomy, where tumor samples, from which OC-PDX derived, were collected. Twelve patients were chemotherapy-naïve, 12 patients were treated with adjuvant chemotherapy and 2 patients underwent neoadjuvant treatment.

Regardless of these aspects, all the patients were treated with a standard-of-care platinum-taxane based chemotherapy, with the addition of bevacizumab in two cases. The patient diagnosed with a mucinous carcinoma was not treated.

At the last recorded follow up, 8 patients were considered resistant to therapy, being in progressive disease; 2 had stable disease and 5 had a partial response. After therapy, 4 patients experienced complete response and 5 did not show any evidence of disease. For one patient no clinical records were available.

ID	Histotype at diagnosis	Patients' specimen source and origin			Neoadjuvant Chemotherapy	Adjuvant Chemotherapy	Follow Up
			Ov	Om			
MNHOC 8	HGS	Primary			X	CBDCA	PR
MNHOC Y8	HGS	Relapse			X	EPI+CTX+DDP	PD
MNHOC 10	HGS	Primary			X	DDP	PD
MNHOC 22	HGS	Relapse			X	DDP	PD
MNHOC 76	HGS	Relapse			X	PAC	PD
MNHOC 84	HGS	Relapse			X	DDP+PTX	N.A
MNHOC 106	HGS	Relapse		X		PAC	PR
MNHOC 107	HGS	Relapse		X		PAC	PR
MNHOC 111/2	HGS	Relapse			X	DDP+PTX	PD
MNHOC 125	HGS	Primary	X			CBDCA	PR
MNHOC 143	HGS	Primary	X			CBDCA+PTX	NED
MNHOC 149	HGS	Primary	X			CBDCA+PTX	NED
MNHOC 500	HGS	Primary	X			CBDCA	NED
MNHOC 506	HGS	Primary			X	CBDCA+PTX	PD
MNHOC 508	HGS	Primary		X		CBDCA+PTX+BEVA	NED
MNHOC 511	HGS	Primary		X		CBDCA+PTX	CR
MNHOC 513	HGS	Primary		X		CBDCA+PTX+BEVA	NED
MNHOC 124	HGS/HGE	Primary	X			CBDCA+PTX	PD
MNHOC 18	HGE	Primary	X			EPI+CTX	PR
MNHOC 78	HGE	Relapse			X	CP	SD
MNHOC 154	HGE	Relapse		X		CBDCA+PTX	CR
MNHOC 79	HGE/CCC	Relapse			X	CDDP	SD
MNHOC 109	LGE	Relapse		X		CBDCA	CR
MNHOC 94/2-C	CCC	Relapse			X	N.A	PD
MNHOC 119	CCC	Primary	X			CBDCA	CR
MNHOC 182	MUC	Primary	X			NO TREATMENT	

Table 3.2 Patients' tumors characteristics of the 26 OC-PDX used in this PhD thesis.

Abbreviations: HGS, high grade serous; HGE, high grade endometrioid; LGE, low grade endometrioid; CCC, clear cell carcinomas; MUC, mucinous.

Ov, ovary; Om, omentum; A, ascites.

CBDCA, carboplatin; EPI, epirubicin; DDP, cisplatin; PTX, paclitaxel; BEVA, bevacizumab; PAC, cisplatin-adriamycin-cyclophosphamide; CP, cisplatin-cyclophosphamide; CTX, cyclophosphamide; N.A, not available.

PR, partial response; PD; progressive disease; NED, non-evident disease; CR, complete response; SD, stable disease; N.A, not available.

3.1.2 OC-PDX recapitulate the morphology and histopathology of ovarian cancer

When available, the histology of OC-PDX was compared with the corresponding patient original tumor; in all cases, morphology and tissue structure were retained (representative histological section in Figure 3.2, panel A). In some cases, cytokeratin pool and CA-125 were assessed, resulting in a strong retention of positivity (Figure 3.2, panel B). The value of OC-PDX as a model to study ovarian cancer was proved also by evaluating morphology and histopathology after several *in vivo* passages (comparison between hematoxylin-eosin section at passage I and higher than V); the architecture of the original tumor was preserved even after several transplants in mice (Figure 3.2, panel C). The subset of patients, from which the 26 OC-PDX were established, resembled the clinical histopathological heterogeneity of ovarian cancer, thus being a powerful tool to study new therapeutic strategies on a wider range of patients that could gain benefit.

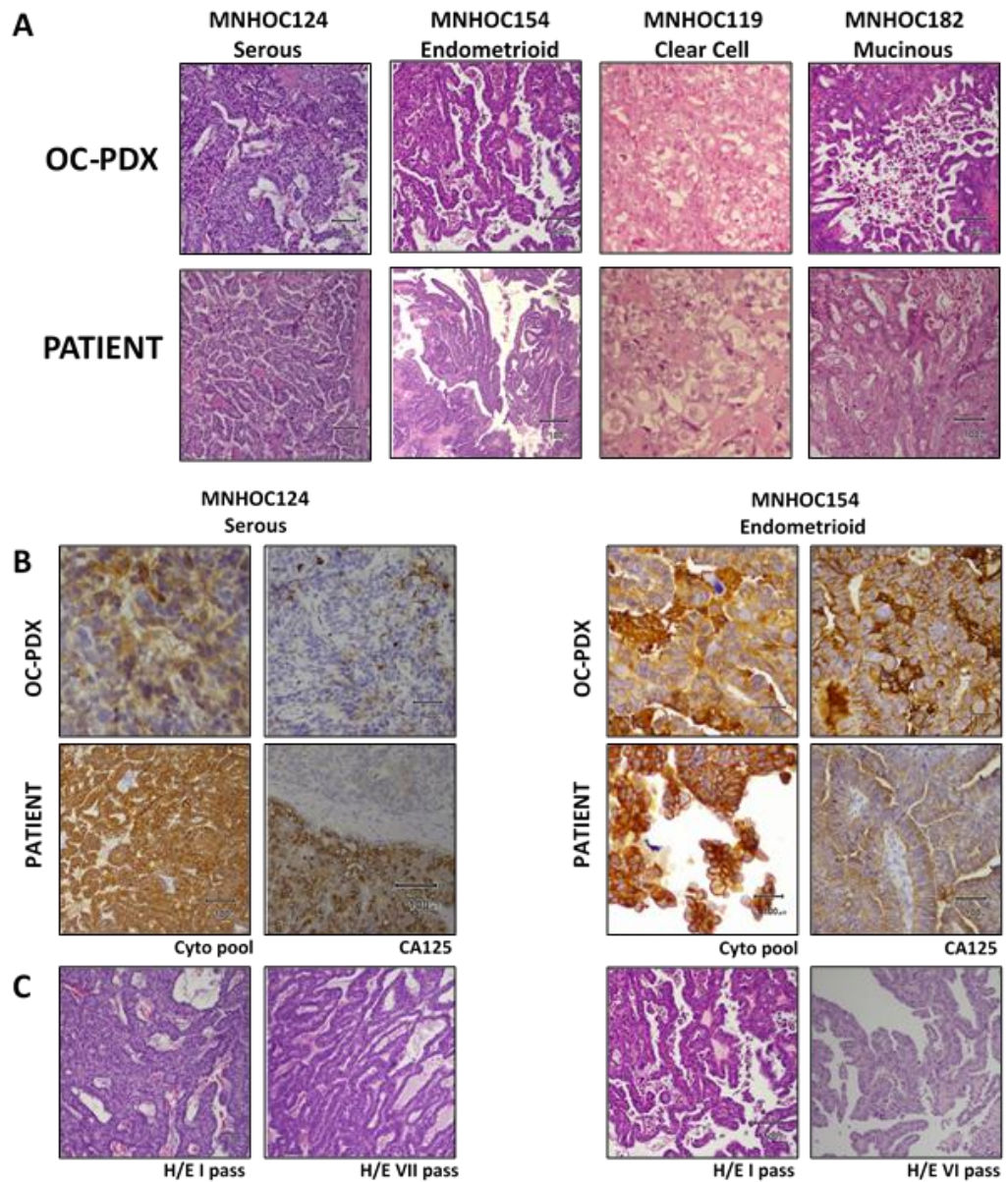


Figure 3.2 Representative histological section of subcutaneous OC-PDX and corresponding patient tumor.

A) Sections from OC-PDX and the corresponding patient (hematoxylin and eosin).
B) Comparative immunohistological analysis of patient tumor and the corresponding xenograft (cytokeratin pool and CA-125).
C) Comparative immunohistochemical analysis of xenografts at different passages.
Images partially reported in "Patient-Derived Ovarian Tumor Xenografts Recapitulate Human Clinicopathology and Genetic Alterations", by Ricci/Bizzaro et al, Cancer Res, 2014.

3.1.3 OC-PDX biological behaviour

Among the 26 OC-PDX chosen for this project, 16 models were transplanted subcutaneously, 8 models were injected and grew in the peritoneal cavity and 2 grown in both sites (Table 3.1, squared in red).

Subcutaneous models were a useful and easy-to-manage tool, especially to conduct preclinical trials in a more simple and controlled environment, thus focusing only on the effects of the therapy on tumor growth. Subcutaneous tumor growth was very variable, from faster progressor OC-PDX, such as MNHOC 18 (approx. 17 days to reach 1200mm³), to slower ones, such as MNHOC 125 (approx. 125 days to reach 1200mm³) (Ricci et al., 2014).

Intraperitoneally growing OC-PDX were a unique and valuable tool to study the biological behaviour and the ability to disseminate in the peritoneal organs, thus mimicking the original patient tumors and allowing us to shed light on the effects of therapy in a more complex microenvironment. Intraperitoneal OC-PDX closely reproduced the dissemination patterns of human ovarian cancer, forming ascites and spreading diffusely through the organs of the peritoneal cavity (ovary, uterus, diaphragm, pancreas, omentum and liver) with various levels of carcinomatosis, ascites formation and median survival time (MST). Ascites production and tumor dissemination were linear in some case, such as MNHOC 111/2 with high levels of fluid formation and carcinomatosis, or completely different, as for MNHOC 8, with the highest levels of ascites among all and the lowest score of dissemination and carcinomatosis (Ricci et al., 2014).

3.1.4 NGS to study the mutational landscape of OC-PDX

NGS on the whole genome was conducted in collaboration with AstraZeneca (see Section 2.2.2 and 2.2.3 Materials and Methods). Molecular characterization was undertaken on the panel of 26 OC-PDX.

For this project the focus was on aberrations and mutations in a set of genes involved in the pathogenesis of ovarian cancer (Table 3.3, e.g. *TP53*, *KRAS*, *BRAF*, *PIK3CA*, *CTNNB1*, *PTEN*, *EGFR*) and genes belonging to the HR DNA repair pathway (Table 3.4, e.g. *BRCA1/2*, *ATM*, *ATR*, *ATRX*, *BARD1*, *BLM*, *CHEK1*, *CHEK2*, *FANCA*, *FANCB*, *FANCC*, *FANCD*, *FANCE*, *FANCF*, *FANCG*, *FANCI*, *FANCL*, *FANCM*, *MRE11A*, *NBN*, *PALB2*, *RAD50*, *RAD51*, *RAD51B*, *RAD51C*, *RAD51D*, *RAD52*, *RAD54L*, *RPA* from (Coleman et al., 2017) and reported in Table 1.1 Introduction).

Sanger sequencing was performed on OC-PDX DNA to validate mutations, designing *ad hoc* primers pairs to amplify 100-200 bp around the region containing the mutation (see Table 2.1, Materials and Methods, Chapter 2, for genes and primers pairs used in Sanger validation). When possible, the same mutation found in OC-PDX was confirmed also in the corresponding patient's DNA.

The detailed mutational spectrum of the most common genes involved in the pathogenesis of ovarian cancer is reported in Table 3.3.

ID	Histotype	TP53	OTHERS OvCa genes
MNHOC 8	HGS	c.514G>T p.V172F	
MNHOC Y8	HGS	c.514G>T p.V172F	
MNHOC 10	HGS	c.659A>G p.Y220C	
MNHOC 22	HGS	g.14755 G:C>T:A, c.993+1G>A	
MNHOC 76	HGS	c.723delC p.S242fs*5	
MNHOC 76 PZ	HGS	wt/ c.723delC p.S242fs*5	
MNHOC 84	HGS	g.14451 G:C>T:A, c.783-1G>T	KRAS wt/ c.35G>C p.G12A
MNHOC 84 PZ	HGS	g.14451 G:C>T:A, c.783-1G>T	KRAS wt/ c.35G>C p.G12A
MNHOC 106	HGS	g.13999 G:C>T:A, c.673-1G>C	
MNHOC 106 PZ	HGS	g.13999 G:C>T:A, c.673-1G>C	
MNHOC 107	HGS	c.517G>A p.V173M	
MNHOC 107 PZ	HGS	wt/ c.517G>A p.V173M	
MNHOC 111/2	HGS	c.839G>A p.R280K	
MNHOC 111/2 PZ	HGS	wt/ c.839G>A p.R280K	
MNHOC 125	HGS	c.517G>A p.V173M	
MNHOC 125 PZ	HGS	wt/ c.517G>A p.V173M	
MNHOC 143	HGS	c.470T>A p.V157D	
MNHOC 143 PZ	HGS	wt/ c.470T>A p.V157D	
MNHOC 149	HGS	c.713 G>A p.C238Y	
MNHOC 149 PZ	HGS	wt/ c.713 G>A p.C238Y	
MNHOC 500	HGS	c.641 A>G p.H214R	
MNHOC 500 PZ	HGS	wt/ c.641 A>G p.H214R	
MNHOC 506	HGS	c.796G>T p.G266*	
MNHOC 506 PZ	HGS	wt/ c.796G>T p.G266*	
MNHOC 508	HGS	splice site, c.782+1G>A	EGFR c.3328T>A p.Y1110N
MNHOC 508 PZ	HGS	splice site, c.782+1G>A	EGFR wt/ c.3328T>A p.Y1110N
MNHOC 511	HGS	c.523C>G p.R175G	
MNHOC 511 PZ	HGS	wt/ c.523C>G p.R175G	
MNHOC 513	HGS	c.338delT p.F113fs	
MNHOC 513 PZ	HGS	wt/ c.338delT p.F113fs	
MNHOC 124	HGS/HGE	c.524G>A p.R175H	
MNHOC 124 PZ	HGS/HGE	wt/ c.524G>A p.R175H	
MNHOC 18	HGE	c.527G>T p.C176F	EGFR c.2884C>T p.R962C
MNHOC 18 PZ	HGE	wt/ c.527G>T p.C176F	EGFR wt/ c.2884C>T p.R962C
MNHOC 78	HGE	c.518T>G p.V173G	
MNHOC 154	HGE	c.844C>T p.R282W	
MNHOC 154 PZ	HGE	c.844C>T p.R282W	
MNHOC 79	HGE/CCC	g.14755 G:C>T:A	
MNHOC 109	LGE	c.639A>G p. wt(R213R)	
MNHOC 109 PZ	LGE	wt/ c.639A>G p.wt(R213R)	
MNHOC 94/2-C	CCC	wt	PTEN c.388C>T p.R130*
MNHOC 119	CCC	wt	
MNHOC 119 PZ	CCC	wt	
MNHOC 182	MUC	wt	KRAS wt/ c.35G>A p.G12D
MNHOC 182 PZ	MUC	wt	KRAS wt/ c.35G>A p.G12D

Table 3.3 Mutational spectrum of most commonly mutated genes in ovarian cancer, verified by Sanger sequencing.

Data are from OC-PDX and corresponding patient (PZ) where available. Abbreviations: HGS, high grade serous; HGE, high grade endometrioid; LGE, low grade endometrioid; CCC, clear cell carcinomas; MUC, mucinous.

Nonsynonymous *TP53* mutations were found in all the high grade serous and endometrioid tumors; clear cell (MNHOC 94/2-C and MNHOC 119), low grade endometrioid (MNHOC 109, synonymous *TP53* mutation c.639A>G, p.R213R) and mucinous (MNHOC 182) harboured wild type *TP53*, in line with clinical data (Ahmed et al., 2010).

All the mutations found in *TP53* were located with a strong predominance in exons 4-9, which encodes the DNA-binding domain of the protein, including the 6 main “hot-spot” residues described (Cho et al., 1994), such as R175, G245, R248, R249, R273, and R282, that are frequent in almost all type of cancer. The majority were missense substitutions, with a pathogenic prediction score.

Among other genes, two cases of mutated *KRAS* were found both in the OC-PDX and corresponding patient’s tumor, one high grade serous MNHOC 84 (p.G12A) and one mucinous MNHOC 182 (p.G12D).

The clear cell MNHOC 94/2-C displayed a truncation/frameshift mutation in *PTEN* (p.R130*), with a high pathogenic prediction score. *EGFR* carried two missense mutations in MNHOC 508 (p.Y1110N) and MNHOC 18 (p.R962C, pathogenic).

The OC-PDX and the corresponding patient tumors whose DNAs were available always displayed the same mutational status.

The detailed mutational spectrum of different HR DNA repair pathway genes is reported in Table 3.4.

ID	Histotype	BRCA 1	BRCA 2	HR pathway genes	
MNHOC 8	HGS				
MNHOC Y8	HGS				
MNHOC 10	HGS			PARP4 c.2873G>A p.R958Q	
MNHOC 22	HGS	c.1687C>T p.Q563*		PALB2 wt/ c.850A>C p. T284P	ATM wt/ c.6167C>T p. P2056L
MNHOC 76	HGS				
MNHOC 76 PZ	HGS				
MNHOC 84	HGS				
MNHOC 84 PZ	HGS				
MNHOC 106	HGS	c.5161delC p.Q1721fs			
MNHOC 106 PZ	HGS	n.t			
MNHOC 107	HGS	c.2727_2730delTCAA p. N909fs			
MNHOC 107 PZ	HGS	n.t			
MNHOC 111/2	HGS				
MNHOC 111/2 PZ	HGS				
MNHOC 125	HGS	c.65T>C p.L225			
MNHOC 125 PZ	HGS	c.65T>C p.L225			
MNHOC 143	HGS			FANCA wt/ c.2134G>A p. E712K	ATM wt/ c.6669C>G p. I2223M
MNHOC 143 PZ	HGS			FANCA wt/ c.2134G>A p. E712K	ATM wt/ c.6669C>G p. I2223M
MNHOC 149	HGS				
MNHOC 149 PZ	HGS				
MNHOC 500	HGS	c.1088delA p.N363fs			
MNHOC 500 PZ	HGS	wt/ c.1088delA p.N363fs			
MNHOC 506	HGS				
MNHOC 506 PZ	HGS				
MNHOC 508	HGS		c.5722_5723delCT p.L1908fs	ATM c.6067G>A p.G2023R	FANCB c.1004G>A p.G335E
MNHOC 508 PZ	HGS		wt/ c.5722_5723delCT p.L1908fs	ATM c.6067G>A p.G2023R	FANCB c.1004G>A p.G335E
MNHOC 511	HGS	c.190T>C p.C64R	c.6212G>C p.S2071T		
MNHOC 511 PZ	HGS	wt/ c.190T>C p.C64R	wt/ c.6212G>C p.S2071T		
MNHOC 513	HGS	LOSS			
MNHOC 513 PZ	HGS	LOSS			
MNHOC 124	HGS/HGE				
MNHOC 124 PZ	HGS/HGE				
MNHOC 18	HGE		wt/ c.3199A>G p.T1067A		
MNHOC 18 PZ	HGE		wt/ c.3199A>G p.T1067A		
MNHOC 78	HGE	c.5266dupC p. Q1756fs			
MNHOC 154	HGE	c.181T>G p.C61G	AMPLIFICATION	ATRX c.2595 C>G p. H865Q	
MNHOC 154 PZ	HGE	wt/ c.181T>G p.C61G	n.t	ATRX c.2595 C>G p. H865Q	
MNHOC 79	HGE/CCC				
MNHOC 109	LGE				
MNHOC 109 PZ	LGE				
MNHOC 94/2-C	CCC				
MNHOC 119	CCC				
MNHOC 119 PZ	CCC				
MNHOC 182	MUC		wt/ c.7399 gaa>gAaa p.E2391EX	ATRX c.2093delA p. K698fs	
MNHOC 182 PZ	MUC		wt/ c.7399 gaa>gAaa p.E2391EX	ATRX wt/ c.2093delA p. K698fs	

Table 3.4 Mutational spectrum of different HR genes, verified by Sanger sequencing.

Data are from OC-PDX and corresponding patient (PZ) where available. Abbreviations: HGS, high grade serous; HGE, high grade endometrioid; LGE, low grade endometrioid; CCC, clear cell carcinomas; MUC, mucinous.

Sequencing of genes related to the HR DNA repair pathway revealed a disparate picture. *BRCA1* and *BRCA2* were found mutated or lost in 11 OC-PDX, notably in the high grade serous and endometrioid types.

Mutations in *BRCA1* were mostly substitution/missense and truncation/frameshift, all described as pathogenic accordingly to ClinVar (<https://preview.ncbi.nlm.nih.gov/clinvar/>). Of note, MNHOC 513 carried a deletion on the exon 23 of *BRCA1*, an event that caused a frameshift leading to a loss of function (LoF) at the protein level (Table 3.4).

Mutations in *BRCA2* included one frameshift described as pathogenic (p.L1908fs on MNHOC 508) and one missense mutation with conflicting interpretation (p.S2071T on MNHOC 511). Interestingly MNHOC 18 exhibited a missense mutation, predicted as neutral non-pathogenic (FATHMM score 0,15) on *BRCA2* (p.T1067A). The mucinous MNHOC 182 displayed a truncation/frameshift mutation in *BRCA2*, despite the low mutation rate described for this type of tumor (Pennington et al., 2014; Soegaard et al., 2008; Zhang et al., 2011). The mutation (p.E2391EX) led to the formation of a stop codon. In both the cases, the mutation induced an absence of locus-specific loss of heterozygosity (LOH), meaning that one allele is wild type and the other is mutated, so functional protein is still produced. This was confirmed also with *ad hoc* Sanger sequencing on cDNA, retro-transcribed from RNA. The homologous recombination pathway was thus functional.

Of note, MNHOC 154 carried a pathogenic amplification of *BRCA2* (Table 3.4).

Among other genes of the HR DNA repair pathway, *PARP4*, *PALB2*, *ATM*, *ATRX*, *FANCA* and *FANCB* were found altered. Mutations were unknown missense with uncertain clinical significance accordingly to ClinVar, except for *PARP4* (p.R958Q) substitution missense described as pathogenic in MNHOC 10, *PALB2* (p.T284P) substitution missense likely benign in MNHOC 22, *FANCB* (p.G335E) and *ATRX* (p.H865Q) substitutions missense described as benign in MNHOC 508 and MNHOC 154 respectively (Table 3.4).

Interestingly, OC-PDX and the corresponding patient's tumor -where human DNA was available- displayed the same somatic mutations.

3.1.5 Gene expression profile analysis to characterize OC-PDX

Gene expression analysis on selected genes was performed using different techniques, including RealTime-PCR (RT-PCR), genome-wide gene expression, fluidigm and RNAseq (see Chapter 2.2, Molecular analysis, Materials and Methods).

The results herein presented a focus on the expression levels of *BRCA1* and *BRCA2* across the 26 OC-PDX selected to perform this PhD research project.

Firstly, absolute copy numbers of mRNA were determined by RT-PCR (ABI-7900, Applied Biosystems) with the SYBR Green technique, using an EPMotion 5075 robot (Eppendorf). Standard curves for each gene were included for absolute quantification of mRNA. Primers for *BRCA1* were designed to cover exons 16-17, and reported in the following table.

<i>BRCA1</i> ex.16-17 Forward	GCCAGAAAACACCACATCAC
<i>BRCA1</i> ex.16-17 Reverse	CAGTGTCCGTTACACACAA

RT-PCR analysis showed that MNHOC 8 and MNHOC 8Y (respectively primary and relapsed ascites of the same patient), MNHOC 149 and MNHOC 182 displayed the lowest levels of *BRCA1* expression. In MNHOC 125, MNHOC 22, MNHOC 18, MNHOC 111/2 and MNHOC 508, *BRCA1* levels of expression were the highest (Figure 3.3).

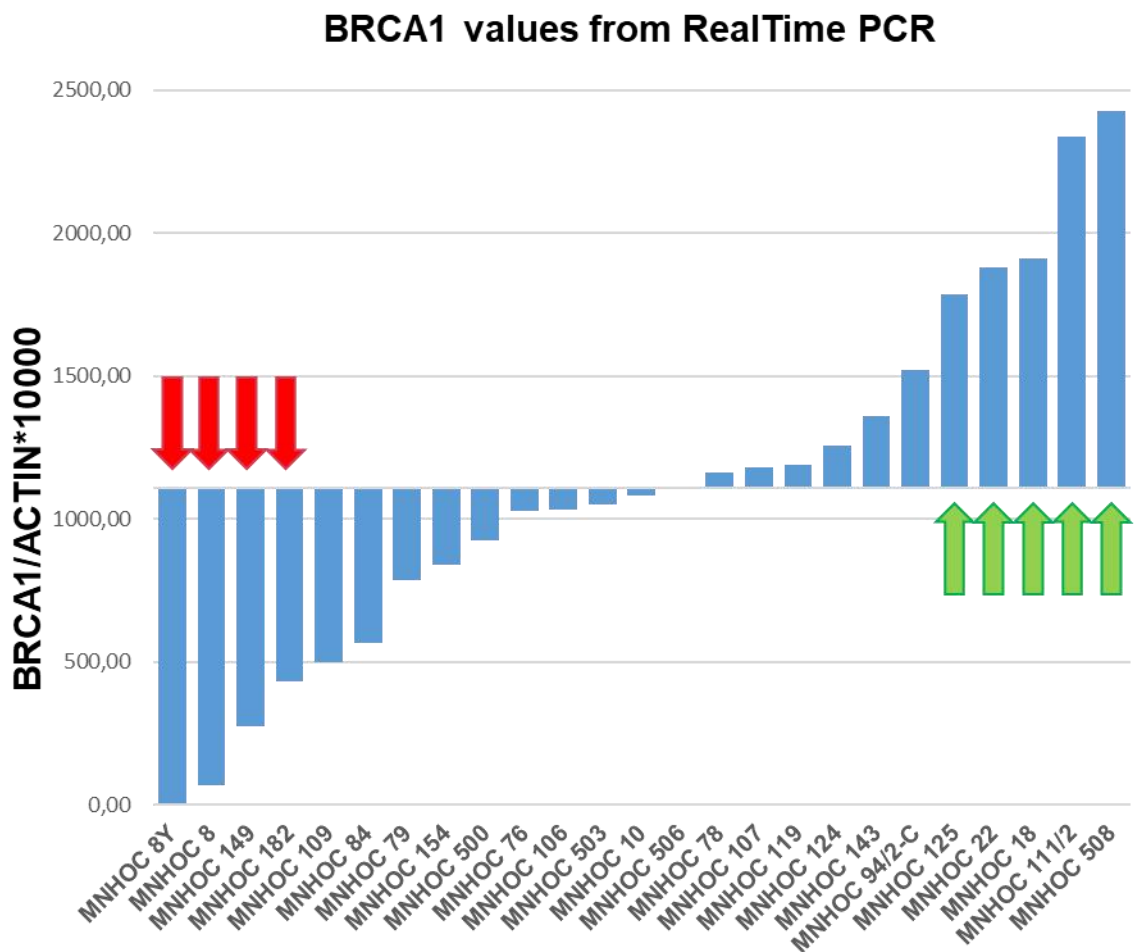


Figure 3.3 Gene expression analysis of OC-PDX from RT-PCR: BRCA1 level of expression.

Absolute copy numbers of mRNA were determined by RT-PCR (ABI-7900, Applied Biosystems) with the SYBR Green technique, using an EPMotion 5075 robot (Eppendorf). Standard curves for each gene were included for absolute quantification of mRNA. Data are expressed as ratio between BRCA1 and actin (housekeeping gene).

Results were then re-confirmed with genome-wide gene expression analysis, focusing our attention both on *BRCA1* and *BRCA2*.

Briefly, arrays were scanned and images analysed by the Feature Extraction Software from Agilent Technologies; raw data were then processed using the LIMMA (Linear Models for Microarray Analysis) package from Bioconductor (Smyth, 2004). Background correction was performed with the normexp method with an offset of 50. Normalization was carried out using the quantile method. Data were expressed as log₂ normalized Intensities (Figure 3.4, panel A and B).

Evaluation of Log₂ Intensity demonstrated that MNHOC 8 and MNHOC 8Y expressed the lowest level of *BRCA1*, with barely detected values compared to the other OC-PDX. High levels of expression were confirmed in MNHOC 111/2 and MNHOC 125, as from RT-PCR data.

Differences in *BRCA2* expression were less pronounced, with Log₂ Intensity values being quite uniform across OC-PDX. *BRCA2* expression appeared to be the lowest in MNHOC 182, MNHOC 10 and MNHOC 8, and the highest in MNHOC 154, due to the pathogenic amplification found in NGS (Figure 3.4, panel A and B).

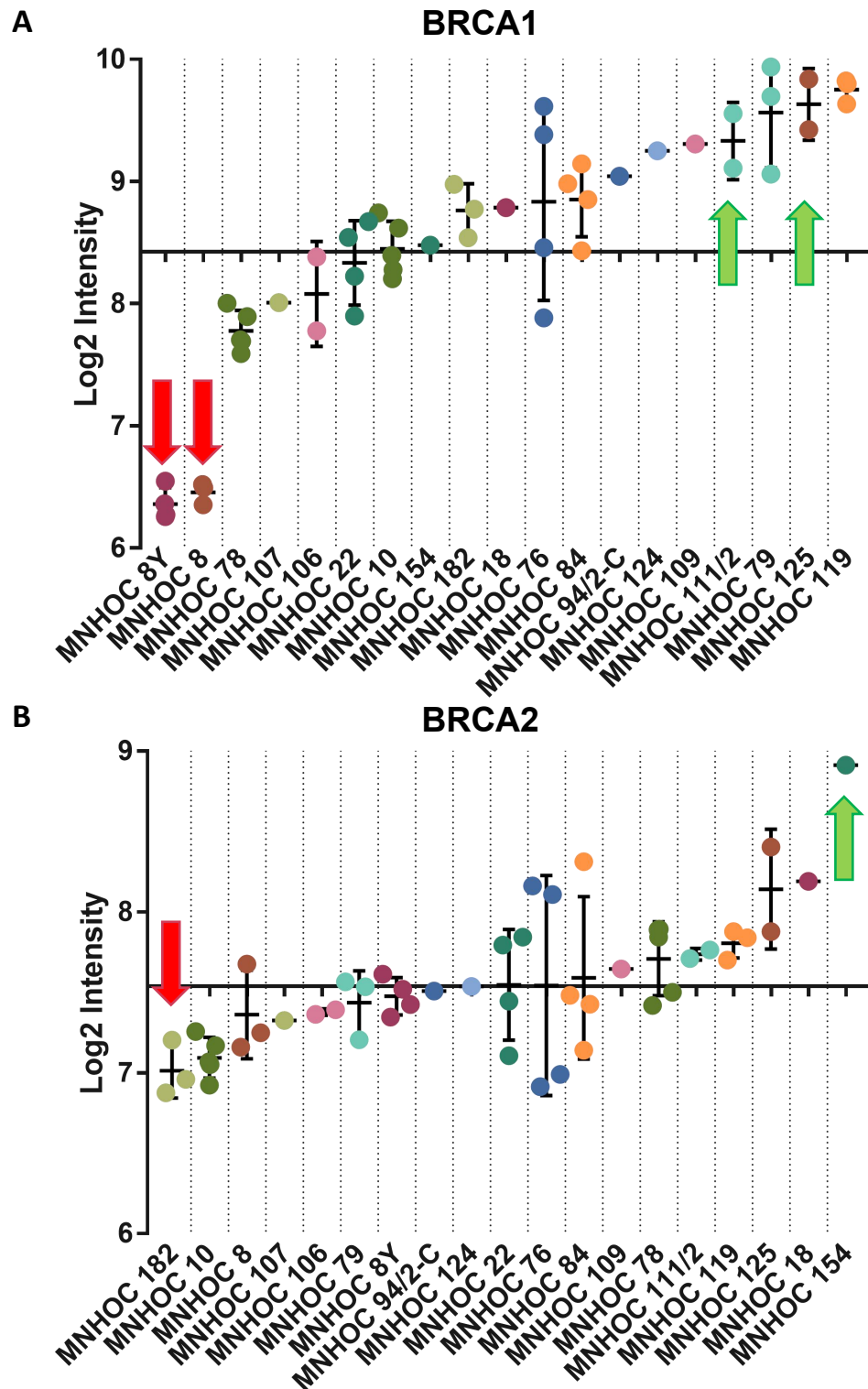


Figure 3.4 Gene expression analysis of OC-PDX from genome-wide gene expression.

A) *BRCA1* and **B)** *BRCA2* levels of expression from genome-wide gene expression analysis. Arrays were scanned and images analysed by the Feature Extraction Software; raw data were processed using the LIMMA (Linear Models for Microarray Analysis) package from Bioconductor (*Smyth, 2004*). Background correction was performed with the normexp method with an offset of 50. Normalization was carried out using the quantile method. Data are expressed as Log2 Intensity and represented on graph as mean \pm SD. Abscissa intercepts ordinate axis at the mean value of Log2 Intensity obtained from all the samples.

Levels of *BRCA1* and *BRCA2* expression were further evaluated with fluidigm (see Chapter 2.2.5 Materials and Methods). To summarize, the mean of Ct values of each replicate was calculated. Then the mean was normalized to housekeeping genes and $\Delta Ct = Ct_{\text{target}} - Ct_{\text{housekeeping}}$ assessed (Figure 3.5, panel A and B). For convenience, values were reported as $-\Delta Ct$, being the lowest value corresponding to the lowest expression.

Results confirmed what was previously assessed by RT-PCR and genome-wide gene expression analysis: MNHOC 8 expressed the lowest and MNHOC 125 the highest values of *BRCA1*, while *BRCA2* was poorly and highly expressed in MNHOC 182 and MNHOC 154 respectively. Results from Fluidigm (Figure 3.5, panel A and B) mirrored what was already highlighted with genome-wide gene expression analysis.

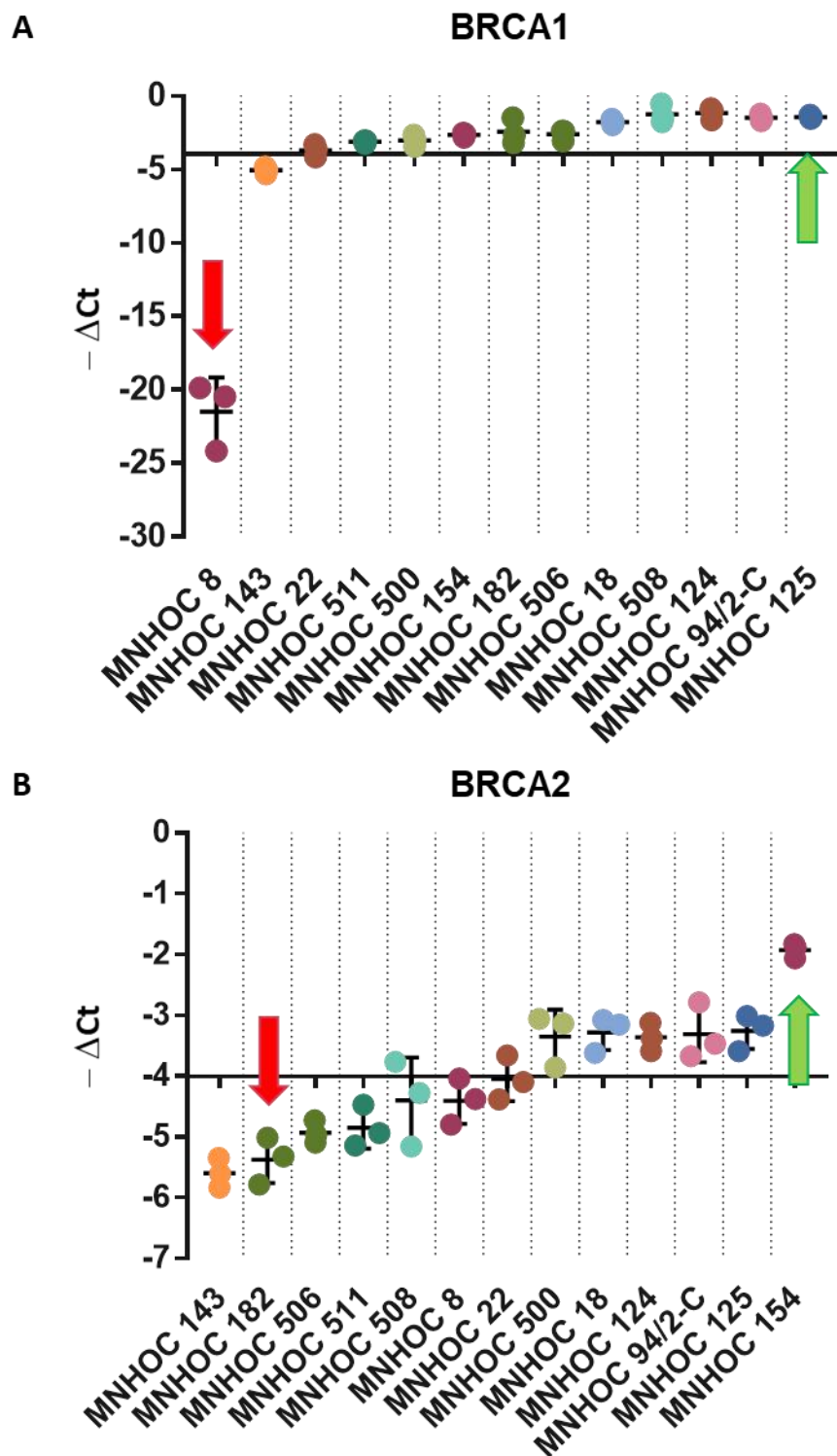


Figure 3.5 Gene expression analysis of OC-PDX at baseline from Fluidigm.

A) *BRCA1* and **B)** *BRCA2* levels of expression from Fluidigm analysis.

Briefly, $\Delta Ct = Ct_{\text{target}} - Ct_{\text{housekeeping}}$ was calculated (housekeeping genes were IPO8 and HPRT1) for each gene under investigation and reported as $-\Delta Ct$, being the lowest value corresponding to the lowest expression. Abscissa intercepts ordinate axis at the average value of $-\Delta Ct$ obtained from all the samples.

RNAseq analysis further strengthened previous results. Log₂*PCM (count per million) values showed that levels of *BRCA1* were the lowest in MNHOC 8 and MNHOC 8Y, while the highest levels of *BRCA2* were detected in MNHOC 154 (Figure 3.6, panel A and B).

Of note, MNHOC 154 was the model with the highest level of expression of *BRCA2* across every gene expression profile analysis performed, confirming NGS results, that indicated a pathogenic amplification in *BRCA2* (as described above in Section 3.1.3 and reported in Table 3.4).

Interestingly, MNHOC 513 carried a deletion in exon 23 of *BRCA1* (as described above in Section 3.1.3 and reported in Table 3.4). However, levels of expression of *BRCA1* were among the highest in MNHOC 513, meaning that the transcript was still produced. The deletion in exon 23 of *BRCA1* led to frameshift and LoF at the protein level.

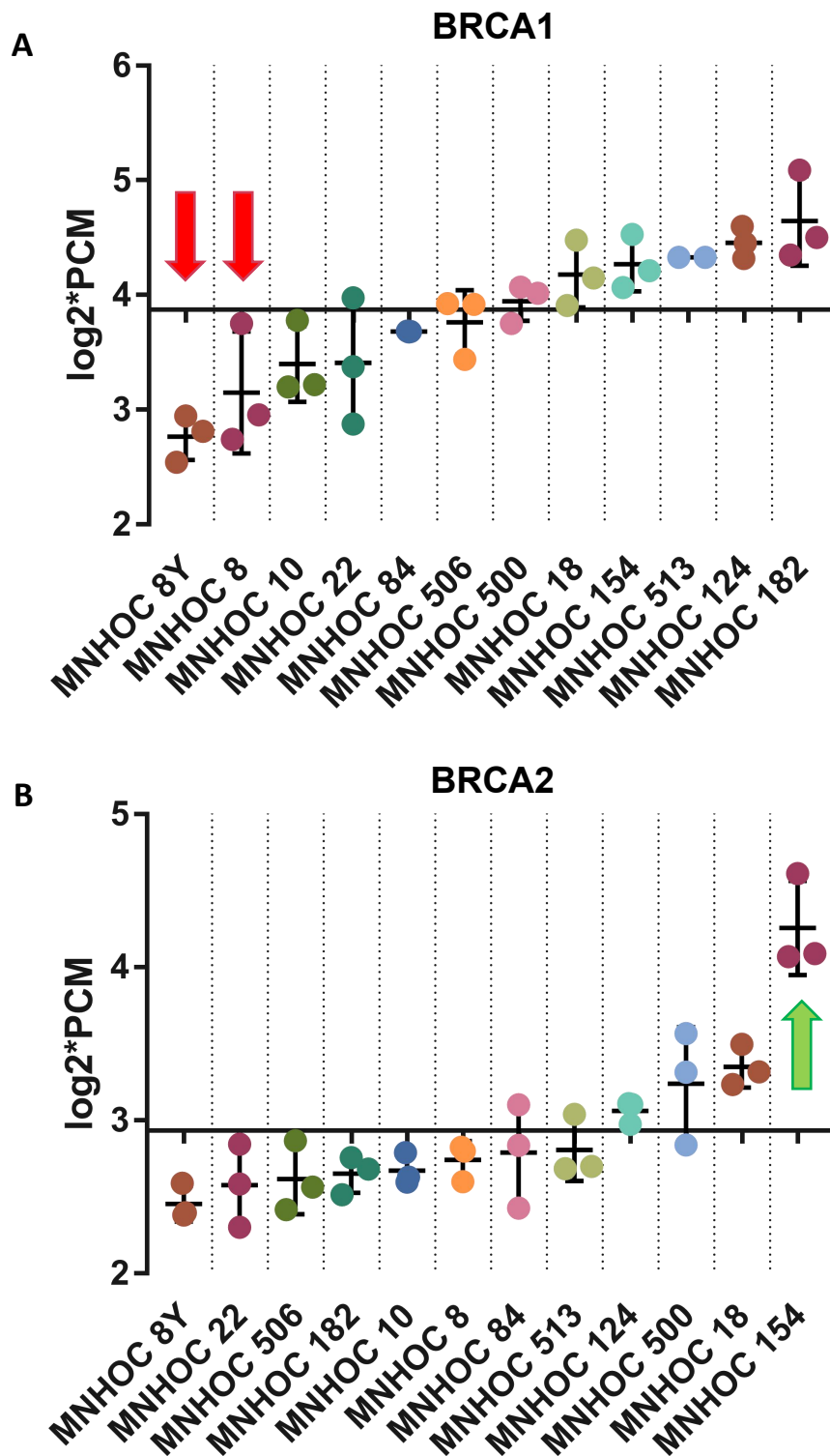


Figure 3.6 Gene expression analysis of OC-PDX from RNAseq.

A) *BRCA1* and **B)** *BRCA2* levels of expression from RNAseq analysis.

Data are expressed Log₂*CPM (count per million) and represented on graph as mean±SD. Abscissa intercepts ordinate axis at the mean value of Log₂*PCM obtained from all the samples.






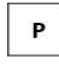




3.2 THE COHORT OF OC-PDX SELECTED TO PERFORM PRECLINICAL DRUG TESTING

The extensive characterization on the 26 OC-PDX chosen to perform this PhD project, based on biological behaviour, histopathological and molecular (mutational landscape and levels of expression of selected genes) aspects, gave us the opportunity to carefully select 13 OC-PDX to perform preclinical testing (Figure 3.7).

HYSTOLOGY	BRCAness							Not BRCAness					
	MNHOC 8	MNHOC 22	MNHOC 500	MNHOC 508	MNHOC 511	MNHOC 513	MNHOC 154	MNHOC 143	MNHOC 506	MNHOC 124	MNHOC 18	MNHOC 94/2-C	MNHOC 182
	HGS	HGS	HGS	HGS	HGS	HGS	HGE	HGS	HGS	HGS	HGE	CCC	MUC
BRCA1		P	P		P	P	P						
BRCA2				P	NP		P				NR		P
ATRX							NP						NP
ATM		NR		NP				NR					
PALB2		NR											
FANCA								NR					
FANCB				NP									
TP53	P	P	P	P	P	P	P	P	P	P	P		
KRAS													P
PTEN												P	
CTNNB1													
BRAF													
PIK3CA													
EGFR				NP							P		

Figure 3.7 The cohort of OC-PDX selected for drug testing.

HGS, high grade serous; HGE, high grade endometrioid; CCC, clear cell carcinomas; MUC, mucinous.

	substitution missense		no locus-specific Loss Of Heterozygosis (LOH)
	splice		no mutation detected
	trunc/frameshift		reported as pathogenic
	deletion		reported as not pathogenic, benign, uncertain clinical significance
	amplification		
	unknown-missense		

In particular, 3 orthotopic intraperitoneal OC-PDX were chosen: MNHOC 8, MNHOC 22 and MNHOC 506. Among subcutaneously growing tumors, 10 models were selected, MNHOC 143, MNHOC 500, MNHOC 508, MNHOC 511, MNHOC 513, MNHOC 124, MNHOC 18, MNHOC 154, MNHOC 94/2-C and MNHOC 182.

The cohort included 8 high grade serous (HGS), 1 mixed high grade serous/endometrioid (HGS/HGE), 2 high grade endometrioid (HGE), 1 clear cell (CCC) and 1 mucinous (MUC). Mutational spectrum and levels of expression of *BRCA1* and *2* were carefully considered for these OC-PDX. Particularly, 6 OC-PDX carried mutations or loss of *BRCA1* and *2*, and of other genes related to HR (MNHOC 22, MNHOC 500, MNHOC 508, MNHOC 511, MNHOC 513, MNHOC 154); MNHOC 8 was the model with the lowest expression of *BRCA1* and one of those with low levels of *BRCA2* expression, verified with several experiments and with different techniques (RT-PCR, genome-wide gene expression, fluidigm and RNAseq).

Among OC-PDX that harboured no mutation or absence of locus-specific loss of heterozygosity (LOH) in *BRCA1* and *BRCA2*, 6 OC-PDX were chosen: MNHOC 143, MNHOC 506, MNHOC 124, MNHOC 18, MNHOC 94/2-C and MNHOC 182.

We decided to classify the 13 OC-PDX, selected *ad hoc* for testing drugs, as BRCAness or Not BRCAness, not only considering the mutational status and pathogenicity of *BRCA1* and *2*, but also the levels of expression and any aberration on other genes involved in the HR DNA repair pathway, as reported in Figure 3.7.

3.3 SUMMARY OF RESULTS AND DISCUSSION

OC-PDX were obtained by transplanting tumor samples, freshly obtained from patients at surgery, subcutaneously and orthotopically in immunocompromised mice.

The choice of the appropriate strain of mice is a critical issue to achieve a high engraftment rate, especially in the first *in vivo* passage. We estimated that the take rate at the first passage after injection is around 50/60% using athymic nude mice (Masazza et al., 1991; Massazza et al., 1989; Ricci et al., 2014). However, accordingly to published data (Shultz et al., 2012), engraftment rate could be improved with the use of NGS mice.

The benefit of OC-PDX models is the limited diversity shown from patient's original tumor (Sausville and Burger, 2006; Siolas and Hannon, 2013; Tentler et al., 2012), compared with the use of an established cell line, which can result in a selected population not truly representative of the original tumor, thus producing responses that are different from those seen in patients.

On the other hand, the biggest issue with PDX as preclinical models is the lack of a murine immune system that makes it impossible to study the effect of the immune system to boost therapy. In fact, it is nowadays well recognized that the immune system plays a critical role in cancer initiation and expansion (Colvin, 2014; Hansen et al., 2016; McLean and Mehta, 2017; Pogge von Strandmann et al., 2017).

This problem/limitation could be overcome thanks to the recent development of "humanized xenograft" models, which are created by co-engrafting patient's tumor fragments with hematopoietic stem cells or human peripheral blood mononuclear cells (Siolas and Hannon, 2013), ideally derived from the same patient to avoid allogenic and graft-versus-host phenomena (Shultz et al., 2012).

A platform of patient-derived ovarian cancer xenografts has been established in the Department of Oncology (Ricci et al., 2014), and new models have been added during this PhD research project (Table 3.1).

Among these, 26 OC-PDX were characterized in depth from the biological, histopathological and molecular point of view (protocol of the study as in Figure 3.1). The panel of the 26 OC-PDX reproduced the plethora of human ovarian carcinomas with all the

different subtypes. OC-PDX, growing both subcutaneously and orthotopically in the peritoneal cavities of mice, maintained the original histotype and tissue architecture even after several passages *in vivo* (Figure 3.2), harboured mutations in genes mostly involved in ovarian cancer disease and progression (*TP53*, *KRAS*, *BRAF*, *PIK3CA*, *CTNNB1*, *PTEN*, *EGFR*) and in HR DNA repair pathway genes (Table 3.3 and Table 3.4). Accordingly to the literature, all the high grade serous and endometrioid OC-PDX harboured mutations on *TP53*, while the clear cell (i.e. MNHOC 94/2-C) and the mucinous (i.e. MNHOC 182) harboured mutations in *PTEN* and *KRAS*. MNHOC 508 and MNHOC 18 carried a missense mutation in *EGFR*. The selected platform of 26 OC-PDX was a useful tool to perform gene expression analysis, with different techniques, leading to reproducible and consistent results (Figure 3.3 – 3.6).

Recently one issue with the use of PDX has been highlighted: Golub and colleagues (Ben-David et al., 2017) have suggested that genomic instability of PDX is underestimated and that the variation in copy number alteration is continuously changing, leading to genetic drift of PDX from the original patient's tumor. *De novo* events during several passages *in vivo* limit the prediction value of these models.

In our platform, when the comparison was possible, OC-PDX showed a strong consistency with the patient's tumor from which they derived, at least in the histopathological and molecular aspect. For this reason, our collection offers an instructive framework to perform preclinical drug testing that could be translated into the clinic (Figure 3.2, Table 3.3 and Table 3.4), as long as OC-PDX are used within a minimum number of *in vivo* passages.

Taking together the data obtained from the NGS and gene expression analysis and considering the histopathology, we further selected 13 OC-PDX for preclinical therapy testing (see Chapter 4, Results). This cohort included mostly high grade serous and

endometrioid ovarian carcinomas (Figure 3.7), with one clear cell and one mucinous model (MHOC 94/2-C and MNHOC 182, as in Figure 3.7).

To resemble the clinical situation and patient stratification, OC-PDX carrying somatic mutations and loss of *BRCA1/2* on both the alleles of the gene were defined as BRCAness types (Figure 3.7); low levels of expression of *BRCA1* and *BRCA2* allowed us to define one particular model, MNHOC 8, as BRCAness, even though no mutations were detected with Sanger sequencing (Figure 3.7). Of note, MNHOC 154, carrying a mutation in *BRCA1*, was defined as BRCAness, even though a high level of expression of *BRCA2*, attributable to an amplification, was described as pathogenic.

OC-PDX that did not carry mutations on *BRCA1* and *BRCA2* or absence of locus-specific loss of heterozygosity (LOH) (such as MNHOC 18 and MNHOC 182) were defined as Not BRCAness (Figure 3.7).

A variety of other genes linked to the HR DNA repair pathway was found mutated across the OC-PDX. The majority of these mutations were reported as non-pathogenic or of uncertain clinical significance.

The panel of 13 OC-PDX offered a useful platform for preclinical testing therapy with cediranib and olaparib, being a powerful tool to study mechanisms of action underlying the effect of the combination (see Chapter 4, Results).

CHAPTER 4.

Results

PRECLINICAL THERAPY TESTING

4.1 CORRELATION BETWEEN THE BRCANESS STATUS AND RESPONSE TO OLAPARIB MONOTHERAPY

PARP inhibitor (PARPi) olaparib was the first molecularly targeted agent validated for high grade ovarian cancer (Ledermann et al., 2012).

To classify the cohort of OC-PDX selected to perform preclinical testing, we used the following criteria:

- OC-PDX carrying somatic mutations and loss of *BRCA1/2* on both the gene alleles were defined as BRCAness. In addition, low expression levels of both *BRCA1* and *BRCA2* allowed us to define one particular model, MNHOC 8, as BRCAness, even though no mutations were detected with Sanger sequencing.
- OC-PDX that did not carry mutations on *BRCA1* and *BRCA2* or did not display locus-specific loss of heterozygosity (LOH) (such as MNHOC 18 and MNHOC 182) were defined as Not BRCAness.

A cohort of 10 subcutaneous OC-PDX was first selected to assess the responsiveness to olaparib monotherapy. Tumor-bearing mice were randomized at an estimated tumor volume of 280-330 mm³ (300 mm³ average) and assigned to treatment groups (see Section 2.3.2 and 2.3.3 Materials and Methods).

Olaparib was administered as a single therapy every day for 5 days on and 2 days off (Q1x5), in a short-term treatment regimen of 4 weeks or in a maintenance schedule (until partial regression - 30% of the tumor volume at random - or complete progression).

Results are shown as waterfall plots, in which each bar represents the course of the disease for each mouse (Figure 4.1).

The BRCAness tumors MNHOC 500, 508, 511, 513 and 154 showed statistically significant responses to olaparib in a short-term regimen (Figure 4.1, panel A) and continued to regress under maintenance treatment (Figure 4.1, panel C), with complete

responses and animals considered cured when tumor-free for approximately 200 days post therapy.

Only a few cases differed from this trend (one MNHOC 508, one MNHOC 511 and two MNHOC 154 tumors), which progressed under treatment, enabling the future possibility of investigating potential mechanisms of resistance to olaparib (beyond the scope of this thesis).

Olaparib was poorly active or inactive in tumor models that were classified as Not BRCAness, such as MNHOC 18, 124, 143, 94/2-C and 182. In each case the course of the disease was progressive after a short-term treatment (Figure 4.1, panel A), and tumor growth also increased markedly (similar to vehicle controls) in a maintenance regimen (Figure 4.1, panel C).

These results confirmed that our OC-PDX models enabled us to recapitulate the drug profile sensitivity seen in patients from which they derived, making them a reliable tool for drug discovery.

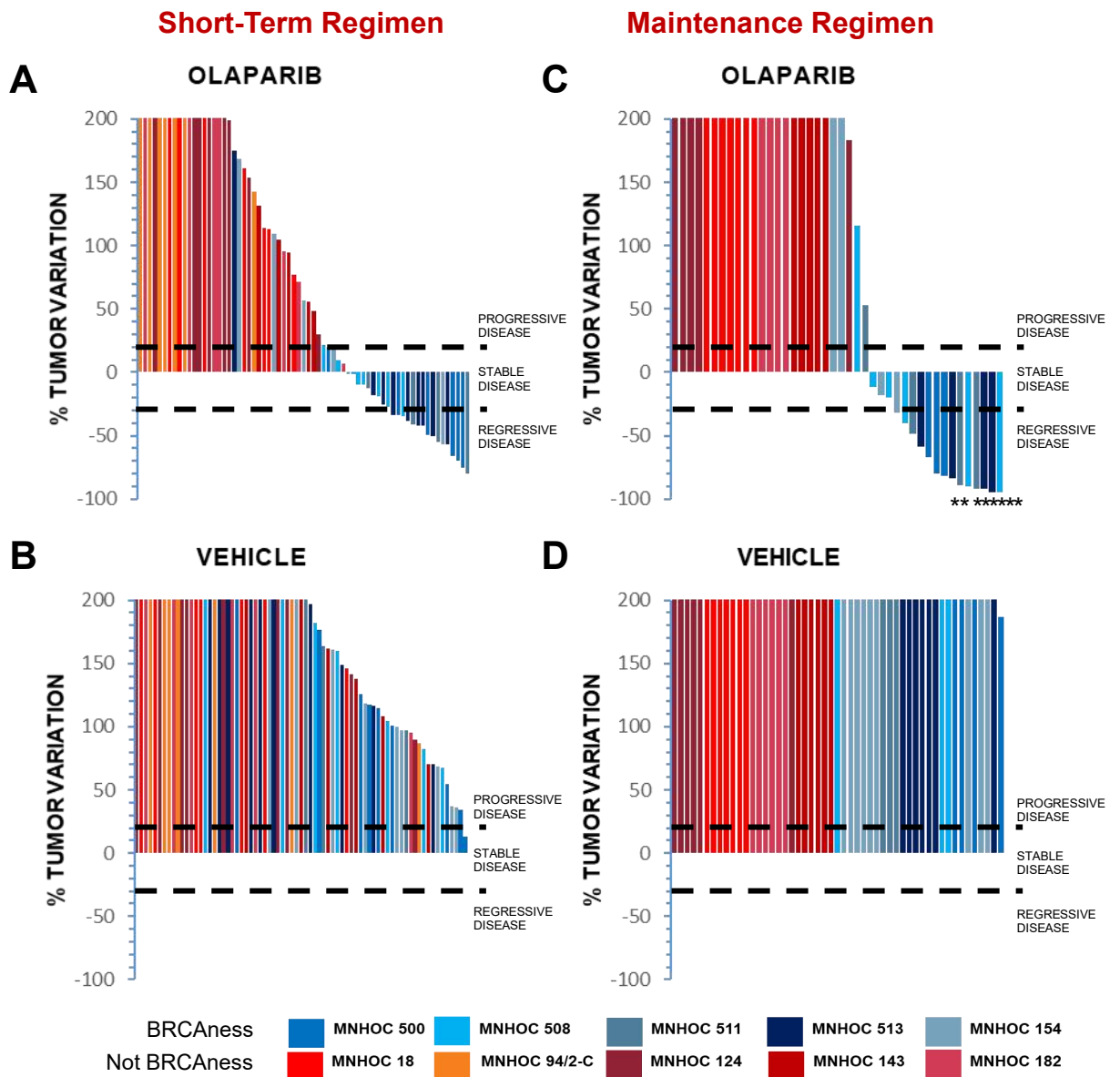


Figure 4.1 Correlation between BRCAness status and response to olaparib monotherapy in a short-term versus maintenance regimen.

Olaparib (100 mg/kg) was administered by oral gavage every day for 5 days on and 2 days off (Q1x5), for four cycles (short-term regimen) or until tumor progression (maintenance regimen).

Treatment efficacy was expressed as % tumor variation after (A – B) short-term (4 weeks, day 28) and (C – D) maintenance (12 weeks, day 100) regimen.

%tumor variation = [(tumor volume day 28 or day 100-tumor volume day 0)/tumor volume day 0] x 100, considering day 0 randomization time.

Disease was considered progressive = tumor variation > 20%; stable = -30% < tumor variation < 20%; regressive = tumor variation > -30%. * Complete responses = tumor free mice at day 200.

N= 4-7 tumors per model.

4.2 THE IMPORTANCE OF THE COMBINATION OF OLAPARIB AND CEDIRANIB

Interest in adding cediranib, an anti-angiogenic agent with activity against VEGF receptors (VEGFR1, 2, 3), c-KIT and PDGFR-alpha, to olaparib has increased recently. Both oral agents have displayed antitumor activity in women with recurrent ovarian cancer (Kaufman et al., 2015; Ledermann et al., 2016) and the combination is ongoing in clinical trials (Liu et al., 2013, 2014).

Olaparib (100 mg/kg) and cediranib (3 mg/kg) in combination were administered orally, every day for 5 days on and 2 days off (Q1x5) with the same doses and scheduled as the single agents, in a short-term treatment regimen of 4 weeks or in a maintenance regimen (until partial regression – 30% of the tumor volume at random - or progression).

After 4 weeks of treatment, the number of progressing single tumors was lower compared to single drug administration (Figure 4.2, panel A), including Not BRCAness tumors that were not responsive to olaparib or cediranib single therapy (all the cases of MNHOC 94/2-C, three MNHOC 124 and one MNHOC 18 tumor).

Of note, the combination increased the number of stable and regressing tumors, most remarkably among the Not BRCAness (most of the MNHOC 18 and 124, all MNHOC 182 and 143) and also those BRCAness cases that marginally responded to olaparib single therapy benefitted from the combination (such as MNHOC 508 and 154) (Figure 4.2, panel A). Moreover, the combination also increased tumor regression rates in those BRCAness tumors that were sensitive to olaparib single therapy (Figure 4.2, panel A).

The long-term administration (maintenance regimen) of the combination possibly boosted the outcome, increasing the number of regressions, equally affecting the BRCAness and Not BRCAness tumors and leading to some complete responses with cured mice (Figure 4.2, panel D).

The short-term (4 weeks) administration of cediranib single therapy caused a heterogeneous response within the OC-PDX. Stable disease and regressions were achieved both for Not BRCAness (MNHOC 124 and MNHOC 143) and almost all the BRCAness models (MNHOC 500, 508, 511, 513 and 154) (Figure 4.2, panel C). Progressive disease was evident especially among Not BRCAness OC-PDX (MNHOC 18, 94/2-C and 182), but also in BRCAness cases (two MNHOC 513, one MNHOC 154 and one MNHOC 508) (Figure 4.2, panel C). The administration of the anti-angiogenic agent in a maintenance regimen resulted in stable disease and regressions in those tumors that already benefitted from the short-term treatment, leaving the not responsive progressing under treatment (Figure 4.2, panel F).

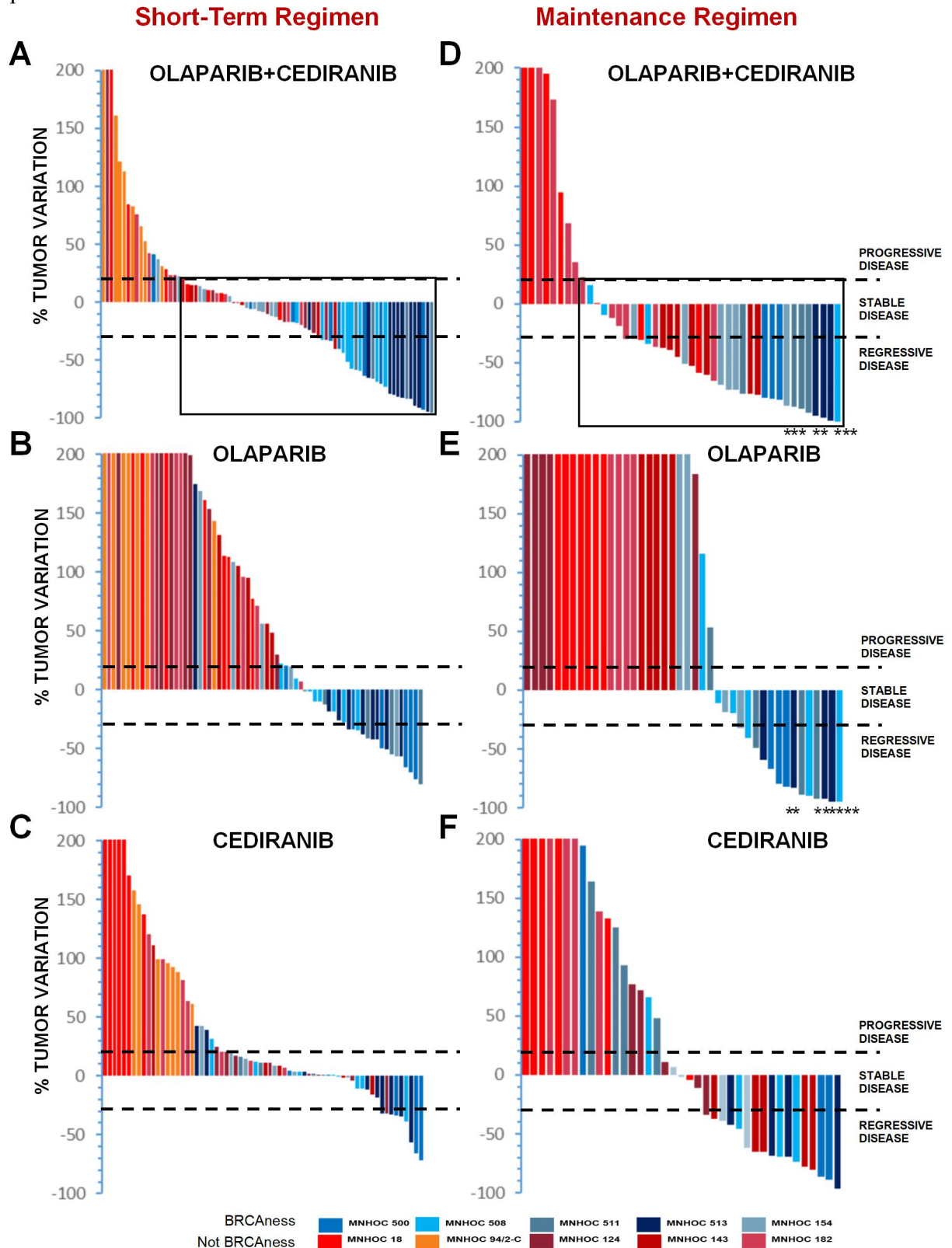


Figure 4.2 The combination of olaparib and cediranib in a short-term and in maintenance (until tumor progression) regimen.

Olaparib (100 mg/kg) and cediranib (3 mg/kg), alone or in combination, were administered by oral gavage every day for 5 days on and 2 days off (Q1x5). Treatment efficacy was expressed as % tumor variation after (A – C) short-term (4 weeks, day 28) and (D – F) maintenance (12 weeks, day 100) regimen. Disease was considered progressive = tumor variation > 20%; stable = -30% < tumor variation < 20%; regressive = tumor variation < -30%. * Complete responses = tumor free mice at day 200. N= 4-7 tumors per model. Waterfall B and E as in Figure 4.1.

Summary of results

- OC-PDX, classified as BRCAness types and carrying mutations or loss of *BRCA1* and 2, responded to olaparib single therapy, both after a short-term treatment and even more notably after a maintenance regimen, with complete responses: there was a strong correlation between homologous recombination deficiency and sensitivity to PARP inhibition.
- OC-PDX displayed a heterogeneous response to cediranib, independent of the homologous recombination status: sensitivity to the anti-angiogenic drugs was dependent on intrinsic features of the tumor or tumor microenvironment.
- The antitumor activity was improved when cediranib was added to olaparib. The superiority of the combination was especially evident for those models that were poorly responsive to the single treatment with olaparib, such as the Not BRCAness types: the results suggested a possible additivity between the two drugs.

4.3 THE COMBINATION OF OLAPARIB AND CEDIRANIB IN ECTOPIC MODELS OF OVARIAN CANCER

To investigate the relevance of the effect of the combination of these two agents, a case-report analysis was performed on the most representative models of OC-PDX, both Not BRCAness and BRCAness

4.3.1 Case-report: MNHOC 18, Not BRCAness

MNHOC 18 was established from a high grade endometrioid primary tumor at the ovary.

The activity of olaparib and the addition of cediranib was tested in a short-term regimen (4 weeks) in the first experiment (Figure 4.3, panel A). Doses, schedules and evaluation of treatment as in Section 2.3.2 and 2.3.3 Materials and Methods.

Tumors progressed rapidly under treatment with olaparib single therapy (T/C 59%), with no significant difference from vehicle-treated controls. Absolute growth delay was 9 days, with a doubling time of 10 days compared to 8 days for the vehicle-treated controls. Cediranib alone was no different from olaparib monotherapy (T/C 57%), with an absolute growth delay and a doubling time of 12 and 13 days respectively (Figure 4.3, panel A).

The combination of olaparib plus cediranib was the most effective treatment (T/C 29%), inducing stable disease until the end of the 4 weeks of administration. As soon as the treatment was stopped, tumors started to re-grow, with an absolute growth delay increased up to 53 days and regrowth doubling time of 51 days compared to vehicle (Figure 4.3, panel A).

The fast regrowth of tumors at the termination of treatment prompted us to investigate the effect of the maintenance regimen (Figure 4.3, panel B). As above, olaparib alone was inactive in reducing or delaying tumor growth (T/C 62%), with the same doubling time as vehicle controls (24 days). The addition of cediranib to olaparib in combination stabilized and controlled tumor progression during 18 weeks of daily administration (T/C 33%). Eventually, tumors progressed under treatment, with an absolute growth delay of 92 days compared to vehicle and 2/7 mice were tumor-free at day 150.

Cediranib in a maintenance regimen was slightly more effective in delaying tumor progression (T/C 41%) than in the short-term treatment, with an absolute growth delay of 55 days.

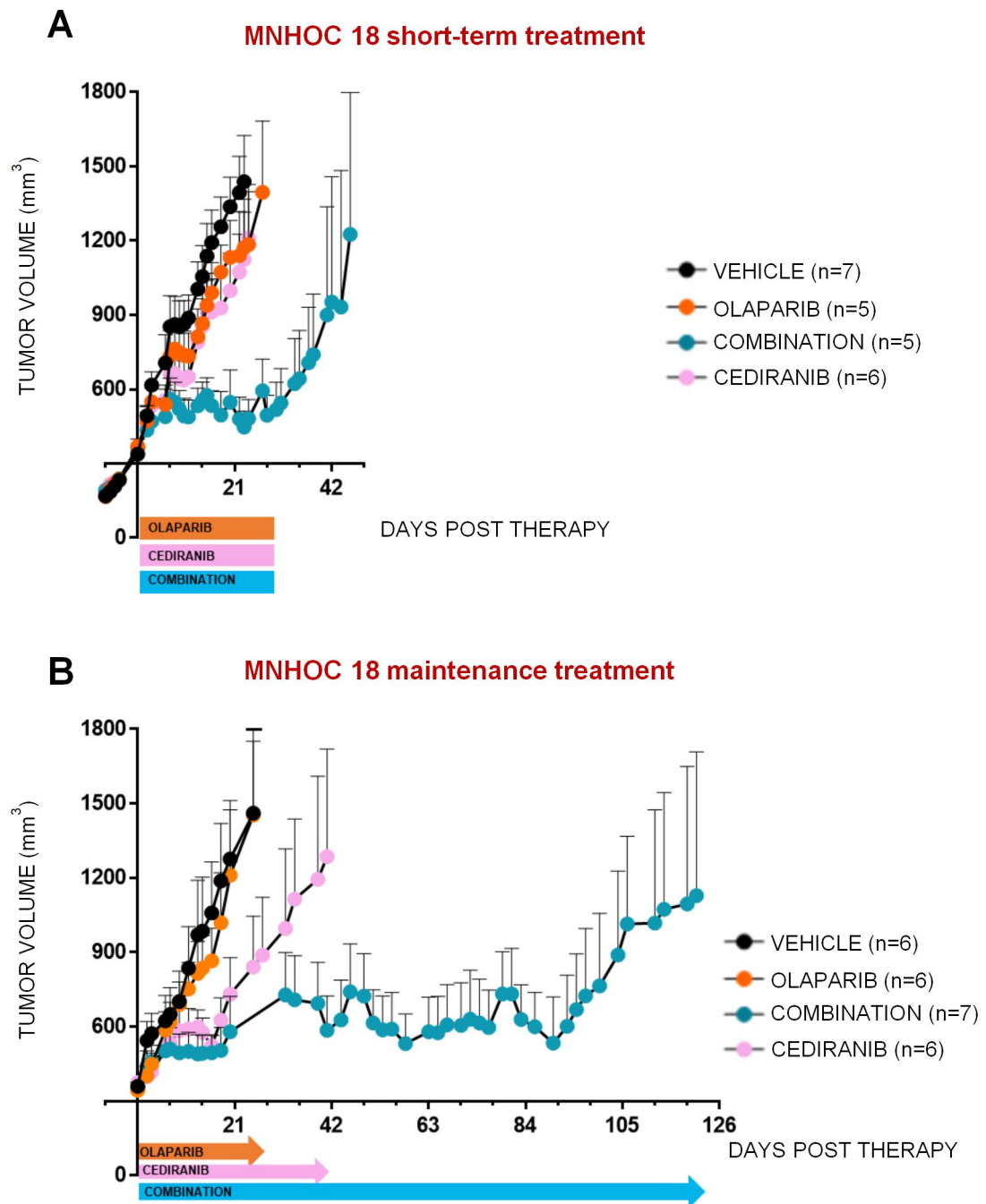


Figure 4.3 The combination in maintenance regimen: the case of MNHOC 18, Not BRCAness.

Mice were randomized to treatment at an average tumor volume of 300 mm³ (subcutaneously growing tumor), doses and schedule as in Materials and Methods (Chapter 2). Responses were **A**) tumor growth after olaparib, cediranib and the combination in a short-term regimen (4 weeks), **B**) tumor growth after olaparib, cediranib and the combination in a maintenance regimen (until tumor progression). Data are mean \pm SD.

4.3.2 Case-report: MNHOC 182, Not BRCAness

MNHOC 182 was established from a mucinous primary tumor in the ovary.

Olaparib slightly reduced tumor growth (T/C 41%), with an absolute growth delay of 14 days; the addition of cediranib to olaparib induced a significant stabilization of tumor volume (T/C 17%), with an absolute growth delay of 276 days. As soon as the therapy was terminated at day 210 (after 30 weeks of treatment), tumors progressed rapidly, with a regrowth doubling time of approximately one month (Figure 4.4).

Cediranib alone was moderately active in delaying tumor progression (T/C 27%), with values of absolute growth delay of 176 days (Figure 4.4).

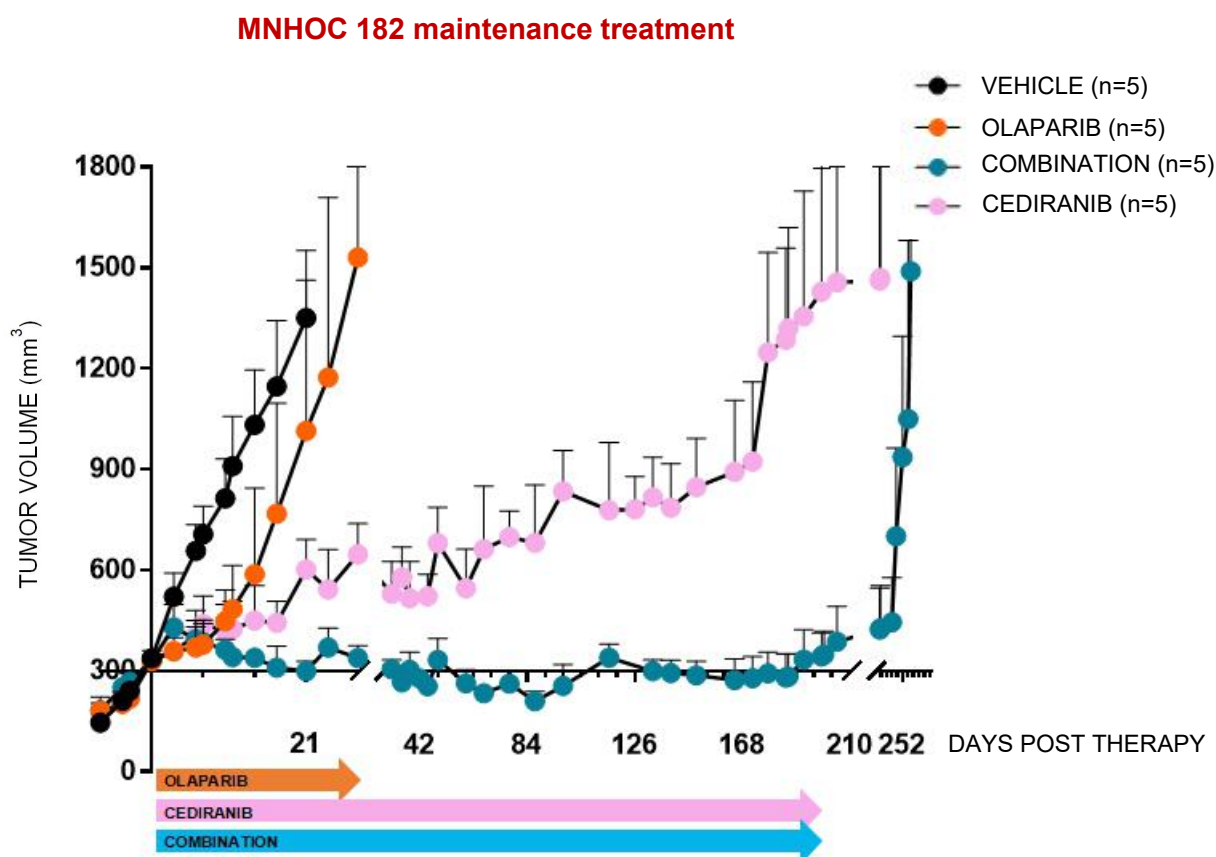


Figure 4.4 The combination in maintenance regimen: the case of MNHOC 182, Not BRCAness.

Antitumor activity of olaparib, cediranib and the combination was evaluated in MNHOC 182, growing subcutaneously. Mice were randomized to treatment at an average tumor volume of 300 mm³, doses and schedule as in Materials and Methods (Chapter 2). Responses were shown as tumor growth after olaparib, cediranib and the combination in a maintenance regimen (until tumor progression). Data are mean \pm SD.

4.3.3 Case-report: MNHOC 508, BRCAness

MNHOC 508 was established from a high grade serous primary tumor in the omentum.

The activity of olaparib and cediranib combination was tested in a short-term regimen (4 weeks) in the first experiment (Figure 4.5, panel A) and in a maintenance regimen (Figure 4.5, panel B). Doses and schedules were described in Section 2.3.2 and 2.3.3, Materials and Methods.

Olaparib and cediranib single agents induced a stabilization of tumor growth under treatment compared to vehicle (T/C 26% and 36% respectively), with olaparib being slightly more effective in delaying tumor growth than cediranib (absolute growth delay - AGD- 46 days and 30 days respectively) (Figure 4.5, panel A).

The combination was more effective in reducing and delaying tumor growth (T/C 14% compared to vehicle, 23% compared to cediranib and 40% compared to olaparib); tumor volume reduction reached its nadir at day 28, concomitantly with the end of the short-term treatment. The regression was maintained for approximately one month from the conclusion of treatment. The delay in tumor growth was 60 days from therapy initiation. In all treatment arms tumors regrew at the end of 4 weeks treatment, with a comparable doubling time (29 days for olaparib, 25 days for cediranib, 25 days for the combination) (Figure 4.5, panel A).

When drugs were given in a maintenance regimen (Figure 4.5, panel B), the effect was more pronounced: cediranib stabilized tumor growth (T/C 34%), both olaparib and the combination induced sustained tumor regressions (T/C 4% and 6% respectively), with tumors reaching their smallest volume at day 63. This prompted us to interrupt all the treatments after 9 weeks of daily administration.

Soon after the suspension of treatment, tumors started to re-grow, reaching the target volume of 300 mm³ in about 35 days for olaparib and 51 days for the combination, while cediranib treated tumors remained stable. Tumors were thus rechallenged to treatment at day 98 with cediranib, olaparib or the combination.

All the treatments delayed tumor growth compared to vehicle (AGD 160 days, 130 days and 176 days respectively), but after treatment restarted the responses were heterogeneous.

At rechallenge, 4/6 tumors progressed rapidly under treatment with olaparib alone; these tumors were no longer responsive to treatment. The potential mechanisms of the resistance to olaparib at relapse would be of interest but are beyond the scope of this PhD research. However, single cell analysis (DNA and RNA sequencing) could be performed, in order to assess if a sub-clonal cell population arise capable of growing under drug pressure in those tumors that progressed at rechallenge, and if tumor cells are enriched in some particular mutation, genomic alteration or change in gene expression induced by the treatment, that could explain the acquired resistance.

When olaparib was administered in combination with cediranib, a more pronounced regression was induced at rechallenge, with tumors reaching the lowest volume at day 147; 2/4 tumors progressed under treatment, with a regrowth doubling time of 45 days (Figure 4.5, panel B).

Cediranib stabilized tumor growth for a longer period (until day 161); then 3/4 tumors progressed under treatment, with a regrowth doubling time of 48 days.

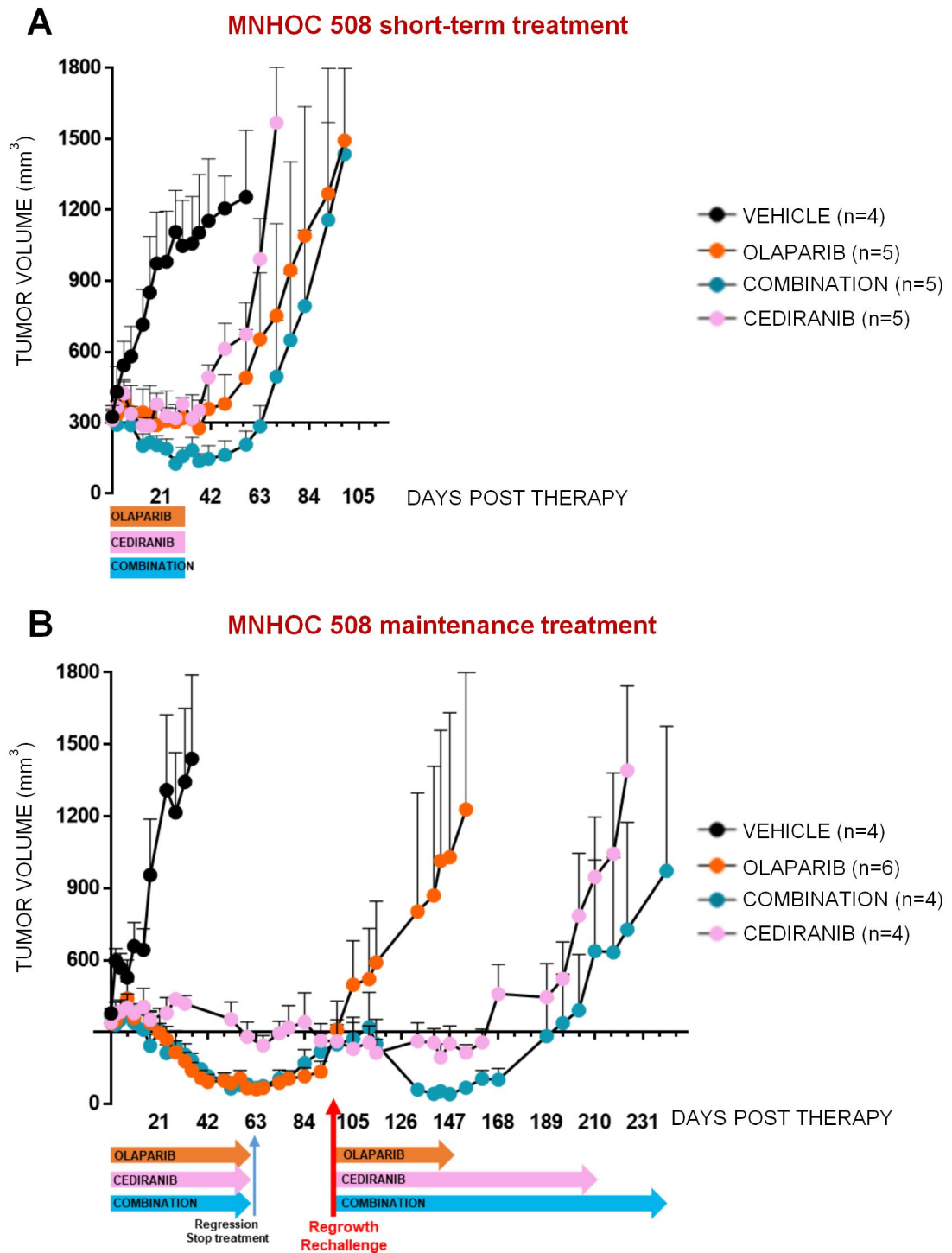


Figure 4.5 The combination in maintenance regimen: the case of MNHOC 508, BRCAness.

Mice were randomized to treatment at an average tumor volume of 300 mm³ (subcutaneously growing tumor), doses and schedule as in Materials and Methods (Chapter 2). Responses were **A**) tumor growth after olaparib, cediranib and the combination in a short-term regimen (4 weeks), **B**) tumor growth after olaparib, cediranib and the combination in a maintenance regimen (until tumor progression). Data are mean \pm SD.

4.3.4 Cases-report: MNHOC 511 and MNHOC 513, BRCAness

Having demonstrated the superiority of the maintenance regimen, MNHOC 511 (Figure 4.6, panel A) and MNHOC 513 (Figure 4.6, panel B) bearing mice were treated until complete regression or progression.

MNHOC 511 was derived from a high grade serous primary tumor from the omentum.

Olaparib itself was very active, such that the combination with cediranib only marginally improved response and treatment was stopped after 9 weeks (day 63).

After treatment suspension, tumors slowly progressed, reaching 300 mm³ in 56 and 84 days for olaparib and the combination respectively. Tumors were then rechallenged at day 119 and day 147 respectively. In both arms a significant regression was induced, that led to complete responses and tumor-free mice at day 200 (Figure 4.6, panel A).

MNHOC 511 proved moderately responsive to cediranib (T/C 33%), with tumors that progressed under treatment and continued to grow after treatment cessation at day 63. The absolute mean tumor growth delay in the group was 45 days and the doubling time 82 days (Figure 4.6, panel A).

Interestingly in this case, treatment information on the corresponding patient, from which MNHOC 511 was established, were available. The MNHOC 511 patient relapsed after first-line chemotherapy and was treated with olaparib; at present, she is still under treatment and showing a complete response. This OC-PDX could be considered a powerful example of perfect correlation between the biological and pharmacological behaviour of the OC-PDX and the corresponding patient, once again stressing the predictive value of xenografts to study the more appropriate treatment for patients (Figure 4.6, panel A).

MNHOC 513 was derived from a high grade serous primary tumor from the omentum.

Olaparib and cediranib single agents were active, inducing tumor regressions when administered in a maintenance regimen (T/C 2% and 4% respectively; AGD 168 and 139 days respectively). At this time point treatment was interrupted (day 84), after 12 weeks, but tumors regrew immediately, reaching a volume of 300 mm³ in 63 days (Figure 4.6, panel B).

At variance of MNHOC 511, tumors progressed rapidly despite re-challenge (day 147), with doubling times of 28 days and 23 days respectively.

When olaparib was administered in combination with cediranib, a stronger tumor regression occurred and treatment was stopped at day 81. After the end of treatment, no regrowth was detected, with complete responses and 3/3 mice considered cured at day 200 (Figure 4.6, panel B).

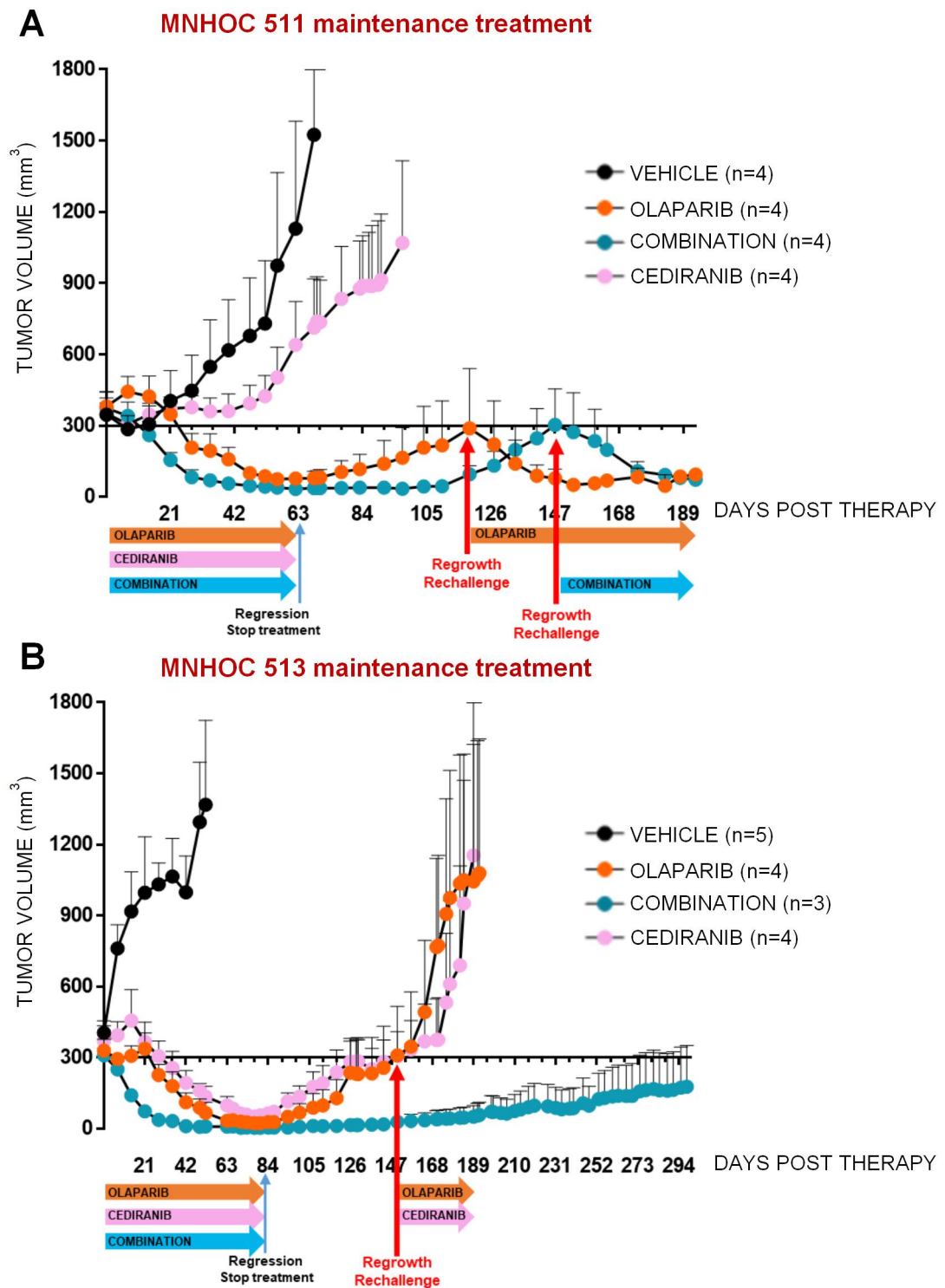


Figure 4.6 The combination in maintenance regimen: the cases of MNHOC 511 and MNHOC 513, BRCAness.

Antitumor activity of olaparib, cediranib and the combination was evaluated in MNHOC 511 and MNHOC 513, growing subcutaneously. Mice were randomized to treatment at an average tumor volume of 300 mm^3 , doses and schedule as in Materials and Methods (Chapter 2). Responses were shown as tumor growth after olaparib, cediranib and the combination in a maintenance regimen (until tumor progression) for **A**) MNHOC 511 and **B**) MNHOC 513. Data are mean \pm SD.

4.3.5 Case-report: MNHOC 154, BRCAness

MNHOC 154 was established from a relapsed tumor at the omentum of a high grade endometrioid patient.

From studies previously carried out in the laboratory, MNHOC 154 was moderately sensitive to cisplatin, with a T/C of 39% (Ricci et al., 2014).

Although MNHOC 154 carried a mutation in *BRCA1*, thus of BRCAness phenotype, the activity of olaparib was heterogeneous, with 2/4 tumors that did not respond and continued to grow under treatment, 1/4 long responder started to regrow at day 150 post therapy and 1/4 was stabilized by the treatment (Figure 4.7). This heterogeneity in olaparib sensitivity could be due to the presence of the amplification in *BRCA2* (see Table 3.4 and Figure 3.4-3.6, Chapter 3).

When cediranib was added to olaparib, tumor regression was induced in all mice (T/C 3%), with treatment being stopped after 13 weeks (day 91). The effect of the combination continued even when treatments were discontinued, with a stabilization of tumor growth and only 3/6 tumors that slowly regrew at day 158 (Figure 4.7). The activity of the combination was more pronounced compared to cediranib single agent, reaching the smallest tumor volume at day 84 (mean tumor volume 125 mm³).

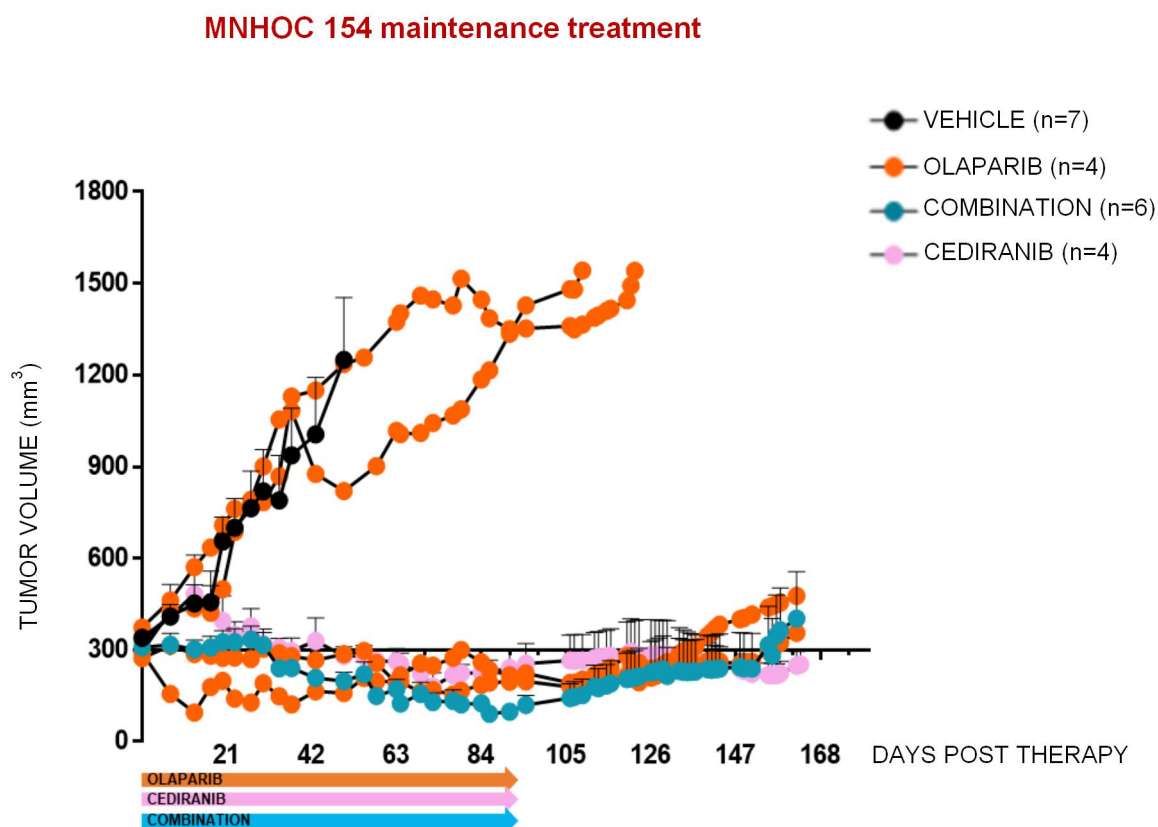


Figure 4.7 The combination in maintenance regimen: the case of MNHOC 154, BRCAness.

Antitumor activity of olaparib, cediranib and the combination was evaluated in MNHOC 154, growing subcutaneously. Mice were randomized to treatment at an average tumor volume of 300 mm³, doses and schedule as in Materials and Methods (Chapter 2). Responses were shown as tumor growth after olaparib, cediranib and the combination in a maintenance regimen (until tumor progression). Data are mean \pm SD for vehicle, cediranib and combination. Data are single tumor volume for olaparib.

Summary of results

- In Not BRCAness models of OC-PDX, olaparib was inactive or very poorly active, with tumors progressing rapidly under treatment, in both MNHOC 18 and MNHOC 182.

When cediranib was added to olaparib, the effect of the combination remarkably improved the outcome. In MNHOC 18, the short-term regimen of 4 weeks induced stable disease while drugs were administered. The cessation of treatment led to a rapid progression.

The maintenance administration of the combination boosted the outcome, mainly stabilizing tumor growth for several weeks (18 weeks for MNHOC18 and 30 weeks for MNHOC182), and then tumors progressed rapidly under treatment. The effect of the combination in a maintenance regimen in MNHOC 182 suggested a greater synergism for all the subtypes of ovarian cancer, not only serous and endometrioid, but also mucinous.

Taken together, these results indicate the importance of adding cediranib to olaparib, especially in a maintenance regimen, as was evident in the waterfall plot (Figure 4.2, panel A and D), analysing the whole panel of Not BRCAness models.

Cediranib was variously effective in delaying tumor growth, with MNHOC 18 being the most resistant. We hypothesise that the effect of the anti-angiogenic is likely linked to the intrinsic microenvironmental features within each model.

- In BRCAness models of OC-PDX, olaparib, in general, stabilized tumor growth when administered in a short-term regimen of 4 weeks. Immediately after removing the drug, tumors progressed. A marked and persistent regression was obtained when the regimen was maintained. When tumors were rechallenged by

monotherapy with olaparib, the responses were heterogeneous: in MNHOC 508 and MNHOC 513, a linear progression under treatment was induced, while in MNHOC 511 regression was again achieved. In MNHOC 154, previously reported as moderately sensitive to platinum, a heterogeneous response to olaparib was observed, with 2/4 single tumors that continued to grow under treatment and 2/4 sustainably inhibited.

The combination of olaparib plus cediranib proved to be the most active regimen, by inducing tumor regression - even after a short-term treatment, as in MNHOC 508 - and further delaying tumor regrowth in a prolonged regimen - as for MNHOC 508 and MNHOC 511. The combination showed the best outcome for MNHOC 513 and MNHOC 154, with complete responses that persisted several weeks after treatment suspension.

Taken together, these results indicate the advantage of adding cediranib to olaparib also in OC-PDX that already gained a benefit from olaparib single therapy, such as the BRCAness types. The results supported the waterfall plot analysis (Figure 4.2, panel A and D) considering all the BRCAness models.

Cediranib was variably effective in delaying (MNHOC 513 and MNHOC 154) or stabilizing (MNHOC 508) tumor growth, except for MNHOC 511, which progressed under treatment.

Ectopic models represent a powerful tool to study pharmacological activity, being easier to continuously monitor over time and being quite reproducible.

However, ectopic models do not reproduce the biology of the disease, lacking, for example, of the ability to disseminate, invade organs of the peritoneal cavity and forming ascites.

To gain further insight into a more “close-to-patient” setting, we studied the effect of the combination on tumor models growing orthotopically in the peritoneal cavity of mice.

4.4 THE COMBINATION OF OLAPARIB AND CEDIRANIB IN ORTHOTOPIC MODELS OF OVARIAN CANCER

4.4.1 Case-report: MNHOC 8, BRCAness

MNHOC 8 was derived from ascites of a patient diagnosed with high grade serous ovarian carcinoma and established as ascites in the mouse peritoneal cavity.

The combination administered in a short-term regimen (4 weeks).

In the first experiment, we assessed the response of MNHOC 8 to olaparib and the addition of cediranib in combination in a short-term regimen (4 weeks), starting treatment at an advanced stage of disease (day 10 after transplantation).

Olaparib increased survival (MST 61 days; ILS 74%) and a similar effect was observed with cediranib (MST 61 day; ILS 71%) (Figure 4.7, panel A).

The addition of the antiangiogenic to olaparib marginally improved the outcome (MST 68 days; ILS 95%), with 1/9 mice alive at day 200, considered cured by necropsy (Figure 4.8, panel A).

At the end of 4 weeks treatment, ascites was present only in vehicle-treated mice, while was almost absent in treated groups, comparable to the level recorded at the beginning of treatment (random group) (Figure 4.8, panel B)

Dissemination to the organs of the peritoneal cavity, assessed using an arbitrary score (see Section 2.1.4.3 Materials and Methods), was diminished in olaparib treated animals, and significantly more when in combination with cediranib, compared to vehicle controls (Figure 4.8, panel B).

The analysis at survival off treatment showed increased ascites, especially in the olaparib group. Cediranib and the combination inhibited ascites formation compared to vehicle controls and olaparib single agent groups (Figure 4.8, panel C).

A macroscopical analysis in the organs of the peritoneal cavity at survival indicated that, despite the effect of olaparib in controlling tumor burden, the combination with cediranib somewhat impaired the outcome, with mice living longer, but dying with a more aggressive disease (Figure 4.8, panel C).

These results suggested that the effectiveness of the combination was present during treatment and was lost when therapy ceased.

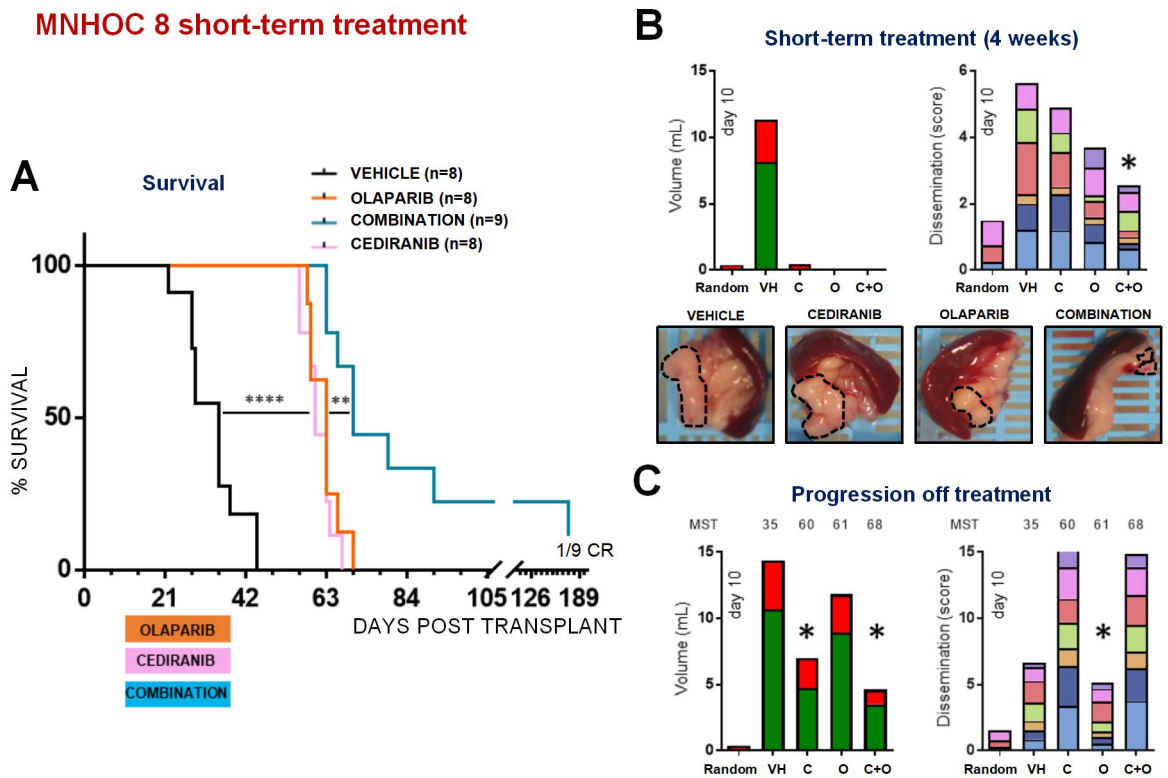
The combination administered in a maintenance regimen.

To confirm the efficacy of the combination with a continuous exposure, in a second experiment cediranib was added to olaparib in a maintenance regimen, until survival. Treatment started at an advanced stage of disease (20 days after transplantation). An additional group was included, in which the combination was terminated on day 142, after approximately 20 weeks of drug administration (COMBINATION stop day 142), as reported in Figure 4.8, panel D.

Olaparib, significantly prolonged survival (MST 56 days and ILS 100%) when given for approximately 13 weeks, until each mouse progressed and was culled. When cediranib was added to olaparib in a maintenance regimen, the outcome was significantly enhanced (MST 105 days and ILS 275%), with 1/6 mice alive at day 300, considered cured. Of note is the fact that when the combination was interrupted at day 142, tumors progressed rapidly and mice were culled within two weeks (MST 148 days and ILS 427%) (Figure 4.8, panel D). At necropsy, olaparib slightly reduced ascites, while cediranib and the combination in maintenance significantly inhibited ascites formation (Figure 4.8, panel E).

However, in contrast, tumor dissemination was significantly affected by olaparib. Interestingly, as observed in the experiment above, the addition of cediranib prolonged survival, despite an apparently increased tumor dissemination (Figure 4.8, panel E).

MNHOC 8 short-term treatment



MNHOC 8 maintenance treatment

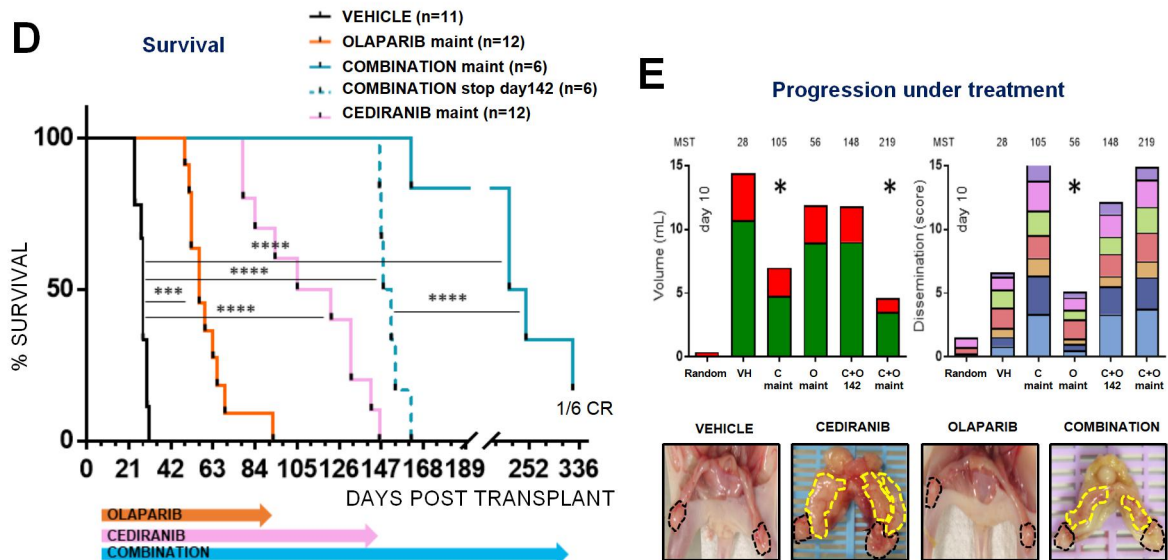


Figure 4.8 The combination in the orthotopic model MNHOC 8, BRCAness.

Doses and schedule as in Materials and Methods (Chapter 2).

A) Survival in a short-term regimen (4 weeks).

Volume of ascites and dissemination were evaluated **B)** at 4 weeks and **C)** at progression-off treatment (survival). Representative images of invaded pancreas at the end of treatment.

D) Survival in a maintenance regimen (until progression) and **E)** volume of ascites and dissemination evaluated at progression under treatment. Representative images of invaded ovaries and uterus are reported.

VH, vehicle; Cstop, cediranib 4 weeks; Cmaint, cediranib in maintenance; Ostop, olaparib 4 weeks; Omaint, olaparib in maintenance; C+O, combination; C+Omaint, combination in maintenance; C+O 142, combination stopped at day 142 MST, median survival times (days). *P<0.05; **P<0.01; ***P<0.001; ****P<0.0001.

The importance of drug sequence in the combination.

To shed light on which of the two players, the PARP inhibitor olaparib or the angiogenesis inhibitor cediranib, was the key effector of the combination, a third experiment was performed (Figure 4.9), with different sequences of the two drugs.

The combination was given for 4 weeks. Then mice were randomized to continue combination (COMBINATION maint) or switched to olaparib (COMBINATION stop/OLAPARIB maint) or cediranib (COMBINATION stop/CEDIRANIB maint).

The combination (COMBINATION stop) was effective in prolong animal survival even after only 4 weeks of treatment (MST 71 days and ILS 109%); the switch to olaparib prolonged survival (MST 98 days and ILS 188% compared to vehicle and 38% compared to COMBINATION stop), with 3/7 long responding mice, culled at day 200. The switch to cediranib increased survival although mice ultimately did not respond to treatment and were culled (MST 101 days and ILS 197% compared to vehicle and 42% compared to COMBINATION stop). The combination of the two inhibitors given in a maintenance regimen (COMBINATION maint), from randomization until progression, was the most effective treatment, strongly increasing survival (MST 142 days and ILS 316%), with 3/8 cured mice culled at day 200 (Figure 4.9, panel A).

Necropsy revealed that the combination administered for 4 weeks (COMBINATION stop) was not sufficient to affect ascites and tumor dissemination, probably explaining the worse survival compared to the other treatment groups (Figure 4.9, panel B).

The switch to olaparib (COMBINATION stop/OLAPARIB maint) decreased ascites and tumor dissemination. The switch to cediranib (COMBINATION stop/CEDIRANIB maint) significantly reduced ascites but was unable to control tumor dissemination, which could explain the rapid loss of response. The combination of the two drugs maintained until

progression (COMBINATION maint) reduced ascites and tumor dissemination (Figure 4.9, panel B).

MNHOC 8: the importance of drug sequence

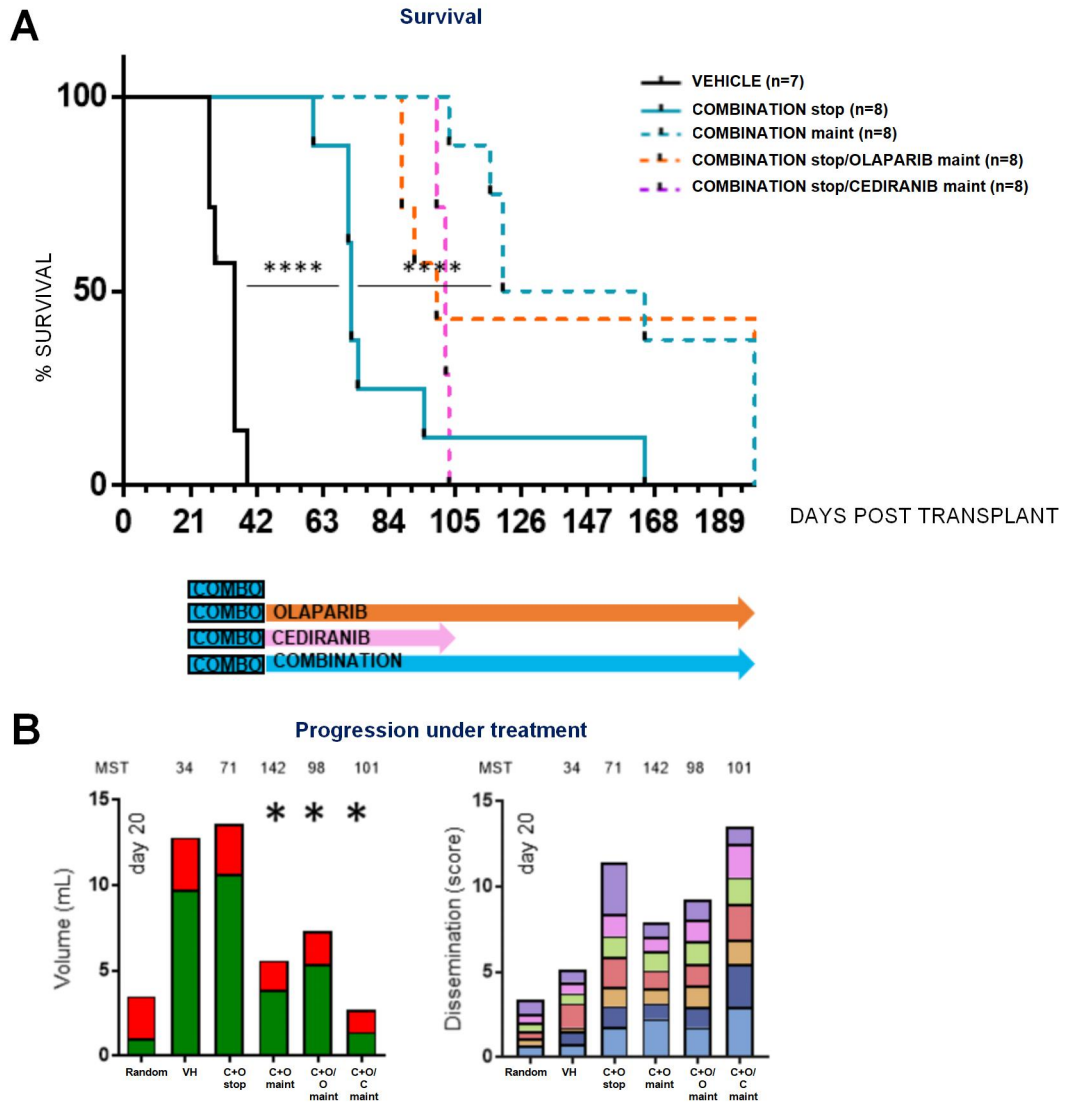


Figure 4.9 The importance of drug sequence in the combination olaparib plus cediranib.

A) Mice bearing intraperitoneal MNHOC 8 were treated with the combination olaparib plus cediranib in short-term regimen (4 weeks), then switched to olaparib or cediranib in maintenance, or maintained until tumor progression under treatment, and survival was evaluated.

B) Volume of ascites and dissemination were evaluated at progression under treatment.

VH, vehicle; C+Ostop, 4 weeks combination; C+O maint, combination in maintenance; C+O/O maint, 4 weeks combination then olaparib in maintenance; C+O/C maint, 4 weeks combination then cediranib in maintenance.

MST, median survival times (days). *P<0.05; ****P<0.0001.

Legend: Pellet (red), Ascites (green), Ovary (blue), Uterus (dark blue), Diaphragm (orange), Pancreas (pink), Gut (light green), Liver (purple), Carcinomatosis (grey).

Summary of results

- The orthotopic model MNHOC 8 could be considered a robust tool to study the effect of drug treatment, due to the resemblance to the original biological features of the patient's tumor.
- In the BRCAness orthotopic model MNHOC 8, olaparib significantly increased survival, mainly when administered in a maintenance regimen until tumor progression

The PARP inhibitor was primarily active on solid “primary” tumors, decreasing dissemination and carcinomatosis. Median survival time was doubled compared to vehicle controls, and mice were culled due to the degree of ascites but with a lower tumor burden.

The combination of olaparib plus cediranib performed better, both in a short-term treatment and even more when administered in a maintenance regimen until tumor progression. Of relevance, the cessation of drug treatment led animals to the need for culling in less than two weeks, endorsing the necessity of the treatment to be maintained, as also demonstrated in different drug sequences. Survival was significantly prolonged to the detriment of a more aggressive disease (tumor dissemination), counteracted by the inhibition of ascites.

This particular effect could be explained by the presence of cediranib, which continued to limit ascites; animals lived longer but suffered from solid masses that compromised the vital function of the peritoneal organs.

4.5 THE COMBINATION OF OLAPARIB WITH OTHER ANGIOGENESIS INHIBITORS

To confirm that the advantage of the combination of olaparib plus cediranib was not related to the pharmacological profile of the angiogenesis inhibitor, we investigated the addition of different angiogenic inhibitors (i.e. bevacizumab and B20) in the ectopic (s.c) MNHOC 18 (Figure 4.10) and orthotopic (i.p) MNHOC 8 model (Figure 4.11).

Bevacizumab is an antibody that recognizes human VEGF, and B20 recognizes both human and mouse VEGF exhibiting an equal affinity (EC50 0.17 nmol/L for h-VEGF and EC50 0.17 nmol/L for m-VEGF) (Liang et al., 2006).

4.5.1 Case-report: MNHOC 18, Not BRCAness

Tumors progressed rapidly under bevacizumab single agent therapy, as well as under bevacizumab added to olaparib (T/C 46% and 36% respectively), with a doubling time of 15 days and 24 days respectively (Figure 4.10, panel B).

Similarly, B20 (B20 TWICE) caused a modest tumor growth delay (T/C 51%) and did not give any advantage when added to olaparib, neither administered once (B20 ONCE+OLA) nor twice a week (B20 TWICE+OLA) (T/C 53% and 60% respectively), with comparable doubling times (18 days, 16 days and 13 days respectively) (Figure 4.10, panel C).

MNHOC 18: olaparib in combination with different angiogenesis inhibitors

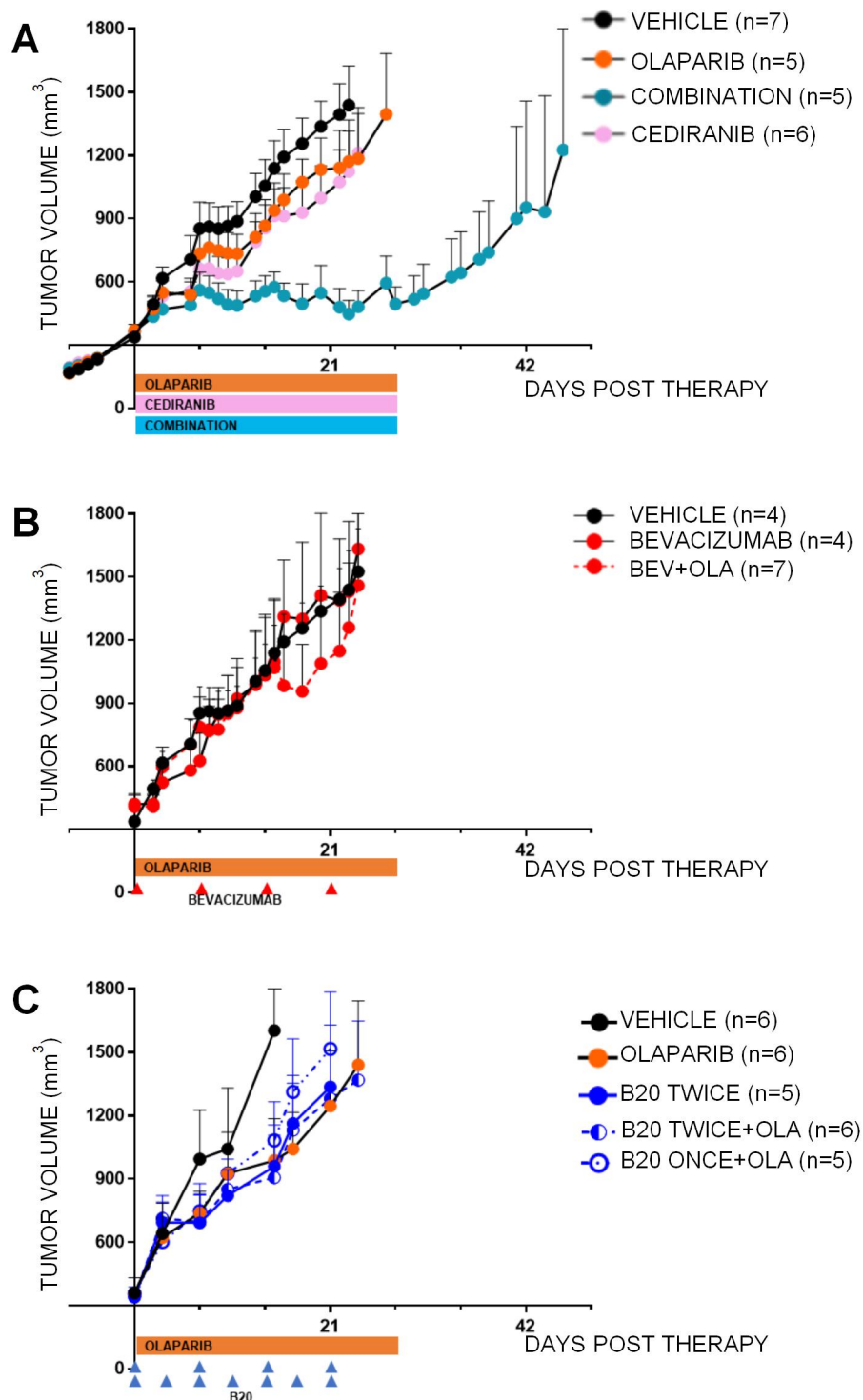


Figure 4.10 Olaparib in combination with different angiogenesis inhibitors: the case of the ectopic MNHOC 18, Not BRCAness.

Mice bearing MNHOC 18 subcutaneously were treated in a short-term regimen (4 weeks) with olaparib (100mg/kg) in combination with:

A) Cediranib (3mg/kg, p.o, daily), same graph of Figure 4.3, panel A;

B) Bevacizumab (5mg/kg, i.v, once a week), the antibody anti-human VEGFA;

C) B20 (5mg/kg, i.v, once or twice a week), the antibody recognising both human and murine VEGFA. Data are mean \pm SD.

4.5.2 Case-report: MNHOC 8, BRCAness

To assess if the effect of the combination was a general phenomenon achievable with other angiogenesis inhibitors in orthotopic OC-PDX, the activity of olaparib was evaluated in combination with bevacizumab in a maintenance regimen in MNHOC 8 (Figure 4.11). Olaparib plus bevacizumab (COMBINATION BEV+OLA) was slightly less effective in prolonging survival (MST 107 days and ILS 213%) compared to olaparib plus cediranib (COMBINATION CED+OLA), even if not significantly different (Figure 4.11, panel A). A similar pattern of tumor dissemination and ascites were observed with the two combinations at progression (Figure 4.11, panel B).

MNHOC 8: olaparib in combination with different angiogenesis inhibitors

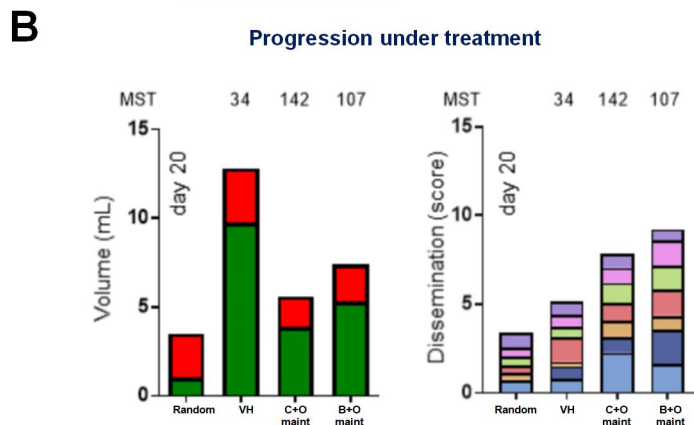
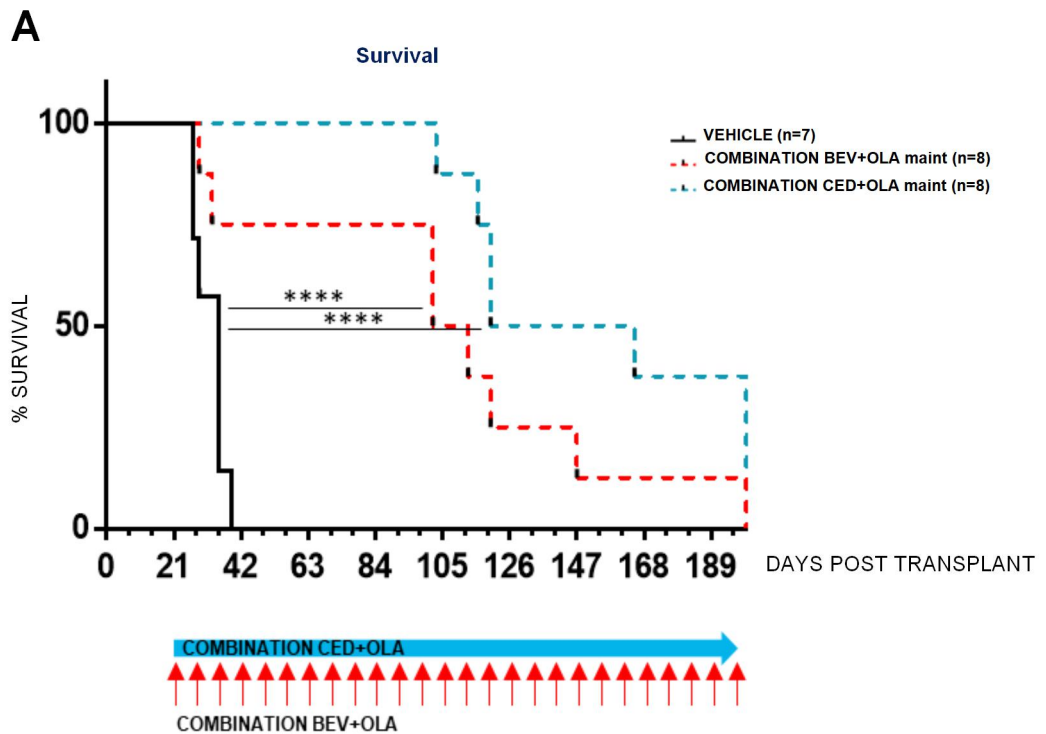


Figure 4.11 Olaparib in combination with a different angiogenesis inhibitor, bevacizumab: the case of the orthotopic MNHOC 8, BRCAness.

A) Effect of the combination olaparib (100mg/kg, p.o, daily) plus cediranib (3mg/kg, p.o, daily) and bevacizumab (5mg/kg, i.v, once a week) in maintenance until tumor progression under treatment in mice bearing intraperitoneal growing MNHOC 8. Vehicle and combination with cediranib as in Fig. 4.9.

B) Volume of ascites and dissemination were evaluated at progression under treatment.

VH, vehicle; C+Omaint, cediranib plus olaparib combination in maintenance; B+Omaint, bevacizumab plus olaparib combination in maintenance. MST, median survival times (days). *P<0.05; ****P<0.0001.

■ Pellet ■ Ascites ■ Ovary ■ Uterus ■ Diaphragm ■ Pancreas ■ Gut ■ Liver ■ Carcinomatosis

Summary of results

- No differences were highlighted comparing the two angiogenesis inhibitors affecting VEGFA, bevacizumab and B20, and the results confirmed the combination of olaparib plus cediranib as the best possible treatment (Figure 4.10).
- The activity of the combination is evident also with other angiogenesis inhibitors (i.e bevacizumab in the orthotopic MNHOC 8, Figure 4.11), although in our OC-PDX models the addition of cediranib to olaparib appeared as the most efficacious in delaying tumor progression (Figure 4.10, the case of the ectopic MNHOC 18) compared with the addition of bevacizumab or B20.

4.6 THE ADVANTAGE OF THE COMBINATION IN OLAPARIB RESISTANT BRCA^{AN} MODELS

4.6.1 Case-report: MNHOC 22, BRCA^{AN}

MNHOC 22 was derived from primary ascites of a patient diagnosed with high grade serous ovarian carcinoma; the OC-PDX was established as ascites, growing orthotopically in the peritoneal cavity.

MNHOC 22 was extensively characterized for its responsiveness to cisplatin, proving to be very sensitive (ILS >150%, at 4 mg/kg), as previously reported (Ricci et al., 2014).

In this model, a truncation/frameshift mutation in *BRCA1* was detected.

Olaparib and the combination with cediranib were administered in a short-term regimen (4 weeks), starting treatment at an advanced stage of disease (6 days after transplant). The engraftment of tumor was verified with necropsy on additional mice (N=3) at the day of randomization; at this point, ascites was barely detected but low levels of carcinomatosis were present in ovaries, liver and gut.

Olaparib single agent therapy was ineffective on survival (ILS 10%), compared to vehicle. The administration of cediranib significantly increased survival (ILS 120%) and the combination performed additively (ILS 159%) (Figure 4.12. panel A).

Tumor burden was evaluated at the end of treatment (Figure 4.12, panel B); at this time vehicle-treated mice had already been culled due to the presence of ascites and dissemination across the organs of the peritoneal cavity (MST 21 days).

Animals which received olaparib single therapy were also culled (MST 21 days as for vehicle), due to the high levels of ascites; however, interestingly, the macroscopical analysis of tumor dissemination revealed a significantly lower burden in term of solid masses and carcinomatosis, compared to vehicle and cediranib treated mice. The effect of the combination of olaparib plus cediranib was “additive”: survival (MST 53 days) was significantly increased, and at the end of treatment ascites and dissemination were undoubtedly reduced compared to vehicle and olaparib. The combination added together effects of cediranib on ascites formation and olaparib action on the formation of tumor masses. Cediranib (MST 46 days) inhibited ascites formation but did not affect tumor dissemination (Figure 4.12, panel B).

The substantial effect of the treatment in reducing ascites formation and dissemination displayed at the end of treatments was completely reversed at progression, after treatment interruption (Figure 4.12, panel C).

The increment of lifespan was however associated with a more aggressive disease. The effect in increasing survival was not associated with tumor burden inhibition (but rather with an aggressive disease), but could be explained by the strong activity of the angiogenic inhibitor in keeping under control the formation of ascites, barely affecting tumor dissemination (as previously reported in MNHOC 8 case with all the schemes of treatment used). On the contrary, the PARP inhibitor displayed a strong action in reducing tumor dissemination.

MNHOC 22: olaparib resistant BRCAness model

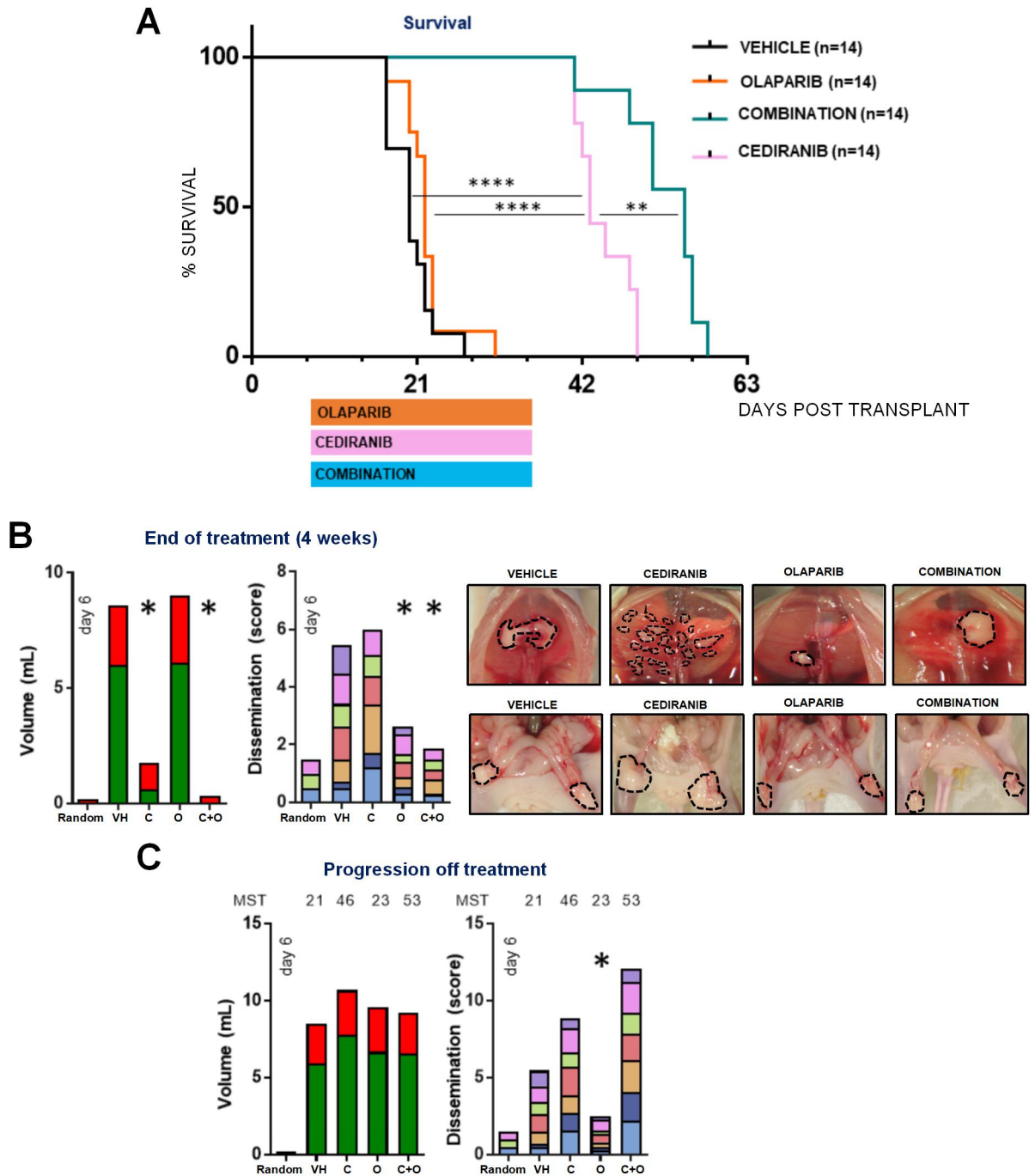


Figure 4.12 The advantage of the combination in olaparib-resistant BRCAness model: the case of the orthotopic MNHOC 22, BRCAness.

Doses and schedule as in Materials and Methods (Chapter 2).

A) Effect of olaparib, cediranib and the combination on survival in a short-term treatment (4 weeks);

B) Volume of ascites and dissemination were evaluated at the end of treatment (4 weeks). Representative images of invaded diaphragm and ovaries at the end of treatment;

C) Volume of ascites and dissemination at progression off treatment (survival).

VH, vehicle; C, cediranib 4 weeks; O, olaparib 4 weeks; C+O, combination. MST, median survival times (days). * $P < 0.05$; ** $P < 0.01$; **** $P < 0.0001$.

Summary of results

MNHOC 22, an orthotopic model of OC-PDX, despite the presence of a truncation/frameshift mutation on *BRCA1*, proved to be resistant to olaparib single agent therapy. A deeper investigation revealed that the PARP inhibitor was not effective in prolonging overall survival, but displayed a great effect in reducing tumor dissemination across the organs of the peritoneal cavity. Cediranib prolonged survival in MNHOC 22 bearing mice, here mainly acting on ascites formation.

The combination of the two drugs was the most active regimen, significantly prolonged survival in MNHOC 22 bearing mice and most actively reduced levels of ascites and dissemination. The short-term effect of the combination on tumor burden was lost at progression off treatment.

4.7 MODELS NOT RESPONSIVE TO THE COMBINATION TO STUDY NEW TREATMENT MODALITIES

Only two OC-PDX among those selected to perform this project did not gain significantly greater advantage from the combination, one ectopic model MNHOC 94/2-C (Figure 4.13) and one orthotopic model MNHOC 506 (Figure 4.14), both Not BRCAness subtypes.

4.7.1 Case-report: MNHOC 94/2-C, Not BRCAness

MNHOC 94/2-C, diagnosed as clear cell carcinoma, was derived from the ascites of a patient at relapse.

MNHOC 94/2-C was moderately sensitive to cisplatin (T/C 34%), but the short-term administration of olaparib had no effect on tumor growth (T/C 54%), with a doubling time comparable to vehicle-treated controls (10 days). Cediranib and the combination with olaparib marginally reduced tumor burden (T/C 36% and 35% respectively), with an

absolute growth delay of 20 days and no differences between the two treatments (Figure 4.13).

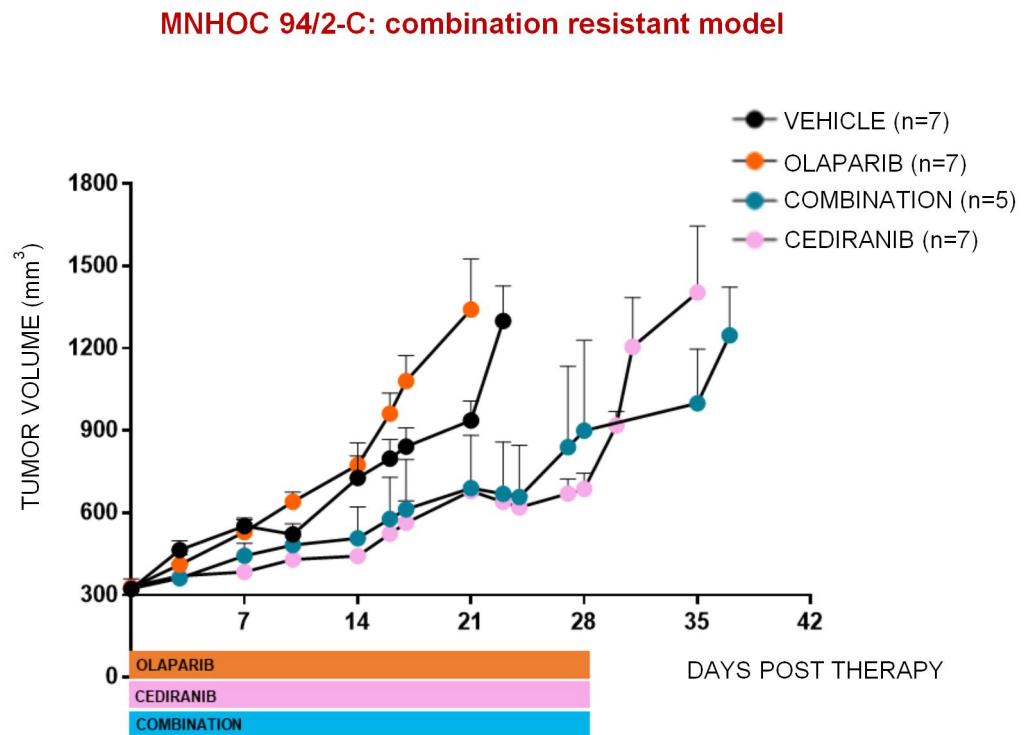


Figure 4.13 The resistance to the combination: the case of the subcutaneous MNHOC 94/2-C, Not BRCAness.

Antitumor activity of olaparib, cediranib and the combination were evaluated in MNHOC 154, growing subcutaneously. Mice were randomized to treatment at an average tumor volume of 300 mm³, doses and schedule as in Materials and Methods (Chapter 2). Responses were shown as tumor growth after olaparib, cediranib and the combination in a maintenance regimen (until tumor progression).

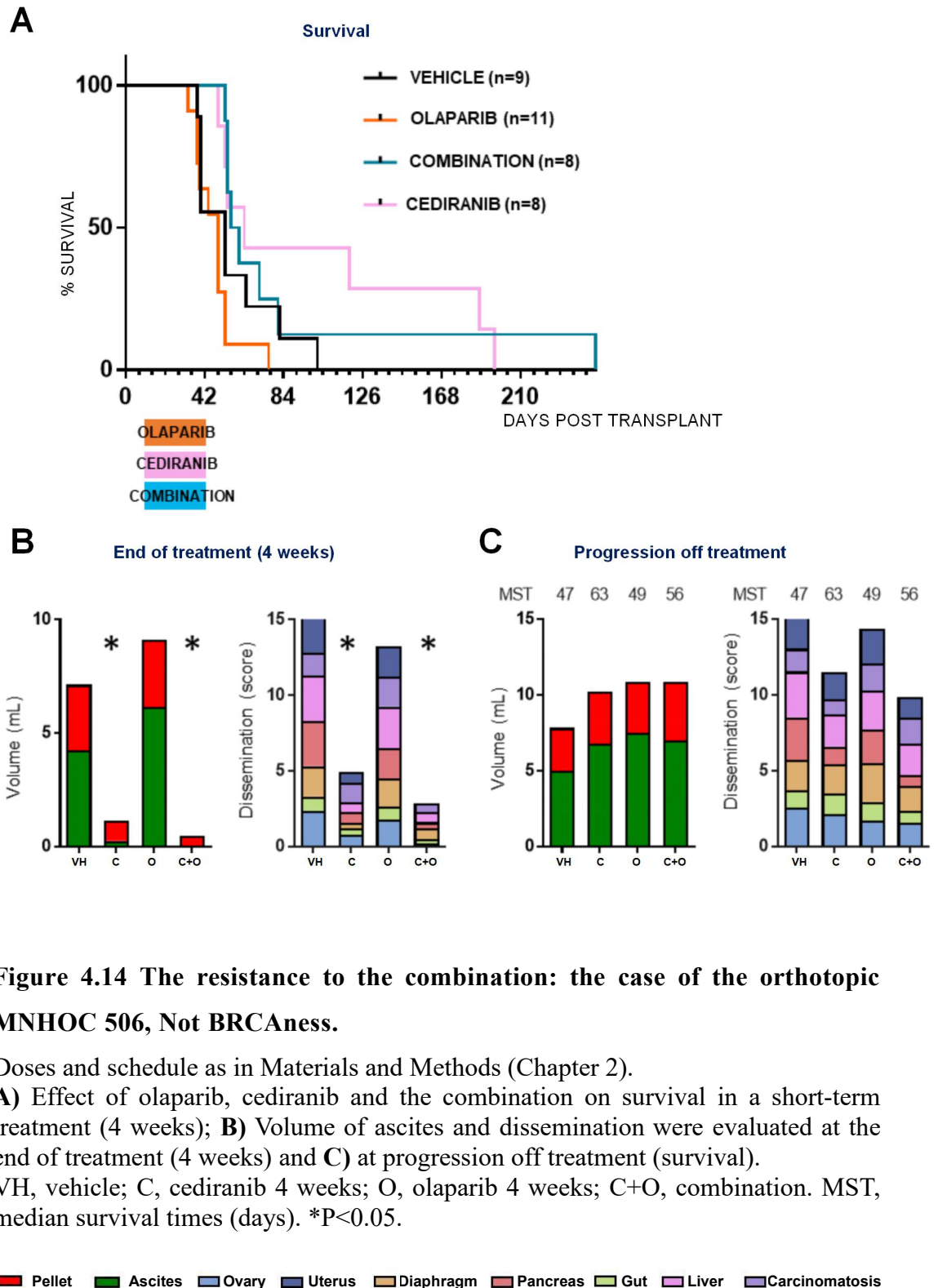
Data are mean \pm SD.

4.7.2 Case-report: MNHOC 506, Not BRCAness

MNHOC 506, diagnosed as a high grade serous carcinoma, was derived from a primary ascites of a patient, who was treated in a neoadjuvant setting with carboplatin and paclitaxel. MNHOC 506 responded to cisplatin (ILS 98%). Short-term administration (4 weeks) of olaparib did not prolong survival compared to vehicle (MST 49 days, ILS 5%), and neither did cediranib (MST 63 days, ILS 16%). The addition of cediranib to olaparib was not more advantageous than single agents (MST 56 days, ILS 20%) (Figure 4.14, panel A).

At necropsy at the end of treatment (4 weeks), the level of ascites and dissemination were reduced by cediranib and the combination (Figure 4.14, panel B). However, at progression, these differences disappeared and necropsy showed a comparable level of ascites and tumor dissemination (Figure 4.14, panel C).

MNHOC 506: combination resistant model



Summary of results

Olaparib was inactive on two Not BRCAness OC-PDX, one orthotopic and one subcutaneous model.

The combination of olaparib with cediranib did not result in a better outcome than single agents; however, a marginal effect on ascites reduction and dissemination at the end of treatment was observed in MNHOC 506 bearing mice and on tumor growth in MNHOC 94/2-C. The fact that this effect was obtained also with cediranib alone suggested that no benefit was gained by olaparib treatment.

These two OC-PDX could be useful to study other treatment modalities when the combination is not significantly advantageous.

4.8 A SYNGENEIC MODEL OF OVARIAN CANCER IN IMMUNOCOMPETENT MICE

In this experiment, we used an orthotopic model of ovarian cancer, designing a complex preclinical trial, with the possibility to follow the response to therapy using magnetic resonance imaging (MRI) analysis. That allowed us to obtain information at different time-points, avoiding the sacrifice of animals.

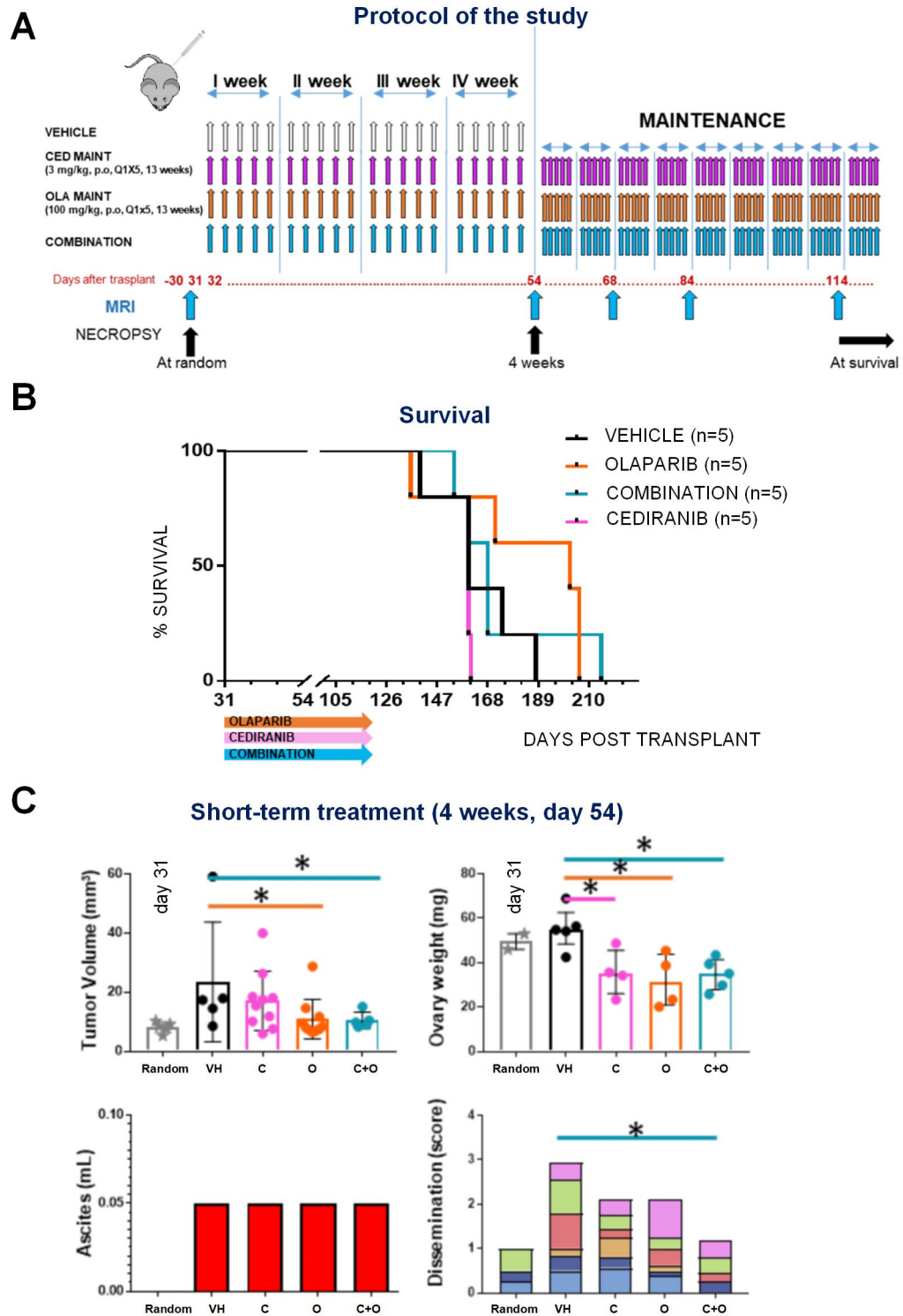
Briefly, 1×10^6 syngeneic ID8-luc cells were injected in the ovary bursa of pathogen-free C57BL/6 mice (see Section 2.1.4.2 Materials and Methods). The protocol of the study was as reported in Figure 4.15, panel A.

MRI was used to confirm tumor engraftment in 5 random mice; 2 mice were culled to perform gross dissemination analysis (Figure 4.15, panel C, Random group). Animals (N=10) were then assigned to vehicle, cediranib, olaparib and the combination based on primary tumor volume at the ovary, assessed with MRI, and considering body weight.

Treatments started at day 31 from tumor injection, at an advanced stage of disease (1/4 of median survival time - MST - of vehicle-treated controls, inferred from previous experiments carried out in the laboratory). Differences in the ovary injected with the tumor compared to the contralateral normal ovary were not macroscopically evident, but signs of tumor dissemination were present mainly at the uterus and gut. Ascites was not yet formed. Olaparib and cediranib single agents were administered every day for 5 days on and 2 days off (Q1x5), for 4 weeks (short-term treatment) to perform interim analysis, and in maintenance (13 weeks treatment) (Figure 4.15, panel A).

Survival analysis did not show significant differences among the vehicle and cediranib treated mice in terms of median survival time (MST vehicle 129 days, cediranib 129 days), with olaparib being slightly, but not significantly, more active (MST olaparib 171 days). No significant advantage was observed combining the two drugs (Figure 4.15, panel B).

However, interim analysis after a short-term treatment (4 weeks, day 54 from tumor transplant) showed that olaparib and the combination with cediranib were the most active in reducing tumor in the ovary, with volume and weight comparable to those registered at random (day 31 from tumor transplant) (Figure 4.15, panel C). The effect of short-term treatment on tumor in the ovary was appraised with MRI and confirmed with necropsy; tumor dimension assessed with MRI (volume, mm³) or weighting the injected ovary (precision balance, mg), was comparable and consistent using the two different methodologies (Figure 4.15, panel C). Ascites was not yet formed, thus peritoneal washout (3 ml NaCl, 0,9%) was performed; pellets were 50 µl on average (Figure 4.15, panel C). Dissemination score analysis showed a strong effect of the combination olaparib plus cediranib in reducing tumor masses and carcinomatosis formation, with a dissemination score comparable to the one registered at random (day 31 from tumor transplant) (Figure 4.15, panel C).



The other halves of each olaparib, cediranib and the combination group (N=5) were treated in a maintenance regimen for an additional 9 weeks and mice monitored with MRI every two/four weeks (Figure 4.15, panel A). Necropsy was performed on each mouse at survival. MRI scans at different time points (day 54, day 68, day 84 and day 116 from injection as latest time point) enabled us to follow tumor burden and plot growth curves (Figure 4.16, panel A). Olaparib monotherapy was active in stabilizing tumor growth compared with vehicle and cediranib (Figure 4.16, panel B). When cediranib was added to olaparib, the combination significantly slowed tumor progression under treatment, with 5/5 tumor with a volume under 100 mm³ and animals still alive at day 114 after transplant, thus indicating the greater effect of the combination in a maintenance regimen in delaying tumor growth (Figure 4.16, panel B).

Eventually, when treatments were terminated at day 121, ascites had developed and tumor had disseminated across the peritoneal cavity, explaining the lack of difference in survival (Figure 4.15, panel B). Nevertheless, the effect of the combination on primary tumor growth was evident at necropsy: injected ovary weights were significantly lower in the combination group, with 4/5 tumors under 400 mg and 1/5 at 1200 mg. Thus, the combination was the most effective regimen in reducing primary tumor growth (Figure 4.16, panel C).

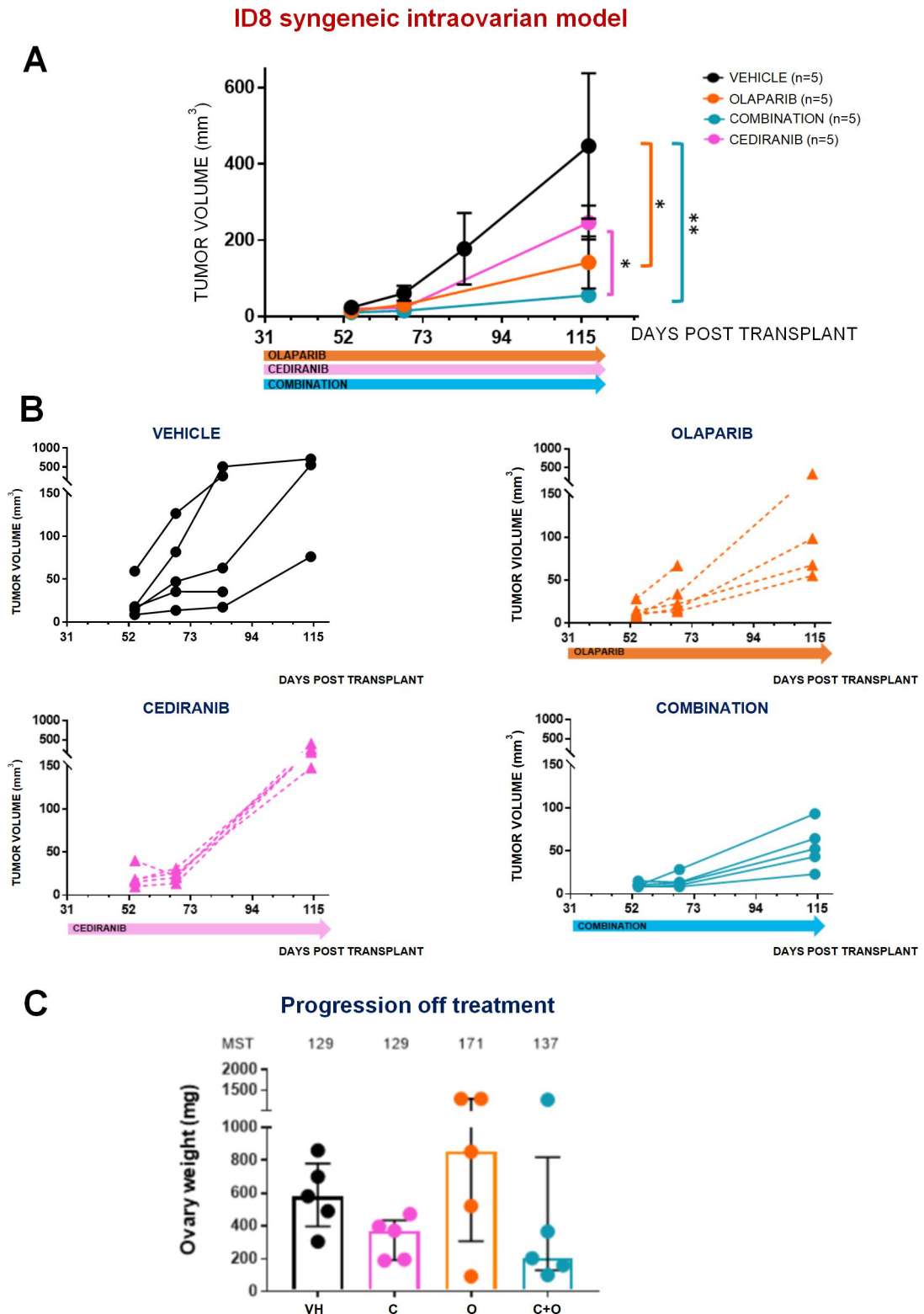


Figure 4.16 The combination in a syngeneic orthotopic model: the intraovarian ID8.

A) Tumor growth in the ovary was evaluated with MRI scans at different time points after the end of the short-term treatment (4 weeks).

B) Single tumor growth curve of vehicle, olaparib, cediranib and the combination are reported.

C) Injected ovary weight for each mice at survival (N=5 mice/group).

VH, vehicle; C, cediranib; O, olaparib; C+O, combination; MST, median survival times (days). *P<0.05, **P<0.01.

Summary of results

The syngeneic Not BRCAness model of ovarian cancer ID8, injected orthotopically in the ovaries of immunocompetent mice, helped us to better understand the effect of olaparib in combination with cediranib.

Olaparib marginally improved survival and slowed tumor progression, mainly at the end of the 4 weeks of treatment (Figure 4.15, panel C). At the end of the study primary tumor weights (Figure 4.16, panel C), levels of ascites, tumor dissemination and carcinomatosis were increased as for vehicle-treated controls.

Cediranib was not active in prolonging survival and marginally in delaying tumor growth; an effect of the angiogenesis inhibitor was just detectable immediately after the end of the 4 weeks treatment (Figure 4.15, panel C), but tended to disappear at tumor progression and when mice were culled (Figure 4.16, panel B and C).

The combination of the two drugs was the most active regimen, not so much in survival, but rather in delaying tumor progression. Primary tumor growth and dissemination were clearly reduced after 4 weeks of treatment (Figure 4.15, panel C) and through the length of the maintenance treatment (13 weeks), as shown by the growth curve inferred by MRI scan (Figure 4.16, panel B). At cull, after the interruption of treatment, the combination affected tumor dissemination and most evidently primary tumor weight (Figure 4.16, panel C).

4.9 MOLECULAR CHARACTERIZATION AFTER TREATMENT

At the beginning of Chapter 4, the 13 OC-PDX selected for testing drug, were classified in BRCAness or Not BRCAness, not only considering the mutational status and pathogenicity

of *BRCA1* and 2, but also the levels of expression and any aberration on other genes involved in HR DNA repair pathway.

Briefly, OC-PDX carrying somatic mutations and loss of *BRCA1/2* on both the gene alleles were defined BRCAness. Low expression levels of both *BRCA1* and *BRCA2* allowed to define one particular model, MNHOC 8, as BRCAness, even though no mutations were detected with Sanger sequencing; OC-PDX that did not carry mutations on *BRCA1* and *BRCA2* or absence of locus-specific loss of heterozygosity (LOH) (such as MNHOC 18 and MNHOC 182) were defined Not BRCAness.

In order to define whether the short-term treatment (4 weeks) with olaparib, cediranib and the combination has or not changed the classification of the OC-PDX models in BRCAness or Not BRCAness, we investigated the mutational landscape and expression of *BRCA1* and *BRCA2* (NGS and gene expression with fluidigm) at the end of treatment (Figure 4.17).

BRCA1 (c.1687C>T, p.Q563* truncation/frameshift, described as pathogenic) was found mutated in MNHOC 22 after cediranib, olaparib and combination treatment, as for vehicle; MNHOC 508 carried one frameshift described as pathogenic on *BRCA2* (c.5722_5723delCT, p.L1908fs) maintained after treatment with cediranib, olaparib and combination. MNHOC 506, MNHOC 18 and MNHOC 94/2-C were defined as Not BRCAness, and no additional mutations harboured on these genes after treatment (Figure 4.17, panel A).

All the pathogenic mutations described for *TP53* were preserved and not changed by treatment (substitution missense c.514G>T, p.V172F for MNHOC 8; c.993+1G>A and c.782+1G>A at splice site for MNHOC 22 and MNHOC 508 respectively; truncation frameshift c.796G>T p.G266* for MNHOC 506; substitution missense c.527G>T p.C176F for MNHOC 18). The clear cell MNHOC 94/2-C did not harbour any alteration in *TP53* as when tested at baseline but maintained *PTEN* truncation frameshift (c.388C>T, p.R130*)

after short-term treatment. In MNHOC 18, *EGFR* carried a substitution missense (c.2884C>T, p.R962C) described as pathogenic and preserved in tumor cells after treatment (4.17, panel A).

MNHOC 8 harboured wild type *BRCA1* and *BRCA2* at baseline and was classified as BRCAness due to the low level of the two genes observed with gene expression analysis with different techniques (Real Time PCR, genome-wide gene expression, Fluidigm and RNAseq, Chapter 3, Figure 3.3 - 3.6). *BRCA1* low expression was retained even after treatment. Of note, short-term treatment of olaparib and the combination with cediranib significantly increased level of expression of *BRCA1* compared to vehicle and cediranib treatment (ΔCt -15.4 vehicle; -15.4 cediranib; -11.4 olaparib; -11.6 combination), but values were still under the mean value of all the models tested (mean ΔCt -6.2) (Figure 4.17, panel B). For convenience, values were reported as $-\Delta\text{Ct}$, being the lowest value corresponding to the lowest expression.

BRCA2 expression in MNHOC 8 was not different compared to the other models, but still under the mean value (mean ΔCt -7.6). No significant differences were pointed out in *BRCA2* among different treatment (ΔCt -10.8 vehicle; -9.4 cediranib; -8.5 olaparib; -8.4 combination) (Figure 4.17, panel B).

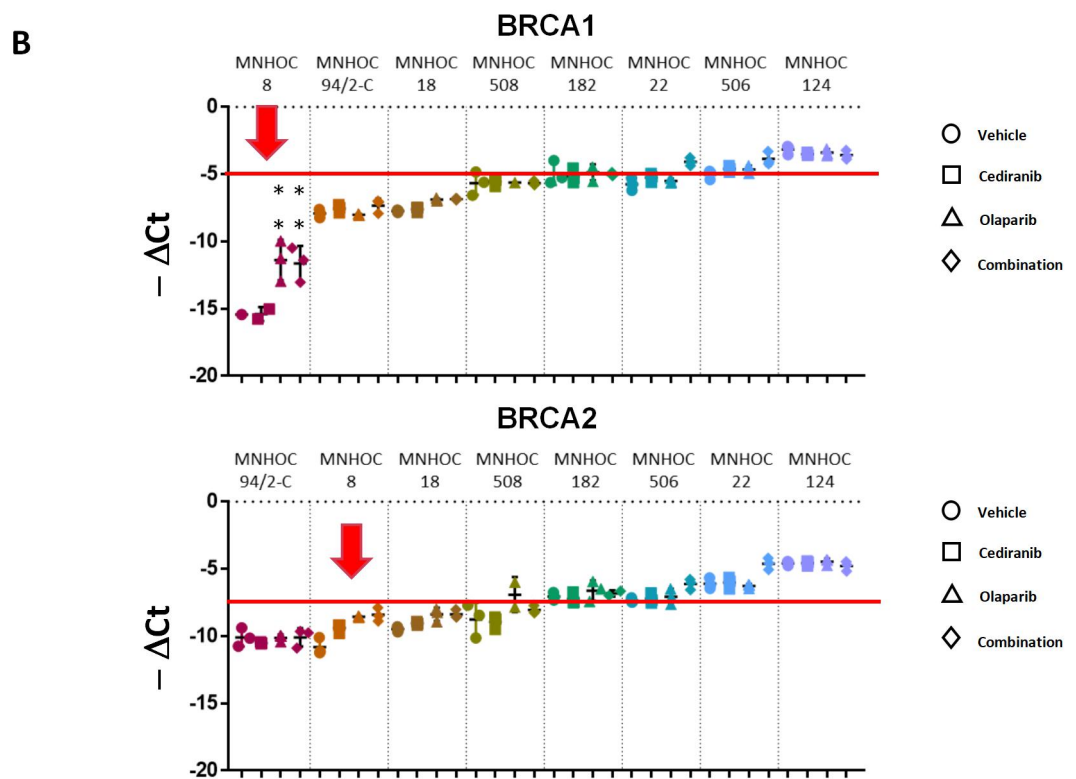
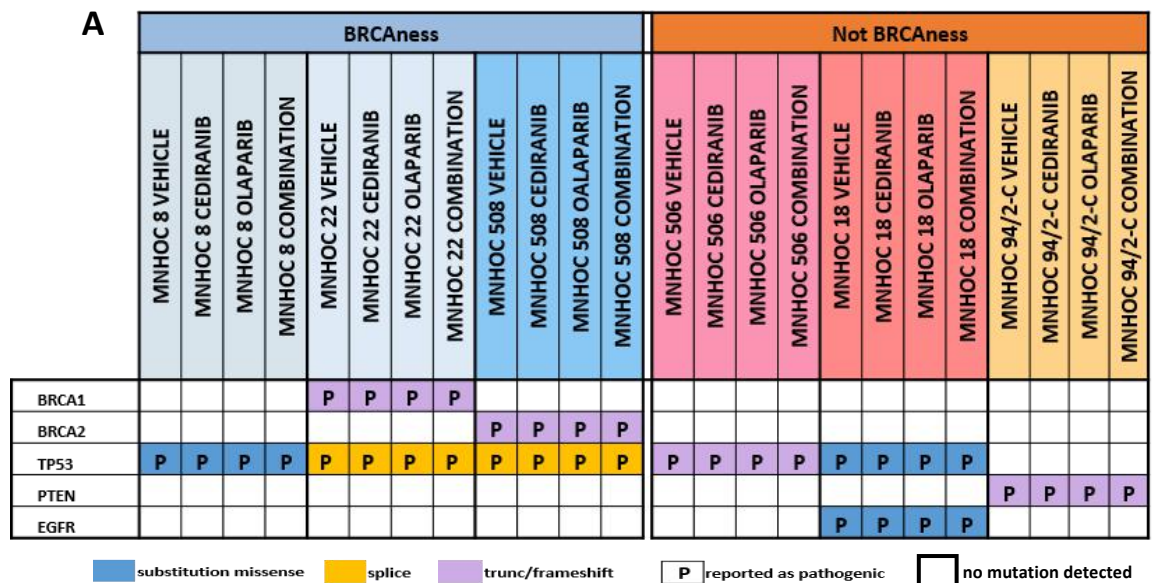


Figure 4.17 OC-PDX classification after treatment.

A) Mutational landscape after treatment with cediranib, olaparib and combination in 6 OC-PDX selected for preclinical testing therapy.

B) *BRCA1* and *BRCA2* level of expression in 8 OC-PDX selected for preclinical testing therapy after four weeks of treatment with cediranib, olaparib and combination.

Data are $\Delta Ct = Ct_{\text{target}} - Ct_{\text{housekeeping}}$ and reported as $-\Delta Ct$, being the lowest value corresponding to the lowest expression. Red line (—) mean value of $-\Delta Ct$ for each gene tested.

4.10 DISCUSSION

Preclinical tumor models recapitulate many aspects of the genesis and progression of human cancers, thus they are valuable resources to investigate the mechanisms of cancer and to predict clinical behaviour, in terms of tumor biological features (i.e. dissemination and ascites formation) and response to therapy.

In particular, patient-derived ovarian tumor xenografts (OC-PDX) are a useful tool to test new therapeutic strategies and efficacy can be determined by mimic the response of the patients (Weroha et al., 2014). A strong correlation between patient and OC-PDX responsiveness to therapy has been demonstrated in ovarian cancer, thus endorsing the reliability of the model to lead translational preclinical and co-clinical trials (Ricci et al., 2014; Masazza et al., 1991; Massazza et al., 1989; Fiebig et al., 1984).

A platform of transplantable OC-PDX has been established in the Department of Oncology (Ricci et al., 2014), and a cohort of 13 OC-PDX was used to perform the preclinical studies reported in Chapter 4.

Firstly, the response to olaparib single therapy was assessed in 10 models of OC-PDX growing subcutaneously, both in a short-term (4 weeks) and in a maintenance regimen (Figure 4.1). Results showed that BRCAness tumors responded to olaparib single therapy, after a short-term treatment and even more so in a maintenance regimen, with complete responses, as seen in the clinic (Fong et al., 2010; Kaufman et al., 2015). Aberrations in *BRCA1/2* are a good predictor for olaparib response. Interestingly, MNHOC 154 was an exception in this context; despite a pathogenic mutation in *BRCA1*, the presence of an amplification in *BRCA2* (confirmed also by high level of gene expression, as reported in Figure 3.4-3.6, Chapter 3, Results) induced a heterogeneous response to olaparib

monotherapy (Figure 4.7), thus MNHOC 154 was a good model to study combination regimens.

In general, the entire cohort of OC-PDX could be considered a reliable tool to deeply analyse the combination of olaparib and other drugs, such as angiogenesis inhibitors. Genomic instability and induced angiogenesis are two of the hallmarks of cancer (Hanahan and Weinberg, 2011), thus targeting both of them could boost the therapeutic outcome. Clinical trials have investigated the combination of olaparib and cediranib (Liu et al., 2013, 2014) in recurrent ovarian cancer patients, showing PFS increase in patients with germline mutations in *BRCA1/2*, but also in homologous recombination proficient patients.

Our models of OC-PDX displayed a heterogeneous response to the angiogenesis inhibitor, both in a short-term and maintenance regimen (Figure 4.2). The response to cediranib seemed to be dependent on the intrinsic features of each single tumor, such as vasculature, factors that determine the metabolic status of the tumor (i.e. fibroblasts), stroma and levels of VEGF. The heterogeneity and diversity of responses seen in our OC-PDX models mimic the clinical scenario, in which patients show different profiles of responsiveness to the anti-angiogenic treatment.

The addition of cediranib to olaparib was favourable for those OC-PDX that were poorly responsive to the olaparib single agent therapy, especially the Not BRCAness subtypes, promoting a stabilization of disease in case of short-term treatment and a strong regression in maintenance regimens, as for MNHOC 18 and MNHOC 182 (Figure 4.3 and 4.4).

The combination was beneficial also for BRCAness models, increasing the number of complete responses and cured mice (Figure 4.2, panel A and D).

Our preclinical data advanced the idea that the combination is worth administering especially in Not BRCAness patients, but also in the BRCAness types to induce more durable and stable effects, persistent several weeks after treatment suspension, as for

MNHOC 511 and MNHOC 513 (Figure 4.6). In particular, the BRCAness MNHOC 511 was a powerful example of the clinical translational impact of these preclinical studies. The patient, from which the OC-PDX was derived, is still under treatment with olaparib and in a complete response. Since MNHOC 511 gained an advantage from the addition of cediranib to olaparib, the combination could be an appropriate treatment if the patient would eventually relapse.

The effect of the combination was evaluated in a case-report fashion, taking into advantage the orthotopic (intraperitoneal) set of available OC-PDX, due to their resemblance to the original biological features of the patient's tumor.

Timing and sequence of angiogenesis and PARP inhibition is an issue that calls for consideration. The BRCAness MNHOC 8 model, for instance, enabled us to analyse in detail the importance of sequence in the combination of cediranib and olaparib. In this model too, the combination was more active than single drugs in increasing survival of mice, particularly when administered in a maintenance regimen (Figure 4.8, panel A and panel D). The gain in survival was accompanied by a substantial control in the levels of ascites; however, dissemination increased, leading mice to live longer, but with the detriment of a more aggressive disease.

The escape from antiangiogenic treatments has been well documented in preclinical studies, including in our models of OC-PDX treated with the anti-VEGFA bevacizumab, which under certain circumstances increased survival but also tumor dissemination (Bizzaro et al., 2018; Decio et al., 2015).

The evidence that cediranib and olaparib should be administered together was obtained when different sequences of drugs were administered (Figure 4.9). The administration of the combination until progression reduced ascites and was more effective in keeping tumor spread across the organs of the peritoneal cavity under control. The combination followed

by a switch to cediranib or olaparib single agent was not effective in increasing survival compared with continuing the combination in maintenance; the switch to olaparib marginally decreased ascites and dissemination; the switch to cediranib significantly reduced ascites, but markedly increased dissemination (Figure 4.9, panel B). The activity of adding cediranib to olaparib, even when treatment was started at a late stage of disease, could be explained as a two-compartment effect, with the effect on the microenvironment produced by the first, and the inhibition of DNA repair system generated by the latter (see also Chapter 5 and Chapter 6, Results).

The benefit of the combination of olaparib and cediranib was further evident when the PARP inhibitor was combined with bevacizumab, the first anti-VEGFA approved for ovarian cancer treatment. A phase III clinical trial, PAOLA-1, is currently testing olaparib versus placebo combined with bevacizumab as maintenance treatment in patients with advanced ovarian cancer following first-line platinum-based chemotherapy plus bevacizumab. In our OC-PDX models, the administration of the combination bevacizumab plus olaparib was ineffective in the case of MNHOC 18 (Figure 4.10, panel B), with subcutaneous tumors progressing rapidly under treatment. A similar outcome was observed when B20, the antibody recognising both human and murine VEGFA, was used (Figure 4.10, panel C).

The effect of the addition of bevacizumab to olaparib was more evident in the orthotopic model MNHOC 8, but not different from the combination with cediranib (Figure 4.11). We could speculate that differences in response between the two OC-PDX tested could be related to the site of growth (subcutaneously growing MNHOC 18 versus intraperitoneally growing MNHOC 8). Moreover, the lack of differences between the combination with cediranib or bevacizumab in the intraperitoneal MNHOC 8 model could be linked to the

effect of the two angiogenic inhibitors on ascites - both reducing it - and on dissemination - both increasing it-, resulting into an equal outcome in survival.

In addition, MNHOC 18 expressed high levels of all the receptors of cediranib, while MNHOC 8 did not (Figure 6.5 and Figure 6.6, Chapter 6); this could explain why there is such a great benefit in combining olaparib with cediranib instead of bevacizumab, at least in MNHOC 18.

Intraperitoneal MNHOC 22 tumor, carrying a mutation in *BRCA1*, was resistant to olaparib single agent, showing no increase in host survival and remarkable production of ascites. The addition of cediranib increased survival and promoted a strong decrease of ascites and dissemination at the end of treatment (Figure 4.12, panel A and B). The additive effect of the combination could be explained by the efficacy of cediranib in controlling ascites formation and olaparib in reducing tumor masses and dissemination. However, after treatment suspension, tumors progressed and mice succumbed with a heavy tumor burden into the peritoneal organs (Figure 4.12, panel C). Thus, the increment of lifespan came along with a more aggressive disease, confirming our previous finding (Bizzaro et al., 2018; Decio et al., 2015; Oliva et al., 2012). However, results obtained on MNHOC 22 (*BRCA1* mutated) and on MNHOC 154 (*BRCA1* mutated but amplified *BRCA2*) suggested that the combination of olaparib with cediranib could be considered the best therapeutic option also for BRCAness platinum-sensitive patients, which are moderately responsive or resistant to olaparib single agent therapy.

If the majority of the selected OC-PDX benefitted from the combination of olaparib with cediranib, cases of poor response need to be taken into consideration and carefully addressed. Poorly responsive OC-PDX, such as the orthotopic MNHOC 506 (Figure 4.14) and the ectopic MNHOC 94/2-C (Figure 4.13), are fundamental tools to study other

treatment modalities for patients in whom the combination would not be so advantageous. A marginal effect could be claimed in reducing ascites and dissemination immediately after the end of treatment in MNHOC 506 bearing mice and marginally in reducing tumor growth in MNHOC 94/2-C.

One last aspect that should be taken into account using OC-PDX, especially to test target therapies, is the fact that the tumor (human) and the host (murine) are different. To address this issue, the orthotopic transplant in the bursa of the ovary of syngeneic murine tumor cells, such as ID8, may enable us to study key aspects of the biological features of the ovarian disease in immunocompetent host, since cancer progression, metastasis formation and response to therapy are similar to those seen in the clinic. Syngeneic murine models provide the opportunity to study the tumor microenvironment, stroma, infiltrating host cells, secreted factors and vasculature. Moreover, in this particular case, we followed disease progression with MRI, a non-invasive imaging technique, that allowed us to obtain several pieces of information, at different time-points, without the need for a sequential culling of animals (Figure 4.16, panel A and B).

The effect of olaparib and the combination with cediranib was tested both in a short-term (4 weeks) and in maintenance regimen (Figure 4.15, panel A). The combination of the two drugs was the most active, not increasing survival in mice, but mostly delaying tumor progression and affecting primary tumor growth at the ovary, both in the short-term treatment (Figure 4.15, panel C) and even after several weeks from treatment suspension (Figure 4.16, panel C).

To summarize, results obtained from preclinical testing trials described in Chapter 4, lead us to believe that the addition of cediranib to olaparib is advantageous in many cases, notably when administered until tumor progression.

Mutational landscape and *BRCA1* and *BRCA2* expression were not modified by short-term treatment (4 weeks) (Figure 4.17, panel A and B). However, preliminary data (not shown) extrapolated from NGS analysis showed that olaparib single agent and the combination with cediranib induced the highest number of novel mutations (as the total number of single-nucleotide-polymorphisms count) in post-treated samples, not observed in vehicle- and cediranib-treated samples at the same time point. This suggested that olaparib is inducing DNA damages in tumor cells during administration.

Biomarkers of response and preliminary data on molecular characterization after short-term treatment described in Chapter 5 and Chapter 6 have the aim to further shed light on the possible mechanisms underlying the biological and pharmacological effects demonstrated in combination treatments.

CHAPTER 5.

Results

BIOMARKERS OF RESPONSE (IMMUNOHISTOCHEMICAL ANALYSES)

5.1 EFFECTS OF THE COMBINATION ON THE TUMOR MICROENVIRONMENT AND HR DNA REPAIR MARKERS

Cediranib binds the three VEGF receptors, with marked selectivity for VEGFR2, together with c-Kit (*KIT*) and PDGFR α (*PDGFRA*) (Sahade et al., 2012), and the use of VEGFR inhibitors can cause local tumor hypoxia. On the other hand, evidence supports the idea that angiogenesis inhibitors can normalize the structure and function of tumor-associated vasculature, thus reducing levels of hypoxia (Jain, 2005).

As a marker of cediranib activity on tumor vasculature, CD31 positive vessels (microvessel density, MVD) and endothelial area (EA) were evaluated; hypoxia was evaluated with CA-9 and pimonidazole. Representative staining showed that both are comparable in formalin-fixed sections of tumors and colocalization is observed, even though differences were highlighted: CA-9 staining tended to be more localized at cell membranes away from vessels, while pimonidazole contributed to a more diffuse signal (Figure 5.1).

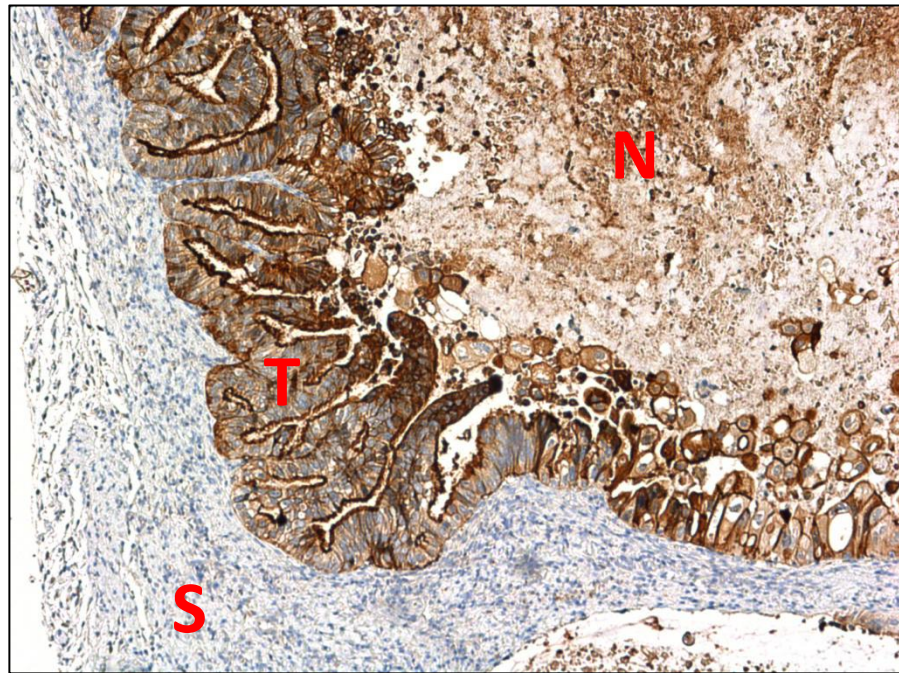
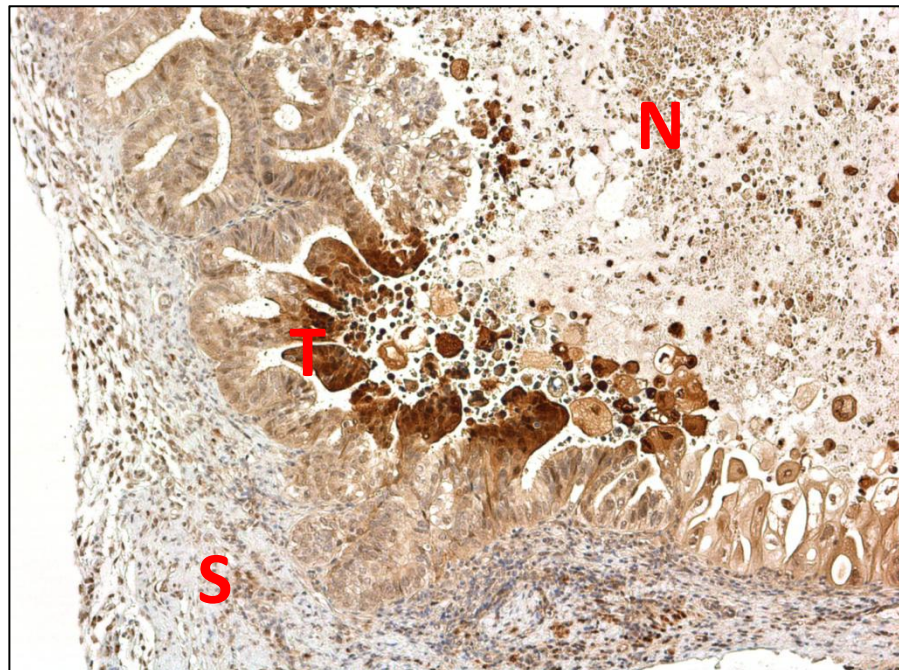
CA-9**Pimonidazole**

Figure 5.1 Tumor hypoxia: CA-9 vs Pimonidazole representative staining on MNHOC 513.

CA-9 and Pimonidazole staining were evaluated in parallel on the same OC-PDX, to assess that results are comparable.

N: necrosis; T: neoplastic tissue; S: stroma.

Acute and chronic hypoxia can lead to a DNA repair-deficient phenotype and genetic instability (Bristow and Hill, 2008; Pires et al., 2010), with decreased expression of proteins involved in the HR DNA repair pathway, leading to an increased sensitivity to DNA cross-linking agents such as Poly(ADP-ribose) polymerase (PARP) inhibitors (Chan et al., 2008, 2010). PARP inhibitors, such as olaparib, are able to induce an increase in DNA damage by “trapping” PARP on DNA single strand breaks, thus inducing the block of replication forks, leading to an evolution and accumulation of double strand breaks.

When DNA damage forms double strand breaks (DSBs), it is always followed by the phosphorylation of the histone H2AX. Newly phosphorylated protein, γ H2AX, is the first step in recruiting and localizing DNA repair proteins. Thus, evaluating levels of expression of γ H2AX within neoplastic tissue could be considered a marker of DNA damage, induced by olaparib.

Analyses were performed on subcutaneous tumors (s.c models) and tumor masses at the ovaries (i.p models) collected at random days (VH at random -when available-) and at the end of short-term treatment (4 weeks, 5 days on and 2 days off), 6 hours after the last dose of vehicle (VH), cediranib (CED), olaparib (OLA) or the combination (COMBO) (n=2-3/per group). Details are reported in Section 2.4, Chapter 2, Materials and Methods.

5.1.1 Subcutaneous tumor models

5.1.1.1 MNHOC 18, Not BRCAness

Administration of the PARP inhibitor olaparib in MNHOC 18 tumor-bearing mice failed in delay tumor progression in a short-term regimen. Lack of responsiveness was displayed with the angiogenesis inhibitor cediranib. The combination was active in stabilizing tumor growth until treatment was ended (Figure 5.2, panel A).

Changes in tumor vasculature indicated that MVD was reduced after cediranib treatment and maintained with the combination (mean number of CD31+ vessels = 12 for cediranib; 14 for the combination), compared with vehicle or olaparib (mean number of CD31+ vessels = 22 for vehicle; 19 for olaparib) (Figure 5.2, panel C).

The same trend was observed on endothelial area (EA) measurements. The PARP inhibitor olaparib induced a modest reduction of the CD31+ area compared with vehicle (mean EA = 2,4% olaparib; 3,9% vehicle). The angiogenesis inhibitor cediranib reduced the CD31+ area compared with vehicle (mean EA = 1,6%) and no further reduction was observed with the combination (mean EA = 1,8%) (Figure 5.2, panel D and representative images in panel E).

This evidence supported results on the level of hypoxia. At randomization, hypoxia was almost undetectable in vehicle-treated tumors (mean of group = 2,5% vehicle at random).

The hypoxic area was similarly increased by cediranib and olaparib after 4 weeks of treatment, with no further improvement by the combination (mean of group = 10% vehicle; 30% cediranib; 20% olaparib; 24% combination) (Figure 5.2, panel B).

Additional analysis on the level of CA-9 mRNA, assessed by fluidigm, showed that cediranib induced an increase in levels of expression (mean $-\Delta Ct = -5.14$). Levels in olaparib treated animals were comparable with vehicle-controls (mean $-\Delta Ct = -7.59$ vehicle; -7.27 olaparib). Accordingly, the addition of cediranib to olaparib did not further increase the expression (mean $-\Delta Ct = -5.77$).

For immunohistochemical analysis of $\gamma H2AX$, the same samples used for hypoxia and tumor-associated vasculature determination were evaluated. Cediranib and olaparib slightly reduced foci formation compared with vehicle (mean of group = 31% vehicle; 15% cediranib; 13% olaparib), and the combination of the two inhibitors induced a significant increase in foci formation (mean of group = 56%) (Figure 5.2, panel F and representative images in panel G).

Not BRCAness MNHOC 18

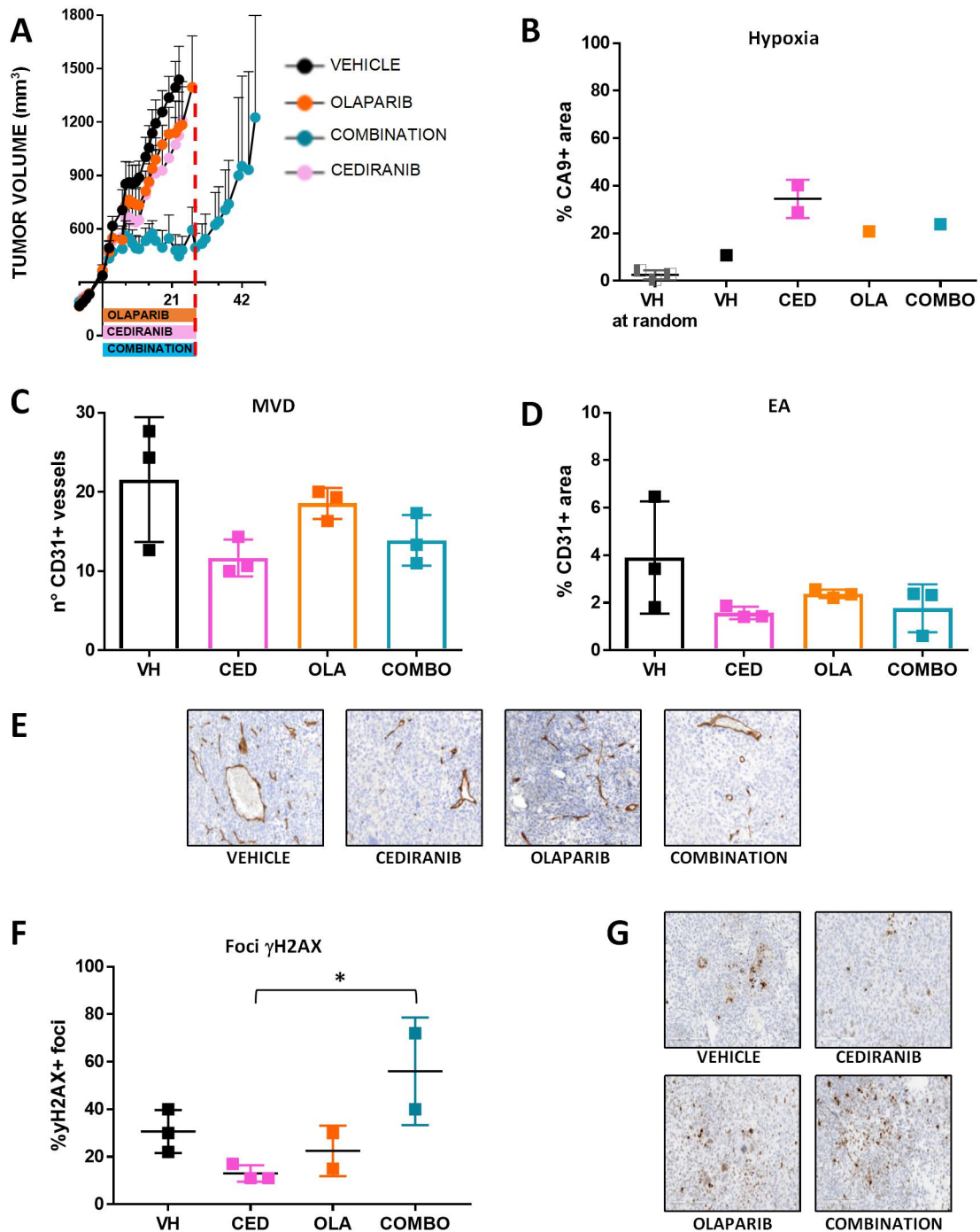


Figure 5.2 Analysis on subcutaneous MNHOC 18.

A) Samples were collected at the end of short-term treatment (---), from figure 4.3 A.
B) % CA-9+ area, **C)** MVD (microvessel density, n° of CD31+ vessels), **D)** EA (endothelial area, CD31 positive area not considering vascular lumen, % of CD31+ area) are reported as the mean \pm SD of 3 200X randomly selected fields in neoplastic tissue. **E)** Representative sections of CD31+ vessels (200X magnification).
F) γ H2AX foci (% γ H2AX+ foci with different patterns) are reported as the mean \pm SD of 3 200X randomly selected fields in neoplastic tissue. **G)** Representative sections of γ H2AX+ cells (200X magnification). *P<0.05.

5.1.1.2 MNHOC 182, Not BRCAness

Short-term administration (4 weeks) of olaparib slightly reduced tumor growth in MNHOC 182 bearing mice and cediranib induced a moderate stabilization of tumor growth. The combination was remarkably active in stabilizing tumor growth, maintaining mean tumor volume closer to values at random day (Figure 5.3, panel A).

Changes in tumor-associated vasculature were estimated. MVD was significantly reduced by cediranib and the combination treatment, compared with vehicle or olaparib (mean n° of CD31+ vessels = 20 for vehicle; 5 for cediranib; 16 for olaparib; 6 for the combination) (Figure 5.3, panel C).

Cediranib reduced EA (mean EA = 0,6%) as much as the combination (mean EA = 0,7%), compared with vehicle (mean EA = 4,3%) or olaparib (mean EA = 4%) (Figure 5.3, panel D).

Of note, evaluation of CD31 stained slides pointed out ectasia of vessels present in vehicle and olaparib groups (Figure 5.3, panel E, black arrows), completely absent after short-term treatment with cediranib and the combination.

Levels of hypoxia were evaluated by assessing the percentage of pimonidazole-positive area (% Pimo+ area) in 2 fields (50x magnification), randomly chosen across the neoplastic tissue. Cediranib induced a reduction of hypoxic area compared with vehicle at random and vehicle after 4 weeks of treatment, but not different from olaparib (mean of groups = 45% vehicle at random; 43% vehicle; 21% cediranib; 21% olaparib). The combination improved the reduction compared to vehicle (mean of group = 12% combination) (Figure 5.3, panel B).

In this model, the formation of γ H2AX foci was in general very low, compared to the other subcutaneous models. No significant differences in foci formation were highlighted among

the different groups (mean of group = 0% vehicle; 1% cediranib; 0% olaparib; 1% combination) (Figure 5.3, panel F).

Not BRCAness MNHOC 182

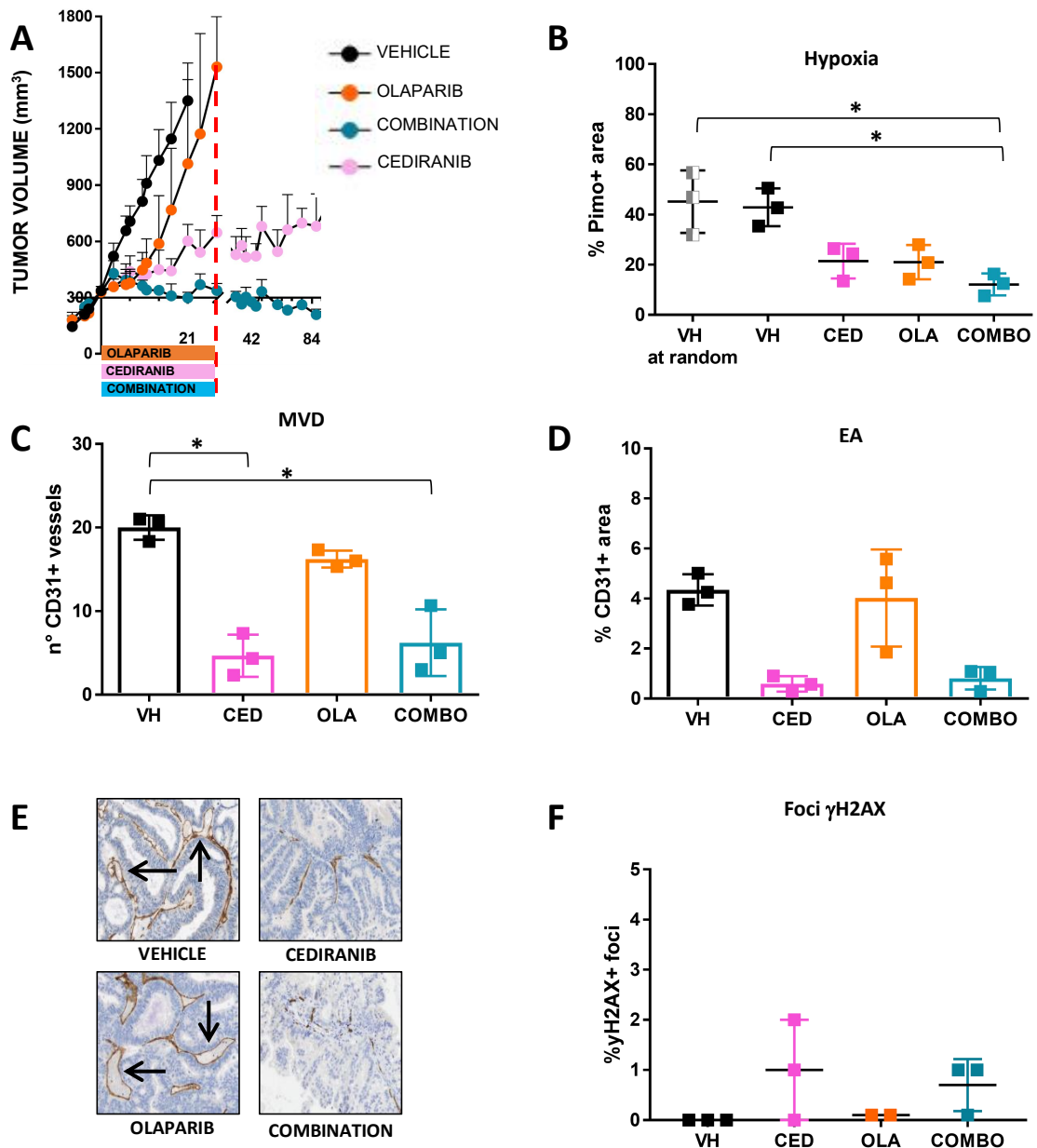


Figure 5.3 Analysis on subcutaneous MNHOC 182.

A) Samples were collected at the end of short-term treatment (---), from figure 4.4.

B) % Pimo+ area, **C)** MVD (microvessel density, n° of CD31+ vessels), **D)** EA (endothelial area, CD31 positive area not considering vascular lumen, % of CD31+ area) are reported as the mean±SD of 3 200X randomly selected fields in neoplastic tissue. **E)** Representative sections of CD31+ vessels (200X magnification).

F) γH2AX foci (% γH2AX+ foci with different patterns) are reported as the mean±SD of 3 200X randomly selected fields in neoplastic tissue. *P<0.05.

5.1.1.3 MNHOC 508, *BRCAness*

Short-term treatment (4 weeks) with olaparib and cediranib induced a stabilization of tumor growth in the MNHOC 508 OC-PDX model. Soon after the end of treatment, tumors regrew again. The combination of the PARP inhibitor with the angiogenesis inhibitor induced a significant regression in tumor growth, maintained for approximately one month after the end of treatment (Figure 5.4, panel A).

MVD analysis revealed a significant reduction in the number of vessels induced by cediranib and the combination compared with vehicle or olaparib alone (mean n° of CD31+ vessels = 12 for vehicle; 15 for olaparib; 3,5 for cediranib; 7 for the combination) (Figure 5.4, panel C).

Analysis of EA showed a decreasing trend of endothelial area driven by cediranib compared with vehicle (mean EA = 0,7% vehicle; mean EA = 0,4% cediranib). Olaparib induced instead a marked increase in EA (mean EA = 1,5% olaparib). The effect of the combination mirrored the situation of vehicle-treated samples (mean EA = 0,8% combination) (Figure 5.4, panel D).

Evaluation of % CA-9+ area confirmed that hypoxic areas were comparable between vehicle at random day and vehicle after 4 weeks (mean of group = 16% vehicle at random; 20% vehicle). Levels of hypoxia were slightly increased after cediranib and reduced by the treatment with olaparib and the combination (mean of group = 30% cediranib; 14% olaparib; 17% combination) (Figure 5.4, panel B and representative images in panel E).

Additional analysis on levels of CA-9 mRNA, assessed by fluidigm, showed comparable values in vehicle and cediranib treated tumors (mean ΔCt = - 4.1 vehicle; -3.6 cediranib) and a decrease in level of CA-9 after olaparib and the combination (mean ΔCt = -7.5 olaparib; -5.2 combination). For convenience, values were reported as $-\Delta\text{Ct}$, being the lowest value corresponding to lowest expression.

Evaluation of DNA damage, assessing % γ H2AX foci formation, showed that cediranib administration did not influence γ H2AX foci formation compared with vehicle (mean of group = 11% vehicle; 11% cediranib), while olaparib and the combination induced a significant increase in DNA damage (mean of group = 48% olaparib; 30% combination) (Figure 5.4, panel F and representative images in panel G).

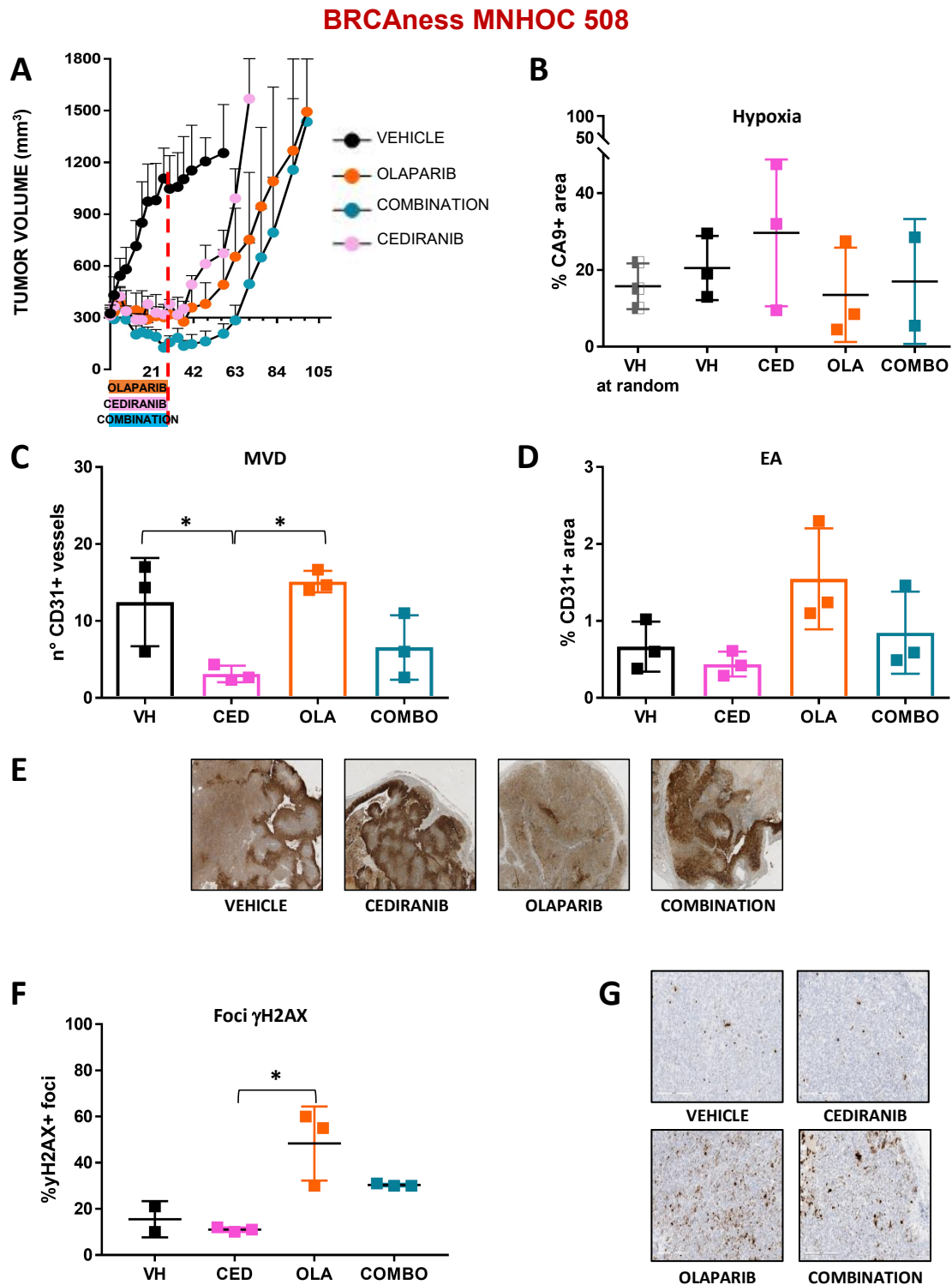


Figure 5.4 Analysis on subcutaneous MNHOC 508.

A) Samples were collected at the end of short-term treatment (---), from figure 4.5 A. **B)** % CA-9+ area, **C)** MVD (microvessel density, n° of CD31+ vessels), **D)** EA (endothelial area, CD31 positive area not considering vascular lumen, % of CD31+ area) are reported as the mean \pm SD of 3 200X randomly selected fields in neoplastic tissue. **E)** Representative sections of CA-9+ area (50X magnification). **F)** γ H2AX foci (% γ H2AX+ foci with different patterns) are reported as the mean \pm SD of 3 200X randomly selected fields in neoplastic tissue. **G)** Representative sections of γ H2AX+ cells (200X magnification). *P<0.05.

5.1.2 Intraperitoneal models

5.1.2.1 MNHOC 8, *BRCAness*

Analysis of changes in tumor-associated vasculature and hypoxia induced by treatment were performed in one intraperitoneal OC-PDX, taken as an illustrative example; the biomarkers of responses were evaluated in neoplastic tissue invading the ovaries.

For the intraperitoneal model MNHOC 8, analyses were carried out taking into consideration two different time points: samples were collected at the end of short-term treatment (4 weeks) (Figure 5.5, panel A) and at progression under treatment (Figure 5.6, panel A).

At short-term treatment (4 weeks), the angiogenesis inhibitor cediranib, PARP inhibitor olaparib and the combination induced a strong reduction in levels of ascites compared with vehicle-treated mice. The combination further improved the outcome, significantly reducing levels of tumor dissemination in the organs of the peritoneal cavity (Figure 5.5, panel A).

MVD and EA evaluation did not show a clear variation in the number of vessels and percentage of CD31+ area detected within the neoplastic tissue, just a general, treatment-independent, decreasing trend in cediranib, olaparib and the combination group compared with vehicle (MVD mean of group = 15 vehicle; 5 cediranib; 8 olaparib; 4 combination. EA mean of group = 1% vehicle; 0,4% cediranib; 0,6% olaparib; 0,5% combination) (Figure 5.5, panel B and C).

Basal levels of hypoxia were assessed evaluating % of CA9+ area in vehicle at random (day 10 after tumor injection) (mean of group = 5%). After 4 weeks, tumor masses in the ovaries were hardly measurable, resulting in poor evaluable hypoxic areas (mean of group = 30% vehicle; 25% cediranib; 30% olaparib; 17% combination) (Figure 5.5, panel D).

BRCAness MNHOC 8

Short-term treatment

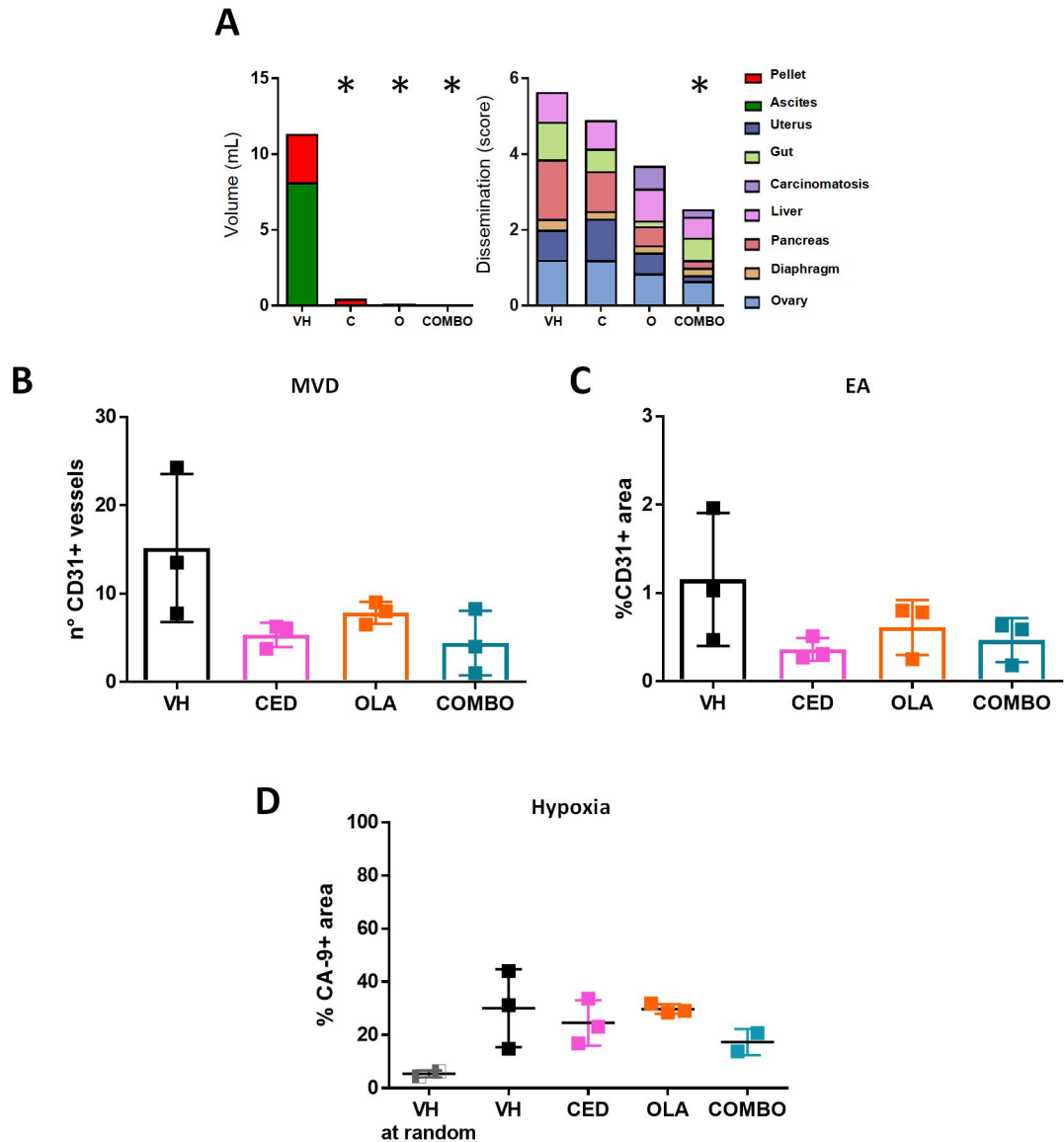


Figure 5.5 Analysis on intraperitoneal MNHOC 8.

Levels of ascites and carcinomatosis at **A)** short-term treatment sample collection time point.

B) MVD (microvessel density, n° of CD31+ vessels), **C)** EA (endothelial area, CD31 positive area not considering vascular lumen, % of CD31+ area) and **D)** %CA-9+ area are reported as the mean±SD of 3 200X randomly selected fields in neoplastic tissue.

At progression under treatment (after more than 20 weeks of treatment administration), cediranib and the combination remarkably controlled ascites formation compared with vehicle or olaparib, nevertheless inducing a substantial spread of carcinomatosis throughout the organs of the peritoneal cavity, especially ovaries. In contrast, olaparib monotherapy did not affect ascites formation, even though it induced a strong reduction in solid tumor masses formation in the ovaries (Figure 5.6, panel A).

At this time point, MVD was halved by cediranib and the combination, compared with vehicle controls or olaparib monotherapy (mean n° of CD31+ vessels = 21 for vehicle; 10 for cediranib; 20 for olaparib; 12 for the combination). The same results were obtained analysing the % CD31+ area (mean of group = 1% vehicle; 0,4% cediranib; 2% olaparib; 0,4% combination) (Figure 5.6, panel B, C and representative images in panel D).

Pimonidazole was used to assess levels of hypoxia (% Pimo+ area). Levels of hypoxia increased significantly at progression under treatment, particularly in vehicle, cediranib and olaparib groups (mean of group = 7% vehicle; 7% cediranib; 9% olaparib). Continuous administration of the combination remarkably diminished % Pimo+ area (mean of group = 1,6% combination) compared to other treatments: despite the fact that tumor masses were larger in animals treated with the combination and changes in tumor-associated vasculature were not further intensified by the combination, hypoxia levels were significantly reduced (Figure 5.6, panel E).

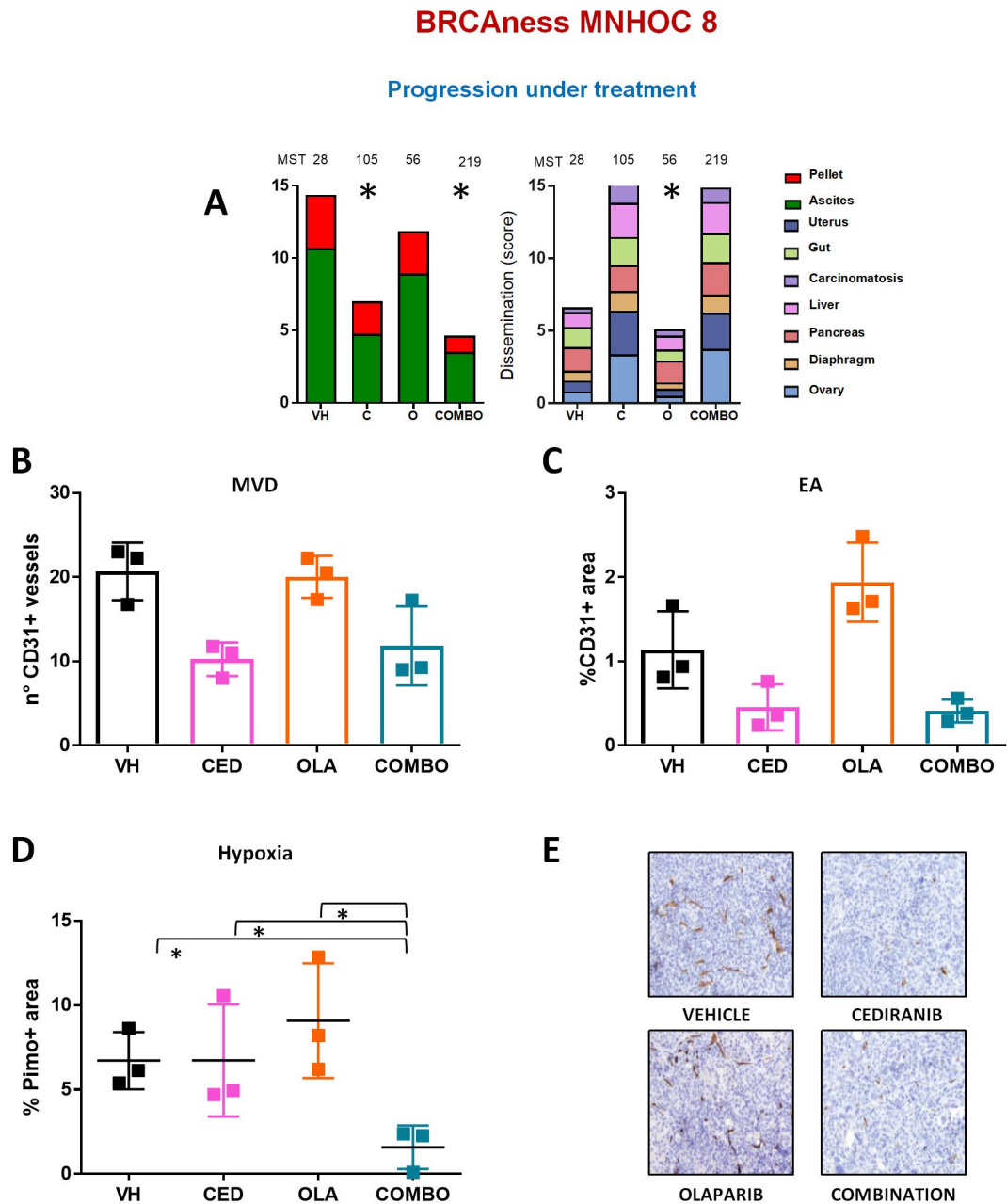


Figure 5.6 Analysis on intraperitoneal MNHOC 8.

Levels of ascites and carcinomatosis at **A**) progression under treatment sample collection time point. **B**) MVD (microvessel density, n° of CD31+ vessels), **C**) EA (endothelial area, CD31 positive area not considering vascular lumen, % of CD31+ area) and **D**) % Pimo+ area are reported as the mean±SD of 3 200X randomly selected fields in neoplastic tissue. **E**) Representative sections of CD31+ vessels (200X magnification). *P<0.05.

5.2 SUMMARY OF RESULTS AND DISCUSSION

It is well recognized that angiogenesis inhibition, using drugs such as the tyrosine-kinase inhibitor cediranib, could lead to a normalization of structure and function of tumor-associated vasculature, reducing hypoxia (Jain, 2005). Nonetheless, there is evidence to support the idea that the use of therapeutic strategies to inhibit angiogenesis can cause local hypoxia in tumors, reducing the number, maturation, patterning and function of vessels and therefore level of oxygen (Liao and Johnson, 2007).

Modification in levels of hypoxia can lead to a DNA repair-deficient phenotype, causing increased genetic instability, with a decrease in the level of expression of HR DNA repair pathway proteins. In this context, tumor cells should be more sensitive to DNA cross-linking agents, such as PARP inhibitors, including olaparib (Bristow and Hill, 2008; Pires et al., 2010).

Moreover, changes in level of hypoxia induced HIF-1 α stabilization and activation, and this might enhance tumor cell dissemination. Enhanced angiogenesis is associated with metastasis, due to the fact that permeable and heterogeneous vasculature facilitates the extravasation and circulation of tumor cells to distant and unaffected organs, thus escaping the hypoxic microenvironment in the primary tumor. Hypoxic cells are indeed more aggressive and invasive, with a better ability to metastatize. Hypoxia influence invasive and migratory behaviour via epithelial-to-mesenchymal transition (EMT), that it is characterized by a decrease in epithelial-associated genes, such as E-cadherin, β -catenin, and an increase in mesenchymal associated gene, such as N-cadherin, vimentin and α -SMA. Tumor cells that undergo EMT are resistant to chemo and radiotherapy.

Changes that the tumor microenvironment and hypoxia cause at a genetic level, could in part explain the promising results of olaparib combined with cediranib in OC-PDX models. For these reasons, changes in tumor-associated vasculature (using CD31 and evaluating vessels number and area), hypoxia (using CA-9 or Pimonidazole staining) and DNA

damage markers (such as γ H2AX foci formation) were evaluated in a limited number of OC-PDX used for preclinical drug testing (see Chapter 4, Results).

In particular, treated samples from 3 subcutaneous (MNHOC 18, MNHOC 182 and MNHOC 508) and one intraperitoneal (MNHOC 8) models were analysed after the end of treatment (4 weeks) and at progression under treatment (only for MNHOC 8).

Results reported in Chapter 5 indicated a general heterogeneity amongst the models, with different levels of hypoxia detected within each model at baseline (vehicle at random and vehicle at short-term treatment), and different baseline expression of γ H2AX.

For example, in the Not BRCAness MNHOC 182, cediranib and the combination reduced hypoxia, with a diminution in vessel number and area, indicating also a normalization of tumor vasculature compared to the ectatic (dilated) vessels present in vehicle and olaparib treated samples (Figure 5.3, panel B, C, D and E). The effect of olaparib and the combination on γ H2AX foci formation was limited, with no significant differences between the groups (Figure 5.3, panel F).

In contrast, in the subcutaneous model MNHOC 18, the number and area of vessels and hypoxia level were mostly affected by cediranib and the combination (Figure 5.2, panel B, C and D). Olaparib induced a slight increase of γ H2AX foci formation (Figure 5.2, panel F). This moderate effect could be linked to the fact that this model is Not BRCAness, so mechanisms of damage repair are functional. Rather, γ H2AX foci formation was significantly increased by the combination with cediranib (Figure 5.2, panel F).

In addition, in the BRCAness MNHOC 508 tumor model, no significant changes in levels of hypoxia were detected, despite a decreased number of vessels induced by cediranib and the combination (Figure 5.4, panel B, C and D). The PARP inhibitor itself induced an increase in γ H2AX foci, and the effect was not further enhanced by the combination, thus

indicating the already strong effect of the PARP inhibitor in boosting genetic instability in this DNA-repair deficient model (Figure 5.4, panel F and G).

In the context of combination therapy, it would be reasonable to hypothesize that i) cediranib played a key role in modifying tumor-associated vasculature and local hypoxia, ii) olaparib caused an enhancement of DNA damage, iii) the combination of the effects sustained the strong stabilization (MNHOC 18, Figure 5.2, panel A) or regression (MNHOC 508, Figure 5.4, panel A) of tumor growth, as long as the therapy is continuously administered.

The intraperitoneal MNHOC 8 model provided the opportunity to study the short and long-term activity of the combination. After only 4 weeks of therapy, minimal changes in tumor-associated vasculature and hypoxia were detected (Figure 5.5, panel B, C and D). At this time point, neoplastic tissue in the ovaries was barely detectable, and that could explain the lack of differences, even with a general reduction in the level of dissemination at necropsy induced by the combination (Figure 5.5, panel A).

When analyses were performed at tumor progression under maintenance treatment (after more than 20 weeks of treatment), vessel number and area were reduced by cediranib and the combination (Figure 5.6, panel B, C and E), but only the latter induced a strong reduction of hypoxia (Figure 5.6, panel D). It is known that long-term exposure to angiogenesis inhibitors can result in tumor growth reduction and in parallel in a more malignant and invasive phenotype (Mountzios et al., 2014). In MNHOC 8 the maintenance treatment with the combination reduced ascites production to the detriment of an increased tumor dissemination through the organs of the peritoneal cavity (Figure 5.6, panel A).

Increased aggressiveness could in part be explained by the fact that angiogenesis inhibitor administration prolong survival in mice, mainly because ascites is drained off and, without it, tumor cells “fall” directly in contact with the surrounding healthy tissues. It is possible

to speculate that the prolonged survival allows resistant and malignant tumor cells to survive and grow, in a microenvironment rich of oxygen and with the correct levels of nutrient.

Correlating results on biomarkers of response, in term of immunohistochemical analysis, with molecular changes (see Chapter 6, Results), in terms of gene expression after treatment, could help to reveal possible mechanisms of action underlying the advantage of adding cediranib to olaparib in both BRCAness and Not BRCAness tumors.

CHAPTER 6.

Results

PRELIMINARY APPROACHES TO DETERMINE MECHANISMS UNDERLYING THE BENEFIT OF COMBINATION THERAPY

In an attempt to investigate mechanisms of action underlying the combination of olaparib (PARP inhibitor) with cediranib (angiogenesis inhibitor), analyses were performed, taking into consideration several complementary aspects of the tumor's biological behaviour.

In Chapter 6 preliminary data on gene expression modulation at the end of 4 weeks of treatment are reported.

6.1 GENE EXPRESSION ANALYSIS AFTER TREATMENT: FLUIDIGM DATA

Cediranib, an oral inhibitor of VEGF signaling, that binds VEGFR1, VEGFR2, VEGFR3, c-Kit and PDGFR-alpha, shown to inhibit blood vessel growth and sprouting both *in vivo* and *in vitro* (Wedge et al., 2005).

Olaparib, an oral inhibitor of PARP, shown a dual activity in preventing DNA damage repair and “trapping” PARP on DNA, thus creating complexes that impair the progression of replication forks (Lord and Ashworth, 2017).

It has been suggested that the use of VEGFR inhibitors (e.g. cediranib) can cause changes in the microenvironment (e.g. local tumor hypoxia, tumor-associated vasculature remodelling) that could lead to a DNA repair-deficient phenotype on tumor cells (Bristow and Hill, 2008; Pires et al., 2010), with a decreased expression of proteins involved in the HR DNA repair pathway. This can increase sensitivity to DNA cross-linking agents such as PARP inhibitors (e.g. olaparib) (Chan et al., 2008, 2010).

As previously reported in the laboratory where this PhD project has been performed, cediranib also caused vascular regression and inhibition of VEGFR3 mediated lymphangiogenesis in ovarian cancer models (Decio et al., 2014). Lim and colleagues (Lim et al., 2014) reported that VEGFR3 inhibition in ovarian cancer cells leads to a decrease in the levels of *BRCA1* and *BRCA2*, both at the mRNA and protein levels of expression.

These multiple findings gave us the rationale to analyse changes induced by the treatment in different classes of genes.

Specifically, gene expression was investigated after 4 weeks of treatment on three OC-PDX: MNHOC 18, MNHOC 182 and MNHOC 124. The three OC-PDX were subcutaneously growing tumors, Not BRCAness, olaparib resistant, but all gained a significant advantage in terms of growth delay when olaparib was administered together with cediranib (Figure 6.1; see also Chapter 4, Results, for details).

Not BRCAness models

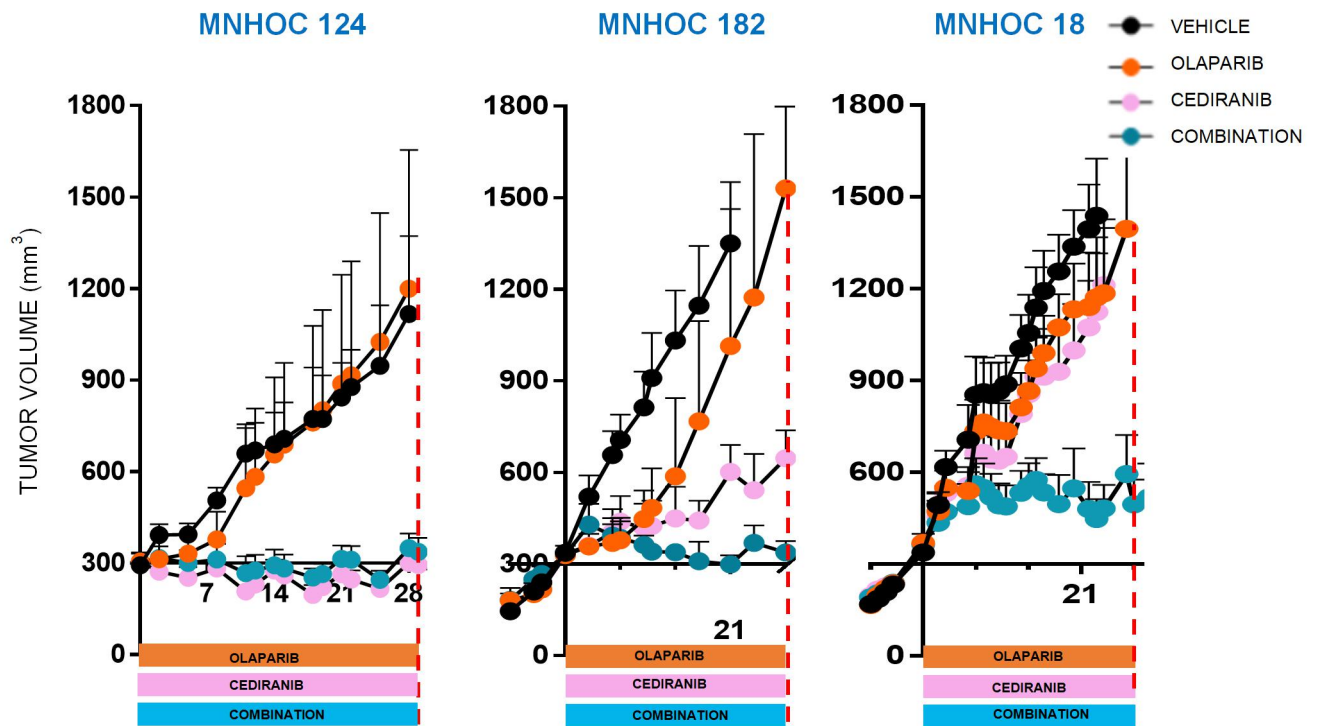


Figure 6.1 OC-PDX models selected to perform gene expression data analysis.

A) MNHOC 124, B) MNHOC 182 and C) MNHOC 18 were Not BRCAness models, resistant to olaparib and gained advantages from the combination. Samples were collected at the end of 4 week treatment (---).

Gene expression analysis was carried out with RealTime PCR. *Ad hoc* murine and human primers were designed, allowing us to consider changes both in the murine (e.g. angiogenesis, cytokine/chemokine, hypoxia, metabolism, immune-stimulatory and suppressive genes) and in the human compartments (e.g. DDR and EMT genes).

Changes in gene expression were initially assessed to identify which classes of genes were overall modulated by the combination treatment.

Modulations at gene expression levels were induced in both cancer cells and tumor microenvironment.

In particular, angiopoietin-2 (m_Angpt2), delta-like protein 4 (m_Dll4), VEGF receptor 2 (m_Kdr) and placental growth factor (m_Pgf) were significantly downregulated, indicating the inhibition of angiogenesis (Figure 6.2, panel A).

Transcript levels (mRNA) of thioredoxin-interacting protein (m_Txnip), an inhibitor of the thioredoxin antioxidative function that leads to the accumulation of reactive oxygen species and cellular stress, were significantly upregulated, suggesting a modulation also in metabolism-associated genes in the microenvironment (Figure 6.2, panel A).

Human XRCC3, which belongs to the DDR pathway and participates in homologous recombination to maintain chromosome stability and repair DNA damage, was significantly upregulated in cancer cells (Figure 6.2, panel B).

Thus, given these overall results, OC-PDX specific changes induced by treatments were then analysed, with a particular focus on all the genes belonging to metabolism and angiogenesis (murine compartment) and DDR (human compartment), comprised in the panel of genes selected for Fluidigm (for the complete list see Section 2.2.5 and Tables 2.2 and 2.3, Materials and Methods, Chapter 2).

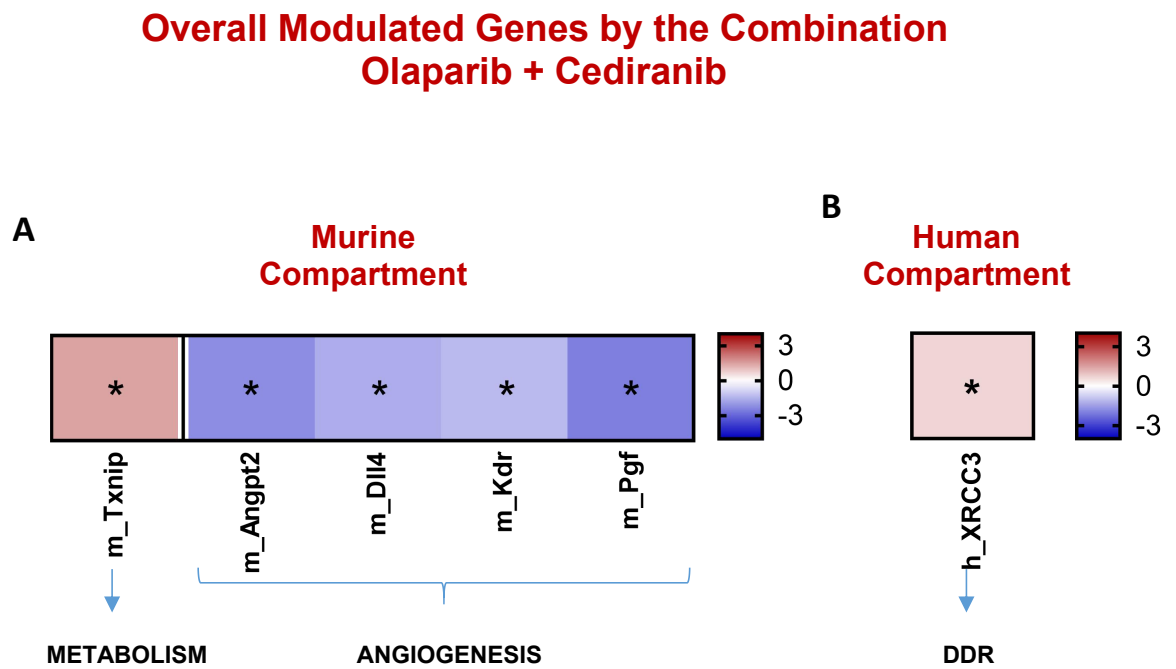


Figure 6.2 Gene expression analysis after 4-week treatment with the combination.

Overall **A)** murine and **B)** human genes, of which levels of expression were significantly modulated by the combination of olaparib and cediranib in responsive tumors undergoing treatment. Briefly $\Delta Ct = Ct_{\text{target}} - Ct_{\text{housekeeping}}$ was calculated (housekeeping genes were IPO8 and HPRT1) for each gene under investigation.

Changes in levels of expression (FC=fold change) were calculated by the $2^{-\Delta\Delta Ct}$ method (comparator were the untreated tumors) (Schmittgen TD and Livak KJ, *Nat Protoc*, 2008). Then the Log_2FC values were analysed for statistical significance. Shown are the significantly modulated genes. * $P < 0.01$. $N = 9$ ($3 \neq$ models).

Murine compartment.

Changes in gene expression induced by the treatment were in general moderate in MNHOC 124 and MNHOC 182 (Figure 6.3, panel A and B). All the treatments induced a significant gene expression modulation in MNHOC 18.

Among genes belonging to metabolism, m_Phgdh (phosphoglycerate dehydrogenase) was significantly upregulated by the three treatment, m_Keap1 (substrate adapter protein for the E3 ubiquitin ligase complex), m_Pfkfb3 (phospho-fructo-kinase/fructose-diphosphatase 3), m_Scd1 (endoplasmic reticulum enzyme Stearoyl-CoA desaturase), m_Slc25a10 (mitochondrial dicarboxylate carrier) and m_Txnip were modulated by olaparib and the combination with cediranib (Figure 6.3, panel C).

The combination of olaparib with cediranib reduced the expression of angiogenesis-related genes, such as m_Angpt2, m_Dll4 and m_Kdr in both MNHOC 124 and MNHOC 182. Unexpectedly, cediranib monotherapy did not modulate gene expression either in metabolism-, or in angiogenesis-related genes (Figure 6.3, panel A and B).

Different angiogenesis genes were downregulated by olaparib, cediranib and the combination in MNHOC 18.

Interestingly, m_Tek (the tyrosine kinase receptor for angiopoietin-1) was significantly upregulated by olaparib, cediranib and the combination (Figure 6.3, panel C).

MICROENVIRONMENT/STROMA
Murine compartment

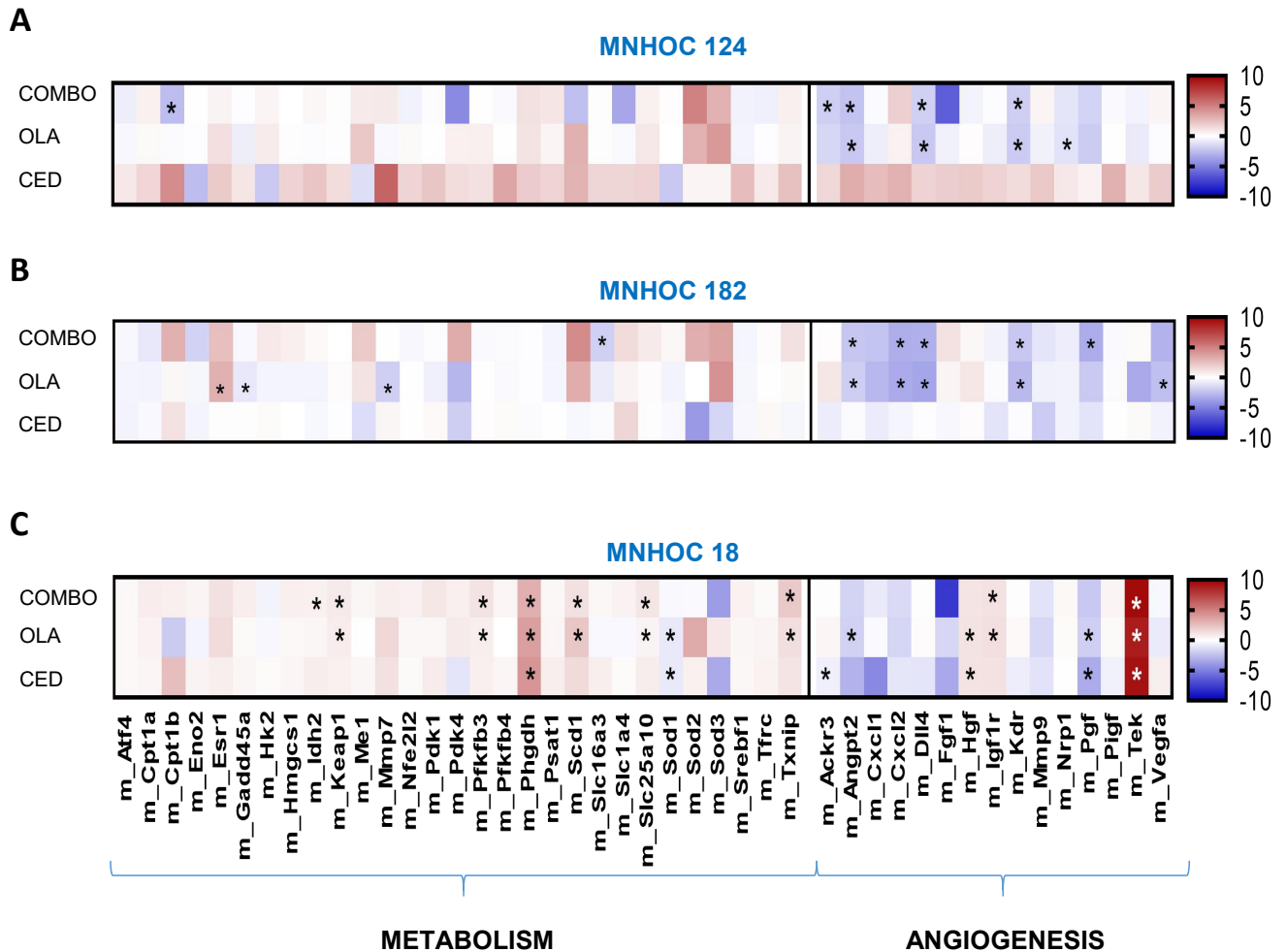


Figure 6.3 Heatmap of relative gene expression ($-\Delta\Delta C_t$ values) induced by 4-week treatment.

Relative expression ($-\Delta\Delta C_t$) of murine genes associated with metabolism and angiogenesis in **A)** MNHOC 124, **B)** MNHOC 182 and **C)** MNHOC 18 after treatment with cediranib, olaparib and the combination. Treated samples were compared with untreated samples. * $P < 0.05$.

N=3

Human compartment.

Results obtained from the analyses on tumor microenvironment (murine compartment) indicated a significant downregulation of angiogenesis induced by treatments. Since it has been reported that changes in the microenvironment (e.g. local hypoxia and changes in tumor-associated vasculature) could induce a downregulation of protein involved in the DNA damage repair system, we analysed gene expression changes on tumor cells (human compartment).

When genes belonging to the DDR pathways were analysed, no significant downregulation was identified (Figure 6.4, panel A and B). On the opposite, a larger number of genes were upregulated in MNHOC 18, mostly when olaparib monotherapy and the combination were administered. Interestingly, also cediranib monotherapy affected the expression levels of DDR genes (Figure 6.4, panel C).

TUMOR CELLS
Human compartment

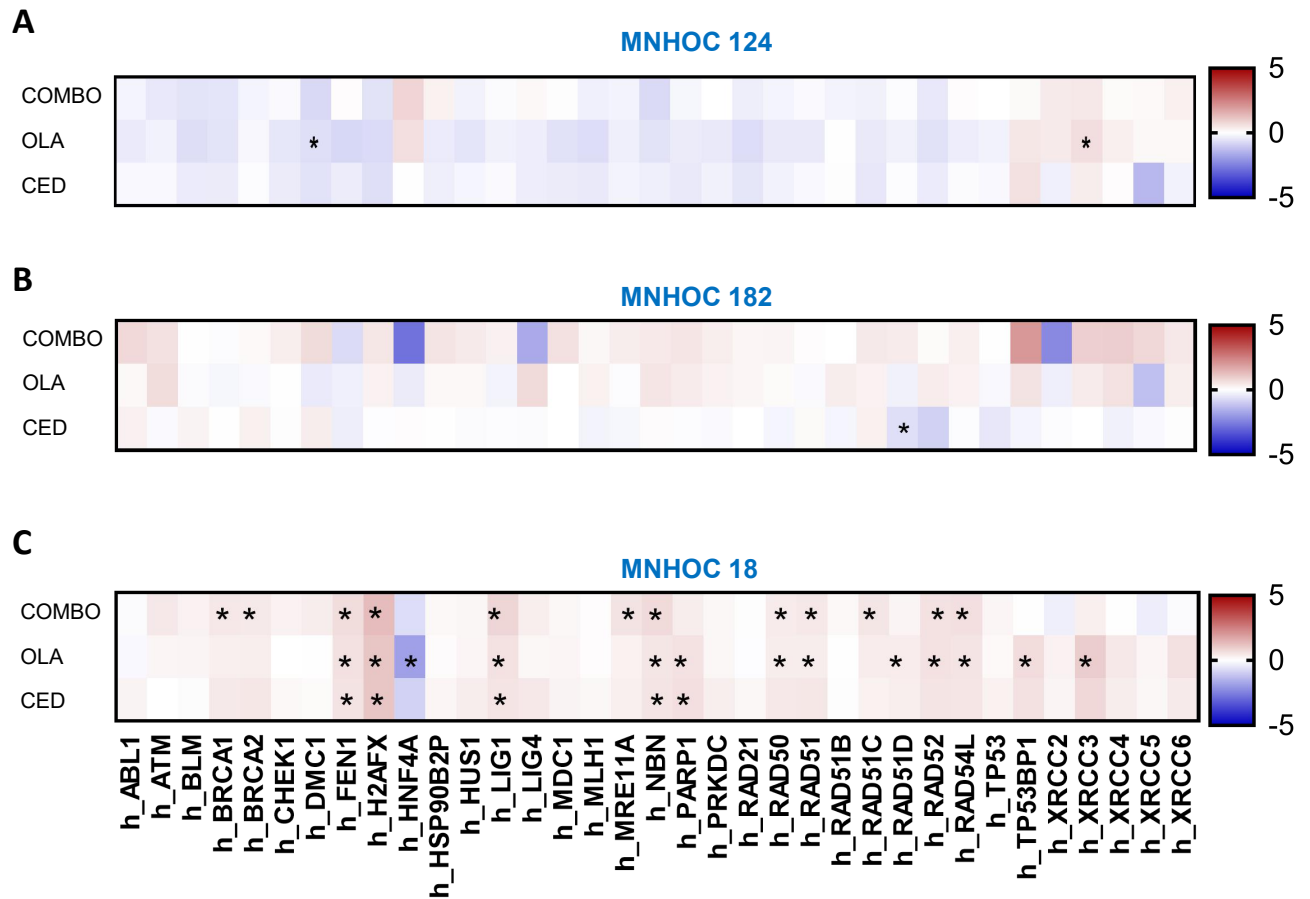


Figure 6.4 Heatmap of relative gene expression ($-\Delta\Delta C_t$ values) induced by 4-week treatment.

Relative expression ($-\Delta\Delta C_t$) of human genes associated with DDR in **A**) MNHOC 124, **B**) MNHOC 182 and **C**) MNHOC 18 after treatment with cediranib, olaparib and the combination. Treated samples were compared with untreated samples. * $P < 0.05$.

N=3

6.2 CEDIRANIB TARGET BASELINE LEVELS OF EXPRESSION

Given the unexpected modulation induced by cediranib of genes belonging to the DDR (human compartment), we investigated whether cediranib could act directly on the tumor cell.

Genome-wide gene expression analyses had previously been carried out on a wider panel of OC-PDX (Ricci et al., 2014). Given the availability of these data, expression levels of cediranib targets, VEGFR1 (*FLT1*), VEGFR2 (*KDR*), VEGFR3 (*FLT4*), c-Kit (*KIT*) and PDGFR-alpha (*PDGFRA*) (Sahade et al., 2012) were analysed on tumor cells.

Results showed that VEGFR1, VEGFR3 and PDGFR-alpha were significantly more highly expressed in MNHOC 18, compared with the other models. Indeed VEGFR1 was scarcely expressed (range 6.1-6.8 Log₂ Intensity) across OC-PDX (n=19), except for MNHOC 18 (7.7 Log₂ Intensity) (Figure 6.5, panel A). Similar results were obtained analysing VEGFR3 and PDGFR-alpha, with MNHOC 18 expressing higher levels (8.9 and 10.2 Log₂ Intensity for VEGFR3 and PDGR-alpha respectively) compared to the other OC-PDX models (range VEGFR3 7-7.9 Log₂ Intensity and range PDGFR-alpha 6.4-10 Log₂ Intensity) (Figure 6.5, panel B and C). No significant differences were seen comparing VEGFR2 and c-KIT levels of expression in MNHOC 18, MNHOC 182 and MNHOC 124 (Figure 6.5, panel D and E).

Genome-wide gene expression analysis

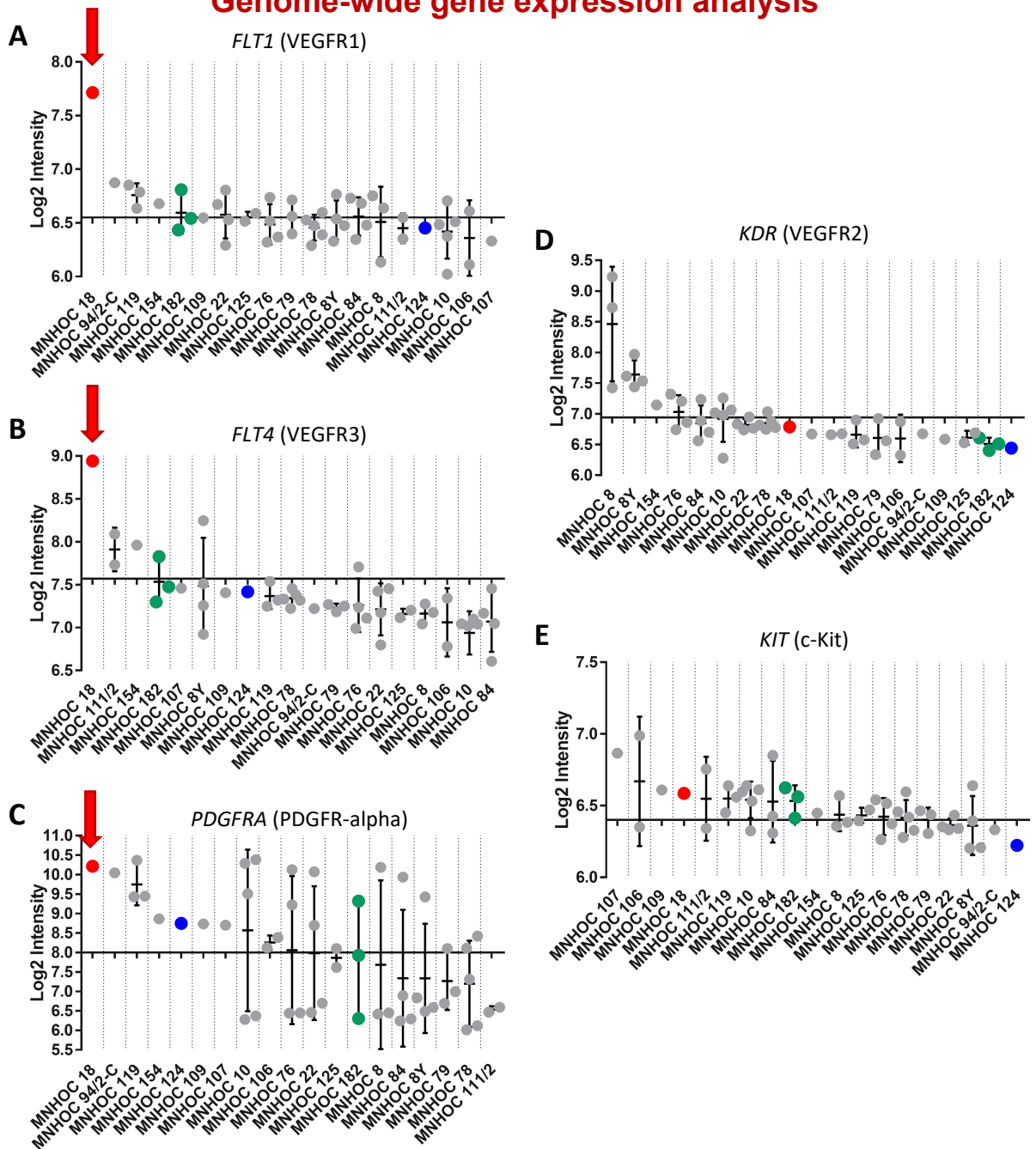


Figure 6.5 Cediranib-target expression level of OC-PDX.

A) *FLT1*, B) *FLT4*, C) *PDGFRA*, D) *KDR* and E) *KIT* levels of expression from genome-wide gene expression analysis.

Arrays were scanned and images analysed by the Feature Extraction Software; raw data were processed using the LIMMA (Linear Models for Microarray Analysis) package from Bioconductor (Smyth, 2004). Background correction was performed with the normexp method with an offset of 50. Normalization was carried out using the quantile method. Data are expressed as Log2 Intensity and represented on graph as mean±SD. Abscissa intercepts ordinate axis at the mean value of Log2 Intensity for each gene.

Thus, to confirm the results obtained from these analyses, *ad hoc* Real-Time PCR assays were performed specifically to study the panel of the 13 OC-PDX used for this PhD research project (see Chapter 3 and Chapter 4, Results). Human-specific primers for VEGFR1, VEGFR2, VEGFR3, c-Kit and PDGFR-alpha were used (Taqman Assay).

VEGFR1 was weakly expressed across all samples (mean ΔCt -15); nevertheless, levels of expression were higher in MNHOC 18 (ΔCt -11.6) compared with MNHOC 124 and MNHOC 182 and above the confidence interval (Figure 6.6, panel A). VEGFR3 and PDGFR-alpha levels of expression were higher in MNHOC 18 (ΔCt -9.5 for VEGFR3 and ΔCt -5.6 for PDGFR-alpha) compared with MNHOC 124 and MNHOC 182 and the other models (mean ΔCt -13 for VEGFR3 and ΔCt -10 for PDGFR-alpha) (Figure 6.6, panel B). MNHOC 18 expressed also the highest level of c-KIT (ΔCt -7.8; mean ΔCt -11) (Figure 6.6, panel E). VEGFR2 levels were within the confidence interval for MNHOC 18 (ΔCt -9.8), but higher compared with the mean of the group (ΔCt -12.3) and different than MNHOC 124 and MNHOC 182 (Figure 6.6, panel D).

RealTime gene expression analysis

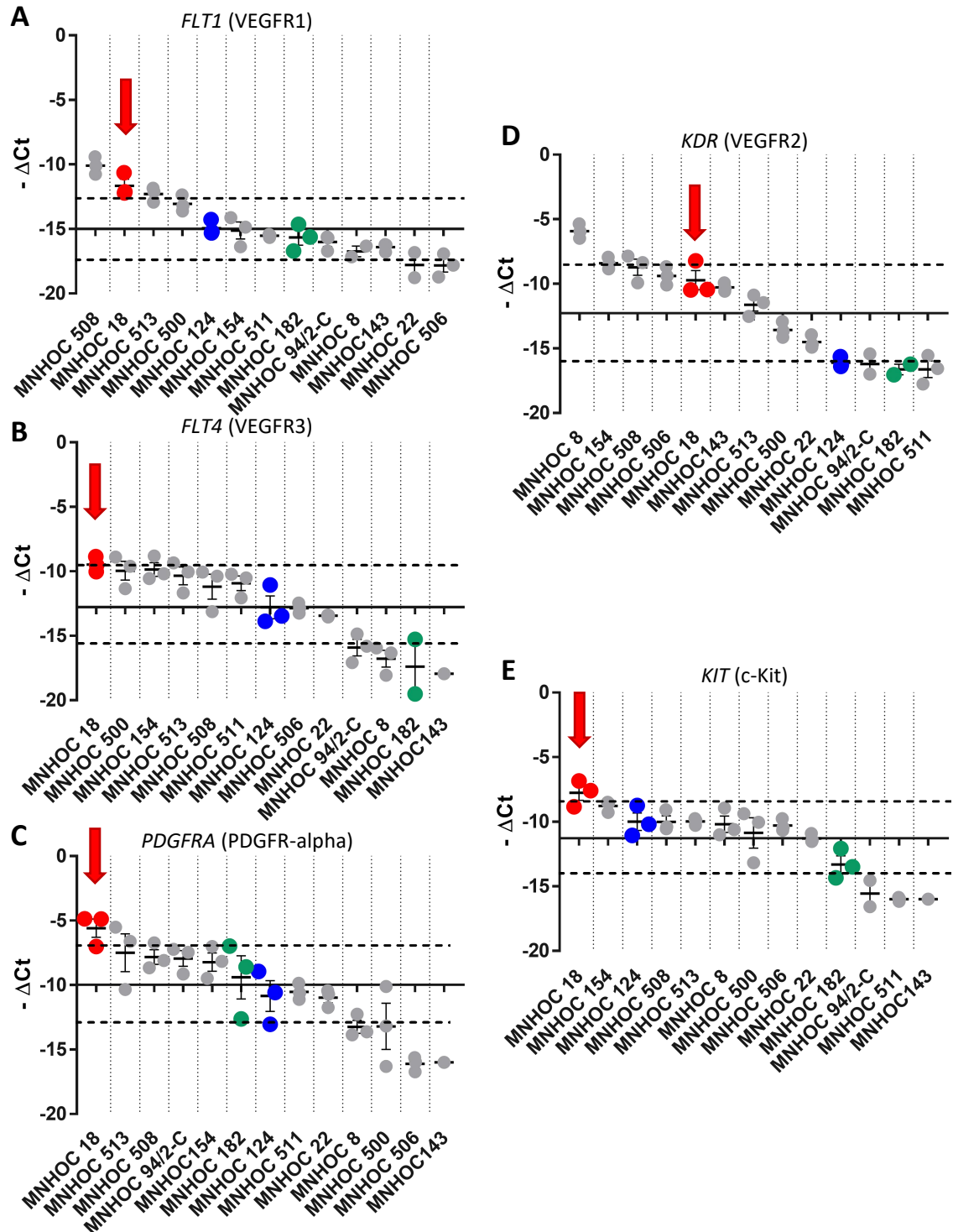


Figure 6.6 Cediranib-target expression level in 13 OC-PDX from RT-PCR.

A) *FLT1*, B) *FLT4*, C) *PDGFRA*, D) *KDR* and E) *KIT* were normalized to beta-actin housekeeping gene and ΔCt calculated.

Reported are results for three biological replicates (mean of three technical replicates each). Data are reported as $-\Delta\text{Ct}$, such that the lowest value corresponds to the lowest expression. Abscissa intercepts ordinate axis at the average value of $-\Delta\text{Ct}$ obtained from all the samples.

When data were analysed considering only MNHOC 18, MNHOC 124 and MNHOC 182 together, the comparison showed that expression of cediranib targets was always higher in MNHOC 18, with the three receptors of VEGF and c-Kit being significantly higher compared with MNHOC 182 (Figure 6.7). Thus, it is conceivable that, particularly in MNHOC 18, cediranib could act not only on the tumor microenvironment but also directly on tumor cells.

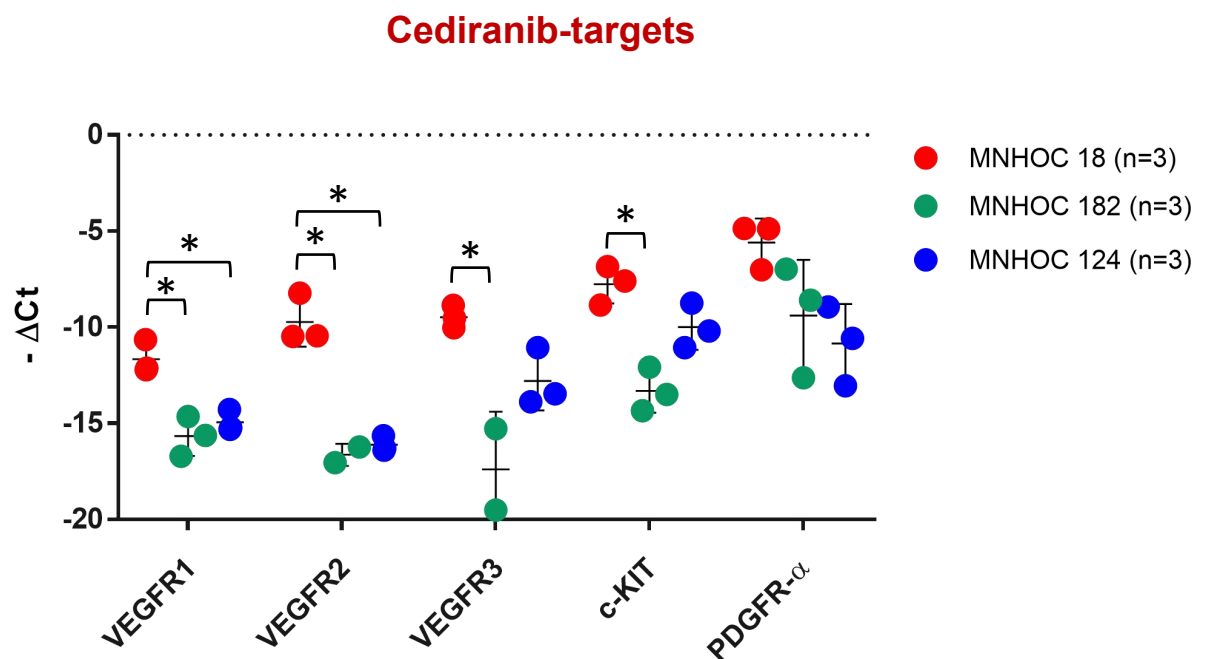


Figure 6.7 Cediranib-target level in MNHOC 18, MNHOC 124 and MNHOC 182.

Reported are results for three biological replicates (mean of three technical replicates each). Data are reported as $-\Delta\text{Ct}$, such that the lowest value corresponds to the lowest expression. * $P < 0.05$. Data comparison from Figure 6.6.

6.3 SUMMARY OF RESULTS AND DISCUSSION

Cediranib (Ledermann et al., 2016) and olaparib (Pujade-Lauraine et al., 2017) have shown promising therapeutic activity in ovarian cancer as single agents. The activity of the combination has led to the two drugs now being considered for a maintenance therapy in patients with ovarian cancer (Liu et al., 2013, 2014).

Preclinical tests with PARP inhibitors combined with angiogenesis inhibitors have suggested that downregulation of homologous recombination repair genes, such as *BRCA1* and *RAD51*, occurs with hypoxia, with an enhancement sensitivity to PARP inhibitor in the hypoxic setting (Bindra et al., 2005; Chan et al., 2008; Scanlon and Glazer, 2015).

Lim and colleagues suggested that VEGFR3 inhibition results in downregulation of both *BRCA1* and *BRCA2* in cancer cells (Lim et al., 2014), and additional preclinical studies indicated that PARP inhibition could increase cytotoxicity in cancer cells under hypoxic compared with normoxic conditions (Lu et al., 2011).

Given these findings, our initial working hypothesis was that the angiogenesis inhibitor cediranib could cause hypoxia, which in turn could induce a downregulation of genes involved in the DNA repair pathway and consequently lead to a “DNA damage repair system-deficient phenotype”, rendering tumor cells more responsive to olaparib.

In this context, the cross talk between an altered microenvironment and tumor cells no longer able to repair DNA damage would lead to synthetic lethality and provide the rationale to the therapeutic advantage of the two drugs administered together.

Indeed, our preclinical testing trials confirmed that the administration of the combination was the regimen with the best outcome, both in models with an impairment in DNA damage repair system (BRCAness) and, most importantly, in those with a proficient

system of repair (Not BRCAness), delaying tumor progression and increasing survival in subcutaneous and in orthotopic OC-PDX.

For these reasons, we investigated changes in gene expression after 4 weeks of treatment in three Not BRCAness models, in which the therapeutic advantage of the combination of olaparib with cediranib was more evident (Figure 6.1).

A panel of both murine and human genes was simultaneously investigated with RealTime PCR gene expression analysis, giving us the opportunity to assess changes in the tumor microenvironment/stroma (murine compartment, cediranib primary target) and in the tumor cell (human compartment, olaparib primary target).

Results indicated that the combination of olaparib with cediranib caused changes in the tumor microenvironment, in particular inducing a significant downregulation of angiogenesis-related genes across the three OC-PDX analysed (Figure 6.2, panel A). Of note, the significant upregulation of m-Tek, the tyrosine kinase receptor (that acts as a cell-surface receptor for angiopoietin-1, angiopoietin-2 and angiopoietin-4) in MNHOC 18, could also support the inhibition of angiogenesis by endorsing vascular instability and vessel quiescence when angiopoietin-2 competes with angiopoietin-1 for binding (Figure 6.3, panel C).

When analyses on changes induced by the treatment on tumor cells (human compartment) were performed, our initial hypothesis that cediranib, by inhibiting angiogenesis, would lead to a decreased expression of proteins involved in the DDR, rendering the tumor cells more sensitive to olaparib, was not confirmed.

No significant downregulation occurred in DDR genes when the combination of olaparib with cediranib was administered; on the contrary and unexpectedly, the treatments induced a significant upregulation of DDR genes in MNHOC 18 (Figure 6.4).

This upregulation could be partially explained by the fact that we have only examined changes in gene expression after 4 weeks of continuous treatment, hence we are likely analysing not the “responder cells” but rather the “survivor cells”.

Thus, it would be better to perform gene expression analyses at different time points to take in consideration changes after a few doses of treatment, when it is reasonable to assume that the treatment has not yet selected resistant cells, could help to better define possible mechanism of action underlying the observed advantage of the combination, both in BRCAness and Not BRCAness tumors.

Olaparib causes DNA damage, due to its “trapping” activity, inducing replication forks to stall. The increased DNA damage is supported by the significantly higher expression of γ H2AX foci detected after the administration of the combination in MNHOC 18 (see Figure 5.2, Chapter 5, Results).

Thus, tumor cells that survived such damage were those able to overcome the insult by increasing the expression of proteins involved in DNA damage repair, and the same occurs in cells that do not respond, explaining also the resistance to olaparib monotherapy.

The fact that the treatments could have induced a clonal selection of cells that have acquired a BRCAness phenotype, thus becoming more sensitive to the combination of olaparib and cediranib, can be excluded. Indeed, mutational analyses at the end of the treatments indicated no acquisition of novel mutations, nor the selection of subclones mutated in *BRCA1*, *BRCA2* or other genes involved in the DNA repair pathway, as reported in Figure 4.17, Chapter 4 of Results.

One last aspect that should be taken into account is the modulation induced by the angiogenesis inhibitor, which led us to investigate the expression of cediranib targets directly on tumor cells across our platform of OC-PDX. Results showed that, especially in MNHOC 18, levels of expression of the three VEGF receptors, c-KIT and PDGFR-alpha,

were higher compared with the other models (Figure 6.5, 6.6 and 6.7), which could explain the modulation of DDR-related genes induced by cediranib monotherapy.

Despite the fact that these preliminary results did not completely clarify the role of cediranib in the beneficial combination with olaparib, it appears not to be linked only to a “general antiangiogenic modulation” on the microenvironment through the inhibition of the VEGFA pathway. Indeed, when bevacizumab or B20 (bevacizumab is an antibody that recognizes human VEGF, and B20 recognizes both human and mouse VEGF exhibiting equal affinity) were administered in combination with olaparib on MNHOC 18 tumor-bearing mice, no tumor growth delay was achieved (as reported in Figure 4.10, Chapter 4, Results).

However, it may be assumed that the growth delay induced by the combination could be due to the sum of the effects given by the single drug; cediranib and olaparib together perturbed the host microenvironment, modulating angiogenesis, and furthermore both directly influenced tumor cells as long as the treatment is administered. In fact, in the MNHOC 18 model, as soon as the combination treatment was interrupted, tumors regrew with the same doubling time as olaparib and vehicle control group.

More detailed analyses are needed to better clarify these preliminary results.

For instance, to mitigate the bias of using only a small panel of selected genes, whole transcriptome (RNA sequencing) analysis is being performed (collaboration with AstraZeneca). Expert bioinformatics colleagues are currently analysing data, taking into consideration changes induced by treatment in each model used in the preclinical testing trials, BRCAness and Not BRCAness, considering both the human and murine compartments.

CHAPTER 7.

Conclusions and Future Perspective

7.1 CONCLUSIONS AND FUTURE PERSPECTIVES

This project was aimed to investigate the effect of the combination therapy of PARP (i.e. olaparib) with angiogenesis inhibitors (i.e. cediranib) in the treatment of ovarian cancer, taking advantage of a platform of established and well characterized (histopathology, biological behaviour and molecular profile) ovarian cancer patients-derived xenografts (OC-PDX).

To this purpose, OC-PDX previously established in the Department of Oncology (Ricci et al., 2014), together with new models established during this PhD research project, as described in Chapter 3, have been used.

Among these, 26 OC-PDX were selected, that reproduced the plethora of ovarian carcinomas with all the different subtypes, growing subcutaneously or orthotopically in the peritoneal cavity of mice. The OC-PDX were deeply characterized for their biological, histopathological and molecular features. Results showed that OC-PDX retained the histotype and tissue architecture even after several *in vivo* passages, harboured mutations in genes mostly involved in ovarian cancer disease and progression (*TP53*, *KRAS*, *BRAF*, *PIK3CA*, *CTNNB1*, *PTEN*, *EGFR*) and in some HR DNA repair pathway genes. Moreover, when a comparison was possible, OC-PDX showed a strong consistency with the patient's tumor they derived from, maintaining the same histotype and mutations. For these reasons, our collection offered an instructive framework to perform preclinical drug testing that could be translated into the clinic.

Taking together data obtained from the Next Generation Sequencing and gene expression analysis and considering their histopathological origin, 13 *ad hoc* OC-PDX models were further selected to preclinical therapy testing with olaparib combined with cediranib, as reported in Chapter 4. This cohort of OC-PDX included mostly high grade serous and endometrioid ovarian carcinomas, with one clear cell and one mucinous model.

OC-PDX carrying somatic mutations and loss of *BRCA1/2* on both gene alleles or expressing low levels of *BRCA1* and *BRCA2* were defined as BRCAness. OC-PDX that did not carry mutations on *BRCA1* and *BRCA2* or did not display locus-specific loss of heterozygosity (LOH) were defined as Not BRCAness.

The response to olaparib monotherapy was assessed in 10 OC-PDX growing subcutaneously, both in a short-term (4 weeks) and in a maintenance regimen, until tumor regression or progression.

Results showed that BRCAness tumors responded to olaparib monotherapy after a short-term treatment and even more in a maintenance regimen, with complete responses. As seen in the clinic, aberrations in *BRCA1/2* were predictive for olaparib response also in our platform of OC-PDX (Fong et al., 2010; Kaufman et al., 2015), increasing the predictive value of these models.

However, some OC-PDX were an exception. The subcutaneous MNHOC 154 carried a pathogenic mutation in *BRCA1*, but the presence of an amplification in *BRCA2* (confirmed also by the high level of gene expression) induced a heterogeneous response to olaparib monotherapy.

The molecular heterogeneity within an individual model is an issue that call for consideration. In this sense, the identification of sub-clone populations of cells within each single tumor of each OC-PDX model and consequently single cell analyses with optimized next generation sequencing technologies, both on DNA, RNA and proteomics could provide a better understanding of the function of an individual cell in the context of its microenvironment. Sequencing the DNA of individual cell clones could provide information about carrier and non-carrier mutations and genomic alteration, while sequencing the RNA could give insight into the differences in gene expression. Taken together, all these aspects could deeply influence the response to targeted therapies, such as

PARP inhibitors and explain the observed heterogeneous responses within one single OC-PDX, as for MNHOC 154.

Similarly, to MNHOC 154, the intraperitoneal MNHOC 22 was resistant to olaparib, showing no increase in host survival and remarkable production of ascites, although carrying a mutation in *BRCA1*.

Not BRCAness and olaparib resistant OC-PDX were good models to study combination regimens and specifically the advantage of adding cediranib to olaparib. Genomic instability and induced angiogenesis are two of the cancer hallmarks (Hanahan and Weinberg, 2011), thus targeting both of them could boost the therapeutic outcome. Clinical trials have investigated the combination of olaparib with cediranib (Liu et al., 2013, 2014) in recurrent ovarian cancer patients, showing an increased PFS in patients with germline mutations in *BRCA1/2*, and most interestingly in homologous recombination proficient patients.

Our preclinical trials indicated that the combination was beneficial for the BRCAness models, inducing more durable and stable effects, persisting several weeks after treatment suspension, and increasing the number of complete responses and cured mice. Most importantly, the combination of olaparib with cediranib was favourable for those OC-PDX that were poorly responsive to olaparib single agent, especially the Not BRCAness subtypes, promoting a stabilization of disease in case of short-term treatment and a regression in maintenance regimens.

Several aspects of the therapeutic advantage of the combination were considered in the orthotopic OC-PDX models, that grow in the peritoneal cavity of immune-deficient mice, resembling the biological features of the patient's tumor.

In particular, the BRCAness MNHOC 8 model enabled us to analyse the importance of drug sequence in the combination of olaparib with cediranib. Survival was increased when

the combination was administered in a maintenance regimen. The gain in survival was accompanied by a substantial control in the ascites levels; however, dissemination increased, leading mice to live longer, but with the detriment of a more aggressive disease.

The escape from antiangiogenic treatments has been well documented in preclinical studies, including in our OC-PDX models treated with bevacizumab, which under certain circumstances increased survival but also tumor dissemination (Bizzaro et al., 2018; Decio et al., 2015).

The benefit of the combination of olaparib with cediranib was further supported when the PARP inhibitor was combined with other angiogenesis inhibitors. In our OC-PDX models, the administration of olaparib with bevacizumab or B20, two anti-VEGF antibodies, was ineffective or not different from the combination with cediranib. Despite the fact that these results did not completely clarify the role of cediranib added to olaparib, its effect appears not to be linked only to a “general antiangiogenic modulation” on the microenvironment through the inhibition of VEGFA pathway.

In this regard, further experiments on the VEGFC/VEGFR3 assay could be of interest, since it has been reported that tumor tissue overexpressing VEGFR3 are characterized by aggressiveness and ability to spread. VEGFC binds VEGFR3, and its expression has been associated with peritoneal and lymph node metastases, since it is the main promoter of lymphangiogenesis and has regulatory functions in tumor progression and dissemination. It has been reported that cediranib caused vascular regression and inhibition of VEGFR3 mediated lymphangiogenesis in ovarian cancer models (Decio et al., 2014). In this context, the effect of adding cediranib to olaparib on the VEGFC/VEGFR3 mediated lymphangiogenesis and dissemination could provide insight into the prolonged survival and the reduced ascites production with the combination treatment, to the detriment of an increased tumor dissemination through the organs of the peritoneal cavity.

In addition, the combination of olaparib with cediranib was the regimen with the best outcome also in the ID8 model, a syngeneic murine ovarian cancer, transplanted in the bursa of the ovary of mice. The combination of olaparib with cediranib did not increase survival in mice, but mostly delayed tumor progression and affected primary tumor growth at the ovary, both in the short-term and in maintenance regimen, inducing stable disease even after several weeks from treatment suspension.

Efforts to determine possible biomarkers of response and to carry out the molecular characterization of OC-PDX after 4 weeks of treatment were described in Chapter 5 and Chapter 6.

Preclinical *in vitro* tests have suggested that downregulation of homologous recombination repair genes, such as *BRCA1* and *RAD51*, occurs with hypoxia, with an enhancement of PARP inhibitor sensitivity in the hypoxic setting (Bindra et al., 2005; Chan et al., 2008; Scanlon and Glazer, 2015).

Lim and colleagues suggested that VEGFR3 inhibition results in downregulation of both *BRCA1* and *BRCA2* in cancer cells (Lim et al., 2014), and additional preclinical studies indicated that PARP inhibition could increase cytotoxicity in cancer cells under hypoxic compared with normoxic conditions (Lu et al., 2011).

Given these, our initial working hypothesis was that the angiogenesis inhibitor cediranib could cause hypoxia, which in turn induced a downregulation of genes involved in the DNA repair pathway and consequently lead to a “DNA damage repair system-deficient phenotype”, thus rendering more responsive to olaparib also DNA repair-proficient tumors. In this context, the cross-talk between an altered microenvironment and tumor cells no more able to repair DNA damage would have led to synthetic lethality and provided the rationale to the therapeutic advantage of the two drugs administered together.

Changes in tumor-associated vasculature (CD31 positive), hypoxia and DNA damage markers (such as γ H2AX foci formation) were evaluated in a limited number of OC-PDX after drug testing, as reported in Chapter 5.

Results indicated a general heterogeneity amongst the models, with different levels of hypoxia and different expression of γ H2AX, detected at baseline.

However, after 4 weeks of treatment, the addition of cediranib to olaparib reduced tumor-associated vasculature and modified hypoxia (microenvironment, cediranib most intended target) and enhanced DNA damage, with γ H2AX foci increased (tumor cells, olaparib most intended target). The double-side effect of the combination sustained the stabilization or regression of subcutaneous tumor growth, as long as the therapy was administered.

When analyses were performed at tumor progression under maintenance treatment in the intraperitoneal MNHOC 8 (after more than 20 weeks of treatment administration), vessel number, vessel area and hypoxia were reduced by the combination. Long-term exposure to angiogenesis inhibitors could result in tumor growth reduction, paralleled by a more malignant and invasive phenotype (Mountzios et al., 2014). In MNHOC 8 the maintenance treatment with the combination reduced ascites production to the detriment of an increased tumor dissemination through the organs of the peritoneal cavity.

Changes in gene expression were analysed after 4 weeks of treatment in three subcutaneously growing Not BRCAness models, in which the therapeutic advantage of the combination of olaparib with cediranib was more evident, as reported in Chapter 6. A panel of both murine and human genes was simultaneously investigated, giving us the opportunity to assess changes in the tumor microenvironment/stroma (murine compartment, cediranib most intended target) and in the tumor cells (human compartment, olaparib most intended target).

Results indicated that the combination of olaparib with cediranib caused changes in the tumor microenvironment, inducing a significant downregulation of angiogenesis-related genes across the three OC-PDX analysed.

However, when changes induced by the treatment on tumor cells were analysed, our initial hypothesis that cediranib, by inhibiting angiogenesis, would have led to a decreased expression of proteins involved in the DDR, rendering the tumor cells more sensitive to olaparib, was not confirmed. On the contrary and unexpectedly, the combination treatment induced a significant upregulation of DDR genes.

These preliminary results could be partially explained by the time-point selected to collect samples for analyses.

Since we looked at changes in gene expression after 4 weeks of continuous treatment, we were likely analysing the “survivor cells”. In these tumor cells, olaparib caused DNA damage, due to its “trapping” activity, inducing replication forks to stall, and that was supported by the significantly higher expression of γ H2AX foci detected after the administration of the combination. Thus, tumor cells that survived such damage were those able to solve the insult by increasing the expression of proteins involved in DNA damage repair, and the same occurs in cells that do not respond, explaining also the resistance to olaparib monotherapy.

Given these, it might be assumed that the effect on growth delay induced by the combination is due to the sum of the effects given by the two single drugs; cediranib and olaparib perturbed together host microenvironment, modulating angiogenesis, and furthermore, both influenced directly tumor cells as long as the treatment was administered.

In conclusion, the results obtained in this PhD thesis compel us to believe that the addition of cediranib to olaparib is advantageous both for BRCAness and Not BRCAness models. The therapeutic effect of the combination in delaying tumor growth, the induction of more durable and stable effects, even several weeks after treatment suspension, and the increased

number of complete responses, is particularly evident when the combination is administered in maintenance.

However, the attempt to investigate possible mechanisms of action underlying the therapeutic effect of the combination of olaparib with cediranib, by immunohistochemical and gene expression analyses, led us to preliminary results that need to be better clarified.

To this purpose, whole transcriptome (RNA sequencing) analysis has been performed, to overcome the bias of using only a small panel of selected genes, as we did with RealTime PCR.

RNA sequencing has been carried out in collaboration with AstraZeneca, on samples collected from subcutaneously and intraperitoneally growing OC-PDX (n=8 both BRCAness and Not BRCAness) after 4 weeks of treatment.

Data are currently under investigation, taking in consideration changes in both the human and murine compartment induced by treatments.

From this genome-wide analysis, more focused gene expression analyses will be performed, to take in consideration changes after a few doses (e.g. 2, 5 and 7 days from treatment initiation), when it would be conceivable to think that the treatment has not selected resistant cells. Looking at cells that are responding to treatment could help to better understand possible mechanisms of action underlying the observed advantage of the combination, both in BRCAness and Not BRCAness tumor.

In this respect performing *ad hoc* preclinical trials, increasing the number of tumors per treatment group (N=8-10) would strengthen the significance of the analyses performed in this PhD project and provide additional material for multiple end-points, both in terms of molecular, such as RNA sequencing, and immunohistochemical analysis.

In terms of immunohistochemical analysis, several other biomarkers of accumulating DNA damage could be investigated in addition to those reported, such as ROS (reactive

oxygen species) production, that is one of the pathway regulated by hypoxia, and also levels of CHECK, ATM, ATR and CASP3.

Vascular architecture is one aspect that could influence drug distribution and response.

In this context, other immunohistochemical analysis could be performed on OC-PDX tumor samples, to assess α -SMA expression, and also to consider EMT (epithelial to mesenchymal transition) status, evaluating E-cadherin and vimentin expression. This evaluation could help to better stratify OC-PDX accordingly to the response to cediranib, olaparib and the combination, and possibly to reveal some mechanism of action underlying to advantage of adding cediranib to olaparib both in BRCAness and Not BRCAness tumor.

Doses of olaparib and cediranib used to perform preclinical therapy testing reported in this PhD project were selected on the basis of those used in clinical trials and converted from human to animal administration. Indeed, in the phase II clinical trial (Liu et al., 2014), olaparib and cediranib were administered as capsule and tablets at the dose of 200 mg and 30 mg; mouse equivalent dose conversion based on FDA Draft Guidelines, led us to select 100 mg/kg and 3 mg/kg respectively. Furthermore, data from clinical trials supported daily oral dosing for both the drugs, that were thus administered with oral gavage in mice.

However, no studies to exclude plasma pharmacokinetic interactions between the two inhibitors and examine whether there is any influence of the combination on drug accumulation in the tumor were performed in OC-PDX.

The collection of a higher number of tumor samples and biological fluids (plasma, serum and ascites) per treatment group, at different time-points from treatment initiation (e.g. 2, 5, 7 and 28), would allow to evaluate steady-state concentrations of the two inhibitors, together with clearance and potential accumulation phenomena.

In this regard, it is known that tyrosine kinase inhibitors, such as cediranib, impair the ATP-ase functionality of the p-glycoprotein (ABCB1), expressed by tumor endothelial

cells, increasing intracellular drug accumulation of different compound that are ABCB1 substrates (doxorubicin, vincristine and paclitaxel).

Ad hoc Real-Time PCR assays or Western Blot analysis could be performed in order to assess level of ABCB1 expression across our OC-PDX.

The availability of AZD2281-BODIPY FL, a modified olaparib in which the cyclopropane group is replaced by the green fluorescent dye boron-dipyromethene (BODIPY) fluorophore (FL), with potential fluorescent imaging activity, would be useful to determine if the administration of cediranib will allow the accumulation of olaparib in the tumor cells of those OC-PDX in which ABCB1 is mostly expressed.

BIBLIOGRAPHY

- Aghajanian C, Blank SV, Goff BA, et al. (2012) OCEANS: a randomized, double-blind, placebo-controlled phase III trial of chemotherapy with or without bevacizumab in patients with platinum-sensitive recurrent epithelial ovarian, primary peritoneal, or fallopian tube cancer. *Journal of Clinical Oncology: Official Journal of the American Society of Clinical Oncology* 30(17): 2039–2045. DOI: 10.1200/JCO.2012.42.0505.
- Ahmed AA, Etemadmoghadam D, Temple J, et al. (2010) Driver mutations in TP53 are ubiquitous in high grade serous carcinoma of the ovary. *The Journal of Pathology* 221(1): 49–56. DOI: 10.1002/path.2696.
- Alsop K, Fereday S, Meldrum C, et al. (2012) BRCA mutation frequency and patterns of treatment response in BRCA mutation-positive women with ovarian cancer: a report from the Australian Ovarian Cancer Study Group. *Journal of Clinical Oncology: Official Journal of the American Society of Clinical Oncology* 30(21): 2654–2663. DOI: 10.1200/JCO.2011.39.8545.
- Antoniou A, Pharoah PDP, Narod S, et al. (2003) Average risks of breast and ovarian cancer associated with BRCA1 or BRCA2 mutations detected in case Series unselected for family history: a combined analysis of 22 studies. *American Journal of Human Genetics* 72(5): 1117–1130. DOI: 10.1086/375033.
- Armstrong DK (2004) Topotecan Dosing Guidelines in Ovarian Cancer: Reduction and Management of Hematologic Toxicity. *The Oncologist* 9(1): 33–42. DOI: 10.1634/theoncologist.9-1-33.
- Ashworth A, Lord CJ and Reis-Filho JS (2011) Genetic interactions in cancer progression and treatment. *Cell* 145(1): 30–38. DOI: 10.1016/j.cell.2011.03.020.
- Audeh MW, Carmichael J, Penson RT, et al. (2010) Oral poly(ADP-ribose) polymerase inhibitor olaparib in patients with BRCA1 or BRCA2 mutations and recurrent ovarian cancer: a proof-of-concept trial. *Lancet (London, England)* 376(9737): 245–251. DOI: 10.1016/S0140-6736(10)60893-8.
- Baldwin RL, Nemeth E, Tran H, et al. (2000) BRCA1 promoter region hypermethylation in ovarian carcinoma: a population-based study. *Cancer Research* 60(19): 5329–5333.
- Banerjee S and Kaye SB (2013) New strategies in the treatment of ovarian cancer: current clinical perspectives and future potential. *Clinical Cancer Research: An Official Journal of the American Association for Cancer Research* 19(5): 961–968. DOI: 10.1158/1078-0432.CCR-12-2243.
- Banerjee S, Kaye SB and Ashworth A (2010) Making the best of PARP inhibitors in ovarian cancer. *Nature Reviews. Clinical Oncology* 7(9): 508–519. DOI: 10.1038/nrclinonc.2010.116.
- Bast RC, Hennessey B and Mills GB (2009) The biology of ovarian cancer: new opportunities for translation. *Nature Reviews. Cancer* 9(6): 415–428. DOI: 10.1038/nrc2644.
- Batchelor TT, Mulholland P, Neyns B, et al. (2013) Phase III randomized trial comparing the efficacy of cediranib as monotherapy, and in combination with lomustine, versus lomustine alone in patients with recurrent glioblastoma. *Journal of Clinical Oncology: Official Journal of the American Society of Clinical Oncology* 31(26): 3212–3218. DOI: 10.1200/JCO.2012.47.2464.

- Ben-David U, Ha G, Tseng Y-Y, et al. (2017) Patient-derived xenografts undergo mouse-specific tumor evolution. *Nature Genetics* 49(11): 1567–1575. DOI: 10.1038/ng.3967.
- Bergers G and Benjamin LE (2003) Tumorigenesis and the angiogenic switch. *Nature Reviews. Cancer* 3(6): 401–410. DOI: 10.1038/nrc1093.
- Bergers G and Hanahan D (2008) Modes of resistance to anti-angiogenic therapy. *Nature Reviews. Cancer* 8(8): 592–603. DOI: 10.1038/nrc2442.
- Bindra RS, Gibson SL, Meng A, et al. (2005) Hypoxia-induced down-regulation of BRCA1 expression by E2Fs. *Cancer Research* 65(24): 11597–11604. DOI: 10.1158/0008-5472.CAN-05-2119.
- Bizzaro F, Falcetta F, D’Agostini E, et al. (2018) Tumor progression and metastatic dissemination in ovarian cancer after dose-dense or conventional paclitaxel and cisplatin plus bevacizumab. *International Journal of Cancer*. DOI: 10.1002/ijc.31596.
- Bolis G, Scarfone G, Raspagliesi F, et al. (2010) Paclitaxel/carboplatin versus topotecan/paclitaxel/carboplatin in patients with FIGO suboptimally resected stage III-IV epithelial ovarian cancer a multicenter, randomized study. *European Journal of Cancer (Oxford, England: 1990)* 46(16): 2905–2912. DOI: 10.1016/j.ejca.2010.06.124.
- Bookman MA, Brady MF, McGuire WP, et al. (2009) Evaluation of new platinum-based treatment regimens in advanced-stage ovarian cancer: a Phase III Trial of the Gynecologic Cancer Intergroup. *Journal of Clinical Oncology: Official Journal of the American Society of Clinical Oncology* 27(9): 1419–1425. DOI: 10.1200/JCO.2008.19.1684.
- Bowtell DDL (2010) The genesis and evolution of high-grade serous ovarian cancer. *Nature Reviews. Cancer* 10(11): 803–808. DOI: 10.1038/nrc2946.
- Brave SR, Ratcliffe K, Wilson Z, et al. (2011) Assessing the activity of cediranib, a VEGFR-2/3 tyrosine kinase inhibitor, against VEGFR-1 and members of the structurally related PDGFR family. *Molecular Cancer Therapeutics* 10(5): 861–873. DOI: 10.1158/1535-7163.MCT-10-0976.
- Bristow RG and Hill RP (2008) Hypoxia and metabolism. Hypoxia, DNA repair and genetic instability. *Nature Reviews. Cancer* 8(3): 180–192. DOI: 10.1038/nrc2344.
- Burger RA, Sill MW, Monk BJ, et al. (2007) Phase II trial of bevacizumab in persistent or recurrent epithelial ovarian cancer or primary peritoneal cancer: a Gynecologic Oncology Group Study. *Journal of Clinical Oncology: Official Journal of the American Society of Clinical Oncology* 25(33): 5165–5171. DOI: 10.1200/JCO.2007.11.5345.
- Burger RA, Brady MF, Bookman MA, et al. (2011) Incorporation of bevacizumab in the primary treatment of ovarian cancer. *The New England Journal of Medicine* 365(26): 2473–2483. DOI: 10.1056/NEJMoal104390.
- Cancer Genome Atlas Research Network (2011) Integrated genomic analyses of ovarian carcinoma. *Nature* 474(7353): 609–615. DOI: 10.1038/nature10166.
- Carmeliet P and Jain RK (2000) Angiogenesis in cancer and other diseases. *Nature* 407(6801): 249–257. DOI: 10.1038/35025220.
- Chan JK, Brady MF, Penson RT, et al. (2016) Weekly vs. Every-3-Week Paclitaxel and Carboplatin for Ovarian Cancer. *The New England Journal of Medicine* 374(8): 738–748. DOI: 10.1056/NEJMoal1505067.

- Chan N, Koritzinsky M, Zhao H, et al. (2008) Chronic hypoxia decreases synthesis of homologous recombination proteins to offset chemoresistance and radioresistance. *Cancer Research* 68(2): 605–614. DOI: 10.1158/0008-5472.CAN-07-5472.
- Chan N, Pires IM, Bencokova Z, et al. (2010) Contextual synthetic lethality of cancer cell kill based on the tumor microenvironment. *Cancer Research* 70(20): 8045–8054. DOI: 10.1158/0008-5472.CAN-10-2352.
- Chen F, Qi X, Qian M, et al. (2014) Tackling the tumor microenvironment: what challenge does it pose to anticancer therapies? *Protein & Cell* 5(11): 816–826. DOI: 10.1007/s13238-014-0097-1.
- Chen VW, Ruiz B, Killeen JL, et al. (2003) Pathology and classification of ovarian tumors. *Cancer* 97(10 Suppl): 2631–2642. DOI: 10.1002/cncr.11345.
- Cho Y, Gorina S, Jeffrey PD, et al. (1994) Crystal structure of a p53 tumor suppressor-DNA complex: understanding tumorigenic mutations. *Science (New York, N.Y.)* 265(5170): 346–355.
- Chura JC, Van Iseghem K, Downs LS, et al. (2007) Bevacizumab plus cyclophosphamide in heavily pretreated patients with recurrent ovarian cancer. *Gynecologic Oncology* 107(2): 326–330. DOI: 10.1016/j.ygyno.2007.07.017.
- Coleman RL, Oza AM, Lorusso D, et al. (2017) Rucaparib maintenance treatment for recurrent ovarian carcinoma after response to platinum therapy (ARIEL3): a randomised, double-blind, placebo-controlled, phase 3 trial. *Lancet (London, England)* 390(10106): 1949–1961. DOI: 10.1016/S0140-6736(17)32440-6.
- Colombo N (2011) Efficacy of trabectedin in platinum-sensitive-relapsed ovarian cancer: new data from the randomized OVA-301 study. *International Journal of Gynecological Cancer: Official Journal of the International Gynecological Cancer Society* 21 Suppl 1: S12-16. DOI: 10.1097/IGC.0b013e318217b321.
- Colvin EK (2014) Tumor-associated macrophages contribute to tumor progression in ovarian cancer. *Frontiers in Oncology* 4: 137. DOI: 10.3389/fonc.2014.00137.
- Coxon A, Bready J, Min H, et al. (2010) Context-dependent role of angiopoietin-1 inhibition in the suppression of angiogenesis and tumor growth: implications for AMG 386, an angiopoietin-1/2-neutralizing peptibody. *Molecular Cancer Therapeutics* 9(10): 2641–2651. DOI: 10.1158/1535-7163.MCT-10-0213.
- Cragun JM (2011) Screening for ovarian cancer. *Cancer Control: Journal of the Moffitt Cancer Center* 18(1): 16–21. DOI: 10.1177/107327481101800103.
- Cramer DW, Hutchison GB, Welch WR, et al. (1983) Determinants of ovarian cancer risk. I. Reproductive experiences and family history. *Journal of the National Cancer Institute* 71(4): 711–716.
- Dawicki-McKenna JM, Langelier M-F, DeNizio JE, et al. (2015) PARP-1 Activation Requires Local Unfolding of an Autoinhibitory Domain. *Molecular Cell* 60(5): 755–768. DOI: 10.1016/j.molcel.2015.10.013.
- De Soto JA, Wang X, Tominaga Y, et al. (2006) The inhibition and treatment of breast cancer with poly (ADP-ribose) polymerase (PARP-1) inhibitors. *International Journal of Biological Sciences* 2(4): 179–185.

- De Vos M, Schreiber V and Dantzer F (2012) The diverse roles and clinical relevance of PARPs in DNA damage repair: current state of the art. *Biochemical Pharmacology* 84(2): 137–146. DOI: 10.1016/j.bcp.2012.03.018.
- Decio A, Taraboletti G, Patton V, et al. (2014) Vascular endothelial growth factor c promotes ovarian carcinoma progression through paracrine and autocrine mechanisms. *The American Journal of Pathology* 184(4): 1050–1061. DOI: 10.1016/j.ajpath.2013.12.030.
- Decio A, Cesca M, Bizzaro F, et al. (2015) Cediranib combined with chemotherapy reduces tumor dissemination and prolongs the survival of mice bearing patient-derived ovarian cancer xenografts with different responsiveness to cisplatin. *Clinical & Experimental Metastasis* 32(7): 647–658. DOI: 10.1007/s10585-015-9734-1.
- Domcke S, Sinha R, Levine DA, et al. (2013) Evaluating cell lines as tumour models by comparison of genomic profiles. *Nature Communications* 4: 2126. DOI: 10.1038/ncomms3126.
- Dowlati A, Gray R, Sandler AB, et al. (2008) Cell adhesion molecules, vascular endothelial growth factor, and basic fibroblast growth factor in patients with non-small cell lung cancer treated with chemotherapy with or without bevacizumab--an Eastern Cooperative Oncology Group Study. *Clinical Cancer Research: An Official Journal of the American Association for Cancer Research* 14(5): 1407–1412. DOI: 10.1158/1078-0432.CCR-07-1154.
- du Bois A, Herrstedt J, Hardy-Bessard A-C, et al. (2010) Phase III trial of carboplatin plus paclitaxel with or without gemcitabine in first-line treatment of epithelial ovarian cancer. *Journal of Clinical Oncology: Official Journal of the American Society of Clinical Oncology* 28(27): 4162–4169. DOI: 10.1200/JCO.2009.27.4696.
- du Bois A, Floquet A, Kim J-W, et al. (2014) Incorporation of pazopanib in maintenance therapy of ovarian cancer. *Journal of Clinical Oncology: Official Journal of the American Society of Clinical Oncology* 32(30): 3374–3382. DOI: 10.1200/JCO.2014.55.7348.
- du Bois A, Kristensen G, Ray-Coquard I, et al. (2016) Standard first-line chemotherapy with or without nintedanib for advanced ovarian cancer (AGO-OVAR 12): a randomised, double-blind, placebo-controlled phase 3 trial. *The Lancet. Oncology* 17(1): 78–89. DOI: 10.1016/S1470-2045(15)00366-6.
- Dvorak HF, Brown LF, Detmar M, et al. (1995) Vascular permeability factor/vascular endothelial growth factor, microvascular hyperpermeability, and angiogenesis. *The American Journal of Pathology* 146(5): 1029–1039.
- Edmondson RJ and Monaghan JM (2001) The epidemiology of ovarian cancer. *International Journal of Gynecological Cancer: Official Journal of the International Gynecological Cancer Society* 11(6): 423–429.
- Ellis LM and Hicklin DJ (2008) Pathways mediating resistance to vascular endothelial growth factor-targeted therapy. *Clinical Cancer Research: An Official Journal of the American Association for Cancer Research* 14(20): 6371–6375. DOI: 10.1158/1078-0432.CCR-07-5287.
- Esteller M, Silva JM, Dominguez G, et al. (2000) Promoter hypermethylation and BRCA1 inactivation in sporadic breast and ovarian tumors. *Journal of the National Cancer Institute* 92(7): 564–569.
- Evers B, Drost R, Schut E, et al. (2008) Selective inhibition of BRCA2-deficient mammary tumor cell growth by AZD2281 and cisplatin. *Clinical Cancer Research: An Official Journal of the American Association for Cancer Research* 14(12): 3916–3925. DOI: 10.1158/1078-0432.CCR-07-4953.

- Farmer H, McCabe N, Lord CJ, et al. (2005) Targeting the DNA repair defect in BRCA mutant cells as a therapeutic strategy. *Nature* 434(7035): 917–921. DOI: 10.1038/nature03445.
- Fathalla MF (1971) Incessant ovulation--a factor in ovarian neoplasia? *Lancet (London, England)* 2(7716): 163.
- Fiebig HH, Schuchhardt C, Henss H, et al. (1984) Comparison of tumor response in nude mice and in the patients. *Behring Institute Mitteilungen* (74): 343–352.
- Fiedler W, Mesters R, Heuser M, et al. (2010) An open-label, Phase I study of cediranib (RECENTIN) in patients with acute myeloid leukemia. *Leukemia Research* 34(2): 196–202. DOI: 10.1016/j.leukres.2009.07.020.
- Folkman J (1971) Tumor angiogenesis: therapeutic implications. *The New England Journal of Medicine* 285(21): 1182–1186. DOI: 10.1056/NEJM197111182852108.
- Fong PC, Boss DS, Yap TA, et al. (2009) Inhibition of poly(ADP-ribose) polymerase in tumors from BRCA mutation carriers. *The New England Journal of Medicine* 361(2): 123–134. DOI: 10.1056/NEJMoa0900212.
- Fong PC, Yap TA, Boss DS, et al. (2010) Poly(ADP)-ribose polymerase inhibition: frequent durable responses in BRCA carrier ovarian cancer correlating with platinum-free interval. *Journal of Clinical Oncology: Official Journal of the American Society of Clinical Oncology* 28(15): 2512–2519. DOI: 10.1200/JCO.2009.26.9589.
- Forsythe JA, Jiang BH, Iyer NV, et al. (1996) Activation of vascular endothelial growth factor gene transcription by hypoxia-inducible factor 1. *Molecular and Cellular Biology* 16(9): 4604–4613.
- Fournier L, Ammari S, Thiam R, et al. (2014) Imaging criteria for assessing tumour response: RECIST, mRECIST, Cheson. *Diagnostic and Interventional Imaging* 95(7). *Interventional radiology in oncology*: 689–703. DOI: 10.1016/j.diii.2014.05.002.
- Friedberg EC, Walker GC, Wolfram S, et al. (2006) *DNA Repair and Mutagenesis*. Second Ed.
- Gama Sosa MA, De Gasperi R and Elder GA (2010) Animal transgenesis: an overview. *Brain Structure & Function* 214(2–3): 91–109. DOI: 10.1007/s00429-009-0230-8.
- Garofalo A, Naumova E, Manenti L, et al. (2003) The combination of the tyrosine kinase receptor inhibitor SU6668 with paclitaxel affects ascites formation and tumor spread in ovarian carcinoma xenografts growing orthotopically. *Clinical Cancer Research: An Official Journal of the American Association for Cancer Research* 9(9): 3476–3485.
- George A, Kaye S and Banerjee S (2017) Delivering widespread BRCA testing and PARP inhibition to patients with ovarian cancer. *Nature Reviews. Clinical Oncology* 14(5): 284–296. DOI: 10.1038/nrclinonc.2016.191.
- Gerber H-P and Ferrara N (2005) Pharmacology and pharmacodynamics of bevacizumab as monotherapy or in combination with cytotoxic therapy in preclinical studies. *Cancer Research* 65(3): 671–680.
- Ghosh S, Sullivan CAW, Zerkowski MP, et al. (2008) High levels of vascular endothelial growth factor and its receptors (VEGFR-1, VEGFR-2, neuropilin-1) are associated with worse outcome in breast cancer. *Human Pathology* 39(12): 1835–1843. DOI: 10.1016/j.humpath.2008.06.004.

- Giavazzi R, Sennino B, Coltrini D, et al. (2003) Distinct role of fibroblast growth factor-2 and vascular endothelial growth factor on tumor growth and angiogenesis. *The American Journal of Pathology* 162(6): 1913–1926. DOI: 10.1016/S0002-9440(10)64325-8.
- Gilks CB and Prat J (2009) Ovarian carcinoma pathology and genetics: recent advances. *Human Pathology* 40(9): 1213–1223. DOI: 10.1016/j.humpath.2009.04.017.
- Glazer PM, Hegan DC, Lu Y, et al. (2013) Hypoxia and DNA repair. *The Yale Journal of Biology and Medicine* 86(4): 443–451.
- Goss GD, Arnold A, Shepherd FA, et al. (2010) Randomized, double-blind trial of carboplatin and paclitaxel with either daily oral cediranib or placebo in advanced non-small-cell lung cancer: NCIC clinical trials group BR24 study. *Journal of Clinical Oncology: Official Journal of the American Society of Clinical Oncology* 28(1): 49–55. DOI: 10.1200/JCO.2009.22.9427.
- Green AE and Rose PG (2006) Pegylated liposomal doxorubicin in ovarian cancer. *International Journal of Nanomedicine* 1(3): 229–239.
- Greenaway J, Moorehead R, Shaw P, et al. (2008) Epithelial-stromal interaction increases cell proliferation, survival and tumorigenicity in a mouse model of human epithelial ovarian cancer. *Gynecologic Oncology* 108(2): 385–394. DOI: 10.1016/j.ygyno.2007.10.035.
- Grunewald T and Ledermann JA (2017) Targeted Therapies for Ovarian Cancer. *Best Practice & Research Clinical Obstetrics & Gynaecology* 41. Epithelial Ovarian Cancer: 139–152. DOI: 10.1016/j.bpobgyn.2016.12.001.
- Hall JM, Lee MK, Newman B, et al. (1990) Linkage of early-onset familial breast cancer to chromosome 17q21. *Science (New York, N.Y.)* 250(4988): 1684–1689.
- Hanahan D and Folkman J (1996) Patterns and emerging mechanisms of the angiogenic switch during tumorigenesis. *Cell* 86(3): 353–364.
- Hanahan D and Weinberg RA (2011) Hallmarks of cancer: the next generation. *Cell* 144(5): 646–674. DOI: 10.1016/j.cell.2011.02.013.
- Hansen JM, Coleman RL and Sood AK (2016) Targeting the tumour microenvironment in ovarian cancer. *European Journal of Cancer* 56: 131–143. DOI: 10.1016/j.ejca.2015.12.016.
- Heckman CA, Holopainen T, Wirzenius M, et al. (2008) The tyrosine kinase inhibitor cediranib blocks ligand-induced vascular endothelial growth factor receptor-3 activity and lymphangiogenesis. *Cancer Research* 68(12): 4754–4762. DOI: 10.1158/0008-5472.CAN-07-5809.
- Hennessy BTJ, Timms KM, Carey MS, et al. (2010) Somatic mutations in BRCA1 and BRCA2 could expand the number of patients that benefit from poly (ADP ribose) polymerase inhibitors in ovarian cancer. *Journal of Clinical Oncology: Official Journal of the American Society of Clinical Oncology* 28(22): 3570–3576. DOI: 10.1200/JCO.2009.27.2997.
- Herbst RS, Hong D, Chap L, et al. (2009) Safety, pharmacokinetics, and antitumor activity of AMG 386, a selective angiopoietin inhibitor, in adult patients with advanced solid tumors. *Journal of Clinical Oncology: Official Journal of the American Society of Clinical Oncology* 27(21): 3557–3565. DOI: 10.1200/JCO.2008.19.6683.
- Hirte H, Lheureux S, Fleming GF, et al. (2015) A phase 2 study of cediranib in recurrent or persistent ovarian, peritoneal or fallopian tube cancer: a trial of the Princess Margaret,

- Chicago and California Phase II Consortia. *Gynecologic Oncology* 138(1): 55–61. DOI: 10.1016/j.ygyno.2015.04.009.
- Hollingsworth HC, Kohn EC, Steinberg SM, et al. (1995) Tumor angiogenesis in advanced stage ovarian carcinoma. *The American Journal of Pathology* 147(1): 33–41.
- Hosaka K, Yang Y, Seki T, et al. (2013) Tumour PDGF-BB expression levels determine dual effects of anti-PDGF drugs on vascular remodelling and metastasis. *Nature Communications* 4: 2129. DOI: 10.1038/ncomms3129.
- Hoskins P, Vergote I, Cervantes A, et al. (2010) Advanced ovarian cancer: phase III randomized study of sequential cisplatin-topotecan and carboplatin-paclitaxel vs carboplatin-paclitaxel. *Journal of the National Cancer Institute* 102(20): 1547–1556. DOI: 10.1093/jnci/djq362.
- Hu L, Hofmann J, Zaloudek C, et al. (2002) Vascular endothelial growth factor immunoneutralization plus Paclitaxel markedly reduces tumor burden and ascites in athymic mouse model of ovarian cancer. *The American Journal of Pathology* 161(5): 1917–1924. DOI: 10.1016/S0002-9440(10)64467-7.
- Indraccolo S, Tisato V, Agata S, et al. (2006) Establishment and characterization of xenografts and cancer cell cultures derived from BRCA1 -/- epithelial ovarian cancers. *European Journal of Cancer (Oxford, England: 1990)* 42(10): 1475–1483. DOI: 10.1016/j.ejca.2006.01.057.
- Jain RK (2005) Normalization of tumor vasculature: an emerging concept in antiangiogenic therapy. *Science (New York, N.Y.)* 307(5706): 58–62. DOI: 10.1126/science.1104819.
- Jaisser F (2000) Inducible gene expression and gene modification in transgenic mice. *Journal of the American Society of Nephrology: JASN* 11 Suppl 16: S95–S100.
- Jemal A, Siegel R, Ward E, et al. (2009) Cancer statistics, 2009. *CA: a cancer journal for clinicians* 59(4): 225–249. DOI: 10.3322/caac.20006.
- Jones S, Wang T-L, Shih I-M, et al. (2010) Frequent mutations of chromatin remodeling gene ARID1A in ovarian clear cell carcinoma. *Science (New York, N.Y.)* 330(6001): 228–231. DOI: 10.1126/science.1196333.
- Karlan BY, Oza AM, Richardson GE, et al. (2012) Randomized, double-blind, placebo-controlled phase II study of AMG 386 combined with weekly paclitaxel in patients with recurrent ovarian cancer. *Journal of Clinical Oncology: Official Journal of the American Society of Clinical Oncology* 30(4): 362–371. DOI: 10.1200/JCO.2010.34.3178.
- Karst AM and Drapkin R (2010) Ovarian cancer pathogenesis: a model in evolution. *Journal of Oncology* 2010: 932371. DOI: 10.1155/2010/932371.
- Kassis JN, Cohen JG, Rasool N, et al. (2007) *Models of Angiogenesis*. Major Reference Works. Malcolm R. Alison.
- Kathleen N. Moore, Paul DiSilvestro, Elizabeth S.Lowe, et al. (2014) SOLO1 and SOLO2: Randomized phase III trials of olaparib in patients (pts) with ovarian cancer and a BRCA1/2 mutation (BRCAm). *Journal of Clinical Oncology* 32(15_suppl): TPS5616-TPS5616. DOI: 10.1200/jco.2014.32.15_suppl.tps5616.
- Katsumata N, Yasuda M, Takahashi F, et al. (2009) Dose-dense paclitaxel once a week in combination with carboplatin every 3 weeks for advanced ovarian cancer: a phase 3, open-label, randomised controlled trial. *Lancet (London, England)* 374(9698): 1331–1338. DOI: 10.1016/S0140-6736(09)61157-0.

- Kaufman B, Shapira-Frommer R, Schmutzler RK, et al. (2015) Olaparib monotherapy in patients with advanced cancer and a germline BRCA1/2 mutation. *Journal of Clinical Oncology: Official Journal of the American Society of Clinical Oncology* 33(3): 244–250. DOI: 10.1200/JCO.2014.56.2728.
- Kim KJ, Li B, Houck K, et al. (1992) The vascular endothelial growth factor proteins: identification of biologically relevant regions by neutralizing monoclonal antibodies. *Growth Factors (Chur, Switzerland)* 7(1): 53–64. DOI: 10.3109/08977199209023937.
- Kindelberger DW, Lee Y, Miron A, et al. (2007) Intraepithelial carcinoma of the fimbria and pelvic serous carcinoma: Evidence for a causal relationship. *The American Journal of Surgical Pathology* 31(2): 161–169. DOI: 10.1097/01.pas.0000213335.40358.47.
- Knudson AG (1971) Mutation and Cancer: Statistical Study of Retinoblastoma. *Proceedings of the National Academy of Sciences* 68(4): 820–823.
- Komiyama S, Aoki D, Tominaga E, et al. (1999) Prognosis of Japanese patients with ovarian clear cell carcinoma associated with pelvic endometriosis: clinicopathologic evaluation. *Gynecologic Oncology* 72(3): 342–346.
- Konstantinopoulos PA, Spentzos D, Karlan BY, et al. (2010) Gene expression profile of BRCAness that correlates with responsiveness to chemotherapy and with outcome in patients with epithelial ovarian cancer. *Journal of Clinical Oncology: Official Journal of the American Society of Clinical Oncology* 28(22): 3555–3561. DOI: 10.1200/JCO.2009.27.5719.
- Korkmaz T, Seber S and Basaran G (2016) Review of the current role of targeted therapies as maintenance therapies in first and second line treatment of epithelial ovarian cancer; In the light of completed trials. *Critical Reviews in Oncology/Hematology* 98: 180–188. DOI: 10.1016/j.critrevonc.2015.10.006.
- Kortmann U, McAlpine JN, Xue H, et al. (2011) Tumor growth inhibition by olaparib in BRCA2 germline-mutated patient-derived ovarian cancer tissue xenografts. *Clinical Cancer Research: An Official Journal of the American Association for Cancer Research* 17(4): 783–791. DOI: 10.1158/1078-0432.CCR-10-1382.
- Krishnakumar R and Kraus WL (2010) The PARP side of the nucleus: molecular actions, physiological outcomes, and clinical targets. *Molecular Cell* 39(1): 8–24. DOI: 10.1016/j.molcel.2010.06.017.
- Kummar S, Allen D, Monks A, et al. (2013) Cediranib for metastatic alveolar soft part sarcoma. *Journal of Clinical Oncology: Official Journal of the American Society of Clinical Oncology* 31(18): 2296–2302. DOI: 10.1200/JCO.2012.47.4288.
- Kurman RJ and Shih I-M (2010) The origin and pathogenesis of epithelial ovarian cancer: a proposed unifying theory. *The American Journal of Surgical Pathology* 34(3): 433–443. DOI: 10.1097/PAS.0b013e3181cf3d79.
- Kurman RJ and Shih I-M (2011) Molecular pathogenesis and extraovarian origin of epithelial ovarian cancer--shifting the paradigm. *Human Pathology* 42(7): 918–931. DOI: 10.1016/j.humpath.2011.03.003.
- Lai Z, Markovets A, Ahdesmaki M, et al. (2016) VarDict: a novel and versatile variant caller for next-generation sequencing in cancer research. *Nucleic Acids Research* 44(11): e108. DOI: 10.1093/nar/gkw227.

- Ledermann J, Harter P, Gourley C, et al. (2012) Olaparib maintenance therapy in platinum-sensitive relapsed ovarian cancer. *The New England Journal of Medicine* 366(15): 1382–1392. DOI: 10.1056/NEJMoa1105535.
- Ledermann JA, Embleton AC, Raja F, et al. (2016) Cediranib in patients with relapsed platinum-sensitive ovarian cancer (ICON6): a randomised, double-blind, placebo-controlled phase 3 trial. *Lancet (London, England)* 387(10023): 1066–1074. DOI: 10.1016/S0140-6736(15)01167-8.
- Leitao MM, Boyd J, Hummer A, et al. (2004) Clinicopathologic analysis of early-stage sporadic ovarian carcinoma. *The American Journal of Surgical Pathology* 28(2): 147–159.
- Lengyel E, Burdette JE, Kenny HA, et al. (2014) Epithelial ovarian cancer experimental models. *Oncogene* 33(28): 3619–3633. DOI: 10.1038/onc.2013.321.
- Leung DW, Cachianes G, Kuang WJ, et al. (1989) Vascular endothelial growth factor is a secreted angiogenic mitogen. *Science* Vol. 246, Issue 4935, pp. 1306-1309 DOI: 10.1126/science.2479986
- Liang W-C, Wu X, Peale FV, et al. (2006) Cross-species vascular endothelial growth factor (VEGF)-blocking antibodies completely inhibit the growth of human tumor xenografts and measure the contribution of stromal VEGF. *The Journal of Biological Chemistry* 281(2): 951–961. DOI: 10.1074/jbc.M508199200.
- Liao D and Johnson RS (2007) Hypoxia: a key regulator of angiogenesis in cancer. *Cancer Metastasis Reviews* 26(2): 281–290. DOI: 10.1007/s10555-007-9066-y.
- Lim HJ and Ledger W (2016) Targeted Therapy in Ovarian Cancer. *Women's Health* 12(3): 363–378. DOI: 10.2217/whe.16.4.
- Lim JJ, Yang K, Taylor-Harding B, et al. (2014) VEGFR3 inhibition chemosensitizes ovarian cancer stemlike cells through down-regulation of BRCA1 and BRCA2. *Neoplasia (New York, N.Y.)* 16(4): 343-353–2. DOI: 10.1016/j.neo.2014.04.003.
- Liu JF, Tolaney SM, Birrer M, et al. (2013) A Phase 1 trial of the poly(ADP-ribose) polymerase inhibitor olaparib (AZD2281) in combination with the anti-angiogenic cediranib (AZD2171) in recurrent epithelial ovarian or triple-negative breast cancer. *European Journal of Cancer (Oxford, England: 1990)* 49(14): 2972–2978. DOI: 10.1016/j.ejca.2013.05.020.
- Liu JF, Barry WT, Birrer M, et al. (2014) Combination cediranib and olaparib versus olaparib alone for women with recurrent platinum-sensitive ovarian cancer: a randomised phase 2 study. *The Lancet. Oncology* 15(11): 1207–1214. DOI: 10.1016/S1470-2045(14)70391-2.
- Lobo MR, Kukino A, Tran H, et al. (2015) Synergistic Antivascular and Antitumor Efficacy with Combined Cediranib and SC6889 in Intracranial Mouse Glioma. *PloS One* 10(12): e0144488. DOI: 10.1371/journal.pone.0144488.
- Lord CJ and Ashworth A (2017) PARP inhibitors: Synthetic lethality in the clinic. *Science (New York, N.Y.)* 355(6330): 1152–1158. DOI: 10.1126/science.aam7344.
- Lu Y, Chu A, Turker MS, et al. (2011) Hypoxia-induced epigenetic regulation and silencing of the BRCA1 promoter. *Molecular and Cellular Biology* 31(16): 3339–3350. DOI: 10.1128/MCB.01121-10.
- Mabuchi S, Terai Y, Morishige K, et al. (2008) Maintenance treatment with bevacizumab prolongs survival in an in vivo ovarian cancer model. *Clinical Cancer Research: An Official Journal*

- of the American Association for Cancer Research* 14(23): 7781–7789. DOI: 10.1158/1078-0432.CCR-08-0243.
- Martinek IE and Kehoe S (2010) When Should Surgical Cytoreduction in Advanced Ovarian Cancer Take Place? Available at: <https://www.hindawi.com/journals/jo/2010/852028/> (accessed 5 July 2018).
- Masazza G, Lucchini V, Tomasoni A, et al. (1991) Malignant behavior and resistance to cisplatin of human ovarian carcinoma xenografts established from the same patient at different stages of the disease. *Cancer Research* 51(23 Pt 1): 6358–6362.
- Massazza G, Tomasoni A, Lucchini V, et al. (1989) Intraperitoneal and subcutaneous xenografts of human ovarian carcinoma in nude mice and their potential in experimental therapy. *International Journal of Cancer* 44(3): 494–500.
- Matulonis UA, Berlin S, Ivy P, et al. (2009) Cediranib, an oral inhibitor of vascular endothelial growth factor receptor kinases, is an active drug in recurrent epithelial ovarian, fallopian tube, and peritoneal cancer. *Journal of Clinical Oncology: Official Journal of the American Society of Clinical Oncology* 27(33): 5601–5606. DOI: 10.1200/JCO.2009.23.2777.
- McLean K and Mehta G (2017) Tumor Microenvironment and Models of Ovarian Cancer: The 11th Biennial Rivkin Center Ovarian Cancer Research Symposium. *International Journal of Gynecological Cancer* 27(9S): S2. DOI: 10.1097/IGC.0000000000001119.
- McNeish IA, Oza AM, Coleman RL, et al. (2015) Results of ARIEL2: A Phase 2 trial to prospectively identify ovarian cancer patients likely to respond to rucaparib using tumor genetic analysis. *Journal of Clinical Oncology* 33(15_suppl): 5508–5508. DOI: 10.1200/jco.2015.33.15_suppl.5508.
- Medeiros F, Muto MG, Lee Y, et al. (2006) The tubal fimbria is a preferred site for early adenocarcinoma in women with familial ovarian cancer syndrome. *The American Journal of Surgical Pathology* 30(2): 230–236.
- Melsens E, Verberckmoes B, Rosseel N, et al. (2017) The VEGFR Inhibitor Cediranib Improves the Efficacy of Fractionated Radiotherapy in a Colorectal Cancer Xenograft Model. *European Surgical Research. Europäische Chirurgische Forschung. Recherches Chirurgicales Europeennes* 58(3–4): 95–108. DOI: 10.1159/000452741.
- Miki Y, Swensen J, Shattuck-Eidens D, et al. (1994) A strong candidate for the breast and ovarian cancer susceptibility gene BRCA1. *Science (New York, N.Y.)* 266(5182): 66–71.
- Miller KD, Sweeney CJ and Sledge GW (2001) Redefining the target: chemotherapeutics as antiangiogenics. *Journal of Clinical Oncology: Official Journal of the American Society of Clinical Oncology* 19(4): 1195–1206. DOI: 10.1200/JCO.2001.19.4.1195.
- Mitamura T, Gourley C and Sood AK (2016) Prediction of anti-angiogenesis escape. *Gynecologic Oncology* 141(1): 80–85. DOI: 10.1016/j.ygyno.2015.12.033.
- Monk BJ, Poveda A, Vergote I, et al. (2016) Final results of a phase 3 study of trebananib plus weekly paclitaxel in recurrent ovarian cancer (TRINOVA-1): Long-term survival, impact of ascites, and progression-free survival-2. *Gynecologic Oncology* 143(1): 27–34. DOI: 10.1016/j.ygyno.2016.07.112.
- Mountzios G, Pentheroudakis G and Carmeliet P (2014) Bevacizumab and micrometastases: revisiting the preclinical and clinical rollercoaster. *Pharmacology & Therapeutics* 141(2): 117–124. DOI: 10.1016/j.pharmthera.2013.09.003.

- Mulders P, Hawkins R, Nathan P, et al. (2012) Cediranib monotherapy in patients with advanced renal cell carcinoma: results of a randomised phase II study. *European Journal of Cancer (Oxford, England: 1990)* 48(4): 527–537. DOI: 10.1016/j.ejca.2011.12.022.
- Murai J, Huang S-YN, Renaud A, et al. (2014) Stereospecific PARP trapping by BMN 673 and comparison with olaparib and rucaparib. *Molecular Cancer Therapeutics* 13(2): 433–443. DOI: 10.1158/1535-7163.MCT-13-0803.
- Nagy JA, Dvorak AM and Dvorak HF (2012) Vascular hyperpermeability, angiogenesis, and stroma generation. *Cold Spring Harbor Perspectives in Medicine* 2(2): a006544. DOI: 10.1101/cshperspect.a006544.
- Nguewa PA, Fuertes MA, Cepeda V, et al. (2006) Poly(ADP-ribose) polymerase-1 inhibitor 3-aminobenzamide enhances apoptosis induction by platinum complexes in cisplatin-resistant tumor cells. *Medicinal Chemistry (Sharjah (United Arab Emirates))* 2(1): 47–53.
- Nimeiri HS, Oza AM, Morgan RJ, et al. (2008) Efficacy and safety of bevacizumab plus erlotinib for patients with recurrent ovarian, primary peritoneal, and fallopian tube cancer: a trial of the Chicago, PMH, and California Phase II Consortia. *Gynecologic Oncology* 110(1): 49–55. DOI: 10.1016/j.ygyno.2008.02.009.
- O'Donovan PJ and Livingston DM (2010) BRCA1 and BRCA2: breast/ovarian cancer susceptibility gene products and participants in DNA double-strand break repair. *Carcinogenesis* 31(6): 961–967. DOI: 10.1093/carcin/bgq069.
- Oliva P, Decio A, Castiglioni V, et al. (2012) Cisplatin plus paclitaxel and maintenance of bevacizumab on tumour progression, dissemination, and survival of ovarian carcinoma xenograft models. *British Journal of Cancer* 107(2): 360–369. DOI: 10.1038/bjc.2012.261.
- O'Malley DM, Richardson DL, Rheaume PS, et al. (2011) Addition of bevacizumab to weekly paclitaxel significantly improves progression-free survival in heavily pretreated recurrent epithelial ovarian cancer. *Gynecologic Oncology* 121(2): 269–272. DOI: 10.1016/j.ygyno.2011.01.009.
- Omura G, Blessing JA, Ehrlich CE, et al. (1986) A randomized trial of cyclophosphamide and doxorubicin with or without cisplatin in advanced ovarian carcinoma. A Gynecologic Oncology Group Study. *Cancer* 57(9): 1725–1730.
- Ozols RF (2003) Progress in ovarian cancer: an overview and perspective. *European Journal of Cancer Supplements* 1(2). New Approaches in Cancer Treatments: 43–55. DOI: 10.1016/S1359-6349(03)00008-9.
- Padera TP, Kuo AH, Hoshida T, et al. (2008) Differential response of primary tumor versus lymphatic metastasis to VEGFR-2 and VEGFR-3 kinase inhibitors cediranib and vandetanib. *Molecular Cancer Therapeutics* 7(8): 2272–2279. DOI: 10.1158/1535-7163.MCT-08-0182.
- Partridge E, Kreimer AR, Greenlee RT, et al. (2009) Results from four rounds of ovarian cancer screening in a randomized trial. *Obstetrics and Gynecology* 113(4): 775–782. DOI: 10.1097/AOG.0b013e31819cda77.
- Pennington KP, Walsh T, Harrell MI, et al. (2014) Germline and somatic mutations in homologous recombination genes predict platinum response and survival in ovarian, fallopian tube, and peritoneal carcinomas. *Clinical Cancer Research: An Official Journal of the American Association for Cancer Research* 20(3): 764–775. DOI: 10.1158/1078-0432.CCR-13-2287.

- Perren TJ, Swart AM, Pfisterer J, et al. (2011) A phase 3 trial of bevacizumab in ovarian cancer. *The New England Journal of Medicine* 365(26): 2484–2496. DOI: 10.1056/NEJMoa1103799.
- Piek JM, van Diest PJ, Zweemer RP, et al. (2001) Dysplastic changes in prophylactically removed Fallopian tubes of women predisposed to developing ovarian cancer. *The Journal of Pathology* 195(4): 451–456. DOI: 10.1002/path.1000.
- Piek JMJ, Verheijen RHM, Kenemans P, et al. (2003) BRCA1/2-related ovarian cancers are of tubal origin: a hypothesis. *Gynecologic Oncology* 90(2): 491.
- Pignata S, Scambia G, Katsaros D, et al. (2014) Carboplatin plus paclitaxel once a week versus every 3 weeks in patients with advanced ovarian cancer (MITO-7): a randomised, multicentre, open-label, phase 3 trial. *The Lancet. Oncology* 15(4): 396–405. DOI: 10.1016/S1470-2045(14)70049-X.
- Pires IM, Bencokova Z, Milani M, et al. (2010) Effects of acute versus chronic hypoxia on DNA damage responses and genomic instability. *Cancer Research* 70(3): 925–935. DOI: 10.1158/0008-5472.CAN-09-2715.
- Pogge von Strandmann E, Reinartz S, Wager U, et al. (2017) Tumor–Host Cell Interactions in Ovarian Cancer: Pathways to Therapy Failure. *Trends in Cancer* 3(2): 137–148. DOI: 10.1016/j.trecan.2016.12.005.
- Poveda A (2005) Gemcitabine in patients with ovarian cancer. *Cancer Treatment Reviews* 31 Suppl 4: S29–37.
- Prat J (2012) Ovarian carcinomas: five distinct diseases with different origins, genetic alterations, and clinicopathological features. *Virchows Archiv: An International Journal of Pathology* 460(3): 237–249. DOI: 10.1007/s00428-012-1203-5.
- Prat J and FIGO Committee on Gynecologic Oncology (2015) FIGO’s staging classification for cancer of the ovary, fallopian tube, and peritoneum: abridged republication. *Journal of Gynecologic Oncology* 26(2): 87–89. DOI: 10.3802/jgo.2015.26.2.87.
- Press JZ, De Luca A, Boyd N, et al. (2008) Ovarian carcinomas with genetic and epigenetic BRCA1 loss have distinct molecular abnormalities. *BMC cancer* 8: 17. DOI: 10.1186/1471-2407-8-17.
- Pujade-Lauraine E, Hilpert F, Weber B, et al. (2014) Bevacizumab combined with chemotherapy for platinum-resistant recurrent ovarian cancer: The AURELIA open-label randomized phase III trial. *Journal of Clinical Oncology: Official Journal of the American Society of Clinical Oncology* 32(13): 1302–1308. DOI: 10.1200/JCO.2013.51.4489.
- Pujade-Lauraine E, Ledermann JA, Selle F, et al. (2017) Olaparib tablets as maintenance therapy in patients with platinum-sensitive, relapsed ovarian cancer and a BRCA1/2 mutation (SOLO2/ENGOT-Ov21): a double-blind, randomised, placebo-controlled, phase 3 trial. *The Lancet. Oncology* 18(9): 1274–1284. DOI: 10.1016/S1470-2045(17)30469-2.
- Pyriochou A, Olah G, Deitch EA, et al. (2008) Inhibition of angiogenesis by the poly(ADP-ribose) polymerase inhibitor PJ-34. *International Journal of Molecular Medicine* 22(1): 113–118.
- Raja FA, Griffin CL, Qian W, et al. (2011) Initial toxicity assessment of ICON6: a randomised trial of cediranib plus chemotherapy in platinum-sensitive relapsed ovarian cancer. *British Journal of Cancer* 105(7): 884–889. DOI: 10.1038/bjc.2011.334.
- Ray-Coquard I, Selle F, Harter P, et al. (2016) PAOLA-1: An ENGOT/GCIG phase III trial of olaparib versus placebo combined with bevacizumab as maintenance treatment in patients

- with advanced ovarian cancer following first-line platinum-based chemotherapy plus bevacizumab. *Journal of Clinical Oncology* 34(15_suppl): TPS5607-TPS5607. DOI: 10.1200/JCO.2016.34.15_suppl.TPS5607.
- Ribatti D (2009) Endogenous inhibitors of angiogenesis: a historical review. *Leukemia Research* 33(5): 638–644. DOI: 10.1016/j.leukres.2008.11.019.
- Ricci F, Brogгинi M and Damia G (2013) Revisiting ovarian cancer preclinical models: implications for a better management of the disease. *Cancer Treatment Reviews* 39(6): 561–568. DOI: 10.1016/j.ctrv.2013.01.005.
- Ricci F, Bizzaro F, Cesca M, et al. (2014) Patient-derived ovarian tumor xenografts recapitulate human clinicopathology and genetic alterations. *Cancer Research* 74(23): 6980–6990. DOI: 10.1158/0008-5472.CAN-14-0274.
- Robert J. Kurman, Carcangiu ML, Herrington SC, et al. (2014) *WHO Classification of Tumors of Female Reproductive Organs*. 4th edition. World Health Organization Classification of Tumours. Lyon: IARC.
- Rottenberg S, Jaspers JE, Kersbergen A, et al. (2008) High sensitivity of BRCA1-deficient mammary tumors to the PARP inhibitor AZD2281 alone and in combination with platinum drugs. *Proceedings of the National Academy of Sciences of the United States of America* 105(44): 17079–17084. DOI: 10.1073/pnas.0806092105.
- Sahade M, Caparelli F and Hoff PM (2012) Cediranib: a VEGF receptor tyrosine kinase inhibitor. *Future Oncology (London, England)* 8(7): 775–781. DOI: 10.2217/fon.12.73.
- Saitou M, Iida Y, Komazaki H, et al. (2015) Success rate and safety of tumor debulking with diaphragmatic surgery for advanced epithelial ovarian cancer and peritoneal cancer. *Archives of Gynecology and Obstetrics* 291(3): 641–646. DOI: 10.1007/s00404-014-3446-7.
- Sancar A, Lindsey-Boltz LA, Unsal-Kaçmaz K, et al. (2004) Molecular mechanisms of mammalian DNA repair and the DNA damage checkpoints. *Annual Review of Biochemistry* 73: 39–85. DOI: 10.1146/annurev.biochem.73.011303.073723.
- Satoh MS and Lindahl T (1992) Role of poly(ADP-ribose) formation in DNA repair. *Nature* 356(6367): 356–358. DOI: 10.1038/356356a0.
- Sausville EA and Burger AM (2006) Contributions of human tumor xenografts to anticancer drug development. *Cancer Research* 66(7): 3351–3354, discussion 3354. DOI: 10.1158/0008-5472.CAN-05-3627.
- Scanlon SE and Glazer PM (2015) Multifaceted control of DNA repair pathways by the hypoxic tumor microenvironment. *DNA repair* 32: 180–189. DOI: 10.1016/j.dnarep.2015.04.030.
- Schmittgen TD and Livak KJ (2008) Analyzing real-time PCR data by the comparative C(T) method. *Nature Protocols* 3(6): 1101–1108.
- Schmoll H-J, Cunningham D, Sobrero A, et al. (2012) Cediranib with mFOLFOX6 versus bevacizumab with mFOLFOX6 as first-line treatment for patients with advanced colorectal cancer: a double-blind, randomized phase III study (HORIZON III). *Journal of Clinical Oncology: Official Journal of the American Society of Clinical Oncology* 30(29): 3588–3595. DOI: 10.1200/JCO.2012.42.5355.
- Schneider CA, Rasband WS and Eliceiri KW (2012) NIH Image to ImageJ: 25 years of image analysis. Available at: <https://www.nature.com/articles/nmeth.2089> (accessed 24 March 2018).

- Shen Y, Rehman FL, Feng Y, et al. (2013) BMN 673, a novel and highly potent PARP1/2 inhibitor for the treatment of human cancers with DNA repair deficiency. *Clinical Cancer Research: An Official Journal of the American Association for Cancer Research* 19(18): 5003–5015. DOI: 10.1158/1078-0432.CCR-13-1391.
- Shih I-M and Kurman RJ (2004) Ovarian tumorigenesis: a proposed model based on morphological and molecular genetic analysis. *The American Journal of Pathology* 164(5): 1511–1518.
- Shultz LD, Brehm MA, Garcia-Martinez JV, et al. (2012) Humanized mice for immune system investigation: progress, promise and challenges. *Nature Reviews. Immunology* 12(11): 786–798. DOI: 10.1038/nri3311.
- Singer G, Stöhr R, Cope L, et al. (2005) Patterns of p53 mutations separate ovarian serous borderline tumors and low- and high-grade carcinomas and provide support for a new model of ovarian carcinogenesis: a mutational analysis with immunohistochemical correlation. *The American Journal of Surgical Pathology* 29(2): 218–224.
- Siolas D and Hannon GJ (2013) Patient-derived tumor xenografts: transforming clinical samples into mouse models. *Cancer Research* 73(17): 5315–5319. DOI: 10.1158/0008-5472.CAN-13-1069.
- Smith EL, Zamarin D and Lesokhin AM (2014) Harnessing the immune system for cancer therapy. *Current Opinion in Oncology* 26(6): 600–607. DOI: 10.1097/CCO.0000000000000128.
- Smith NR, James NH, Oakley I, et al. (2007) Acute pharmacodynamic and antivascular effects of the vascular endothelial growth factor signaling inhibitor AZD2171 in Calu-6 human lung tumor xenografts. *Molecular Cancer Therapeutics* 6(8): 2198–2208. DOI: 10.1158/1535-7163.MCT-07-0142.
- Smyth GK (2004) Linear models and empirical bayes methods for assessing differential expression in microarray experiments. *Statistical Applications in Genetics and Molecular Biology* 3: Article3. DOI: 10.2202/1544-6115.1027.
- Soegaard M, Kjaer SK, Cox M, et al. (2008) BRCA1 and BRCA2 mutation prevalence and clinical characteristics of a population-based series of ovarian cancer cases from Denmark. *Clinical Cancer Research: An Official Journal of the American Association for Cancer Research* 14(12): 3761–3767. DOI: 10.1158/1078-0432.CCR-07-4806.
- Stordal B, Timms K, Farrelly A, et al. (2013) BRCA1/2 mutation analysis in 41 ovarian cell lines reveals only one functionally deleterious BRCA1 mutation. *Molecular Oncology* 7(3): 567–579. DOI: 10.1016/j.molonc.2012.12.007.
- Stuart GCE, Kitchener H, Bacon M, et al. (2011) 2010 Gynecologic Cancer InterGroup (GCIG) consensus statement on clinical trials in ovarian cancer: report from the Fourth Ovarian Cancer Consensus Conference. *International Journal of Gynecological Cancer: Official Journal of the International Gynecological Cancer Society* 21(4): 750–755. DOI: 10.1097/IGC.0b013e31821b2568.
- Tan DSP, Yap TA, Hutka M, et al. (2013) Implications of BRCA1 and BRCA2 mutations for the efficacy of paclitaxel monotherapy in advanced ovarian cancer. *European Journal of Cancer (Oxford, England: 1990)* 49(6): 1246–1253. DOI: 10.1016/j.ejca.2012.11.016.
- Tavtigian SV, Simard J, Rommens J, et al. (1996) The complete BRCA2 gene and mutations in chromosome 13q-linked kindreds. *Nature Genetics* 12(3): 333–337. DOI: 10.1038/ng0396-333.

- Tentler JJ, Tan AC, Weekes CD, et al. (2012) Patient-derived tumour xenografts as models for oncology drug development. *Nature Reviews. Clinical Oncology* 9(6): 338–350. DOI: 10.1038/nrclinonc.2012.61.
- Tentori L, Lacal PM, Muzi A, et al. (2007) Poly(ADP-ribose) polymerase (PARP) inhibition or PARP-1 gene deletion reduces angiogenesis. *European Journal of Cancer (Oxford, England: 1990)* 43(14): 2124–2133. DOI: 10.1016/j.ejca.2007.07.010.
- Terada M, Fujiki H, Marks PA, et al. (1979) Induction of erythroid differentiation of murine erythroleukemia cells by nicotinamide and related compounds. *Proceedings of the National Academy of Sciences* 76(12): 6411–6414.
- Therasse P, Arbuck SG, Eisenhauer EA, et al. (2000) New guidelines to evaluate the response to treatment in solid tumors. European Organization for Research and Treatment of Cancer, National Cancer Institute of the United States, National Cancer Institute of Canada. *Journal of the National Cancer Institute* 92(3): 205–216.
- Topp MD, Hartley L, Cook M, et al. (2014) Molecular correlates of platinum response in human high-grade serous ovarian cancer patient-derived xenografts. *Molecular Oncology* 8(3): 656–668. DOI: 10.1016/j.molonc.2014.01.008.
- Turner N, Tutt A and Ashworth A (2004) Hallmarks of ‘BRCAness’ in sporadic cancers. *Nature Reviews. Cancer* 4(10): 814–819. DOI: 10.1038/nrc1457.
- Wedge SR, Kendrew J, Hennequin LF, et al. (2005) AZD2171: a highly potent, orally bioavailable, vascular endothelial growth factor receptor-2 tyrosine kinase inhibitor for the treatment of cancer. *Cancer Research* 65(10): 4389–4400. DOI: 10.1158/0008-5472.CAN-04-4409.
- Weroha SJ, Becker MA, Enderica-Gonzalez S, et al. (2014) Tumorgrafts as in vivo surrogates for women with ovarian cancer. *Clinical Cancer Research: An Official Journal of the American Association for Cancer Research* 20(5): 1288–1297. DOI: 10.1158/1078-0432.CCR-13-2611.
- Wood RD, Mitchell M, Sgouros J, et al. (2001) Human DNA repair genes. *Science (New York, N.Y.)* 291(5507): 1284–1289. DOI: 10.1126/science.1056154.
- Wooster R, Bignell G, Lancaster J, et al. (1995) Identification of the breast cancer susceptibility gene BRCA2. *Nature* 378(6559): 789–792. DOI: 10.1038/378789a0.
- Workman P, Aboagye EO, Balkwill F, et al. (2010) Guidelines for the welfare and use of animals in cancer research. *British Journal of Cancer* 102(11): 1555–1577. DOI: 10.1038/sj.bjc.6605642.
- Wu R, Hendrix-Lucas N, Kuick R, et al. (2007) Mouse model of human ovarian endometrioid adenocarcinoma based on somatic defects in the Wnt/beta-catenin and PI3K/Pten signaling pathways. *Cancer Cell* 11(4): 321–333. DOI: 10.1016/j.ccr.2007.02.016.
- Wu R, Baker SJ, Hu TC, et al. (2013) Type I to type II ovarian carcinoma progression: mutant Trp53 or Pik3ca confers a more aggressive tumor phenotype in a mouse model of ovarian cancer. *The American Journal of Pathology* 182(4): 1391–1399. DOI: 10.1016/j.ajpath.2012.12.031.
- Xue Y, Lim S, Yang Y, et al. (2011) PDGF-BB modulates hematopoiesis and tumor angiogenesis by inducing erythropoietin production in stromal cells. *Nature Medicine* 18(1): 100–110. DOI: 10.1038/nm.2575.

- Yu JL, Coomber BL and Kerbel RS (2002) A paradigm for therapy-induced microenvironmental changes in solid tumors leading to drug resistance. *Differentiation; Research in Biological Diversity* 70(9–10): 599–609. DOI: 10.1046/j.1432-0436.2002.700913.x.
- Yushkevich PA, Piven J, Hazlett HC, et al. (2006) User-guided 3D active contour segmentation of anatomical structures: significantly improved efficiency and reliability. *NeuroImage* 31(3): 1116–1128. DOI: 10.1016/j.neuroimage.2006.01.015.
- Zhang S, Royer R, Li S, et al. (2011) Frequencies of BRCA1 and BRCA2 mutations among 1,342 unselected patients with invasive ovarian cancer. *Gynecologic Oncology* 121(2): 353–357. DOI: 10.1016/j.ygyno.2011.01.020.

APPENDICES

A.1 Work by the candidate preceding the work described in this thesis

PUBLICATIONS

Ricci F[§], **Bizzaro F[§]**, Cesca M, Guffanti F, Decio A, Ghilardi C, Perego P, Fruscio R, Buda A, Ostano P, Chiorino G, Bani MR, Damia G and Giavazzi R.

Patient-derived ovarian tumor xenografts recapitulate human clinicopathology and genetic alterations. Cancer Res, 2014. Dec 1;74(23):6980-90. doi: 10.1158/0008-5472.CAN-14-0274. Epub 2014 Oct 10.

§equal contribution

CONGRESS PRESENTATIONS

Bizzaro F, Cesca M, Decio A, Scarlato V, Figini S, Ghilardi C, Bani MR and Giavazzi R.

A panel of patient-derived tumor xenografts representing the heterogeneity of epithelial ovarian cancer (EOC).

5th Freiburg Symposium on Anticancer Drug Discovery “Preclinical models of cancer: towards enhanced clinical relevance and predictivity”, Freiburg, Germany, April 24-27, 2013.

Bizzaro F, Ricci F, Cesca M, Guffanti F, Decio A, Ghilardi C, Perego P, Fruscio R, Ostano P, Chiorino G, Bani MR, Damia G, Giavazzi R.

Establishment of a platform of patient-derived tumor xenografts (EOC-PDX) to study the biology and therapy of epithelial ovarian cancer.

56th Annual Meeting of the Italian Society of Cancer, “Dangerous Liaisons: translating cancer biology into better patients management”, Ferrara, September 11-13, 2014.

Abstract selected for Oral Presentation.

A.2 Work by the candidate emanating from the work described in this thesis

CONGRESS PRESENTATIONS

Bizzaro F, Decio A, Barry ST, O'Connor MJ, Mannarino L, Ricci F, Bani MR and Giavazzi R.

Preclinical models of patient-derived ovarian cancer xenograft to study the response of the PARP inhibitor olaparib.

2nd Special Conference EACR AACR SIC, “The Challenge of Optimising Immuno and Target Therapies, From Cancer Biology to the Clinic”, Florence, June 24-27, 2017.

Abstract awarded with Best Poster Presentation sponsored by Fondazione Guido Berlucci and with Travel Grant.

Bizzaro F, Marchetti AC, Decio A, Ricci F, O'Connor MJ, Taylor MA, Lai Z, Barry ST, Bani MR and Giavazzi R.

Patient-derived ovarian cancer xenograft (OC-PDX) to study the response of the PARP inhibitor olaparib.

AACR Annual Meeting 2018, “Driving Innovative Cancer Science to Patient Care”, Chicago, April 14-18, 2018.

Abstract awarded with AACR-Società Italiana di Cancerologia Scholar-in-Training Award.

Bizzaro F, Marchetti AC, Decio A, Ricci F, O'Connor MJ, Taylor MA, Lai Z, Barry ST, Bani MR and Giavazzi R.

Patient-derived ovarian cancer xenograft (OC-PDX) to study the response of the PARP inhibitor olaparib.

PhD student Meeting, Istituto di Ricerche Farmacologiche Mario Negri IRCCS, Milan, June 14-15, 2018.

Abstract selected for Oral Presentation.

A.3 Work by the candidate not pertaining to the work described in this thesis

PUBLICATIONS

Bizzaro F, Falcetta F, D'Agostini E, Decio A, Minoli L, Erba E, Peccatori A.F, Scanziani E, Colombo N, Zucchetti M, Bani MR, Ubezio P and Giavazzi R.

Tumor progression and metastatic dissemination in ovarian cancer after dose-dense versus conventional paclitaxel plus bevacizumab.

International Journal of Cancer, 2018. May 11. doi: 10.1002/ijc.31596.

Guffanti F, Fratelli M, Ganzinelli M, Bolis M, Ricci F, **Bizzaro F**, Chilà R, Sina FP, Fruscio R, Lupia M, Cavallaro U, Cappelletti MR, Generali D, Giavazzi R, Damia G.

Platinum sensitivity and DNA repair in a recently established panel of patient-derived ovarian carcinoma xenografts.

Oncotarget, 2018. 15;9(37):24707-24717. doi: 10.18632/oncotarget.25185. eCollection 2018 May 15.

Falcetta F, **Bizzaro F**, D'Agostini E, Bani MR, Giavazzi R and Ubezio P.

Modelling cytostatic and cytotoxic responses to new treatment regimens for ovarian cancer.

Cancer Res, 2017. Dec 1;77(23):6759-6769. doi: 10.1158/0008-5472.CAN-17-1099. Epub 2017 Sep 26.

Fuso Nerini I, Cesca M, **Bizzaro F**, Giavazzi R.

Combination therapy in cancer: effects of angiogenesis inhibitors on drug pharmacokinetics and pharmacodynamics.

Chin J Cancer, 2016. Jun 29;35(1):61. doi: 10.1186/s40880-016-0123-1. Review.

Decio A, Cesca M, **Bizzaro F**, Porcu L, Bettolini R, Ubezio P, Taraboletti G, Belotti D, Giavazzi R.

Cediranib combined with chemotherapy reduces tumor dissemination and prolongs the survival of mice bearing patient-derived ovarian cancer xenografts with different responsiveness to cisplatin.

Clin Exp Metastasis, 2015. 2015 Oct;32(7):647-58. doi: 10.1007/s10585-015-9734-1. Epub 2015 Jul 17.

Pinessi D, Ostano P, Borsotti P, Bello E, Guffanti F, **Bizzaro F**, Frapolli R, Bani MR, Chiorino G, Taraboletti G, Resovi A.

Expression of thrombospondin-1 by tumor cell in patient-derived ovarian carcinoma xenografts.

Connect Tissue Res, 2015. 2015;56(5):355-63. doi: 10.3109/03008207.2015.1045065. Epub 2015 Jun 15.

Cesca M, **Bizzaro F**, Zucchetti M e Giavazzi R.

Tumor delivery of chemotherapy combined with inhibitors of angiogenesis and vascular targeting agents.

Front Oncol, 2013. Oct 1;3:259. doi: 10.3389/fonc.2013.00259. Review.

CONGRESS PRESENTATIONS

Bizzaro F, D'Agostini E, Decio A, Falcetta F, Erba E, Ubezio P and Giavazzi R.

Paclitaxel drives response to combination therapy with bevacizumab in ovarian cancer preclinical models.

Special Conference EACR AACR SIC, "Anticancer Drug Action and Drug Resistance: from Cancer Biology to the Clinic", Florence, June 20-23, 2015.

Bizzaro F, D'Agostini E, Decio A, Falcetta F, Erba E, Ubezio P and Giavazzi R¹.

Paclitaxel drives response to combination therapy with bevacizumab in ovarian cancer preclinical models.

PhD student Meeting, Istituto di Ricerche Farmacologiche Mario Negri IRCCS, Milan, July 9-10, 2015.

Bizzaro F, D'Agostini E, Decio A, Falcetta F, Erba E, Minoli L, Scanziani E, Bani MR, Ubezio P and Giavazzi R.

"Dose-dense" paclitaxel combined with bevacizumab in preclinical models of ovarian cancers.

58th Annual Meeting of the Italian Society of Cancer, "Revolutionary Road: accelerating conversion of cancer biology into personalized clinical oncology", Verona, September 5-8, 2016.

Bizzaro F, D'Agostini E, Decio A, Falcetta F, Erba E, Minoli L, Scanziani E, Bani MR, Ubezio P and Giavazzi R.

“Dose-dense” paclitaxel combined with bevacizumab in preclinical models of ovarian cancers.

PhD student Meeting, Istituto di Ricerche Farmacologiche Mario Negri IRCCS, Milan, July 13-14, 2016.

Abstract awarded with the Best Poster Presentation sponsored by Carlo Erba.

A.4 Abstract from paper as a first name author

Ricci F[§], **Bizzaro F[§]**, Cesca M, Guffanti F, Decio A, Ghilardi C, Perego P, Fruscio R, Buda A, Ostano P, Chiorino G, Bani MR, Damia G and Giavazzi R.

Patient-derived ovarian tumor xenografts recapitulate human clinicopathology and genetic alterations.

Epithelial ovarian cancer (EOC) is the most lethal gynecologic malignancy. On the basis of its histopathology and molecular-genomic changes, ovarian cancer has been divided into subtypes, each with distinct biology and outcome. The aim of this study was to develop a panel of patient-derived EOC xenografts that recapitulate the molecular and biologic heterogeneity of human ovarian cancer. Thirty-four EOC xenografts were successfully established, either subcutaneously or intraperitoneally, in nude mice. The xenografts were histologically similar to the corresponding patient tumor and comprised all the major ovarian cancer subtypes. After orthotopic transplantation in the bursa of the mouse ovary, they disseminate into the organs of the peritoneal cavity and produce ascites, typical of ovarian cancer. Gene expression analysis and mutation status indicated a high degree of similarity with the original patient and discriminate different subsets of xenografts. They were very responsive, responsive, and resistant to cisplatin, resembling the clinical situation in ovarian cancer. This panel of patient-derived EOC xenografts that recapitulate the recently type I and type II classification serves to study the biology of ovarian cancer, identify tumor-specific molecular markers, and develop novel treatment modalities.

Cancer Res, 2014. Dec 1;74(23):6980-90. doi: 10.1158/0008-5472.CAN-14-0274. Epub 2014 Oct 10.

§equal contribution

Bizzaro F, Falcetta F, D'Agostini E, Decio A, Minoli L, Erba E, Peccatori A.F, Scanziani E, Colombo N, Zucchetti M, Bani MR, Ubezio P and Giavazzi R.

Tumor progression and metastatic dissemination in ovarian cancer after dose-dense versus conventional paclitaxel plus bevacizumab.

The efficacy of therapeutic regimens incorporating weekly or every-3-weeks paclitaxel (PTX) for ovarian cancer is debated. We investigated the addition of bevacizumab in regimens of chemotherapy with different PTX doses and schedules in preclinical models. Treatments were cisplatin (DDP) with weekly PTX (conventional), or dose-dense-equi (every other day to the conventional cumulative dose), or dose-dense-high (total dose 1.5 times higher), with or without bevacizumab. Treatment efficacy was evaluated analyzing

tumor growth in different time-windows in two patient-derived ovarian cancer xenografts with different sensitivity to cisplatin. Tumor progression, metastasis and survival were studied in ovarian cancer models growing orthotopically and disseminating in the mouse peritoneal cavity. Short-term effects on cell cycle, tumor cell proliferation/apoptosis and vasculature were evaluated by flow cytometry and immunohistochemistry. PTX dose-dense (with/without DDP) was superior to the conventional scheme in a dose-dependent manner; the high efficacy was confirmed by the lower ratio of tumor to normal cells. All schemes benefited from bevacizumab, which reduced tumor vessels. However, DDP/PTX dose-dense-high (only chemotherapy) was at least as active as DDP/PTX conventional plus bevacizumab. DDP/PTX dose-dense-high plus bevacizumab was the most effective in delaying tumor progression, though it did not prolong mouse survival and the continuous treatment with bevacizumab was associated to a malignant disease. These findings indicate that the effect of bevacizumab in combination with chemotherapy depends on the schedule-dose of the treatment and help to explain the unclear benefits after bevacizumab. *International Journal of Cancer*, 2018. May 11. doi: 10.1002/ijc.31596.